Université de Montréal

Drug and gene delivery systems based on polymers derived from bile acids

Par Alexander Joseph Cunningham

Département de Chimie

Faculté des Arts et Sciences

Thèse présentée à la Faculté des études supérieures et postdoctorales
en vue de l'obtention du grade de Philosophiae Doctor (Ph. D.)
en chimie

Avril 2021

Université de Montréal

Faculté des études supérieures – Département de chimie

Cette thèse intitulée

Drug and gene delivery systems based on polymers derived from bile acids

Présentée par

Alexander Joseph Cunningham

A été évaluée par un jury composé des personnes suivantes

Suzanne Giasson
Présidente-rapportrice

Julian Zhu
Directeur de recherche

Jeanne Chain
Codirectrice

Xavier Banquy
Codirecteur

Michel Lafleur
Membre du jury

Juntao Luo
Examinateur externe

Résumé

Grâce à de récentes percées scientifiques, certains médiateurs clés dans divers états pathologiques ont été identifiés et de nouveaux composés thérapeutiques ont été développés pour les inhiber. Bien que très efficaces, ces composés possèdent souvent des propriétés physico-chimiques incompatibles avec celles du corps humain et deviennent, donc, difficiles à formuler. Au cours des dernières décennies, les systèmes de vectorisation de médicaments ont été étudiés comme une solution potentielle promettant une augmentation de la concentration du médicament au site d'action tout en atténuant les problèmes de stabilité et de solubilité. Plus particulièrement, les polymères ont démontré un succès en tant que matière première dans la conception de ces formulations. Cependant, un obstacle majeur à leur développement clinique est le faible niveau d'encapsulation du principe actif. Afin de remédier à cette limitation, les travaux présentés dans cette thèse se sont concentrés sur l'utilisation de copolymères blocs en forme d'étoile et à base d'acide cholique pour faciliter l'encapsulation. Divers principes actifs aux propriétés physico-chimiques variables ont été encapsulés dans nos systèmes polymères, témoignant ainsi de leur grande efficacité et ceci à travers une large gamme de médicaments.

Dans un premier temps, les propriétés physico-chimiques de notre système ont été étudiées. Les copolymères bloc sont composés d'un noyau d'acide cholique (CA) sur lequel le poly (allyl glycidyl éther) (PAGE) et le poly (éthylène glycol) (PEG) sont polymérisées séquentiellement pour donner lieu au CA-(PAGE-*b*-PEG)$_4$ amphiphiles à quatre branches. De plus, le bloc PAGE a été fonctionnalisé pour porter des groupements amines primaires. Les effets de la longueur du bloc PEG et des groupements amines sur le comportement thermosensible des polymères dans l'eau ont été examinés. Cette thermosensibilité a aussi été étudiée en présence de diverses concentrations de sels. Il a été découvert que l'augmentation de la longueur du PEG augmente la température du point de trouble. De même, la fonctionnalisation des blocs PAGE pour porter des groupements amines a augmenté le point de trouble en l'absence de sel, mais a significativement diminué en présence de sel. Cette observation a été attribuée au « salting-out » des polymères.

Dans un second temps, employée comme un médicament hydrophobe modèle, la doxorubicine (Dox) a été encapsulée à l'aide de nos copolymères blocs CA-(PAGE-*b*-

PEG)$_4$. Dans ce cas, les interactions polymère-médicament régissant l'encapsulation de la Dox ont été étudiées. Plus précisément, les interactions hydrophobes et électrostatiques ont été comparées pour leur influence sur la charge de médicament à l'intérieur des copolymères blocs. Une charge élevée de Dox a été obtenue à l'aide des interactions électrostatiques par rapport aux interactions hydrophobes avec ou sans la présence d'acide oléique comme co-tensioactif. De plus, les interactions électrostatiques conféraient au système de relargage une réactivité au pH permettant ainsi un relargage de la Dox en présence d'un pH acide. Les copolymères blocs ont présenté une bonne biocompatibilité lors d'essai in vitro. Les nouveaux copolymères blocs en étoile et à base d'acide cholique ont montré un grand potentiel en tant que vecteurs de relargage de médicaments pour l'encapsulation de la Dox.

Pour démontrer l'étendue de l'application de notre système, des petits acides ribonucléiques interférant (pARNi) ont été encapsulés à l'aide des copolymères blocs CA-(PAGE-*b*-PEG)$_4$ où le PAGE a été fonctionnalisé pour porter des groupements amines. Les pARNi sont des composés thérapeutiques hydrophiles chargés négativement et nécessitant une méthodologie d'encapsulation différente de celle utilisée pour la Dox. Les groupements allyles du bloc PAGE ont été fonctionnalisés pour porter des amines primaires ou tertiaires. Également, l'acide folique a été greffé sur l'extrémité de la chaîne PEG pour augmenter l'absorption cellulaire. Les (CA-PAGE-*b*-PEG)$_4$ fonctionnalisés avec des amines primaires ou tertiaires ont présenté une forte complexation des pARNi. Des agrégats micellaires uniformes ont ainsi été obtenus. De plus, des lipides ont été ajoutés comme co-tensioactifs pour aider à stabiliser les nanoparticules dans les milieux de culture cellulaire. Ces systèmes micellaires mixtes avaient une charge élevée de pARNi et une absorption cellulaire améliorée avec une augmentation concomitante de la transfection des pARNi dans des cellules modèles de HeLa et HeLa-GFP, respectivement. Les résultats présentés dans cette thèse témoignent du grand potentiel de l'utilisation de copolymères blocs en forme d'étoile et à base d'acide cholique dans la conception de systèmes de vectorisation de médicaments. Ces résultats offrent des conclusions pertinentes sur les différents paramètres clés contrôlant l'efficacité des systèmes de vectorisation des médicaments à base de polymères pouvant être traduits dans d'autres systèmes. Les stratégies développées ici aideront grandement au développement des

systèmes de vectorisation de médicaments et accéléreront potentiellement leur évolution vers la clinique.

Mots Clés : copolymère bloc, relargage de médicament, thérapie génique, thermosensible, pH sensible, biocompatible, acide cholique.

Abstract

Recent scientific breakthroughs have fostered the identification of key mediators of various diseased states while permitting the development of novel therapeutic compounds to address them. Although very potent, these compounds often possess physico-chemical properties that are incompatible with those of the human body and are becoming increasingly difficult to formulate. In the recent decades, drug delivery systems have been studied as a potential solution in the formulation of these therapeutic compounds promising improved accumulation at the site of action while mitigating issues of stability and solubility. Most notably, polymers have shown tremendous success as starting material in the design of these drug formulations. However, one major hurdle curtailing their clinical translatability is their low drug loading levels. In an effort to address this limitation, the work presented in this thesis focused on the use of cholic acid-based star-shaped block copolymers for the encapsulation of active pharmaceutical ingredients with varying physico-chemical properties thereby demonstrating their successful application to a broad range of compounds.

First, the physico-chemical properties of our proposed system were studied. The block copolymers are composed of a cholic acid (CA) core onto which poly(allyl glycidyl ether) (PAGE) and poly(ethylene glycol) (PEG) are polymerized sequentially to afford an amphiphilic CA-(PAGE-*b*-PEG)$_4$ with four branches. The PAGE block was further functionalized to bear pendant amine groups. The effects of PEG length and of the amine groups on the thermoresponsive behavior of the polymers in water at various salt concentrations were examined. It was discovered that increasing the length of PEG increases the cloud point temperature. Similarly, functionalizing the PAGE blocks to bear pendant amine groups increased the cloud point in the absence of salt, but significantly decreased the cloud point in the presence of salt. This observation was attributed to the salting-out of the polymers.

Acting as a model hydrophobic drug, doxorubicin (Dox) was first encapsulated using our proposed CA-(PAGE-*b*-PEG)$_4$ block copolymers. In this case, the polymer-drug interactions driving the loading of Dox was studied. Specifically, hydrophobic and electrostatic interactions were compared for their influence on the drug loading inside the block copolymers. A high loading of Dox was achieved vis electrostatic interactions

compared to hydrophobic interactions with or without the presence of oleic acid as a cosurfactant. Also, the electrostatic interactions conferred a pH responsiveness to the system where the Dox remained encapsulated at physiological pH but was released in acidic pH. The block copolymers displayed good biocompatibility in vitro. The new functionalized star block copolymers based on cholic acid showed great potential as drug delivery carriers for the loading of Dox.

To demonstrate the widespread application of our proposed system, small interfering RNA (siRNA) was loading using the CA-(PAGE-*b*-PEG)$_4$ block copolymers where PAGE was functionalized with amine. siRNA is a hydrophilic, negatively charged therapeutic compound necessitating a different loading methodology than that used for Dox. The allyl groups of PAGE were functionalized to bear primary or tertiary amines and folic acid was grafted onto the PEG chain end to increase cell uptake. (CA-PAGE-*b*-PEG)$_4$ functionalized with either primary or tertiary amines show high siRNA complexation. Uniform micellar aggregates were obtained. Lipids were added as co-surfactants to help stabilize the nanoparticles in the cell culture media. The mixed micelles had high siRNA loading and improved cell uptake with a concomitant increase in siRNA transfection in HeLa and HeLa-GFP model cells, respectively.

The results presented in this thesis, demonstrate the feasibility of using cholic acid-based star-shaped block copolymers in the design of drug delivery systems and offers insights into key parameters controlling their efficacy which can be translated to other polymer-based systems. The strategies developed herein will greatly aid in the development of drug delivery systems and potentially accelerate their progress into the clinic.

Keywords: bloc copolymer, drug delivery, gene delivery, thermosensitive, pH-responsive, biocompatible, cholic acid.

Acknowledgements

First and foremost, I would like to thank God for his unwavering presence in my life. His grace, His wisdom, His strength, and His unending love has uplifted me not only throughout this thesis, but ever since I have seen His light. Also, I would like to take the time to honour my parents who have always been there for me and I am grateful for their love and support. As if it weren't enough, I was blessed further with two additional parents that have always treated me like their son and for this I am forever grateful and would like to thank them for their unending love and support. Finally, I would like to thank God for these exceptional men I have the honour to call my brothers, Mattieu, Emmanuel, Stephane, and Alexandru. They have always been there for me with love and encouragement. Words cannot express the gratitude I have towards God for this extraordinary family and the love I have for them. Their presence in my life has been a blessing that is abundantly above what anyone can ever think of.

The work in this thesis is multidisciplinary in nature and needed expertise in chemistry and pharmacy. I would like to thank my thesis supervisors, Professors Julian Zhu, Jeanne Leblond-Chain, and Xavier Banquy for their mentorship and guidance during my PhD. They have helped me in numerous ways in shaping me into becoming a great scientist. They have helped me develop and attain my goals, always present and accessible, always prompt to teach and instruct, yet friendly and welcoming.

Thank you to the members of the jury and my committee members, Professors Michel Lafleur and Suzanne Giasson, for doing me the honor of taking your time to evaluate this thesis. A big thank you also to all the co-authors of the articles who participated intellectually or manually on the merits of the publications.

I would also like to thank all the students, colleagues, professors, and research assistants that I have worked with during my thesis. Thank you for all the helpful discussions and insightful advice.

Finally, I would like to thank the Université de Montréal, the Charron-Lam Foundation, the Camille-Sandorfy Foundation, l'École Polytechnique de Montréal and the Church Le Refuge, especially the Pastor Daniel Cheri, for the scholarships which were able to lighten my financial burden.

Table of contents

List of Tables

List of Schemes

List of Figures

List of acronyms, abbreviations, and symbols

ABC	Accelerated blood clearance
ADR	Adriamycin
AGE	Allyl glycidyl ether
AIBN	Azobisisobutyronitrile
API	Active pharmaceutical ingredient
AT-II	Angiotensin-II
AUC	Area under the concentration-time curve
BBB	Blood brain barrier
BCS	Biopharmaceutical classification system
CA	Cholic acid
CMC	Critical micellar concentration
CP	Cloud point
BA	Bile acid
Đ	Polydispersity
DCA	Deoxycholic acid
DDS	Drug delivery system
D_h	Hydrodynamic diameter
DLC	Drug loading content
DLE	Drug loading efficiency
DLS	Dynamic light scattering
DMEM	Dulbecco's modified eagle medium
DMF	Dimethylformamide
DMSO	Dimethyl sulfoxide
DOPE	1,2-dioleoyl-sn-glycero-3-phosphoethanolamine
DOX	Doxorubicin
DSC	Dynamic scanning calorimetry
DSPE	1,2-distearoyl-sn-glycero-3-phosphoethanolamine
DTT	Dithiothreitol
EE	Encapsulation efficiency
EPR	Enhanced permeation and retention effect
ER	Estrogen receptor
FA	Folic acid
FACS	Fluorescence activated cell sorting
FBS	Fetal bovine serum
GFP	Green fluorescent protein
GSH	Glutathione
IC_{50}	Half maximal inhibitory concentration
IgG	Immunoglobulin G
iRGD	Cyclic 9-amino acid arginine-glycine-aspartic acid peptide
LCA	Lithocholic acid
LCST	Lower critical solution temperature
LDL	Low-density lipoprotein
LPM	Lipid-polymer mixed micelles
MD	Molecular dynamics

MEC	Maximum effective concentration
MTC	Maximum tolerated concentration
MTD	Maximum tolerated dose
NMR	Nuclear magnetic resonance
NP	Nanoparticle
N/P	Nitrogen/phosphate ratio
OA	Oleic acid
PAAc	Poly(acrylic acid)
PAGE	Poly(allyl glycidyl ether)
PAMAM	Polyamidoamine
PAsp	Poly(L-aspartate)
PbAE	Poly(β-amino esters)
PBS	Phosphate buffered saline
PCAE	Poly(acryloyloxy ethyl cholate)
PCL	Poly(caprolactone)
PDMAEMA	Poly(2-(dimethylamino) ethyl methacrylate)
pDNA	Plasmid deoxyribonucleic acid
PEG	Poly(ethylene glycol)
PEI	Poly(ethylene imine)
PHis	Poly(L-histidine)
PLA	Polylactide
PLGA	Poly(lactic-*co*-glycolic acid)
PLL	Poly(L-lysine)
PMMA	Poly(methyl methacrylate)
PNIPAAM	Poly(N-isopropylacrylamide)
PPO	Poly(propylene oxide)
PS	Polystyrene
PTX	Paclitaxel
PVA	Poly(vinyl alcohol)
PVL	Polyvalerolactone
PVP	Polyvinylpyrrolidone
RES	Reticular endothelial system
RGD	Arginine-glycine-aspartic acid peptide
ROS	Reactive oxygen species
SEC	Size exclusion chromatography
siRNA	Small interfering ribonucleic acid
T_{cp}	Cloud-point temperature
TEM	Transmission electron microscopy
T_g	Glass transition temperature
THF	Tetrahydrofuran
UV	Ultraviolet
VEGFR	Vascular endothelial growth factor receptor

Chapter 1. Introduction

Equipped with modern computer simulations and aided with crystal structures of target proteins and enzymes, chemists can now use structure-activity relationships and combinatorial chemistry to develop a library of potential drug candidates. The lead compounds undergo further testing eventually producing new therapeutic drugs. These tools enabled the discovery of drugs with superior potency and specificity, but this often came at a cost. Currently, there are thousands of compounds in the drug pipeline that are undergoing testing for their efficacy in the treatment of a range of diseases. However, recent estimates indicate that 90% of these drugs and 40% of those that get approval are poorly water-soluble.[1] The main challenge associated with these active pharmaceutical ingredients (API) resides in their poor water solubility, rapid metabolism and elimination and low permeability which negatively impacts their dissolution, absorption and bioavailability. The low bioavailability and absorption hamper the pharmacokinetics of the drugs leading to variable patient outcomes. In addition to the low permeability and/or solubility, certain APIs also present issues with high toxicity, low stability, and poor cell uptake. Specifically pertaining to cancer therapy, chemotherapeutic agents and gene products present additional hurdles with respect to their stability and toxicity. These concerns drove the impetus for the development of suitable formulations.

The pharmaceutical industry is currently dominated by solid APIs that are administered orally in the formulation of the biopharmaceutical classification system (BCS) class II and IV drugs.[1] In most cases, these solid APIs are formulated as salts (active ingredient and a counter-ion), solvates or hydrates (active ingredient and water or solvent), crystals (crystalline form of the active ingredient), or pro-drugs.[2] The purpose of these different formulations is to increase the permeability of the APIs through the gastrointestinal tract for better absorption and increase the solubility of the APIs to prevent crystallisation and precipitation of the drug. These strategies have led to successful drug formulations but are also prone to several limitations. For example, salification of current APIs is a common technique to ameliorate the essential properties of bioavailability and solubility.[3] There is an estimated 50% of all drugs in the pharmaceutical industry developed as salts.[2] However, salification of API can only be achieved on compounds that are ionizable and therefore is of limited use. These formulation strategies were successful

in the formulation of a range of therapeutic agents. Nonetheless, they are characterized with their respective limitations and cannot be employed for all therapeutics.

Table 1.1. The Biopharmaceutics Classification System (BCS) for the classification of API for oral administration.

Class I: High Solubility High Permeability	Class II: Low Solubility High Permeability
Class III: High Solubility Low Permeability	Class IV: Low Solubility Low Permeability

In addition, certain APIs are unstable and degrade rapidly before reaching their therapeutic target. For example, small interfering RNAs (siRNA) used in gene therapy are rapidly cleaved in the bloodstream, due to the presence of nucleases, and require protection from nucleases to improve its plasma concentration and enable a therapeutic response.[4] Other compounds, such as chemotherapeutic agents, possess high toxicity, in particular nephrotoxicity, neurotoxicity and ototoxicity.[5] Their use in the treatment of cancer hangs on a delicate balance between response and toxicity. The cytotoxic action of the chemotherapeutic drug does not select between malignant and healthy cells and its distribution inside the patient is the main cause for severe toxic side effects, a hallmark of chemotherapy. To address these limitations, drug formulations have evolved into drug delivery systems (DDS). Inspired by Paul Ehrlich's century-old concept of the magic bullet, DDS function as excipients for the encapsulation of APIs and delivers this API to the target cells without harming healthy tissues and while preventing its degradation. DDS have many advantages: loading and release of hydrophobic APIs, spatio-temporal release of a drug for improved specificity and lower side effects, overcoming multi-drug resistance for chemotherapeutic compounds, reduced toxicity, increased cell uptake for large and charged compounds, loading of more than one API for combination therapy, and diverse platforms including theranostic.[6-11]

DDS offer great possibilities for improving drug formulations. The nanoparticle drug delivery system protects its cargo during transport to the target site. This property

can be useful for drugs that are easily degraded in certain environments such as the gastrointestinal (GI) tract in the oral delivery of compounds. For example, cylcosporin-loaded poly(lactide-*co*-glycolide) nanoparticles were used in the oral delivery of cyclosporin and markedly improved its bioavailability compared to the commercially available formulation due to increased stability in the GI tract.[12] The protection of the cargo also extends to decreasing the first-pass metabolism effect encountered in drugs administered orally.[13-14] The potential of DDS to protect its cargo and increase the bioavailability of the drug is also a key feature in their parenteral delivery driving their use in the realm of gene delivery. Indeed, various reports have described the potential of DDS to protect siRNA degradation from plasmatic nucleases and renal filtration thereby improving their bioavailability and therapeutic efficiency.[15-17] DDS are also useful to increase the solubility of poorly water-soluble APIs. These APIs can form hydrophobic-hydrophobic interactions with the core of the micelle and the micelles can increase their water solubility through increased stability in the aqueous environment.[18] For example, Genexol-PM© was the first FDA approved polymer-based formulation for the encapsulation of Paclitaxel. Paclitaxel has a very low water solubility and, through encapsulation into the poly(ethylene glycol)-*b*-poly(D,L-lactide) micelles, its water solubility was increased by three orders of magnitude thereby increasing its bioavailability.[18-19] Another possibility achieved with the use of DDS is the targeted delivery of the API to its site of action. It is now customary to attach on the DDS a ligand that will recognize specific cell-surface receptors and promote cell uptake of the DDS and its encapsulated cargo.[20] This targeting of the DDS enables a targeted distribution of drugs or biological macromolecules inside the body thereby limiting off-target effects. A library of ligands have been designed thus far and these can recognize a range of different receptors to target different tissues and cell types.[20] Stimuli-responsive drug release is another modality that is often used to promote a targeted delivery of the API. In response to endogenous or exogenous stimuli, the drug-polymer interactions are broken, and the drug is released. As will be discussed in section 1.1.4, tuning of the cleavable linkage can afford a spatio-temporal drug release. Finally, prolonging drug circulation is another advantage afforded through the use of DDS. These DDS can effectively act as reservoirs and release the drug in a controlled and sustained fashion to prolong the blood circulation

half-life and further improve its pharmacokinetics.[21] Prolonging the blood circulation of Doxorubicin through the liposomal formulation Doxil© is one of the reason behind its clinical success.[22]

There are countless examples of drug delivery systems in the literature with only a number of these reaching clinical phase trials and receiving FDA approval for clinical use in the treatment of a range of pathological conditions.[23] Specifically, DDS have had enormous success in the field of cancer therapy for the delivery of chemotherapeutic agents with several formulations currently approved for clinical use. However, there are limitations that persist with the current strategies, most notably with regards to excipient toxicity and insufficient drug loading. In an effort to remediate these limitations, the work presented herein proposes a bile acid- and polymer-based material in the design and formulation of drug delivery systems to be used in cancer therapies. The pertinence of DDS goes beyond the realm of cancer, but for the sake of clarity and brevity, the topic of this thesis will be limited to DDS as it pertains to cancer therapy. The following introduction is separated into two chapters. In the first chapter, polymer-based nanoparticles, micellization, drug loading and drug release is examined, followed by the different barriers to drug delivery. The second chapter of the introduction will focus on bile acids and their potential towards nanomaterials with emphasis on drug delivery.

1.1 Polymer-based nanoparticles

Polymers are materials of choice in the design and synthesis of nanoparticulate drug delivery systems. Their prevalence in ongoing clinical trials testifies to their utility in enhancing therapeutic and diagnostic strategies in the treatment of a range of diseases. Indeed, two of the top ten most sold drugs in the US during the course of 2013 were the two polymeric drugs Copaxone and Neulasta.[24-25] Most polymers in this field can be categorized as hydrogels, polymer-drug conjugates or micelles. Hydrogels are composed of a crosslinked polymer network and a large amount of water (typically 70-99% water).[26] Their high water content provides tunable physical properties that can be varied to match those of soft tissues in the body providing better biocompatibility; their stiffness can be varied from 0.5 kPa to 5 MPa.[27-30] Moreover, the crosslinked network serves as a barrier preventing enzymes from accessing the drug-loaded core and metabolizing the drug before its release.[26, 31] The hydrogels' mesh and pore size can be adjusted to afford the

desired rate of drug release.[32] In addition, recent stimuli-responsive methods added another level of control over the diffusion rate.[32] Hydrogels hold great potential as drug delivery systems, however certain challenges limit their broad application. Most notably, control over drug release has been difficult to achieve and most systems that demonstrate on-demand release are proof-of-concepts and suffer from significant baseline release.

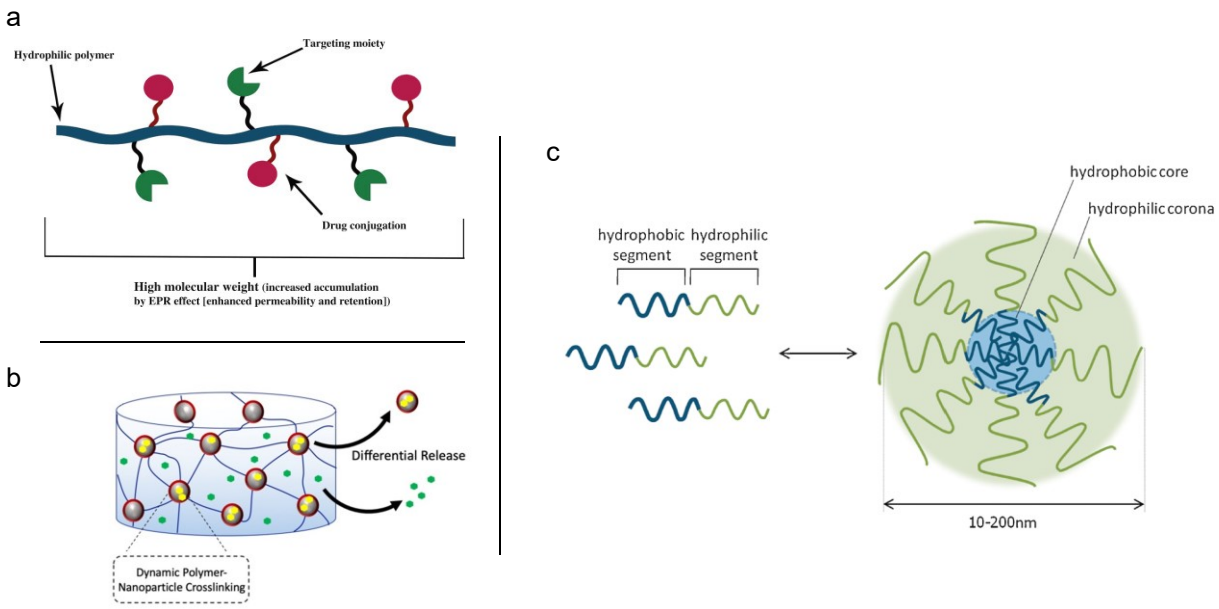

Figure 1.1 Schematic representation of (a) polymer-drug conjugates,[33] (b) hydrogels,[32] and (c) block copolymer micelles.[34] In the case of micelles, the hydrophobic block forms the core of the micelle, while the hydrophilic block constitutes the corona. (Reproduced with permission from © 2012 Elsevier).

Polymer-drug conjugates are macromolecular constructs composed of an API covalently linked to a polymeric carrier.[35] In this case, the polymer-conjugate increases the solubilization and/or stability of the API while providing a controlled delivery and pharmacokinetics and increased efficacy.[35] For these systems, the linker molecule is of great interest and mandates the drug release, a crucial step in achieving a therapeutic response. Without a stable linker, the drug can suffer from premature release whereas an overly stable linker prevents drug release and, hence, prevents a therapeutic response.[35] The most frequently employed linkers include esters,[36-39] enzymatically-cleavable peptide linkers,[40-42] acid-labile linkers,[43-47] and reduction-responsive linkers.[48-51] In terms of

polymer conjugates, poly(ethylene glycol) (PEG) has been the most studied candidate both for its biocompatibility and its potential for prolonging blood circulation. Alternatives to PEG include natural polysaccharides like dextran, polysialic acid and hyaluronic acid,[52-53] and poly(2-oxazoline).[54-56]

Polymer nanoparticles are supramolecular constructs ranging in size from tens to hundreds of nanometers and are composed of amphiphilic copolymers. These amphiphilic polymers self-assemble in an aqueous environment above their critical micellar concentration (CMC) with the hydrophobic block forming the core of the micelle and the hydrophilic block forming the corona and providing colloidal stability (Figure 1.1). This self-assembly process is entropically and energetically driven where the amphiphiles aggregate to minimize the unfavored hydrophobic-water interactions.[57] The morphology of the micelle depends on the size of each blocks, their relative hydrophobicity and hydrophilicity and the solvent conditions.[58] The different morphologies that have been described in the literature include spheres, rods, vesicles, tubules and lamellar.[58-60] These different nanostructures can be predicted based on a dimensionless packing parameter *p*,[57, 61-62]

$$p = \frac{v}{a \times l} \qquad (1)$$

where v is the volume of the hydrophobic chain, a is the optimal area of the head group, and l is the length of the hydrophobic tail.[57, 61-62] When $p \leq 1/3$ spherical micelles are obtained, when $1/3 \leq p \leq 1/2$ cylindrical micelles are obtained and when $1/2 \leq p \leq 1$ vesicles and polymersomes are obtained.[63] These morphologies can have an impact on the drug delivery system and reports show that rod-shaped nanoparticles exhibit higher cell uptake and drug delivery efficiencies than their spherical counterpart.[64] Morphology can be a determining factor in the success of a DDS and should be taken into account in the design of a successful DDS. For example, Cai et al. designed poly(ethylene oxide)-*b*-poly(ε-caprolactone) block copolymers for the encapsulation of paclitaxel.[65] Both worm-like filomicelles and spherical micelles were constructed with the same material and prepared under similar conditions. Their results show that the filomicelles had superior properties with twice the loading content of their spherical counterpart while displaying better safety and efficacy *in vitro*.[65]

1.1.1 Polymers in the design of nanoparticles

A vast array of polymers can self-assemble to form micelles in solution provided they possess amphiphilic character. However, only a small subset of these polymers is amenable for drug delivery applications due to the strict conditions set forth by the human body. For clinical applications, these polymers need to be biocompatible and ideally biodegradable with a low immunogenicity. The most common hydrophilic polymers that have populated the literature or have translated into the clinic include PEG,[66] poly(N-vinyl pyrrolidone) (PVP),[67-68] polyvinyl alcohol (PVA),[69] dextran,[69] and poly(N-isopropylacrylamide) (pNIPAAm) (Figure 1.2).[70]

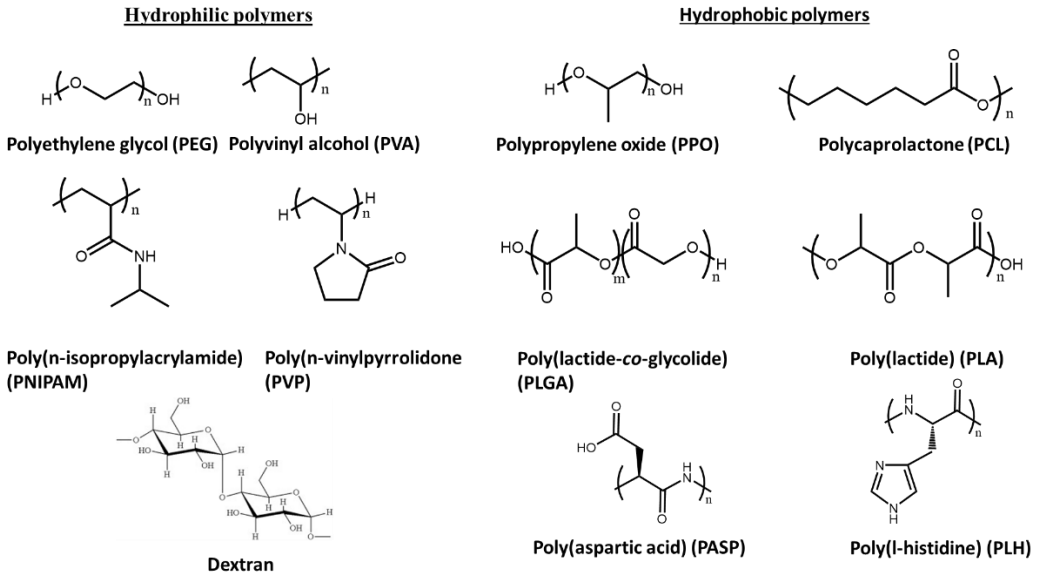

Figure 1.2 Chemical structures for hydrophilic and hydrophobic polymers commonly used in the design of polymer-based drug delivery systems.

PEG is an FDA-approved, biocompatible hydrophilic polymer that is flexible, uncharged and widely used in the pharmaceutical industry. PEG can shield its cargo through steric repulsion which reduces the immunogenicity, opsonization and degradation of the latter.[35, 71] Two to three water molecules are tethered per ethylene oxide units generating a hydrated state that diminishes aggregation and immunogenicity.[66] PEG-

based drug delivery systems has seen success at the clinical stage. Doxil, for example, was the first marketed nanomedicine.[23] A liposomal formulation of doxorubicin, Doxil was approved by the FDA for the treatment of AIDS-related Kaposi's sarcoma in 1995 and ovarian cancer in 1998.[72] Doxil is composed of a PEGylated disteroyl phosphatidyl ethanolamine (DSPE) lipid.[72] Part of its success can be attributed to the formulation stability and its increased circulation time compared to free doxorubicin which enables a sufficient enhanced-permeation and retention effect (EPR) and increased dose accumulation in tumor tissues compared to free doxorubicin.[73-75] PVP, a water-soluble and biocompatible polymer, has also been used in the design of drug delivery nanoparticles.[76-77] The group of Leroux has demonstrated the potential of poly(N-vinylpyrrolidone)-*b*-poly(D,L-lactide) (PVP-*b*-PLA) for the encapsulation and delivery of paclitaxel (PTX), a hydrophobic chemotherapeutic agent.[78-80] They successfully encapsulated PTX in stable PVP-*b*-PLA micelles and showed greater antitumor activity for their formulation over free drug. PVP-coated nanoparticles have been shown to possess higher circulation times compared to other hydrophilic polymers with minimal tissue distribution thereby enhancing the EPR effect.[69] Typically, micelles tend to accumulate in highly vascularized tissues such as the liver and spleen which diminishes their circulation time, decreases the delivery of the therapeutic agents and leads to higher toxicity. PVP-based micelles has been shown to reduce their uptake in liver and spleen.[81] Moreover, an increasing body of evidence indicate that, upon repeated injection, the plasma concentration of PEGylated micelles are dramatically reduced in a process known as accelerate blood clearance (ABC).[82-84] An advantage for PVP-based micelles is their ability to minimize this ABC phenomenon providing improved and reproducible pharmacokinetic and pharmacodynamic profiles.[82] For the hydrophobic block, the most studied polymers include poly(propylene oxide (PPO),[85] poly (ε-caprolactone) (PCL),[86-87] polylactide (PLA),[88] poly(lactide-co-glycolide) (PLGA),[89] poly(L-aspartic acid) (pAsp),[90-91] poly(L-histidine) (pHis),[92] and poly(β-amino esters) (PbAE) (Figure 1.2).[93] PLA is the most widely used hydrophobic polymer for biomedical applications. It is FDA-approved for clinical use and has been exploited in the design of a range of biomedical devices such as sutures,[94] scaffolds for tissue engineering,[95-97] bioabsorbable screws for bone fractures,[97-98] biodegradable meniscus repair,[99-100] bone regeneration,[101] and drug

delivery systems.[102-105] PLA has the advantage of being biocompatible, biodegradable via hydrolysis and enzymatic activity and has low immunogenicity thereby facilitating its clinical translatability.[106-107] Indeed, PLA-based drug delivery systems has reached the clinic with Genexol-PM. Genexol-PM is a PEG-*b*-PLA PTX-loaded drug delivery system approved in South Korea for the treatment of ovarian cancer.[108] These micelles are 20-50 nm in diameter and have a 3-fold increase in the maximum tolerated dose (MTD) of PTX and 2-3 fold higher drug accumulation in tumor tissues compared to Taxol, a 1:1 (v/v) Cremophor-EL and dehydrated alcohol formulation.[19, 109]

1.1.2 Influence of PEG length

The length of polymers constituting the block copolymers is an important aspect controlling the physico-chemical and biological properties of the corresponding nanoparticles. Micelle size, drug loading, and cell interactions are all parameters influenced by block length. Certain reports in the literature have described the influence of both hydrophobic and hydrophilic block on these parameters. PEG has been chosen as the hydrophilic block in the synthesis of star-shaped bile acid-based block copolymers discussed throughout this thesis, hence, particular attention will focus on the influence of PEG length in PEG-based block copolymers.

In one report, star-shaped block copolymers of poly(L-lactide)-*b*-poly(ethylene glycol) (PLLA-*b*-PEG) were prepared with varying PEG length to determine its impact on the physico-chemical properties of the nanoparticles.[110] Three PEGs of 2000, 4000 and 6000 g/mol were studied and the results show that micelles prepared with a longer PEG had a larger diameter than those prepared with a shorter PEG. This observation falls in line with other reports.[111-118] Poly(ethylene glycol)–distearoylphosphatidylethanolamine (PEG-DSPE) micelles with PEG chain length of 750, 2000 and 5000 g/mol and poly(ethylene glycol)-*b*-poly(propylene oxide)-*b*-poly(ethylene glycol) (PEG-b-PPO-b-PEG) triblock copolymer micelles with PEG chain length of 1144, 3344, and 4400 g/mol were prepared and their physico-chemical properties were compared.[116] The results show a clear trend of increasing hydrodynamic diameter with increasing PEG length.[116] Hydrophilic PEG extends into solution thereby shielding the surface of the nanoparticle and conferring colloidal stability, per discussion in Section 1.1. These PEG chains interact with water via hydrophilic interactions, such as hydrogen bonding and dipole-dipole

forces.[33, 119] With longer PEG chains, steric repulsion between individual chains forces the polymers into a more rigid and extended, brush-like conformation thereby increasing the hydrodynamic diameter of the micelle.[33, 119] A similar observation was noted for PEGylates bile acids. Different bile acids were grafted with PEG chains of varying lengths and their micelle sizes were compared.[120-121] It was observed that the bile acids with the longer PEG chains were characterized with larger micelle diameters. As will be discussed in Section 1.2, particle size has a strong influence on the circulation, tumor accumulation and cell uptake of nanoparticles, therefore the length of the block copolymers and their concomitant size are important parameters that need to be optimized to obtain a DDS with high efficacy.

In addition to micelle size, the critical micellar concentration (CMC) is strongly influenced by the length of the hydrophobic and hydrophilic blocks.[122] Numerous reports describe an increase in the CMC when the length of the hydrophilic block is increased.[123-124] It is noteworthy that the CMC also decreases when the hydrophobic block is increased and that variations in hydrophobic block length has greater impact on the CMC than variations of the hydrophilic block length.[122] The CMC is an important parameter controlling the in vivo stability of nanoparticles.[122] Copolymer systems with lower CMCs have a higher in vivo stability and are less prone to premature disassembly during transport to the target tissue.[122]

Interestingly, with regards to drug loading, the longer the hydrophilic block, the lower the drug loading.[113, 115-116] As mentioned previously, longer PEG chains increases the CMC. Yet, the increase in CMC decreases the number of micelles in solution by decreasing the number of polymers present as micelles.[122] Since there are fewer micelles, the degree of solubilization decreases because of a decreased hydrophobic volume. Therefore, there exists an inverse relationship between hydrophilic block length and drug loading where the longer the hydrophilic block, the lower the drug loading. Doxorubicin (DOX) loading was studied in linear block copolymers of acid- or urea-functionalized polycarbonate and PEG of either 5,000 or 10,000 g/mol.[118] It was demonstrated that, keeping the length and structure of hydrophobic block constant, there was an inverse relationship between PEG chain length and DOX loading. The decrease in DOX loading for longer PEG chains was attributed to the increased hydrophilicity which resulted in

increased CMC, fewer micelles and lower hydrophobic content.[118] The influence of hydrophilic block length on drug loading was also studied for bile acid-based star-shaped polymers.[120-121] Bile acid-based polymers are believed to assemble with the hydrophobic face of the bile acid constituting the core of the aggregate.[125] Numerous reports demonstrate that the bile acid molecules favor the formation of internal cavities due to the convex molecular structure of their steroid core.[125-127] Consequently, these bile acids tend to form small hollow-core micelles. The attachment of PEG on the hydrophilic surface of the bile acids is known to increase the repulsive forces of the system, constraining the micelle to decrease in size.[125] The group of Lam et al. have studied in details the influence of the PEG length on the formation of internal cavities of PEGylated cholic acid micelles.[125] The results of molecular dynamics simulation show that increasing the PEG chain length decreases the size of the internal cavity. Hence, lower PEG chains have a greater potential for high drug loading, and the authors demonstrated that PEG chains with 20 EG repeating units have the highest drug loading potential.[125] The impact of the PEG chain length on drug loading for bile acid-based polymers was demonstrated empirically for PEGylated cholic, deoxycholic and lithocholic acids with either 9 or 16 repeating units of EG for the encapsulation of itraconazole.[120] Irrespective of the bile acid, increasing the PEG chain length led to a decrease in itraconazole loading in the micelles.[120] Interestingly, the authors measured the solubilisation capacity of the bile acid-based polymer and determined it was a measure of the partitioning of the drug between two phases, i.e., either inside or outside the micellar aggregates. Their results show that the higher the PEG chains, the lower the solubilisation capacity and, hence, the lower the drug loading.[120]

1.1.3 Drug loading

Upon self-assembly, hydrophobic therapeutic compounds can reside within the core of these micelles, whereas hydrophilic APIs will remain adsorb to the surface of the micelle. The micelles can increase the aqueous solubility of hydrophobic APIs while protecting it during transport to its site of action. Typically, micelles are larger than the renal clearance threshold of 5.5 nm for nanoparticles and can prolong the circulation time of its therapeutic cargo and improve its pharmacokinetics.[128] Loading of the drug inside the micellar core is a function of the miscibility between the polymer core and the drug

which is governed by polymer-drug interactions.[107] Hydrophobic interactions,[129] hydrogen bonding,[130] electrostatic,[131-132] host-guest,[133-135] stereocomplex,[136] and coordination interactions[137-138] between the drug and the polymer core are known to be crucial in determining the extent of drug loading and the stability of the polymeric micelle.[139-140] These interactions are necessary in providing a stable drug loaded formulation. As previously mentioned, polymers associate to form micelles, however these micelles are in a dynamic equilibrium with the bulk phase, and polymers constantly shuttle among micelles and between the micelles and the bulk phase.[141-142] A strong interaction between the polymer core and the drug ensures a stable loading and diminishes the extent of premature release during transport of the cargo to the desired tissue. Drug loading inside nanoparticles is reported with respect to two important parameters: drug loading content (DLC) (equation 2) which is the weight ratio of drug to polymer, and as drug loading efficiency (DLE) (equation 3) which is the ratio of loaded drug to the amount of drug in the feed.[138] The DLC content is a function of the polymer structure and the physico-chemical properties of the carrier and drug, whereas the DLE is influenced by the loading mechanism and conditions, as well as the amount of drug in the feed.[138]

$$DLC\ (wt\ \%) = \frac{mass\ of\ drug\ in\ micelle}{mass\ of\ polymer} \times 100\% \qquad (2)$$

$$DLE\ (wt\ \%) = \frac{mass\ of\ drug\ in\ micelle}{mass\ of\ drug\ in\ feed} \times 100\% \qquad (3)$$

High DLCs are important to achieve a successful drug delivery system and has been the Achilles heel of polymer-based nanoparticles. With low DLCs, administering a sufficient dose at the target site requires a large amount of the carrier material which can cause systemic toxicity and unwanted side effects. This is also observed with biocompatible and biodegradable polymers;[138] the old adage persists, “the dose makes the poison”. Various strategies have been designed to increase the loading of the therapeutic cargo. For example, in the case of hydrophobic interactions, inclusion of hydrophobic moieties with high hydrophobic indexes in the backbone of the polymer or as pendant groups were a fruitful strategy.[138] Compounds such as cholesterol,[129, 143-144] bile acids,[121, 145-147] all-*trans* retinoic acid,[148] and α-tocopherol (vitamin E)[149] have been employed in the design of DDS affording high DLC. For example, LeDevedec et al. prepared self-

emulsifying drug delivery systems composed of PEGylated bile acids and oleic acid for the encapsulation of itraconazole.[121] A high loading efficiency of 20 wt% were obtained with stable formulations. Similarly, hyaluronic acid was conjugated to deoxycholic acid generating amphiphilic molecules were the hyaluronic acid served as hydrophilic moieties and the steroid ring of deoxycholic acid imparted hydrophobicity.[147] These conjugates formed nano-sized micelles in an aqueous environment and loaded paclitaxel with 34.1% DLC and 93.2% DLE. Zhang et al. recently developed a novel triblock copolymer of poly(β-aminoesters-*g*-cholesterol)-*b*-PEG-*b*- poly(β-aminoesters-*g*-cholesterol).[144] Their system was used for the encapsulation of doxorubicin and achieved a DLC of 20% with a DLE of 60%. In this thesis, cholic acid is used as a core forming block to demonstrate its potential towards increasing the DLC for polymer-based nanoparticles.

1.1.4 Drug release

Once the nanoparticle has reached its target, the loaded drug needs to be released from within the nanoparticle to elicit its therapeutic response. In terms of drug release, the mechanism is largely dependent on the type of nanoparticle formed and the method of drug loading. Drug release from within polymeric micelles occur mostly by diffusion and the rate of diffusion is a function of the drug partition coefficient, amount of drug loaded, and the length of the core forming block.[150] Also, the physical state of the core forming block plays an important role in the drug release where cores composed of glassy polymers are characterized by slower release than those formed from viscous polymers.[150]

For polymeric nanoparticles, the drug release mechanism is more complex. Drug release from within the core of polymeric nanoparticles is governed by four mechanisms, namely (1) diffusion through water-filled pores, (2) diffusion through the polymer matrix, (3) osmotic pumping and (4) erosion (Figure 1.3).[151-152] For the diffusion through water-filled pores, drug molecules escape the core of the nanoparticle by diffusion along a network of pores through a random process driven by the chemical potential difference generated between the drug-filled reservoir and the outer milieu.[151] This process is typically observed for biodegradable polymers where a pore network is generated through the degradation of the polymer and evolves over time as a function of the degradation rate generating larger pores for the diffusion process to occur.[153] For nondegradable polymers, drugs are mostly released *via* diffusion through the polymer matrix, a process that is

constant and unaffected by concentration gradients.[151] In osmotic pumping, the DDS contains an osmogen which drives the absorption of water within the core of the DDS.[154] As water penetrates the core, it swells and pushes the drug into solution in a process that is independent of both pH and hydrodynamics of the dissolution environment.[154] In terms of erosion, there are two types, surface erosion and bulk erosion.[151, 155] In surface erosion, the polymers at the surface of the DDS are eroded and the NP diminishes in size until all is consumed, going from the exterior to the interior.[155] This process is mostly observed when the rate of diffusion for penetration of water inside the core is lesser than the rate of erosion. In bulk erosion, water penetrates the core of the nanoparticle and the polymer matrix is uniformly degraded; here, the rate of diffusion of water inside the core dominates the rate of erosion.[155] An ideal DDS would follow a zero-order release profile which would provide a constant plasma drug concentration within the minimum effective concentration (MEC) and the maximum toxic concentration (MTC) as depicted in Figure 1.4.[151]

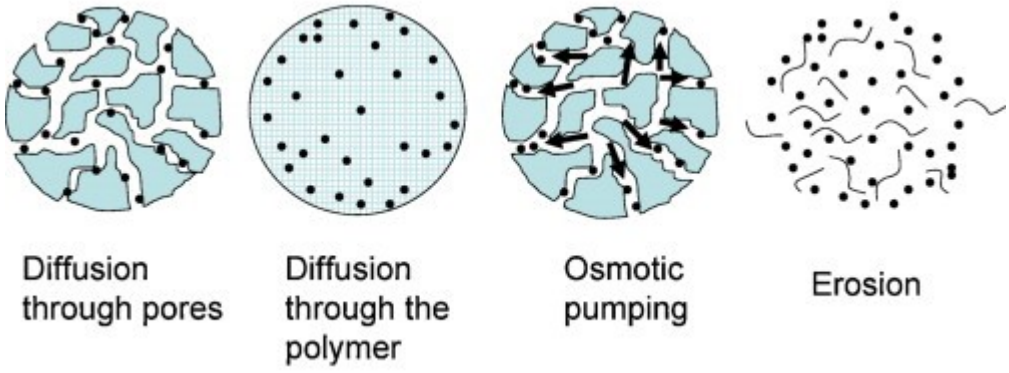

Figure 1.3 The different mechanisms that govern the drug release from polymeric nanoparticle cores.[151] (Reproduced with permission from © 2016 American Chemical Society)

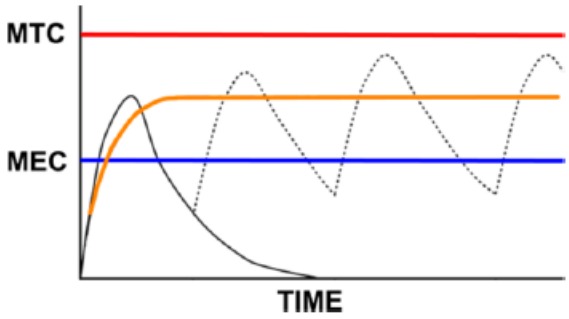

Figure 1.4 Ideal drug plasma concentration (orange line) should remain between the maximum toxic concentration (MTC) and minimum effective concentration (MEC). A rapidly absorbed and eliminated drug (black line) require frequent dosing (dashed line) in order to remain within this therapeutic window.[151] (Reproduced with permission from © 2016 American Chemical Society)

Unfortunately, this release profile has yet to be achieved using polymeric carriers. Instead, biphasic and triphasic profiles are most often encountered (Figure 1.5).[152] For these profiles, the first phase is referred to as the burst release and results from the release of drug molecules that are either adsorbed to the surface of the nanoparticle or encapsulated at the interface of the hydrophobic and hydrophilic layers.[151-152] The second phase consist of a slow release of the drug through the polymer matrix or through pores and occurs *via* the aforementioned *diffusion through water-filled pores* and *diffusion through the polymer matrix* mechanisms.[151-152] The second phase depends on the physico-chemical properties of the polymer matrix where densely packed polymer cores lead to a slower second phase.[151] The third phase, is observed with biodegradable polymers and is a function of the erosion process. The burst release effect is an undesirable trait of the DDS. It is unpredictable, uncontrollable and can lead to unwanted toxicity arising from an initial high dose.[156] Certain strategies have been designed to circumvent this limitation; for example, the use of high molecular weight polymers have been shown to reduce this effect.[156] Decreasing the hydrophilicity of the corona has been linked to a reduction in the hydration of the nanoparticle and minimizes the solubilization of drugs on the outer layer, hence decreasing the burst effect.[156]

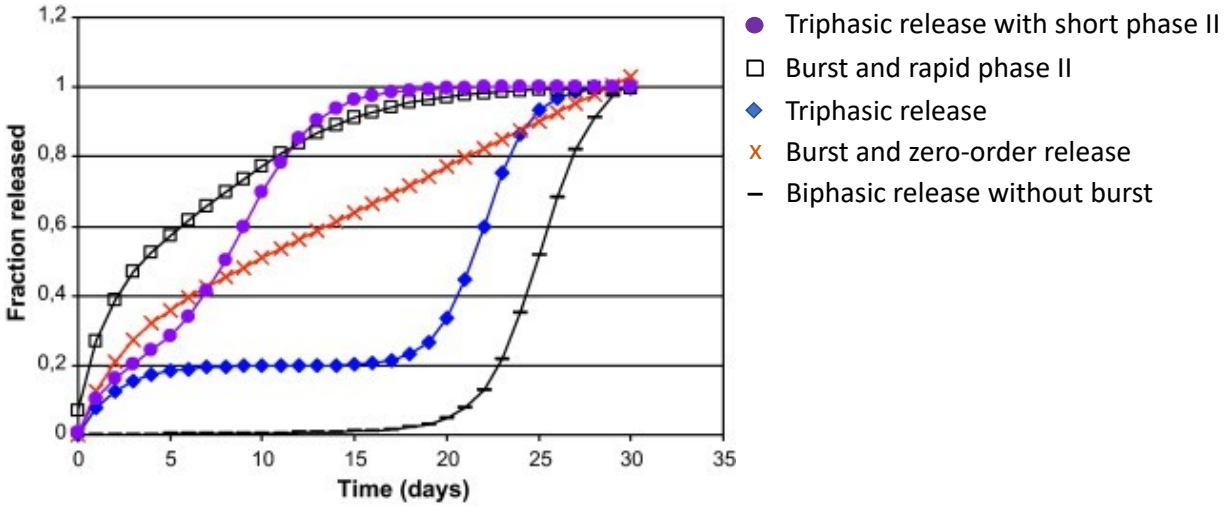

Figure 1.5 Typical release profiles observed in polymer-based DDS.[152] Open squares represent a biphasic release with a burst release and rapid phase II. Filled circles represent a triphasic release with a short phase II. Crosses represent a combination of a burst and zero-order release profile. Dashes represent a biphasic release profile in the absence of a burst release. Diamonds represent a triphasic release. (Reproduced with permission from © 2016 American Chemical Society)

1.1.5 Stimuli-responsive drug delivery systems

A recent advancement in the release mechanisms has been obtained with stimuli-responsive drug release. In essence, the carrier holds the drug within its core in a controlled fashion reducing premature drug release and its associated toxicity while releasing the cargo in response to a stimulus. This stimulus can be endogenous, e.g. change in pH, reactive oxygen species or elevated enzymatic activity, or exogenous, e.g. heat, light, electrical or ultrasound induction.[157] Stimuli-responsive drug release permitted a minimization of systemic toxicities, better dosing of the drug and a decrease in unfavourable interactions of drug with plasma proteins.[151] Examples of DDS employing the stimuli-responsive strategy have dominated the literature in the recent years and three stimuli-responsive strategies employing endogenous stimuli are presented here in details.

Redox-responsive delivery systems employ the gradient of reducing agents that exists within cells. Glutathione (GSH), a tripeptide of glutamate-cysteine-glycine, is an endogenous reducing agent with an intracellular concentration of 2-10 mM and an extracellular concentration of 2-20 μM.[158] GSH is also overexpressed in numerous cancer

cell lines with intracellular concentrations much higher than those in healthy cells generating a gradient that is about four times higher than typically observed in healthy cells.[159] This reducing gradient across the cell membrane has been utilized as a method for promoting drug release inside tumor cells. Disulfide and diselenide bonds are targets for GSH and reduce to thiols and selenols, respectively.[160] Adding disulfide or diselenide bonds in the architecture of the polymer promotes higher drug release in response to a reducing environment. The group of Zhong et al. developed so called shell-sheddable micelles with a PEG block linked to a PCL block through a disulfide bond (PEG-SS-PCL) (Figure 1.6).[161] In the presence of 10 mM DTT, mimicking the reducing environment inside the cell, the disulfide bond is cleaved, and the PEG shell is released exposing the core of the micelle and causing drug release. Loaded with DOX, these micelles exhibited close to 100% drug release within 12 h when exposed to DTT and < 20% DOX release in the absence of DTT.

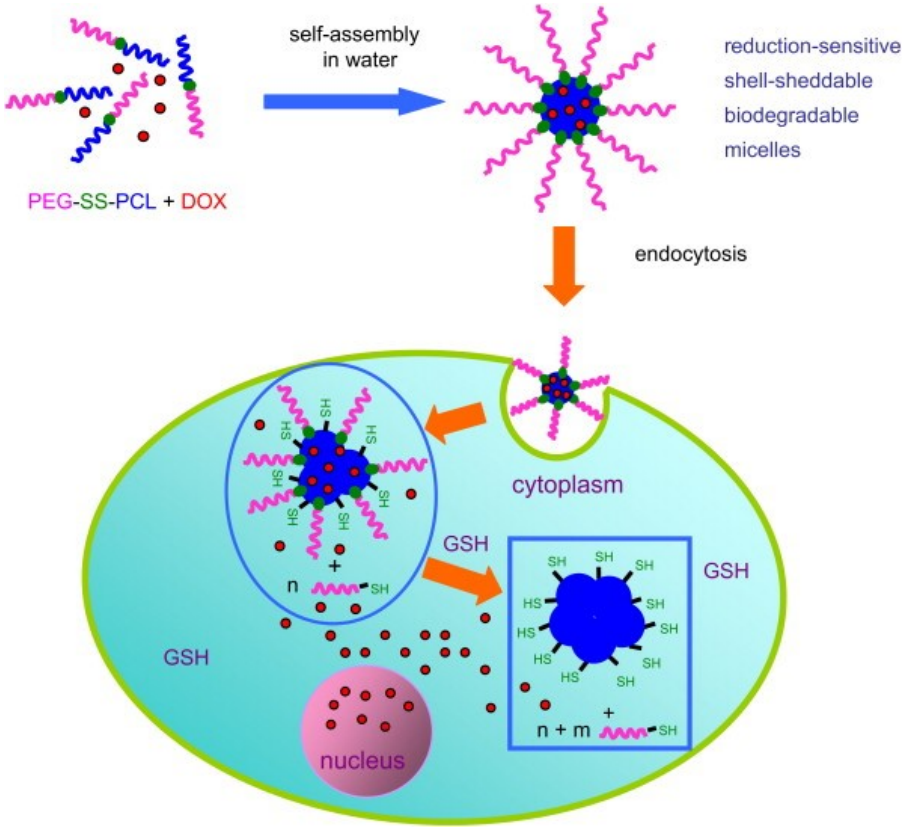

Figure 1.6 Reduction-sensitive sheddable PEG-*b*-PCL block copolymers. In a reducing environment, the disulfide bonds are reduced releasing the encapsulated cargo.[161] (Reproduced with permission from © 2009 Elsevier)

Oxidation is another stimulus that can be used for triggered drug release. Reactive oxygen species (ROS) are present in healthy cells and their levels are maintained through homeostasis.[151] However, certain pathological conditions can cause these levels to rise, e.g. cancer, inflammatory diseases, diabetes and infections.[151] Designing polymers that degrade in response to elevated ROS can be utilized to deliver drugs specifically to these diseased tissues.[151] Thioketals[162] and arylboronic esters[163-164] respond to ROS species by cleavage of the functional group or through a switch in solubility of the polymer, respectively. For example, a monomer containing an arylboronic ester was polymerized to afford a ROS-responsive system (Figure 1.7).[164] In the presence of ROS, the boronic ester is cleaved causing a degradation of the polymer backbone and drug release. Using Nile Red and fluorescein diacetate as surrogates for drug loading, ROS triggered a 50% Nile Red release from this system after 26 hours.

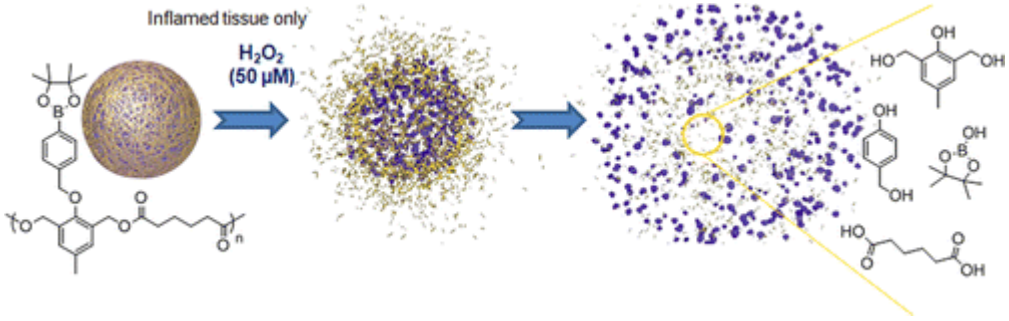

Figure 1.7 ROS-responsive polymeric nanoparticle. In the presence of hydrogen peroxide, the arylboronic esters are cleaved thereby causing the nanoparticles to burst and release the encapsulated cargo.[164] (Reproduced with permission from © 2012 American Chemical Society)

pH-responsive DDS are the most encountered systems in the literature, especially for systems pertaining to cancer therapy. In a process known as the Warburg effect, cancer cells rewire their metabolism towards increased glucose uptake and its fermentation into lactate.[165] As a result of the lactic acid build up, tumor microenvironments have been linked with a significantly lower pH than healthy tissue environment.[165] In addition, the pH of endosomes and lysosomes, the compartments micelles encounter once internalized inside the cell, are acidic with a measured pH of 5-6 and 4-5, respectively.[166] Designing polymers with acid-labile groups in the polymer architecture enables a triggered drug

release in response to lowering of the pH. Various methods have been employed to design pH-responsive DDS.[167] In one method, the pH-responsive polymers respond to a change in pH with a change in solubility thereby causing micelle instability and drug release.[167] For example, a block copolymer of poly(L-histidine)-*co*-(L-phenylalanine)-*b*-PEG was synthesized and characterized for pH-responsive drug delivery.[168] This block copolymer forms a micelle when the pH is higher than the pK_a of histidine (6.5) due to its hydrophobic character. However, in a lower pH, the histidine is protonated and becomes hydrophilic causing the micelles to disintegrate and release their content. Another method to induce pH-responsiveness is to design the polymer backbone to include acid-labile groups such as acetals, ketals, orthoesters, hydrazone, oxime, and boronic esters.[167] In the presence of a lowered pH, these bonds are cleaved. Appropriately placed within the polymer backbone, the cleavage of these acid-labile bonds can cause the release of loaded drugs. Recently, a three-armed star-shaped block copolymer composed of PEG and PCL was synthesized (Figure 1.8).[169] The PEG and PCL blocks were linked with a pH-responsive acetal group and the micelles were loaded with DOX. The results show that at physiological pH (7.4), the micelles released 40% DOX after 28 hr whereas, at a pH of 6 the micelles released 60% of DOX and at a pH of 5 the micelles release 80% of DOX. The DOX release was ascribed to the cleavage of the acetal group and the disruption of the micelle integrity. These are examples of different strategies that have been used in the design of stimuli-responsive DDS responding to endogenous stimuli. There also exists many examples for the design of DDS responding to exogenous stimuli, however it is beyond the scope of this thesis and has been thoroughly reviewed.[151, 157, 159]

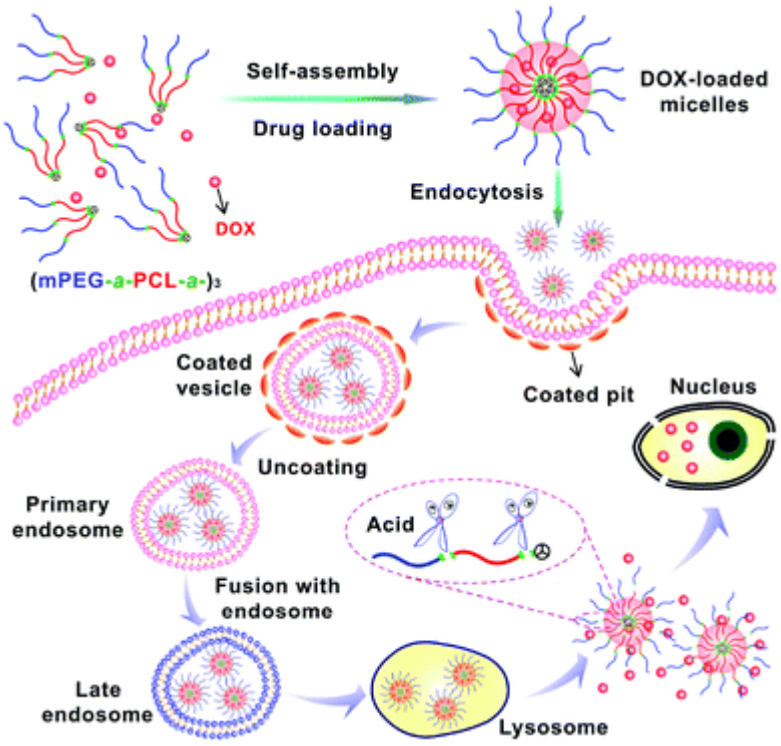

Figure 1.8 Acid-labile PEG-*b*-PCL block copolymers for Dox release. The acid-labile acetal groups are positioned between the PEG and PCL blocks such that when the pH is reduced the acetal groups are cleaved and the blocks disassemble causing micellar instability and drug release.[169] (Reproduced with permission from © 2015 Royal Society of Chemistry)

1.1.6 Lower critical solution temperature and thermoresponsive polymers

Block copolymers that respond to temperature variations are an important class of materials gaining attention in the field of drug delivery. Polymers that possess a lower critical solution temperature (LCST) respond to variations in temperature by undergoing a sol-gel transition at a critical temperature.[170-171] This thermally controlled transition can be understood by the Gibbs free energy of mixing for the polymer solution.[170] Below a certain temperature called the LCST, the enthalpy of mixing is negative due to the formation of hydrogen bonds between the hydrophilic block and surrounding water molecules.[172] There is also an ordering of water molecules surrounding the hydrophobic block that generates a negative entropic cost, but the Gibbs free energy of mixing remains negative.[172] However, above the LCST, the enthalpic contribution of hydrogen bonding

between water and polymer chains is less than the entropic gain from the release of ordered water molecules surrounding the polymer.[172] This leads to a positive Gibbs free energy of mixing and the collapse of the polymers and loss of solubility. The polymers possessing a LCST are versatile in the design of drug delivery systems. Examples include injectable hydrogels,[173-174] nanogels,[175-176] core-shell nanodevices,[177] and thermo-sensitive liposomes.[178] The most appealing strategy behind the use of a LCST polymer is for thermo-responsive hydrophilic polymers with a LCST close to physiological temperature. In this case, the thermo-responsive hydrophilic corona allows the formation of core-shell micelles below its transition temperature. When the LCST is reached, the corona collapses over the hydrophobic core leading to the formation of large aggregates. These large aggregates serve as drug depots slowly releasing its loaded drug over the time course of the treatment. Here the advantage is to design a polymer system with a LCST that is slightly higher than physiological temperature and utilize the natural temperature gradient that exists amongst different tissues or through the application of heat.

A great deal of polymers with thermo-responsive properties have been studied and poly(*N*-isopropylacrylamide) (PNIPAM) is the most prominent example. PNIPAM has been extensively studied in the design of smart biomaterials since its LCST is in the range of 30-35 °C which is very close to that of human physiological temperature.[179] PEG polymers also have a LCST, with the LCST spanning a large temperature range depending on its molecular weight, where the LCST decreases with increasing PEG molecular weight.[179-180] Various strategies have been developed to tune the LCST temperature of a polymer to fit a desired application. For example, PNIPAM polymers can be functionalized at their isopropyl group with either carboxyl, amide, or hydroxyl groups to modify the LCST to a desired temperature.[179, 181-183] Similarly, PEG polymers have been copolymerized with various hydrophobic blocks such as PLA and poly(N-acryloyl-2,2-dimethyl-1,3-oxazolidine) (PADMO) to obtain a tunable LCST between 20 to 85 °C.[184-185] Copolymerization with water soluble polymers increases the energy required to break a hydrogen bond during heating and thereby increases the LCST.[179] On the other hand, copolymerization with hydrophobic monomers decreases the LCST.[179] As an example, the PEG chain length was varied in a triblock copolymer of PNIPAM-*b*-PEG-*b*-PNIPAM and the LCST measured as a function of PEG chain length.[186] PNIPAM-*b*-PEG-*b*-

PNIPAM triblock copolymers with PEG chains of 23, 34, or 77 repeating units had LCSTs of 35, 37, and 38 °C, respectively. The triblock copolymer with PEGs of 165 repeating units did not show a LCST at the measured temperatures indicating a much higher LCST, hence copolymerization of PNIPAM with hydrophilic PEG increased the LCST with increasing PEG chain length.[186]

There are a variety of ways in which the LCST of a polymer can be controlled and tuned for the desired application other than copolymerization. These factors include pH,[187-188] salt concentration,[189-191] surfactants,[192-193] and co-solvents,[194] and these affect the polymer-solvent interactions thereby tuning the LCST. Salt has been previously studied for its effect on the LCST.[195-196] Indeed, salts are known to cause a salting-out effect and the Hofmeister series was identified and developed to classify these salts. This series classifies these salts as either strongly hydrated, kosmotropes, or weakly hydrated, chaotropes.[197] Kosmotropes decrease the LCST through a polarization of the interfacial water molecules involved in hydrating the hydrophilic groups of the polymer.[198] In this situation, the salt essentially breaks the hydrogen bonding of the hydrophilic groups and water. Chaotropes decreases the LCST through increase in surface tension between the hydrophobic/water interface and this effect increases with increasing salt concentration.[197] Understanding the LCST behavior of drug delivery systems in salt solutions is of crucial importance due to the high salt concentrations typically found at physiological conditions. These high salt concentrations can be deleterious to the desired application. For example, studying the effect of salt concentration on the transfection potential of poly(ethylene imine) (PEI) complexed to plasmid deoxyribonucleic acid (pDNA), physiological concentrations of NaCl were shown to severely decrease the transfection potential of the polyplexe.[199] This decrease in the transfection potential was ascribed to a salting-out of the polyplex due to a decrease in the LCST.[199]

1.2 Barriers to drug delivery

1.2.1 Micelle stability

From the site of injection to the targeted tumor cells, the drug delivery system encounters a great deal of barriers that can potentially mitigate its effectiveness. A successful delivery system will need to overcome each of these barriers while maintaining

its integrity and stability to avoid unwanted side effects and ensure a therapeutic dose of the compound is delivered. Therefore, a thorough understanding of these barriers is warranted for the design of a successful DDS and is reviewed here in details to justify our proposed bile acid-based nanoparticles for their use as DDS.

Upon injection, the drug-loaded nanoparticles encounter a large volume of dilution which can impact the stability of the nanoparticles. There are two concepts that describe the stability of the micelles: thermodynamic stability and kinetic stability. Thermodynamic stability is intricately linked to the critical micellar concentration (CMC) and describes the formation of the micelles and the position of the equilibrium, whereas kinetic stability characterizes the behavior of the micelle over time including the dissociation of the micelle and the exchange of individual polymer chains amongst micelles.[33] Equation 4 shows the Gibbs free energy of micellization as a function of the CMC concentration where the lower the CMC the lower the Gibbs free energy and the more readily the polymer will form a micelle.[33]

$$\Delta G°mic = RT \ln (CMC) \quad (4)$$

where $\Delta G°mic$ is the change in Gibbs free energy of micellization, R is the universal gas constant, T is the absolute temperature, and CMC is the critical micellar concentration.

Thermodynamic stability implies that a polymer will remain in micellar form if its concentration is above the CMC. Factors that affect the value of the CMC include: the nature and length of the core-forming block and the length of the hydrophilic block.[33] Looking at the impact of the hydrophobic block length, numerous reports show that the longer the hydrophobic block, the lower the CMC value.[33] Jette et al. demonstrated with a block copolymer of poly(ethylene glycol) (PEG) and poly(ε-caprolactone) (PCL) that varying the ratio of PCL/PEG from 0.2 to 0.8 induced a change in the CMC from 2.7 to 0.2 μmol/L, i.e. the higher the hydrophobicity, the lower the CMC.[200] Similarly, Adams et al. showed that the longer the acyl chain length in a block copolymer of poly(ethylene oxide)-*b*-poly(N-hexyl-L-Aspartamide) the lower the CMC.[201] Also, the length of the hydrophilic block has an inverse relationship with the CMC value.[123-124, 202-203] Kabanov et al. varied the length of PEO blocks in a triblock copolymer of PEO-*b*-PPO-*b*-PEO and found that longer PEO chains promoted contact between the PEO and PPO blocks thereby decreasing the overall hydrophobicity of the micellar core and resulted in destabilization

of the micelles and an increase in the CMC values.[204] Finally, the higher the hydrophobicity of the core forming block, the lower the CMC value. In a model block copolymer of PEG-*b*-poly(alkyl methacrylate), a positive relationship was found between the CMC value and the degree of hydrophobicity in the alkyl methacrylate blocks.[205]

In terms of kinetic stability, the rate of disassembly depends on the physical state of the micellar core. Polymers with a semi-crystalline core, such as polycaprolactone (PCL) and polyvalerolactone (PVL) typically have a higher kinetic stability than polymers with an amorphous core, such as poly(D,L)lactide (PDLLA).[206] Indeed, stereocomplex formation between poly(N,N-dimethylaminoethyl methacrylate)-*b*-poly(d-lactic acid)-*b*-poly(N,N-dimethylaminoethyl methacrylate) showed higher kinetic stability when 1:1 D/L mixtures were prepared than when the isotactic or racemic mixtures were prepared.[207] Another factor influencing kinetic stability is polymer exchange between micelles where the higher the exchange rate the lower the stability.[33] In a model block copolymer of poly((dimethylamino)alkyl methacrylate)-sodium methacrylate, Creuz et al. discovered a decrease in the rate of unimer exchange between micelles when there was an increase in the hydrophobic/hydrophilic balance.[208] There is strong evidence that the presence of an encapsulated hydrophobic drug or molecule can increase the kinetic stability of a micelle upon dilution. The group of Kataoka et al. showed that the presence of adriamycin (ADR) in the core of a PEG-*b*-poly(aspartic acid) increased stability of the micelle and the higher the concentration of ADR the greater the stability.[209]

1.2.2 Blood circulation

Upon injection, the nanoparticles navigate throughout the blood circulation before reaching its target tissue (Figure 1.9). The next hurdle in a nanoparticle's path is the adsorption of serum proteins. Protein adsorption plays an important role in determining the fate of the DDS and tissue distribution.[210] In a process called opsonisation, specific serum proteins adsorb on the surface of pathogens triggering their uptake by cells of the reticular endothelial system (RES); namely, monocytes, macrophages, and dendritic cells. Although an effective immune response for invading pathogens, the RES can sequester NPs to the liver and spleen decreasing effectiveness and causing unwanted noxious effects.[210] The adsorption of proteins on the surface of NP was found to be a complex process that is unique to each nanomaterial and NP.[210-211] Also, the presence of these

proteins provides a biological identity to the NP and have profound influence on its stability and fate. Indeed, increased complement protein C3 and immunoglobulin G (IgG) adsorbed on NPs was directly linked to increased uptake by Kupffer cells of the liver.[212]

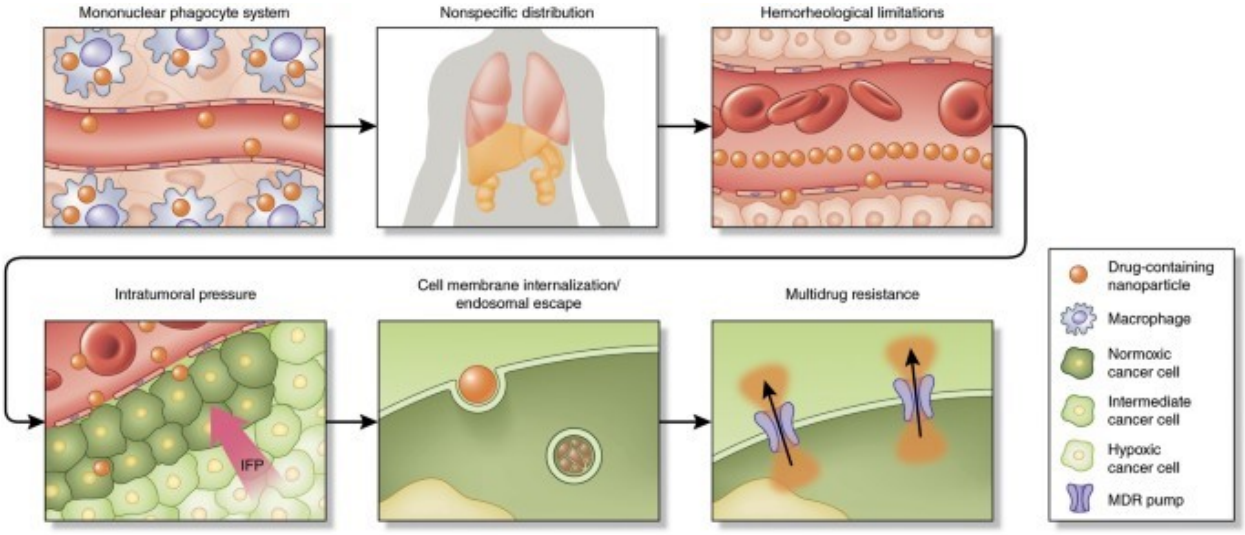

Figure 1.9 Different physiological barriers preventing drug delivery to the target tissue.[213] (Reproduced with permission from © 2015 Springer Nature)

To date no hydrophilic block has been able to completely prevent protein adsorption on the surface of nanoparticles; rather the hydrophilic corona modifies the type and decreases the extent of protein adsorption. There has been a great deal of research dedicated towards understanding this phenomenon and the impact of hydrophilic block length, type, and density. The most studied systems employ PEG as the hydrophilic corona. Factors that affect the nature and formation of the protein corona on the surface of the NP include the NP size, shape, charge and functional groups.[211] Extensive research was conducted by the group of Chan et al. on the phenomenon of protein adsorption.[214-217] They found over 70 different serum proteins adsorbed to varying extent on the surface of PEG-functionalized gold NP and the type and variations of protein adsorption was linked to the mechanism and efficiency of NP uptake by macrophage cells.[214] There exists a negative correlation between PEG grafting density and protein adsorption where the higher the density the lower the adsorption.[215] Also, the higher the density the lower the macrophage uptake with densities of 0.5 PEG/nm^2 giving the optimal results; densities higher than 0.5 PEG/nm^2 led to lower adsorption but not lower uptake from RES cells.[215]

Moreover, hydrophobic and charged surfaces have a greater tendency to adsorb and denature proteins than hydrophilic and neutral surfaces[218]. However, there exists a certain threshold for PEG density beyond which PEG becomes too sterically constrained and act as a surface on which proteins can adsorb.[215] Also, curvature of the nanoparticle has a large influence on the adsorption where smaller NP led to higher curvature allowing the PEG chains to adopt more extended chain configurations which ultimately decreases the thermodynamic barrier for protein adsorption and leads to higher adsorption.[217] Moreover, reports indicate that the optimal PEG chain length is between 2 kDa and 5 kDa,[219-221] although the exact value is heavily debated with reports showing 5 kDa as the optimal PEG chain length[219] while others citing 2 kDa as the optimal value.[222-223] As mentioned earlier, the phenomenon of protein adsorption has a huge impact on the residence time of NP due to the RES uptake, but it also imparts lower NP stability. It was reported that the adsorption of proteins leads to the destabilization of the NP and a premature release of the cargo.[224] Therefore, a suitable method to minimize and control this protein adsorption is necessary to achieve a successful DDS. One such method is the pre-coating of NPs with proteins or an *ad-hoc* design of the block copolymers to promote the adsorption of a specific type of protein.[225] For example, tween 80 (polysorbate-80) is known to promote the adsorption of members of the apolipoprotein family with ApoE being the most influential.[226] NPs were designed to bear this tween 80 shell for targeting through the blood brain barrier (BBB) since low-density lipoprotein (LDL) receptors on the BBB can promote the crossing of ApoE-bound NPs.[226-228] In another strategy, adsorption of proteins before administration was attempted for selected targeting.[229] These findings indicate that protein adsorption on the NP surface plays an important role in the NP fate and stability and establishes its biological identity. Although not necessarily the most efficient but surely the most studied, PEG is a useful hydrophilic block for decreasing the extent of protein adsorption.

1.2.3 Tissue accumulation and penetration

Following blood circulation, the next step for a NP is accumulation at the tumor site. Coined the enhanced permeation and retention effect (EPR), this mechanism is responsible for the accumulation of drug-loaded NPs to the site of action (Figure 1.10).[230-231]

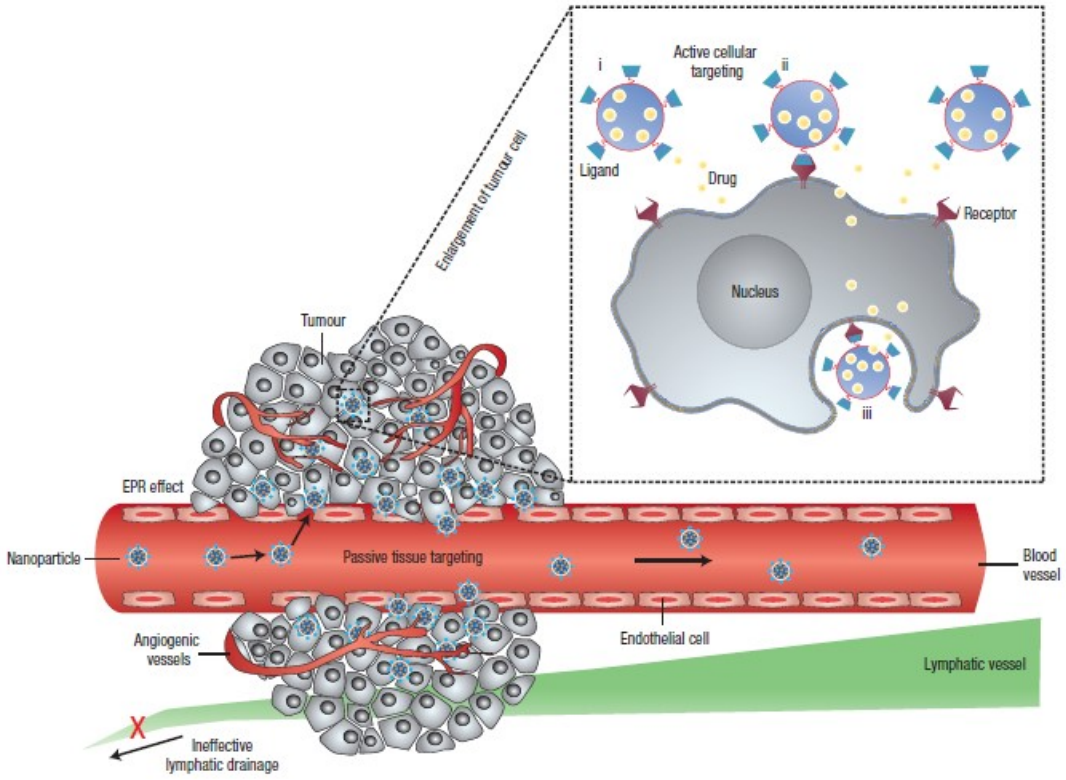

Figure 1.10 Enhanced permeation and retention (EPR) effect accounting for increased nanoparticle uptake in tumor tissues compared to healthy tissues.[231] (Reproduced with permission from © 2007 Springer Nature Ltd.)

Blood vessels are responsible for the transport of nutrients, oxygen, and molecules for maintenance of homeostasis and normal tissue function. The endothelial cells composing these blood vessels are divided into three categories, namely continuous, discontinuous, and fenestrated; each of which are characterized by their own morphology and properties.[212] Continuous endothelium typically compose the blood vessels, arteries, and pulmonary arterioles.[212] Fenestrated endothelial cells are present in tissues with elevated trans-endothelial transport or roles with increased filtration like glands, kidney and villi of the intestine.[212] They are more permeable than the continuous one and are composed of perforations of 50-60 nm that are sealed with a 5-6 nm thick diaphragm.[232] Discontinuous endothelia are characterized with the loss of a structured basal membrane and fenestrations of 100-200 nm.[232] These are mostly found in the liver, spleen and bone marrow.[233] Angiogenesis is the formation of new blood vessels and is a key player in the

spreading and maintenance of tumor tissues.[234] Angiogenesis in tumor growth is an imperfect process due to the aggressive growth of neoplastic cells and their overexpression of pro-angiogenic factors.[234] As a result, tumor vasculature is typically immature with the loss of arterioles, capillaries, and venules, archetypes of proper neovascularisation.[235] The resulting hyperpermeable, disorganized, and tortuous vasculature has abnormal structural dynamics and is composed of gaps with diameters between 100 nm and 2 μm depending on the tumor tissue.[236] Tumor vasculature is also coupled with poor lymphatic drainage due to dilated, leaky, and discontinuous blood vessels.[237-238] As a result, there is a leakiness associated with these blood vessels which allows diffusion of the nanoparticles out of the blood circulation and into tumor microenvironments. Unfortunately, this leakiness also results in elevated interstitial fluid pressure and aberrant osmotic forces which acts as a barrier to the extravasation of the nanoparticles (Figure 1.9).[235] This is what the literature has coined the EPR effect. Increasing the circulation time of NPs through the minimization of protein adsorption enables the NPs a greater likelihood of escaping the blood circulation and entering the tumor tissue through the EPR effect.[230] Particles larger than 40 kDa (renal clearance threshold) showed slower clearance, higher AUC (area under the concentration-time curve) and greater accumulation in tumor tissues.[239] Hence, in designing a successful DDS there is an ideal size range where the nanoparticles are larger than the 40 kDa (5.5 nm) renal clearance threshold yet smaller than the 200 nm limit imposed by the RES system. For PEGylated nanoparticles, this renal threshold was found to be 20 kDa. This EPR effect is what enabled Doxil, the liposomal formulation of Doxorubicin (Dox), to improve the delivery of free Dox to tumor tissues thereby increasing its effectiveness and decreasing its toxicity.[240] Unfortunately, it also increases the possibility to escape the blood vessel through the discontinuous endothelia of liver and spleen and accumulate in these organs causing unwanted side effects. Indeed, NPs that are smaller than 200 nm (the size of the liver fenestrae) can extravasate and accumulate in the space of Disse interacting directly with hepatocytes.[241]

A novel strategy to increase the EPR effect is through the addition of mediators of the EPR effect during drug delivery.[236] The EPR effect is mediated by a range of factors such as Bradykinin, vascular epidermal growth factor, cyclooxygenase and prostaglandin,

nitric oxide, etc.[236] It is hypothesized that by increasing the EPR effect, drug delivery can be improved. For example, when angiotensin-II (AT-II) is infused, normal blood vessels are constricted due to hypertension, but not tumor blood vessels due to their lack of smooth muscle cells. Li et al. tested this hypothesis using rats with Walker carcinoma.[242] AT-II increased the blood pressure in rats from 65-95 mmHg to 150 mmHg. Their results show that poly(styrene-co-maleic acid) conjugated with neocarzinostatin administered to these rats had 1.2 to 1.8 fold increased accumulation in the tumor tissues as compared to normal tissues after only 1 hr. This higher DDS accumulation persisted for up to 6 hr after administration. They also observed a 60-80% decrease of DDS in bone marrow and small intestine compared to rats under a normotensive state. With respect to tumor vascularisation, there is the emerging practice of blood vessel normalization to improve drug delivery to tumor site.[243] The elevated interstitial fluid pressure acts as a barrier to nanoparticle extravasation and this elevated pressure is a result of the poorly constructed blood vessels.[243-244] Therefore, normalization of the blood vessels has the potential to reduce the vascular density, increase perfusion, and limit hypoxia all of which can increase drug delivery and improve anti-tumor efficacy.[244] During normalization, there is a decrease in proangiogenic factors which leads to maturing of the blood vessels resulting in homogeneous blood flow and reduced vessel permeability and hypoxia.[245] Consequently, there is a trade off with normalization where large nanoparticles suffer from reduced extravasation due to a decrease in the fenestration.[244] Examples of mediators of blood vessel normalization include inhibition of vascular endothelial growth factor receptor-2 (VEGFR2).[244-245] Inhibiting VEGFR2 led to tumor vessel normalization and a decrease in interstitial fluid pressure.[244-245] In the presence of VEGFR2 inhibitors, it was demonstrated that there was an increase in nanoparticle extravasation into tumor tissues for particles up to 40 nm with the smaller nanoparticles penetrating deeply into the tumor tissue.[246]

Pertaining to the extravasation of nanoparticles across endothelial cells into the tumor microenvironments, there is a second school of though which proposes transcytosis as the main mechanism for nanoparticle extravasation.[247-248] There is an increasing body of evidence that suggests the abnormal vascular fenestrations and leakiness typically observed in the EPR effect can arise as an experimental artifact.[248] Accordingly, various

reports have described a network of tubular vesicles inside vascular endothelial cells of different tumor types. These tubular vesicles, or vesico-vacuolar organelles (VVO), appear as a cluster of vesicles and vacuoles that are interconnected and typically span the entire length of the vascular endothelium.[249-250] This interconnected network allows the nanoparticles to penetrate through the apical surface of endothelial cells and reach the extravascular space into the tumor microenvironment.[249-250] It has been recently demonstrated that neuropilin-1 (NRP-1), a receptor expressed on the surface of tumor blood vessels, triggers an endocytic transcytosis process.[251] Interestingly, a variety of growth factors including VEGF and TGF-β are known ligands for this receptor and triggers the transcytosis mechanism.[251] To date, it is unknown to which extent each of the two mechanisms, EPR vs. transcytosis, affect the extravasation of nanoparticles. Although there is undeniable clinical evidence bolstering the validity of the EPR, the transcytosis mechanism has been demonstrated in various reports pointing to a possible combination of the two mechanisms to explain the process of extravasation.

1.2.4 Tumor penetration

Extravasation of the nanoparticle *via* the EPR effect is hindered due to the elevated interstitial fluid pressure build up in solid tumor tissues.[252] Typically, Starling forces of a capillary drive the hydrostatic pressure causing filtration of water and solutes out of the capillary into the tissue micro-environment.[253] On the other hand, an oncotic pressure, created mostly by plasma proteins like albumins, causes a net flow of water and by-products of cell metabolism back into the blood circulation by way of venous transport.[254] The tight junctions of capillaries allow salts and small molecules to filter into the interstitial space, while larger proteins are retained creating an osmotic driving force for the flow of fluid back into the capillaries.[254] In a healthy tissue, there is a balance between these two forces with hydrostatic forces providing fluids, oxygen and salts necessary for proper cell maintenance and oncotic forces preventing edema and ensuring proper waste removal.[254] Unfortunately, the leaky vasculature of tumor tissues causes the extravasation of proteins and large solutes which decreases the osmotic force responsible for the oncotic pressure.[252] The net result is a decrease of the hydrostatic and oncotic pressures which causes elevated interstitial fluid pressure. This elevated interstitial fluid pressure acts as a physical barrier for the extravasation of nanoparticles and their diffusion into the tumor

interstitium.[252] In addition, the tumor microenvironment consists of a collagen matrix acting as a primary structural element with roles in cell adhesion and migration. This extracellular collagen matrix further impedes the diffusion of nanoparticles into the tumor microenvironment.[252] Various reports demonstrate that nanoparticles whose diameter is greater than 60 nm cannot penetrate deeply and are most often found at the periphery of the tumor tissues.[255-258] These reports seem to indicate a preference for small nanoparticles over larger ones for effective tissue penetration.[259]

1.2.5 Cell uptake

Upon extravasation and tissue penetration, the last hurdle is the uptake of nanoparticles into cells. The lipid bilayer prevents the diffusion of large and hydrophilic molecules across the cell membrane. Thus, nanoparticle's cell uptake must occur through different mechanisms. The entry of nanoparticles into cells occurs through endocytic pathways and is governed by their size, shape, and surface properties.[260] In Figure 1.11, the different endocytic pathways are presented along with their shuffling through the cell. There are two main approaches a nanoparticle can interact with a cell membrane leading to internalization.[260] The nanoparticles either interact directly with membrane-bound receptors or *via* hydrophobic or electrostatic interactions with the membrane.[260] Phagocytosis describes the entry of nanoparticles through an engulfment mechanism. Only specialized cells such as those composing the reticular endothelial system (macrophages, neutrophils and dendritic cells) are amenable to phagocytosis where opsonization plays a key role in determining the extent of cell uptake.[261] Contrary to phagocytosis, pinocytosis is common to nearly all cell types. Of the different mechanisms of pinocytosis, clathrin-mediated endocytosis is the most studied mechanism and occurs with the help of receptors that recruit clathrin through adaptor proteins at the site of internalization causing an invagination of the membrane followed by budding inside the cell.[261-262] As a result, a large amount of research effort has been directed towards coupling ligands to nanoparticles to promote cell uptake through this mechanism. Caveolae-mediated endocytosis is another mechanism of pinocytosis and involves the dimeric protein caveolin-1.[261] In this case, dynamin causes a scissoring of the vesicle from the membrane, in a similar fashion to clathrin-mediated endocytosis, where the vesicles formed in the cytosol fuse with caveosome and bypass the lysosomes.[261] Although less

studied, this uptake mechanism can help in the drug delivery field where endosomal escape tends to limit the delivery of cargo.[261] Finally, macropinocytosis is responsible for the engulfment of a large volume of extracellular fluid and has been shown to be induced by growth factors.[263] There exist other mechanisms that are clathrin- and caveolae-independent, however their description is beyond the scope of this thesis and has been thoroughly reviewed.[264-265]

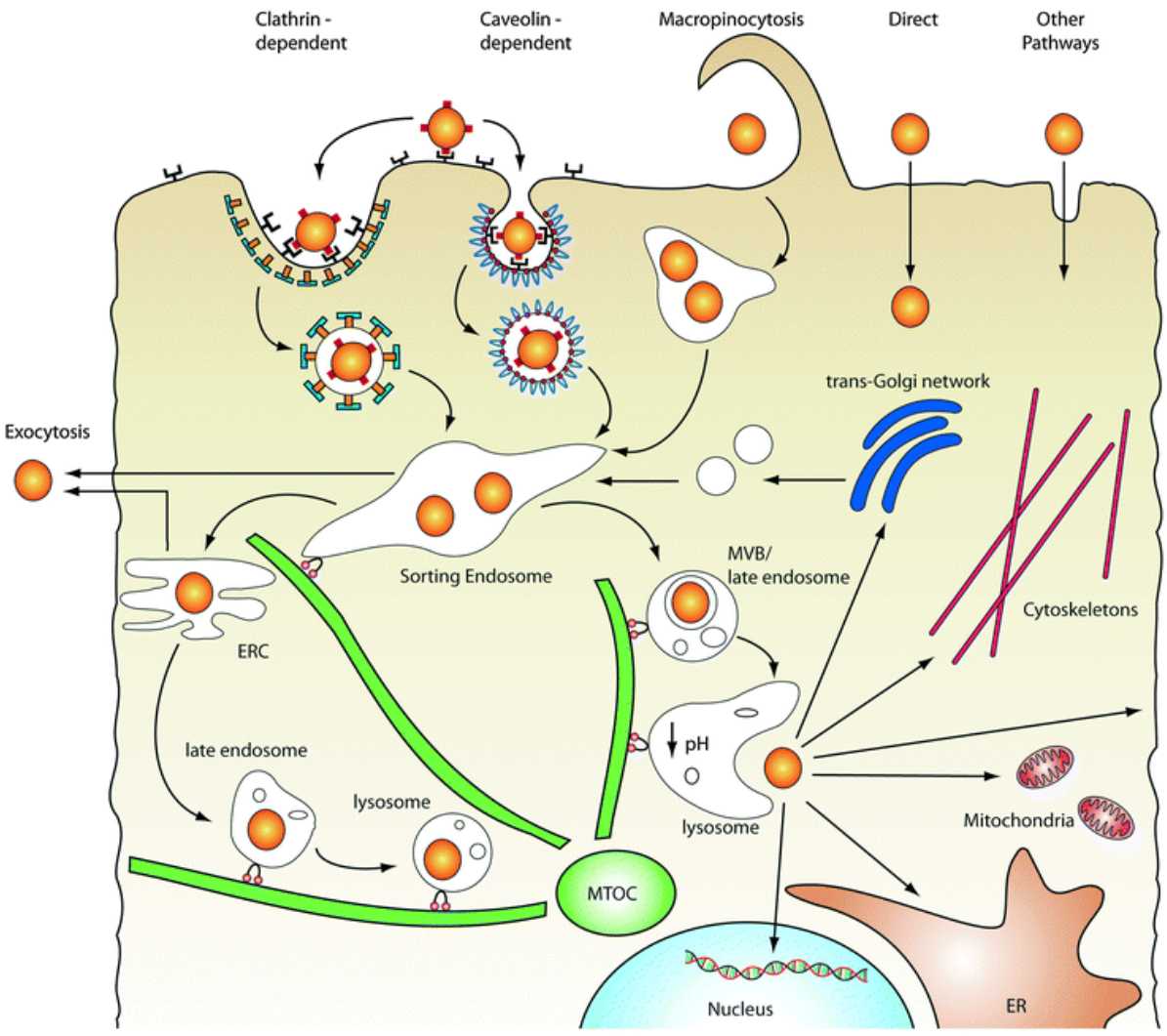

Figure 1.11 Fate of nanoparticles inside the cell following uptake.[260] (Reproduced with permission from © 2011 Royal Society of Chemistry Ltd.).

The physico-chemical properties of nanoparticles readily influence their interaction with cell membranes and, by extension, their cell uptake. It has been shown that the nanoparticle size, shape, surface charge, surface hydrophobicity/hydrophilicity, mechanical properties and surface functionalization all have an impact on cell uptake.[266] Size was discovered to be a key factor controlling the uptake of nanoparticles.[266] Smaller nanoparticles of a few to several hundred nm are engulfed via macro- and micropinocytosis.[267] Those between 250 nm and 3 μm are taken up mostly by phagocytosis whereas those between 120-150 nm are taken up by clathrin- or caveolae-mediated endocytosis.[267] The maximum size taken up *via* clathrin- and caveolae-mediated endocytosis have diameters of 200 nm due to the limiting size of the caveolae- and clathrin-coated pits that are formed during budding from the plasma membrane.[268-270] Studies carried out using Au nanoparticles of various sizes and shapes cite 50 nm as the optimal size for higher efficiency and uptake rate in internalization with lower uptake for both smaller and larger nanoparticles.[271-275] In terms of the effect of shape, the picture is less clear where conflicting results have been observed albeit with different materials. With regards to transferrin-coated Au nanoparticle, the uptake route followed the clathrin-mediated endocytosis with wrapping of the membrane around the nanoparticles.[271] The wrapping time was found to be a function of size and aspect ratio of the nanoparticles where higher aspect ratio led to lower uptake rates.[271] As a result, rod-shaped Au nanoparticles showed lower rates of uptake than spherical ones.[271] In another report, monodispersed hydrogels of different sizes and shapes were studied for their uptake in HeLa cells.[276] Interestingly, the high aspect ratio, rod-like hydrogels had higher uptake rates compared to lower aspect ratio hydrogels with spherical or cubic shapes. Despite these conflicting results and the lack of a clear shape-dependent uptake mechanism, the shapes of nanoparticles can limit or bolster the delivery of nanoparticles inside cells. In terms of surface charge, the literature is unequivocal, the negatively charged plasma membrane favors the uptake of positively charged nanoparticles over neutral or negatively charged nanoparticles.[266] Negatively- and positively-charged polystyrene (PS) nanoparticles were studied for their uptake inside synthetic lipid bilayers of giant unilamellar vesicles.[277] Positively charged PS had strong electrostatic interactions with the cell membrane leading to membrane binding and enhanced membrane surface tension

which resulted in transient pore formation and cell uptake. These results show a higher uptake for positively charged nanoparticles. In addition to the degree of uptake, the uptake mechanism has been shown to vary according to surface charge. Macropinocytosis tends to favor positively charged nanoparticles whereas clathrin- and caveolae-mediated endocytosis favors negatively charged nanoparticles.[278-279] Other than surface charge, another physical property affecting cell uptake is hydrophobicity. It is a noteworthy understanding that nanoparticle surface hydrophobicity will be tainted by opsonisation where the mere presence of opsonin will steer the uptake mechanism to that of receptor-mediated cell uptake. As a result, limited empirical data are available for these systems and the only information available employ molecular dynamics (MD) simulations.[266] Nevertheless, these MD simulations demonstrate that nanoparticles with a hydrophilic surface adsorbed onto the cell with a wrapping of the membrane around these nanoparticles before internalization, whereas hydrophobic nanoparticles penetrate directly inside the membrane embedding themselves within the inner hydrophobic core of the bilayer.[280-282]

To further increase the uptake of nanoparticles that are characterized with poor cell uptake, nanoparticles are conjugated with ligands at their surface. These ligands recognize receptors on the cell surface and promote uptake. Various transmembrane proteins located on the cell surface act as transporters and functionalization of the nanoparticles with agents or ligands that resemble the endogenous substrates of these transmembrane transporters enable cell uptake of the nanoparticle.[283] There is a slew of transmembrane receptors that are overexpressed in diseased tissues and can serve as targets to promote cell uptake.[283] For example, transferrin, folate, integrin, and cell adhesion molecule receptors have all been studied as targets to promote the uptake of drug delivery systems.[283-284] Transferrin receptors are over-expressed in cancer cells with 2- to 10-fold higher concentration than compared to healthy cells.[284] Transferrin is a type II trans-membrane glycoprotein which mediates iron uptake in cells through binding of the transferrin protein.[284] Various nanoparticles have been shown to be readily internalized inside tumor cells following conjugation with transferrin ligands.[284] Interestingly, folate receptors are overexpressed in various cancers such that it is often used as a tumor marker.[285] Indeed, it is expressed in the ovarian carcinoma of over 90% of afflicted

individuals. Folate receptor is a promising target to promote the uptake of nanoparticles in cancerous cells and selecting cancerous cells over healthy cells since it is absent in most healthy tissues.[285] Folic acid is a key starting material in the biosynthesis of nucleotide bases and is internalized inside cells through receptor-mediated endocytosis *via* folate receptors.[286] Folic acid can be conjugated on the surface of PEG-based block copolymers to promote uptake of drug delivery to cancerous cells.[285-286] For example, PEG-*b*-PLA micelles were conjugated with folic acid for the delivery of Doxorubicin to human ovarian cancer cells.[287] The conjugated micelles were shown to have higher cytotoxicity than non-conjugated micelles and delivered a higher amount of Doxorubicin to the cancer cells. Similarly, folic acid-conjugated block copolymers of poly[aminopoly(ethylene glycol)cyanoacrylate-*co*-hexadecyl cyanoacrylate] [poly(H_2NPEGCA-*co*-HDCA)] were studied for their specific interaction with folate-binding transmembrane protein.[288] Surface plasmon resonance showed that the folate-conjugated nanoparticles were bound to folate receptors and that this receptor binding drove the cell uptake of the nanoparticles.

Recently, evidence of a direct transfer of the loaded drug from the nanoparticle to the cell interior without the internalization of the nanoparticles has added complexity to our current understanding of cargo delivery inside cells. The uptake of a block copolymer of PEG-*b*-PCL loaded with Pheophorbide-a (Pheo) inside MCF-7 cells was studied using Förster resonance energy transfer.[289] These results demonstrate that most of the Pheo was delivered to the cells upon collision of the nanoparticles with the cells causing a direct transfer of the drug through the membrane rather than engulfment of the entire nanoparticle. This direct process accounted for a fast uptake of the loaded drug, followed by the slower uptake of the nanoparticle. A similar effect was observed for the delivery of Pheo inside human colorectal cells HCT-116.[290] This mechanism was also observed for block copolymers of PEG-*b*-PLA loaded with DiL and Nile Red.[291-292]

Upon internalization, the nanoparticle is trafficked through to the endocytic pathway. It is noteworthy to specify that internalization *via* caveolae-mediated endocytosis can bypass the endosomal compartments under certain circumstances.[293] Although the mechanism has not been thoroughly investigated, it is believed that the trafficking of the caveosomes generated upon cellular entry are regulated by a complex interplay between a family of kinases and phosphatases.[293] As many as 43 kinases have

been reported as effectors in the signal transduction pathways determining the sorting destination following uptake of SV40 viruses in HeLa cells.[294-295] For DDS entering through macropinocytosis or clathrin-dependent endocytosis, membrane-bound endosomal vesicles are formed and contain the nanoparticles. These endosomes are classified into three types, namely early, late, and recycling endosomes.[267] Early endosomes carry the cargo to different cellular destinations using motor proteins shuttling these vesicles along microtubules inside the cell.[267] A portion of these endosomes will recycle to the plasma membrane through recycling endosomes and release its contents outside the cell.[260] The remainder of the early endosomes differentiate and mature into late endosomes which will integrate with lysosomes to form the endo-lysosomal compartments.[260] During this maturation process, there is a rapid acidification of the vesicle with a lowering of the pH from 6 to 4, followed with the recruitment of hydrolytic enzymes whose purpose is to digest the vesicular content.[260] For a successful delivery strategy, the DDS needs to escape the endo-lysosomal compartments and release its cargo in the cytoplasm before succumbing to this strong degradation condition. Various strategies have been developed that enable such a feat and the aforementioned pH-responsive DDS is a prominent example. These strategies employ the proton sponge effect (Figure 1.12).[260] During the acidification process, ATPase proton pumps drive an influx of H^+ ions inside the lumen of the endosome.[260] During this process, there is a concomitant influx of Cl^- ions and water to maintain electrical neutrality inside the lysosome.[260] Polymers that have a buffering capacity inhibit the drop in pH and causes an increase in the amount of H^+ ions pumped inside the lysosome. This increase in protons is accompanied by an increase in Cl^- and water influx which leads to an increase in the osmotic pressure inside the lysosome culminating with bursting of the vesicular compartment thereby releasing its content.[296] Polymers that promote the proton sponge effect include polyethyleneimine (PEI),[297-299] poly(N,N-(dimethylamino)ethyl methacrylate)) (PDMAEMA),[300] and polyamidoamie (PAMAM).[301] PEI has a broad buffering capacity with a second pK_a at 4.5 which explains its buffering capacity at the lysosomal pH.[299] Finally, once outside the lysosome the nanoparticles can release their content and mediate their therapeutic effect.

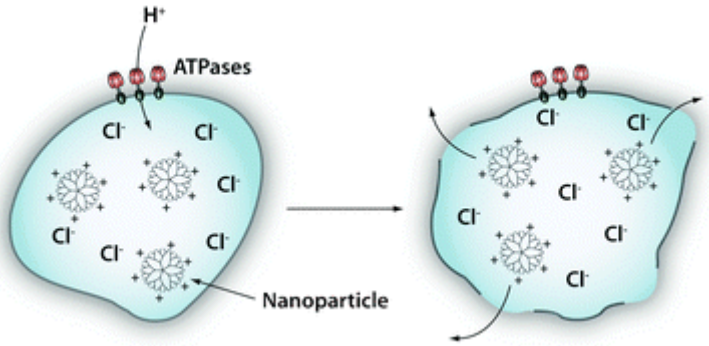

Figure 1.12 Proton-sponge effect.[260] (Reproduced with permission from © 2011 Royal Society of Chemistry Ltd.)

1.3 Scope of the thesis

Within our research group, the synthesis of bile acid-based star-shaped block copolymers using anionic polymerization has been previously described.[127, 302-303] With this polymerization technique, different architectures were designed with varying block positions, i.e. CA-(PAGE)$_4$, CA-(PEG)$_4$, CA-(PEG-*b*-PAGE)$_4$, and CA-(PAGE-*b*-PEG)$_4$. Moreover, the type of bile acid constituting the hydrophobic core has also been varied affording tunable hydrophobicity, aggregation properties and hydrodynamic diameters.[120] Employing CA-(PAGE)$_4$ as main excipient, a self-emulsifying drug delivery system was designed for the encapsulation of itraconazole, a hydrophobic anti-fungal drug.[121] This DDS showed promise for both enteral and parenteral administration of itraconazole in a pre-clinical model. In another report, PEGylated bile acids were prepared for the encapsulation of ibuprofen using different bile acids as core forming blocks and yielded formulations with varying drug loading and efficiency.[120] Based on these observations, it was hypothesized that CA-(PAGE-*b*-PEG)$_4$ could be used for the encapsulation of Dox. Following the description of the influence of the PEG block length on the physico-chemical properties of the DDS, a PEG length between 20 and 45 units will be used in the preparation of the cholic acid-based block copolymers. Numerous reports show that the shorter the PEG block, the higher the drug loading.[113, 115-116] Typically, for bile acid-based block copolymers, MD simulations show that lower PEG chains with 20 units are optimal for achieving highest drug loading.[125] However, the length of PEG chains should be long

enough to prevent micellar aggregation and prevent protein adsorption during systemic circulation with reports citing a PEG chain length of 45 units as the optimal value.[222-223] Therefore, the PEG chain length will be varied between 20 and 45 units to achieve the best performances. Moreover, the allyl groups could be functionalized to bear amine groups for the complexation with siRNA and promote gene delivery. Therefore, in this thesis the colloidal properties of CA-(PAGE-*b*-PEG)$_4$ and its potential towards both Dox and siRNA delivery was studied *in vitro*.

The objective of this thesis is to design a drug delivery system using bile acid-based block copolymers as starting materials that would satisfy each of the properties necessary for a successful formulation, i.e., biocompatible, high drug loading, high cell uptake, controlled release, and low toxicity. The formulation is designed to be versatile where therapeutics of different physico-chemical properties can be loaded at high concentrations with a simple tuning of the system. Ultimately, this formulation would serve as a drug delivery system for the encapsulation of therapeutic compounds for the treatment of breast cancer, i.e., chemotherapeutic agents, and siRNA molecules for gene therapy. Polymer based-drug delivery systems are often limited with low drug loading and premature release of the drugs. For Dox loading through hydrophobic interactions, the loading level is typically lower than 5 wt%.[137, 304-305] The use of cholic acid will be examined for its use as a reservoir for the loaded drugs and determine if it can help in increasing drug loading and stability of the formulation during transport to the desired tissue. It is hypothesized that using the biocompatible materials cholic acid, PAGE and PEG as building blocks, a biocompatible drug delivery system with low cytotoxicity will be obtained. Also, with respect to siRNA delivery, the star shaped structure of the formulation will be tested for its improved siRNA loading which can potentially decrease the amount of polymers needed to elicit a gene knockdown and potentially mitigate the high toxicities often encountered with using polyplexes as vectors for gene therapies. Moreover, it is hypothesized that the allyl groups of PAGE can be modified by a simple click reaction to afford electrostatic binding to govern the type of therapeutic compounds which can be loaded inside the drug delivery system. Towards this goal, the solution properties of the bile acid-based drug delivery system are studied first, followed by its potential towards Dox and siRNA loading and release.

Chapter 2 is a review article discussing the application of bile acids as building blocks in the design and construction of biomaterials for various applications. These materials were divided into two broad categories, soft materials for those that are held by weak intermolecular forces and hard materials for those that are mechanically stronger. For each of these two categories, the impact of using bile acids on the physico-chemical properties of the material is explained along with the advantages and limitations of using bile acids. For soft materials, the discussion is focused on the use of bile acids for drug delivery applications.[306]

Chapter 3 describes the thermoresponsive properties of the bile acid-based block copolymers in aqueous media to determine the factors affecting the LCST. PAGE and PEG blocks were grafted from a cholic acid (CA) core to yield the star-shaped block copolymers with 4 arms CA-(PAGE-*b*-PEG)$_4$. The PAGE block was further functionalized to bear pendant amine groups. The effects of PEG length and of the amine groups on the LCST behavior in water at various salt concentrations were examined. This work has been submitted to Langmuir and is currently under revision for publication.

Chapter 4 investigates the use of bile acid-based block copolymers for the encapsulation of doxorubicin as drug delivery systems for the treatment of breast cancer. In this article, hydrophobic and electrostatic interactions between the drug and polymer core is compared for its potential towards higher drug loading and stability. The pH-responsiveness afforded by electrostatic interaction between the drug and the polymer core is also examined for its influence on drug release and compared with drug loading by hydrophobic interaction. The potential of this bile acid-based DDS towards anti-cancer therapy is tested in HeLa cells; the IC_{50} of the nanoparticles is measured and compared with that of free doxorubicin.[307]

Chapter 5 explores the use of cholic acid-based block copolymers for the encapsulation and delivery of siRNA towards gene therapy. The impact of block length on siRNA loading and stability of the polyplexes is studied. Moreover, folic acid was conjugated on the surface of the micelles to promote higher cell uptake. To promote higher stability in the cell environment, mixed micelles were prepared. The mixed micelles are composed of cholic acid-based block copolymers with 10 wt % lipids as co-surfactants. The cholic acid-based micelles and mixed micelles were studied for their potential to serve as drug

delivery systems for the encapsulation and release of siRNA inside the cell. The transfection potential and cell uptake were measured for each of these systems in different conditions.[308]

Chapter 6 concludes the thesis with an overall summary of the work that was carried out in the course of this thesis project and presents future work that remain for the implementation of bile acids as a platform in the design of drug delivery systems.

1.4 References

1. Loftsson, T.; Brewster, M. E., Pharmaceutical applications of cyclodextrins: basic science and product development. *J. Pharm. Pharmacol.* **2010,** *62* (11), 1607-1621.
2. Shamshina, J. L.; Barber, P. S.; Rogers, R. D., Ionic liquids in drug delivery. *Expert Opin. Drug Deliv.* **2013,** *10* (10), 1367-1381.
3. Cerreia Vioglio, P.; Chierotti, M. R.; Gobetto, R., Pharmaceutical aspects of salt and cocrystal forms of APIs and characterization challenges. *Adv. Drug Deliv. Rev.* **2017,** *117*, 86-110.
4. Pack, D. W.; Hoffman, A. S.; Pun, S.; Stayton, P. S., Design and development of polymers for gene delivery. *Nat. Rev. Drug Discov.* **2005,** *4* (7), 581-593.
5. Saha, R. N.; Vasanthakumar, S.; Bende, G.; Snehalatha, M., Nanoparticulate drug delivery systems for cancer chemotherapy. *Mol. Membr. Biol.* **2010,** *27* (7), 215-231.
6. Bobo, D.; Robinson, K. J.; Islam, J.; Thurecht, K. J.; Corrie, S. R., Nanoparticle-based medicines: a review of FDA-approved materials and clinical trials to date. *Pharm. Res.* **2016,** *33* (10), 2373-2387.
7. Caster, J. M.; Patel, A. N.; Zhang, T.; Wang, A., Investigational nanomedicines in 2016: a review of nanotherapeutics currently undergoing clinical trials. *Nanomed. Nanobiotechnol.* **2017,** *9* (1), 1-18.
8. Ventola, C. L., The nanomedicine revolution: part 1: emerging concepts. *P. T.* **2012,** *37* (9), 512-25.
9. Havel, H. A., Where Are the Nanodrugs? An industry perspective on development of drug products containing nanomaterials. *AAPS J.* **2016,** *18* (6), 1351-1353.
10. Havel, H.; Finch, G.; Strode, P.; Wolfgang, M.; Zale, S.; Bobe, I.; Youssoufian, H.; Peterson, M.; Liu, M., Nanomedicines: from bench to bedside and beyond. *AAPS J.* **2016,** *18* (6), 1373-1378.
11. Sainz, V.; Conniot, J.; Matos, A. I.; Peres, C.; Zupancic, E.; Moura, L.; Silva, L. C.; Florindo, H. F.; Gaspar, R. S., Regulatory aspects on nanomedicines. *Biochem. Biophys. Res. Commun.* **2015,** *468* (3), 504-510.
12. Italia, J. L.; Bhatt, D. K.; Bhardwaj, V.; Tikoo, K.; Kumar, M. N. V. R., PLGA nanoparticles for oral delivery of cyclosporine: nephrotoxicity and pharmacokinetic studies in comparison to Sandimmune Neoral®. *J. Control. Release* **2007,** *119* (2), 197-206.
13. Mittal, G.; Sahana, D. K.; Bhardwaj, V.; Ravi Kumar, M. N. V., Estradiol loaded PLGA nanoparticles for oral administration: effect of polymer molecular weight

and copolymer composition on release behavior in vitro and in vivo. *J. Control. Release* **2007,** *119* (1), 77-85.
14. Anand, P.; Kunnumakkara, A. B.; Newman, R. A.; Aggarwal, B. B., Bioavailability of curcumin: Problems and promises. *Mol. Pharm.* **2007,** *4* (6), 807-818.
15. Zhu, X.; Lu, L.; Currier, B. L.; Windebank, A. J.; Yaszemski, M. J., Controlled release of NFkappaB decoy oligonucleotides from biodegradable polymer microparticles. *Biomaterials* **2002,** *23* (13), 2683-2692.
16. Mountziaris, P. M.; Sing, D. C.; Chew, S. A.; Tzouanas, S. N.; Lehman, E. D.; Kasper, F. K.; Mikos, A. G., Controlled release of anti-inflammatory siRNA from biodegradable polymeric microparticles intended for intra-articular delivery to the temporomandibular joint. *Pharm. Res.* **2011,** *28* (6), 1370-1384.
17. Akhtar, S.; Lewis, K. J., Antisense oligonucleotide delivery to cultured macrophages is improved by incorporation into sustained-release biodegradable polymer microspheres. *Int. J. Pharm.* **1997,** *151* (1), 57-67.
18. Kalepu, S.; Nekkanti, V., Insoluble drug delivery strategies: review of recent advances and business prospects. *Acta Pharm. Sin. B* **2015,** *5* (5), 442-453.
19. Ma, P.; Mumper, R. J., Paclitaxel nano-delivery systems: A comprehensive review. *J. Nanomed. Nanotechnol.* **2013,** *4* (2), 1000164.
20. Li, B.; Li, Q.; Mo, J.; Dai, H., Drug-loaded polymeric nanoparticles for cancer stem cell targeting. *Front. Pharmacol.* **2017,** *8* (51), 1-12.
21. Fam, S. Y.; Chee, C. F.; Yong, C. Y.; Ho, K. L.; Mariatulqabtiah, A. R.; Tan, W. S., Stealth coating of nanoparticles in drug-delivery systems. *Nanomaterials* **2020,** *10* (4), 787-805.
22. Zhang, L.; Gu, F.; Chan, J.; Wang, A.; Langer, R.; Farokhzad, O., Nanoparticles in medicine: Therapeutic applications and developments. *Clin. Pharmacol. Ther.* **2008,** *83* (5), 761-769.
23. Anselmo, A. C.; Mitragotri, S., Nanoparticles in the clinic: An update. *Bioeng. Transl. Med.* **2019,** *4* (3), e10143.
24. Duncan, R., Polymer therapeutics: Top 10 selling pharmaceuticals — What next? *J. Control. Release* **2014,** *190*, 371-380.
25. Bobo, D.; Robinson, K. J.; Islam, J.; Thurecht, K. J.; Corrie, S. R., Nanoparticle-based medicines: A review of FDA-approved materials and clinical trials to date. *Pharm. Res.* **2016,** *33* (10), 2373-2387.
26. Li, J.; Mooney, D. J., Designing hydrogels for controlled drug delivery. *Nat. Rev. Mater.* **2016,** *1* (12), 16071-16088.
27. Calvert, P., Hydrogels for soft machines. *Adv. Mater.* **2009,** *21* (7), 743-756.
28. Arakaki, K.; Kitamura, N.; Fujiki, H.; Kurokawa, T.; Iwamoto, M.; Ueno, M.; Kanaya, F.; Osada, Y.; Gong, J. P.; Yasuda, K., Artificial cartilage made from a novel double-network hydrogel: In vivo effects on the normal cartilage and ex vivo evaluation of the friction property. *J. Biomed. Mater. Res. Part A* **2010,** *93* (3), 1160-1168.
29. Li, J.; Illeperuma, W. R. K.; Suo, Z.; Vlassak, J. J., Hybrid hydrogels with extremely high stiffness and toughness. *ACS Macro Letters* **2014,** *3* (6), 520-523.
30. Bodugoz-Senturk, H.; Macias, C. E.; Kung, J. H.; Muratoglu, O. K., Poly(vinyl alcohol)–acrylamide hydrogels as load-bearing cartilage substitute. *Biomaterials* **2009,** *30* (4), 589-596.

31. Su, J.; Hu, B.-H.; Lowe, W. L.; Kaufman, D. B.; Messersmith, P. B., Anti-inflammatory peptide-functionalized hydrogels for insulin-secreting cell encapsulation. *Biomaterials* **2010,** *31* (2), 308-314.
32. Narayanaswamy, R.; Torchilin, V. P., Hydrogels and their applications in targeted drug delivery. *Molecules* **2019,** *24* (3), 603-621.
33. Owen, S. C.; Chan, D. P. Y.; Shoichet, M. S., Polymeric micelle stability. *Nano Today* **2012,** *7* (1), 53-65.
34. Deb, P. K.; Kokaz, S. F.; Abed, S. N.; Paradkar, A.; Tekade, R. K., Chapter 6 - Pharmaceutical and biomedical applications of polymers. In *Basic Fundamentals of Drug Delivery*, Tekade, R. K., Ed. Academic Press: 2019; pp 203-267.
35. Ekladious, I.; Colson, Y. L.; Grinstaff, M. W., Polymer–drug conjugate therapeutics: advances, insights and prospects. *Nat. Rev. Drug Discov.* **2019,** *18* (4), 273-294.
36. Ekladious, I.; Liu, R.; Zhang, H.; Foil, D. H.; Todd, D. A.; Graf, T. N.; Padera, R. F.; Oberlies, N. H.; Colson, Y. L.; Grinstaff, M. W., Synthesis of poly(1,2-glycerol carbonate)-paclitaxel conjugates and their utility as a single high-dose replacement for multi-dose treatment regimens in peritoneal cancer. *Chem. Sci.* **2017,** *8* (12), 8443-8450.
37. Chan, J. M.; Zhang, L.; Tong, R.; Ghosh, D.; Gao, W.; Liao, G.; Yuet, K. P.; Gray, D.; Rhee, J. W.; Cheng, J.; Golomb, G.; Libby, P.; Langer, R.; Farokhzad, O. C., Spatiotemporal controlled delivery of nanoparticles to injured vasculature. *Proc. Natl. Acad. Sci.* **2010,** *107* (5), 2213-2218.
38. Crielaard, B. J.; Rijcken, C. J. F.; Quan, L.; van der Wal, S.; Altintas, I.; van der Pot, M.; Kruijtzer, J. A. W.; Liskamp, R. M. J.; Schiffelers, R. M.; van Nostrum, C. F.; Hennink, W. E.; Wang, D.; Lammers, T.; Storm, G., Glucocorticoid-loaded core-cross-linked polymeric micelles with tailorable release kinetics for targeted therapy of rheumatoid arthritis. *Angew. Chem. Int. Ed.* **2012,** *51* (29), 7254-7258.
39. Tong, R.; Cheng, J., Paclitaxel-initiated, controlled polymerization of lactide for the formulation of polymeric nanoparticulate delivery vehicles. *Angew. Chem. Int. Ed.* **2008,** *47* (26), 4830-4834.
40. Peng, Z. H.; Kopecek, J., Enhancing accumulation and penetration of HPMA copolymer-doxorubicin conjugates in 2D and 3D prostate cancer cells via iRGD conjugation with an MMP-2 cleavable spacer. *J. Am. Chem. Soc.* **2015,** *137* (21), 6726-6729.
41. Miller, K.; Erez, R.; Segal, E.; Shabat, D.; Satchi-Fainaro, R., Targeting bone metastases with a bispecific anticancer and antiangiogenic polymer–alendronate–taxane conjugate. *Angew. Chem. Int. Ed.* **2009,** *48* (16), 2949-2954.
42. Zhu, L.; Wang, T.; Perche, F.; Taigind, A.; Torchilin, V. P., Enhanced anticancer activity of nanopreparation containing an MMP2-sensitive PEG-drug conjugate and cell-penetrating moiety. *Proc. Natl. Acad. Sci.* **2013,** *110* (42), 17047-17052.
43. Pang, X.; Jiang, Y.; Xiao, Q.; Leung, A. W.; Hua, H.; Xu, C., pH-responsive polymer-drug conjugates: Design and progress. *J. Control. Release* **2016,** *222*, 116-129.
44. Quan, L. D.; Purdue, P. E.; Liu, X. M.; Boska, M. D.; Lele, S. M.; Thiele, G. M.; Mikuls, T. R.; Dou, H.; Goldring, S. R.; Wang, D., Development of a macromolecular prodrug for the treatment of inflammatory arthritis: mechanisms

involved in arthrotropism and sustained therapeutic efficacy. *Arthritis. Res. Ther.* **2010,** *12* (5), 170-180.
45. Du, J. Z.; Du, X. J.; Mao, C. Q.; Wang, J., Tailor-made dual pH-sensitive polymer-doxorubicin nanoparticles for efficient anticancer drug delivery. *J. Am. Chem. Soc.* **2011,** *133* (44), 17560-17563.
46. Takahashi, A.; Yamamoto, Y.; Yasunaga, M.; Koga, Y.; Kuroda, J.; Takigahira, M.; Harada, M.; Saito, H.; Hayashi, T.; Kato, Y.; Kinoshita, T.; Ohkohchi, N.; Hyodo, I.; Matsumura, Y., NC-6300, an epirubicin-incorporating micelle, extends the antitumor effect and reduces the cardiotoxicity of epirubicin. *Cancer Sci.* **2013,** *104* (7), 920-925.
47. Mukai, H.; Kogawa, T.; Matsubara, N.; Naito, Y.; Sasaki, M.; Hosono, A., A first-in-human Phase 1 study of epirubicin-conjugated polymer micelles (K-912/NC-6300) in patients with advanced or recurrent solid tumors. *Invest. New Drugs* **2017,** *35* (3), 307-314.
48. Dubikovskaya, E. A.; Thorne, S. H.; Pillow, T. H.; Contag, C. H.; Wender, P. A., Overcoming multidrug resistance of small-molecule therapeutics through conjugation with releasable octaarginine transporters. *Proc. Natl. Acad. Sci.* **2008,** *105* (34), 12128-12133.
49. Mishra, M. K.; Beaty, C. A.; Lesniak, W. G.; Kambhampati, S. P.; Zhang, F.; Wilson, M. A.; Blue, M. E.; Troncoso, J. C.; Kannan, S.; Johnston, M. V.; Baumgartner, W. A.; Kannan, R. M., Dendrimer brain uptake and targeted therapy for brain injury in a large animal model of hypothermic circulatory arrest. *ACS Nano* **2014,** *8* (3), 2134-2147.
50. Hu, X.; Liu, G.; Li, Y.; Wang, X.; Liu, S., Cell-penetrating hyperbranched polyprodrug amphiphiles for synergistic reductive milieu-triggered drug release and enhanced magnetic resonance signals. *J. Am. Chem. Soc.* **2015,** *137* (1), 362-368.
51. Luo, C.; Sun, J.; Liu, D.; Sun, B.; Miao, L.; Musetti, S.; Li, J.; Han, X.; Du, Y.; Li, L.; Huang, L.; He, Z., Self-assembled redox dual-responsive prodrug-nanosystem formed by single thioether-bridged paclitaxel-fatty acid conjugate for cancer chemotherapy. *Nano Lett.* **2016,** *16* (9), 5401-5408.
52. Steinbach, T.; Wurm, F. R., Degradable polyphosphoester-protein conjugates: "PPEylation" of proteins. *Biomacromolecules* **2016,** *17* (10), 3338-3346.
53. Urakami, H.; Guan, Z., Living ring-opening polymerization of a carbohydrate-derived lactone for the synthesis of protein-resistant biomaterials. *Biomacromolecules* **2008,** *9* (2), 592-597.
54. Knop, K.; Hoogenboom, R.; Fischer, D.; Schubert, U. S., Poly(ethylene glycol) in drug delivery: pros and cons as well as potential alternatives. *Angew. Chem. Int. Ed.* **2010,** *49* (36), 6288-6308.
55. Luxenhofer, R.; Han, Y.; Schulz, A.; Tong, J.; He, Z.; Kabanov, A. V.; Jordan, R., Poly(2-oxazoline)s as polymer therapeutics. *Macromol. Rapid Commun.* **2012,** *33* (19), 1613-1631.
56. Gangloff, N.; Ulbricht, J.; Lorson, T.; Schlaad, H.; Luxenhofer, R., Peptoids and polypeptoids at the frontier of supra- and macromolecular engineering. *Chem. Rev.* **2016,** *116* (4), 1753-1802.

57. Blanazs, A.; Armes, S. P.; Ryan, A. J., Self-assembled block copolymer aggregates: From micelles to vesicles and their biological applications. *Macromol. Rapid Commun.* **2009,** *30* (4), 267-277.
58. Mai, Y.; Eisenberg, A., Self-assembly of block copolymers. *Chem. Soc. Rev.* **2012,** *41* (18), 5969-5985.
59. Jones, M.; Leroux, J., Polymeric micelles - a new generation of colloidal drug carriers. *Eur. J. Pharm. Biopharm.* **1999,** *48* (2), 101-111.
60. Giorgio, G.; Colafemmina, G.; Mavelli, F.; Murgia, S.; Palazzo, G., The impact of alkanes on the structure of Triton X100 micelles. *RSC Advances* **2016,** *6* (1), 825-836.
61. Nagarajan, R., Molecular packing parameter and surfactant self-assembly: The neglected role of the surfactant tail. *Langmuir* **2002,** *18* (1), 31-38.
62. Bhattacharya, A.; Bourov, G. K. In *Effect of Packing Parameter on Amphiphilic Self-Assembly: A Brownian Dynamics Study*, Berlin, Heidelberg, Springer Berlin Heidelberg: Berlin, Heidelberg, 2004; pp 123-128.
63. Israelachvili, J. N., 20 - Soft and biological structures. In *Intermolecular and Surface Forces (Third Edition)*, Israelachvili, J. N., Ed. Academic Press: Boston, 2011; pp 535-576.
64. Wang, W.; Gaus, K.; Tilley, R. D.; Gooding, J. J., The impact of nanoparticle shape on cellular internalisation and transport: what do the different analysis methods tell us? *Mater. Horiz.* **2019,** *6* (8), 1538-1547.
65. Cai, S.; Vijayan, K.; Cheng, D.; Lima, E. M.; Discher, D. E., Micelles of different morphologies--advantages of worm-like filomicelles of PEO-PCL in paclitaxel delivery. *Pharm. Res.* **2007,** *24* (11), 2099-2109.
66. Kolate, A.; Baradia, D.; Patil, S.; Vhora, I.; Kore, G.; Misra, A., PEG — A versatile conjugating ligand for drugs and drug delivery systems. *J. Control. Release* **2014,** *192*, 67-81.
67. Bailly, N.; Thomas, M.; Klumperman, B., Poly(N-vinylpyrrolidone)-block-poly(vinyl acetate) as a drug delivery vehicle for hydrophobic drugs. *Biomacromolecules* **2012,** *13* (12), 4109-4117.
68. Zhu, Z.; Xie, C.; Liu, Q.; Zhen, X.; Zheng, X.; Wu, W.; Li, R.; Ding, Y.; Jiang, X.; Liu, B., The effect of hydrophilic chain length and iRGD on drug delivery from poly(ε-caprolactone)-poly(N-vinylpyrrolidone) nanoparticles. *Biomaterials* **2011,** *32* (35), 9525-9535.
69. Kaneda, Y.; Tsutsumi, Y.; Yoshioka, Y.; Kamada, H.; Yamamoto, Y.; Kodaira, H.; Tsunoda, S.-i.; Okamoto, T.; Mukai, Y.; Shibata, H.; Nakagawa, S.; Mayumi, T., The use of PVP as a polymeric carrier to improve the plasma half-life of drugs. *Biomaterials* **2004,** *25* (16), 3259-3266.
70. Kim, D. H.; Vitol, E. A.; Liu, J.; Balasubramanian, S.; Gosztola, D. J.; Cohen, E. E.; Novosad, V.; Rozhkova, E. A., Stimuli-responsive magnetic nanomicelles as multifunctional heat and cargo delivery vehicles. *Langmuir* **2013,** *29* (24), 7425-7432.
71. Caliceti, P.; Veronese, F. M., Pharmacokinetic and biodistribution properties of poly(ethylene glycol)-protein conjugates. *Adv. Drug Deliv. Rev.* **2003,** *55* (10), 1261-1277.

72. Allen, T. M.; Cullis, P. R., Drug delivery systems: entering the mainstream. *Science* **2004,** *303* (5665), 1818-1822.
73. Matsumura, Y.; Maeda, H., A new concept for macromolecular therapeutics in cancer chemotherapy: mechanism of tumoritropic accumulation of proteins and the antitumor agent smancs. *Cancer Res.* **1986,** *46* (12), 6387-6392.
74. Haran, G.; Cohen, R.; Bar, L. K.; Barenholz, Y., Transmembrane ammonium sulfate gradients in liposomes produce efficient and stable entrapment of amphipathic weak bases. *Biochim. Biophys. Acta* **1993,** *1151* (2), 201-215.
75. Horowitz, A. T.; Barenholz, Y.; Gabizon, A. A., In vitro cytotoxicity of liposome-encapsulated doxorubicin: dependence on liposome composition and drug release. *Biochim. Biophys. Acta* **1992,** *1109* (2), 203-209.
76. Pound, G.; McKenzie, J. M.; Lange, R. F. M.; Klumperman, B., Polymer–protein conjugates from ω-aldehyde endfunctional poly(N-vinylpyrrolidone) synthesised via xanthate-mediated living radical polymerisation. *Chem. Commun.* **2008,** (27), 3193-3195.
77. Torchilin, V. P., Polymer-coated long-circulating microparticulate pharmaceuticals. *J. Microencapsul.* **1998,** *15* (1), 1-19.
78. Benahmed, A.; Ranger, M.; Leroux, J.-C., Novel polymeric micelles based on the amphiphilic diblock copolymer poly(N-vinyl-2-pyrrolidone)-block-poly(D,L-lactide). *Pharm. Res.* **2001,** *18* (3), 323-328.
79. Le Garrec, D.; Gori, S.; Luo, L.; Lessard, D.; Smith, D. C.; Yessine, M. A.; Ranger, M.; Leroux, J. C., Poly(N-vinylpyrrolidone)-block-poly(D,L-lactide) as a new polymeric solubilizer for hydrophobic anticancer drugs: in vitro and in vivo evaluation. *J. Control. Release* **2004,** *99* (1), 83-101.
80. Gaucher, G.; Asahina, K.; Wang, J.; Leroux, J. C., Effect of poly(N-vinyl-pyrrolidone)-block-poly(D,L-lactide) as coating agent on the opsonization, phagocytosis, and pharmacokinetics of biodegradable nanoparticles. *Biomacromolecules* **2009,** *10* (2), 408-416.
81. Zhu, Z.; Li, Y.; Li, X.; Li, R.; Jia, Z.; Liu, B.; Guo, W.; Wu, W.; Jiang, X., Paclitaxel-loaded poly(N-vinylpyrrolidone)-b-poly(epsilon-caprolactone) nanoparticles: preparation and antitumor activity in vivo. *J. Control. Release* **2010,** *142* (3), 438-446.
82. Ishihara, T.; Maeda, T.; Sakamoto, H.; Takasaki, N.; Shigyo, M.; Ishida, T.; Kiwada, H.; Mizushima, Y.; Mizushima, T., Evasion of the accelerated blood clearance phenomenon by coating of nanoparticles with various hydrophilic polymers. *Biomacromolecules* **2010,** *11* (10), 2700-2706.
83. Wang, X.; Ishida, T.; Kiwada, H., Anti-PEG IgM elicited by injection of liposomes is involved in the enhanced blood clearance of a subsequent dose of PEGylated liposomes. *J. Control. Release* **2007,** *119* (2), 236-244.
84. Xu, H.; Wang, K. Q.; Deng, Y. H.; Chen, D. W., Effects of cleavable PEG-cholesterol derivatives on the accelerated blood clearance of PEGylated liposomes. *Biomaterials* **2010,** *31* (17), 4757-4763.
85. Sharma, A. K.; Zhang, L.; Li, S.; Kelly, D. L.; Alakhov, V. Y.; Batrakova, E. V.; Kabanov, A. V., Prevention of MDR development in leukemia cells by micelle-forming polymeric surfactant. *J. Control. Release* **2008,** *131* (3), 220-227.

86. Kanazawa, T.; Akiyama, F.; Kakizaki, S.; Takashima, Y.; Seta, Y., Delivery of siRNA to the brain using a combination of nose-to-brain delivery and cell-penetrating peptide-modified nano-micelles. *Biomaterials* **2013,** *34* (36), 9220-9226.
87. Laouini, A.; Koutroumanis, K. P.; Charcosset, C.; Georgiadou, S.; Fessi, H.; Holdich, R. G.; Vladisavljević, G. T., pH-sensitive micelles for targeted drug delivery prepared using a novel membrane contactor method. *ACS Appl. Mater. Interfaces* **2013,** *5* (18), 8939-8947.
88. Tyler, B.; Gullotti, D.; Mangraviti, A.; Utsuki, T.; Brem, H., Polylactic acid (PLA) controlled delivery carriers for biomedical applications. *Adv. Drug Deliv. Rev.* **2016,** *107*, 163-175.
89. Koyamatsu, Y.; Hirano, T.; Kakizawa, Y.; Okano, F.; Takarada, T.; Maeda, M., pH-responsive release of proteins from biocompatible and biodegradable reverse polymer micelles. *J. Control. Release* **2014,** *173*, 89-95.
90. Yokoyama, M.; Miyauchi, M.; Yamada, N.; Okano, T.; Sakurai, Y.; Kataoka, K.; Inoue, S., Characterization and anticancer activity of the micelle-forming polymeric anticancer drug adriamycin-conjugated poly(ethylene glycol)-poly(aspartic acid) block copolymer. *Cancer. Res.* **1990,** *50* (6), 1693-1700.
91. Kagaya, H.; Oba, M.; Miura, Y.; Koyama, H.; Ishii, T.; Shimada, T.; Takato, T.; Kataoka, K.; Miyata, T., Impact of polyplex micelles installed with cyclic RGD peptide as ligand on gene delivery to vascular lesions. *Gene Therapy* **2012,** *19* (1), 61-69.
92. Wu, H.; Zhu, L.; Torchilin, V. P., pH-sensitive poly(histidine)-PEG/DSPE-PEG co-polymer micelles for cytosolic drug delivery. *Biomaterials* **2013,** *34* (4), 1213-1222.
93. Min, K. H.; Kim, J. H.; Bae, S. M.; Shin, H.; Kim, M. S.; Park, S.; Lee, H.; Park, R. W.; Kim, I. S.; Kim, K.; Kwon, I. C.; Jeong, S. Y.; Lee, D. S., Tumoral acidic pH-responsive MPEG-poly(beta-amino ester) polymeric micelles for cancer targeting therapy. *J. Control. Release* **2010,** *144* (2), 259-266.
94. Jain, R. A., The manufacturing techniques of various drug loaded biodegradable poly(lactide-co-glycolide) (PLGA) devices. *Biomaterials* **2000,** *21* (23), 2475-2490.
95. Cai, J.; Peng, X.; Nelson, K. D.; Eberhart, R.; Smith, G. M., Permeable guidance channels containing microfilament scaffolds enhance axon growth and maturation. *J. Biomed. Mater. Res. Part A* **2005,** *75* (2), 374-386.
96. Patist, C. M.; Mulder, M. B.; Gautier, S. E.; Maquet, V.; Jérôme, R.; Oudega, M., Freeze-dried poly(d,l-lactic acid) macroporous guidance scaffolds impregnated with brain-derived neurotrophic factor in the transected adult rat thoracic spinal cord. *Biomaterials* **2004,** *25* (9), 1569-1582.
97. Suuronen, R., Biodegradable fracture-fixation devices in maxillofacial surgery. *Int. J. Oral Maxillofac. Surg.* **1993,** *22* (1), 50-57.
98. Larsen, M. W.; Pietrzak, W. S.; DeLee, J. C., Fixation of osteochondritis dissecans lesions using poly(l-lactic acid)/ poly(glycolic acid) copolymer bioabsorbable screws. *Am. J. Sports Med.* **2005,** *33* (1), 68-76.
99. Athanasiou, K. A.; Agrawal, C. M.; Barber, F. A.; Burkhart, S. S., Orthopaedic applications for PLA-PGA biodegradable polymers. *Arthroscopy* **1998,** *14* (7), 726-737.

100. Oksman, K.; Skrifvars, M.; Selin, J. F., Natural fibres as reinforcement in polylactic acid (PLA) composites. *Compos. Sci. Technol.* **2003,** *63* (9), 1317-1324.
101. Senatov, F. S.; Niaza, K. V.; Zadorozhnyy, M. Y.; Maksimkin, A. V.; Kaloshkin, S. D.; Estrin, Y. Z., Mechanical properties and shape memory effect of 3D-printed PLA-based porous scaffolds. *J. Mech. Behav. Biomed. Mater.* **2016,** *57*, 139-148.
102. Jain, D. S.; Athawale, R. B.; Bajaj, A. N.; Shrikhande, S. S.; Goel, P. N.; Nikam, Y.; Gude, R. P., Poly lactic acid (PLA) nanoparticles sustain the cytotoxic action of temozolomide in C6 Glioma cells. *Biomed. Aging Pathol.* **2013,** *3* (4), 201-208.
103. Senthilkumar, M.; Mishra, P.; Jain, N. K., Long circulating PEGylated poly(d,l-lactide-co-glycolide) nanoparticulate delivery of Docetaxel to solid tumors. *J. Drug Target.* **2008,** *16* (5), 424-435.
104. Zhao, L.; Yang, C.; Dou, J.; Xi, Y.; Lou, H.; Zhai, G., Development of RGD-functionalized PEG-PLA micelles for delivery of curcumin. *J. Biomed. Nanotechnol.* **2015,** *11* (3), 436-446.
105. Frounchi, M.; Shamshiri, S., Magnetic nanoparticles-loaded PLA/PEG microspheres as drug carriers. *J. Biomed. Mater. Res. Part A* **2015,** *103* (5), 1893-1898.
106. Casalini, T.; Rossi, F.; Castrovinci, A.; Perale, G., A perspective on polylactic acid-based polymers use for nanoparticles synthesis and applications. *Front. Bioeng. Biotechnol.* **2019,** *7* (259), 1-16.
107. Ding, J.; Chen, L.; Xiao, C.; Chen, L.; Zhuang, X.; Chen, X., Noncovalent interaction-assisted polymeric micelles for controlled drug delivery. *Chem. Comm.* **2014,** *50* (77), 11274-11290.
108. Lee, S.-W.; Kim, Y.-M.; Cho, C. H.; Kim, Y. T.; Kim, S. M.; Hur, S. Y.; Kim, J.-H.; Kim, B.-G.; Kim, S.-C.; Ryu, H.-S.; Kang, S. B., An open-label, randomized, parallel, phase II trial to evaluate the efficacy and safety of a cremophor-free polymeric micelle formulation of paclitaxel as first-line treatment for ovarian cancer: A korean gynecologic oncology group study (KGOG-3021). *Cancer Res. Treat.* **2018,** *50* (1), 195-203.
109. Kim, S. C.; Kim, D. W.; Shim, Y. H.; Bang, J. S.; Oh, H. S.; Wan Kim, S.; Seo, M. H., In vivo evaluation of polymeric micellar paclitaxel formulation: toxicity and efficacy. *J. Control. Release* **2001,** *72* (1), 191-202.
110. Ding, A.; Zhou, Y.; Chen, P.; Nie, W., Ibuprofen-loaded micelles based on star-shaped erythritol-core PLLA-PEG copolymer: effect of molecular weights of PEG. *Colloid Polym. Sci.* **2017,** *295* (9), 1609-1619.
111. Kumar, R.; Tyagi, R.; Shakil, N. A.; Parmar, V. S.; Kumar, J.; Watterson, A. C., Self-assembly of PEG and diester copolymers: Effect of PEG length, linker, concentration and temperature. *J. Macromol. Sci. Part A* **2005,** *42* (11), 1523-1528.
112. Wang, D.; Zhou, Y.; Li, X.; Qu, X.; Deng, Y.; Wang, Z.; He, C.; Zou, Y.; Jin, Y.; Liu, Y., Mechanisms of pH-sensitivity and cellular internalization of PEOz-b-PLA micelles with varied hydrophilic/hydrophobic ratios and intracellular trafficking routes and fate of the copolymer. *ACS Appl. Mater. Interfaces* **2017,** *9* (8), 6916-6930.
113. Maksym, P.; Neugebauer, D., Self-assembling polyether-b-polymethacrylate graft copolymers loaded with indomethacin. *Int. J. Polym. Mater. Polym. Biomater.* **2017,** *66* (7), 317-325.

114. Logie, J.; Owen, S. C.; McLaughlin, C. K.; Shoichet, M. S., PEG-graft density controls polymeric nanoparticle micelle stability. *Chem. Mater.* **2014,** *26* (9), 2847-2855.
115. Wang, J.; del Rosario, L. S.; Demirdirek, B.; Bae, A.; Uhrich, K. E., Comparison of PEG chain length and density on amphiphilic macromolecular nanocarriers: self-assembled and unimolecular micelles. *Acta Biomater.* **2009,** *5* (3), 883-892.
116. Sezgin, Z.; Yüksel, N.; Baykara, T., Preparation and characterization of polymeric micelles for solubilization of poorly soluble anticancer drugs. *Eur. J. Pharm. Biopharm.* **2006,** *64* (3), 261-268.
117. Du, X.-J.; Wang, J.-L.; Liu, W.-W.; Yang, J.-X.; Sun, C.-Y.; Sun, R.; Li, H.-J.; Shen, S.; Luo, Y.-L.; Ye, X.-D.; Zhu, Y.-H.; Yang, X.-Z.; Wang, J., Regulating the surface poly(ethylene glycol) density of polymeric nanoparticles and evaluating its role in drug delivery in vivo. *Biomaterials* **2015,** *69*, 1-11.
118. Attia, A. B.; Yang, C.; Tan, J. P.; Gao, S.; Williams, D. F.; Hedrick, J. L.; Yang, Y. Y., The effect of kinetic stability on biodistribution and anti-tumor efficacy of drug-loaded biodegradable polymeric micelles. *Biomaterials* **2013,** *34* (12), 3132-3140.
119. Owens, D. E., 3rd; Peppas, N. A., Opsonization, biodistribution, and pharmacokinetics of polymeric nanoparticles. *Int. J. Pharm.* **2006,** *307* (1), 93-102.
120. Le Dévédec, F.; Fuentealba, D.; Strandman, S.; Bohne, C.; Zhu, X. X., Aggregation behavior of pegylated bile acid derivatives. *Langmuir* **2012,** *28* (37), 13431-13440.
121. Le Dévédec, F.; Strandman, S.; Hildgen, P.; Leclair, G.; Zhu, X. X., PEGylated bile acids for use in drug delivery systems: Enhanced solubility and bioavailability of itraconazole. *Mol. Pharm.* **2013,** *10* (8), 3057-3066.
122. Allen, C.; Maysinger, D.; Eisenberg, A., Nano-engineering block copolymer aggregates for drug delivery. *Colloids Surf. B: Biointerfaces* **1999,** *16* (1), 3-27.
123. Astafieva, I.; Zhong, X. F.; Eisenberg, A., Critical micellization phenomena in block polyelectrolyte solutions. *Macromolecules* **1993,** *26* (26), 7339-7352.
124. Astafieva, I.; Khougaz, K.; Eisenberg, A., Micellization in block polyelectrolyte solutions. 2. fluorescence study of the critical micelle concentration as a function of soluble block length and salt concentration. *Macromolecules* **1995,** *28* (21), 7127-7134.
125. Despa, F.; Luo, J. T.; Li, J.; Duan, Y.; Lam, K. S., Cholic acid micelles—controlling the size of the aqueous cavity by PEGylation. *Phys. Chem. Chem. Phys.* **2010,** *12* (7), 1589-1594.
126. Ju, C.; Bohne, C., Dynamics of probe complexation to bile salt aggregates. *J. Phys. Chem.* **1996,** *100* (9), 3847-3854.
127. Luo, J.; Giguère, G.; Zhu, X. X., Asymmetric poly(ethylene glycol) star polymers with a cholic acid core and their aggregation properties. *Biomacromolecules* **2009,** *10* (4), 900-906.
128. Soo Choi, H.; Liu, W.; Misra, P.; Tanaka, E.; Zimmer, J. P.; Itty Ipe, B.; Bawendi, M. G.; Frangioni, J. V., Renal clearance of quantum dots. *Nat. Biotechnol.* **2007,** *25* (10), 1165-1170.
129. Lee, A. L.; Venkataraman, S.; Sirat, S. B.; Gao, S.; Hedrick, J. L.; Yang, Y. Y., The use of cholesterol-containing biodegradable block copolymers to exploit hydrophobic interactions for the delivery of anticancer drugs. *Biomaterials* **2012,** *33* (6), 1921-1928.

130. Yang, C.; Attia, A. B.; Tan, J. P.; Ke, X.; Gao, S.; Hedrick, J. L.; Yang, Y. Y., The role of non-covalent interactions in anticancer drug loading and kinetic stability of polymeric micelles. *Biomaterials* **2012,** *33* (10), 2971-2979.
131. Wang, C.; Wang, Z.; Zhang, X., Amphiphilic building blocks for self-assembly: from amphiphiles to supra-amphiphiles. *Acc. Chem. Res.* **2012,** *45* (4), 608-618.
132. Cha, E. J.; Kim, J. E.; Ahn, C. H., Stabilized polymeric micelles by electrostatic interactions for drug delivery system. *Eur. J. Pharm. Sci.* **2009,** *38* (4), 341-346.
133. Lübtow, M. M.; Marciniak, H.; Schmiedel, A.; Roos, M.; Lambert, C.; Luxenhofer, R., Ultra-high to ultra-low drug-loaded micelles: Probing host–guest interactions by fluorescence spectroscopy. *Chemistry* **2019,** *25* (54), 12601-12610.
134. Geng, W.-C.; Sessler, J. L.; Guo, D.-S., Supramolecular prodrugs based on host–guest interactions. *Chem. Soc. Rev.* **2020**, *49*, 2303-2315.
135. Braegelman, A. S.; Webber, M. J., Integrating stimuli-responsive properties in host-guest supramolecular drug delivery systems. *Theranostics* **2019,** *9* (11), 3017-3040.
136. Matsui, H.; Ueda, M.; Makino, A.; Kimura, S., Molecular assembly composed of a dendrimer template and block polypeptides through stereocomplex formation. *Chem. Comm.* **2012,** *48* (49), 6181-6183.
137. Lv, S.; Wu, Y.; Cai, K.; He, H.; Li, Y.; Lan, M.; Chen, X.; Cheng, J.; Yin, L., High drug loading and sub-quantitative loading efficiency of polymeric micelles driven by donor–receptor coordination interactions. *J. Am. Chem. Soc.* **2018,** *140* (4), 1235-1238.
138. Shen, S.; Wu, Y.; Liu, Y.; Wu, D., High drug-loading nanomedicines: progress, current status, and prospects. *Int. J. Nanomedicine* **2017,** *12*, 4085-4109.
139. Shi, Y.; van Steenbergen, M. J.; Teunissen, E. A.; Novo, L.; Gradmann, S.; Baldus, M.; van Nostrum, C. F.; Hennink, W. E., Pi-pi stacking increases the stability and loading capacity of thermosensitive polymeric micelles for chemotherapeutic drugs. *Biomacromolecules* **2013,** *14* (6), 1826-1837.
140. Wang, H.; Chen, J.; Xu, C.; Shi, L.; Tayier, M.; Zhou, J.; Zhang, J.; Wu, J.; Ye, Z.; Fang, T.; Han, W., Cancer nanomedicines stabilized by π-π stacking between heterodimeric prodrugs enable exceptionally high drug loading capacity and safer delivery of drug combinations. *Theranostics* **2017,** *7* (15), 3638-3652.
141. Zana, R.; Marques, C.; Johner, A., Dynamics of micelles of the triblock copolymers poly(ethylene oxide)-poly(propylene oxide)-poly(ethylene oxide) in aqueous solution. *Adv. Colloid Interface Sci.* **2006,** *123* (12), 345-351.
142. Haliloğlu, T.; Bahar, I.; Erman, B.; Mattice, W. L., Mechanisms of the exchange of diblock copolymers between micelles at dynamic equilibrium. *Macromolecules* **1996,** *29* (13), 4764-4771.
143. Gao, M.; Yang, Y.; Bergfel, A.; Huang, L.; Zheng, L.; Bowden, T. M., Self-assembly of cholesterol end-capped polymer micelles for controlled drug delivery. *J. Nanobiotechnol.* **2020,** *18* (1), 13-23.
144. Huang, X.; Liao, W.; Zhang, G.; Kang, S.; Zhang, C. Y., pH-sensitive micelles self-assembled from polymer brush (PAE-g-cholesterol)-b-PEG-b-(PAE-g-cholesterol) for anticancer drug delivery and controlled release. *Int. J. Nanomedicine* **2017,** *12*, 2215-2226.

145. Xiao, K.; Li, Y.; Luo, J.; Lee, J. S.; Xiao, W.; Gonik, A. M.; Agarwal, R. G.; Lam, K. S., The effect of surface charge on in vivo biodistribution of PEG-oligocholic acid based micellar nanoparticles. *Biomaterials* **2011,** *32* (13), 3435-3446.
146. Zeng, X.; Tao, W.; Mei, L.; Huang, L.; Tan, C.; Feng, S. S., Cholic acid-functionalized nanoparticles of star-shaped PLGA-vitamin E TPGS copolymer for docetaxel delivery to cervical cancer. *Biomaterials* **2013,** *34* (25), 6058-6067.
147. Li, J.; Huo, M.; Wang, J.; Zhou, J.; Mohammad, J. M.; Zhang, Y.; Zhu, Q.; Waddad, A. Y.; Zhang, Q., Redox-sensitive micelles self-assembled from amphiphilic hyaluronic acid-deoxycholic acid conjugates for targeted intracellular delivery of paclitaxel. *Biomaterials* **2012,** *33* (7), 2310-2320.
148. Wang, R.; Xiao, H.; Song, H.; Zhang, Y.; Hu, X.; Xie, Z.; Huang, Y.; Jing, X.; Li, Y., Co-delivery of all-trans-retinoic-acid and cisplatin(iv) prodrug based on polymer–drug conjugates for enhanced efficacy and safety. *J. Mater. Chem.* **2012,** *22* (48), 25453-25462.
149. Yang, C.; Wu, T.; Qi, Y.; Zhang, Z., Recent advances in the application of vitamin E TPGS for drug delivery. *Theranostics* **2018,** *8* (2), 464-485.
150. Kedar, U.; Phutane, P.; Shidhaye, S.; Kadam, V., Advances in polymeric micelles for drug delivery and tumor targeting. *Nanomedicine* **2010,** *6* (6), 714-729.
151. Kamaly, N.; Yameen, B.; Wu, J.; Farokhzad, O. C., Degradable controlled-release polymers and polymeric nanoparticles: Mechanisms of controlling drug release. *Chem. Rev.* **2016,** *116* (4), 2602-2663.
152. Fredenberg, S.; Wahlgren, M.; Reslow, M.; Axelsson, A., The mechanisms of drug release in poly(lactic-co-glycolic acid)-based drug delivery systems--a review. *Int. J. Pharm.* **2011,** *415* (1), 34-52.
153. Webber, W. L.; Lago, F.; Thanos, C.; Mathiowitz, E., Characterization of soluble, salt-loaded, degradable PLGA films and their release of tetracycline. *J. Biomed. Mater. Res.* **1998,** *41* (1), 18-29.
154. Keraliya, R. A.; Patel, C.; Patel, P.; Keraliya, V.; Soni, T. G.; Patel, R. C.; Patel, M. M., Osmotic drug delivery system as a part of modified release dosage form. *ISRN Pharm.* **2012,** *2012*, 528079.
155. Uhrich, K. E.; Cannizzaro, S. M.; Langer, R. S.; Shakesheff, K. M., Polymeric systems for controlled drug release. *Chem. Rev.* **1999,** *99* (11), 3181-3198.
156. Huang, X.; Brazel, C. S., On the importance and mechanisms of burst release in matrix-controlled drug delivery systems. *J. Control. Release* **2001,** *73* (2), 121-136.
157. Yin, Q.; Shen, J.; Zhang, Z.; Yu, H.; Li, Y., Reversal of multidrug resistance by stimuli-responsive drug delivery systems for therapy of tumor. *Adv. Drug Deliv. Rev.* **2013,** *65* (13), 1699-1715.
158. Schafer, F. Q.; Buettner, G. R., Redox environment of the cell as viewed through the redox state of the glutathione disulfide/glutathione couple. *Free Radic. Biol. Med.* **2001,** *30* (11), 1191-1212.
159. Cheng, W.; Gu, L.; Ren, W.; Liu, Y., Stimuli-responsive polymers for anti-cancer drug delivery. *Mater. Sci. Eng. C* **2014,** *45*, 600-608.
160. Huo, M.; Yuan, J.; Tao, L.; Wei, Y., Redox-responsive polymers for drug delivery: from molecular design to applications. *Polym. Chem.* **2014,** *5* (5), 1519-1528.

161. Sun, H.; Guo, B.; Cheng, R.; Meng, F.; Liu, H.; Zhong, Z., Biodegradable micelles with sheddable poly(ethylene glycol) shells for triggered intracellular release of doxorubicin. *Biomaterials* **2009,** *30* (31), 6358-6366.
162. Han, K.; Zhu, J.-Y.; Wang, S.-B.; Li, Z.-H.; Cheng, S.-X.; Zhang, X.-Z., Tumor targeted gold nanoparticles for FRET-based tumor imaging and light responsive on-demand drug release. *J. Mater. Chem. B* **2015,** *3* (41), 8065-8069.
163. Broaders, K. E.; Grandhe, S.; Fréchet, J. M. J., A biocompatible oxidation-triggered carrier polymer with potential in therapeutics. *J. Am. Chem. Soc.* **2011,** *133* (4), 756-758.
164. de Gracia Lux, C.; Joshi-Barr, S.; Nguyen, T.; Mahmoud, E.; Schopf, E.; Fomina, N.; Almutairi, A., Biocompatible polymeric nanoparticles degrade and release cargo in response to biologically relevant levels of hydrogen peroxide. *J. Am. Chem. Soc.* **2012,** *134* (38), 15758-15764.
165. Liberti, M. V.; Locasale, J. W., The warburg effect: How does it benefit cancer cells? *Trends Biochem. Sci.* **2016,** *41* (3), 211-218.
166. Ulbrich, K.; Šubr, V. r., Polymeric anticancer drugs with pH-controlled activation. *Adv. Drug Deliv. Rev.* **2004,** *56* (7), 1023-1050.
167. Kocak, G.; Tuncer, C.; Bütün, V., pH-Responsive polymers. *Polym. Chem.* **2017,** *8* (1), 144-176.
168. Kim, G. M.; Bae, Y. H.; Jo, W. H., pH-induced micelle formation of poly(histidine-co-phenylalanine)-block-poly(ethylene glycol) in aqueous media. *Macromol. Biosci.* **2005,** *5* (11), 1118-1124.
169. Hu, J.; He, J.; Zhang, M.; Ni, P., Precise modular synthesis and a structure–property study of acid-cleavable star-block copolymers for pH-triggered drug delivery. *Polym. Chem.* **2015,** *6* (9), 1553-1566.
170. Zhang, Q.; Weber, C.; Schubert, U. S.; Hoogenboom, R., Thermoresponsive polymers with lower critical solution temperature: from fundamental aspects and measuring techniques to recommended turbidimetry conditions. *Mater. Horiz.* **2017,** *4* (2), 109-116.
171. Parmar, I. A.; Shedge, A. S.; Badiger, M. V.; Wadgaonkar, P. P.; Lele, A. K., Thermo-reversible sol–gel transition of aqueous solutions of patchy polymers. *RSC Advances* **2017,** *7* (9), 5101-5110.
172. Sponchioni, M.; Capasso Palmiero, U.; Moscatelli, D., Thermo-responsive polymers: Applications of smart materials in drug delivery and tissue engineering. *Mater. Sci. Eng. C* **2019,** *102*, 589-605.
173. Klouda, L.; Mikos, A. G., Thermoresponsive hydrogels in biomedical applications. *Eur. J. Pharm. Biopharm.* **2008,** *68* (1), 34-45.
174. Bromberg, L. E.; Ron, E. S., Temperature-responsive gels and thermogelling polymer matrices for protein and peptide delivery. *Adv. Drug Deliv. Rev.* **1998,** *31* (3), 197-221.
175. Gandhi, S. S.; Yan, H.; Kim, C., Thermoresponsive gelatin nanogels. *ACS Macro Lett.* **2014,** *3* (11), 1210-1214.
176. Wu, H.-Q.; Wang, C.-C., Biodegradable smart nanogels: A new platform for targeting drug delivery and biomedical diagnostics. *Langmuir* **2016,** *32* (25), 6211-6225.

177. Zhang, J. L.; Srivastava, R. S.; Misra, R. D. K., Core−shell magnetite nanoparticles surface encapsulated with smart stimuli-responsive polymer: Synthesis, characterization, and LCST of viable drug-targeting delivery system. *Langmuir* **2007,** *23* (11), 6342-6351.
178. Wang, J.; Ayano, E.; Maitani, Y.; Kanazawa, H., Tunable surface properties of temperature-responsive polymer-modified liposomes induce faster cellular uptake. *ACS Omega* **2017,** *2* (1), 316-325.
179. Kim, Y.-J.; Matsunaga, Y. T., Thermo-responsive polymers and their application as smart biomaterials. *J. Mater. Chem. B* **2017,** *5* (23), 4307-4321.
180. Bae, Y. C.; Lambert, S. M.; Soane, D. S.; Prausnitz, J. M., Cloud-point curves of polymer solutions from thermooptical measurements. *Macromolecules* **1991,** *24* (15), 4403-4407.
181. Aoyagi, T.; Ebara, M.; Sakai, K.; Sakurai, Y.; Okano, T., Novel bifunctional polymer with reactivity and temperature sensitivity. *J. Biomater. Sci.* **2000,** *11* (1), 101-110.
182. Yoshida, T.; Aoyagi, T.; Kokufuta, E.; Okano, T., Newly designed hydrogel with both sensitive thermoresponse and biodegradability. *J. Polym. Sci. Part A: Polym. Chem.* **2003,** *41* (6), 779-787.
183. Maeda, T.; Yamamoto, K.; Aoyagi, T., Importance of bound water in hydration-dehydration behavior of hydroxylated poly(N-isopropylacrylamide). *J. Colloid Inter. Sci.* **2006,** *302* (2), 467-474.
184. Yu, L.; Ding, J., Injectable hydrogels as unique biomedical materials. *Chem. Soc. Rev.* **2008,** *37* (8), 1473-1481.
185. Guo-liang, Y.; Qian-ling, C.; Yu-xi, Z.; Er-jian, W.; Fei-peng, W. Thermo-responsive block copolymers based on linear-type poly(ethylene glycol): Tunable LCST within the physiological range. *Chinese J. Polym. Sci.* **2012,** *30*, 770-776.
186. Maleki, A.; Zhu, K.; Pamies, R.; Schmidt, R. R.; Kjøniksen, A.-L.; Karlsson, G.; Hernández Cifre, J. G.; García de la Torre, J.; Nyström, B., Effect of polyethylene glycol (PEG) length on the association properties of temperature-sensitive amphiphilic triblock copolymers (PNIPAAMm-b-PEGn-b-PNIPAAMm) in aqueous solution. *Soft Matter* **2011,** *7* (18), 8111-8119.
187. Tamaki, M.; Kojima, C., pH-Switchable LCST/UCST-type thermosensitive behaviors of phenylalanine-modified zwitterionic dendrimers. *RSC Advances* **2020,** *10* (18), 10452-10460.
188. Pei, Y.; Chen, J.; Yang, L.; Shi, L.; Tao, Q.; Hui, B.; Li, J., The effect of pH on the LCST of poly(N-isopropylacrylamide) and poly(N-isopropylacrylamide-co-acrylic acid). *J. Biomater. Sci.* **2004,** *15* (5), 585-594.
189. Freitag, R.; Garret-Flaudy, F., Salt effects on the thermoprecipitation of Poly-(N-isopropylacrylamide) oligomers from aqueous solution. *Langmuir* **2002,** *18* (9), 3434-3440.
190. Liu, X.; Cheng, F.; Liu, H.; Chen, Y., Unusual salt effect on the lower critical solution temperature of hyperbranched thermoresponsive polymers. *Soft Matter* **2008,** *4* (10), 1991-1994.
191. Du, H.; Wickramasinghe, R.; Qian, X., Effects of salt on the lower critical solution temperature of poly (N-isopropylacrylamide). *J. Phys. Chem. B* **2010,** *114* (49), 16594-16604.

192. Lee, S. B.; Song, S. C.; Jin, J. I.; Sohn, Y. S., Surfactant effect on the lower critical solution temperature of poly(organophosphazenes) with methoxy-poly(ethylene glycol) and amino acid esters as side groups. *Colloid Polym. Sci.* **2000,** *278* (11), 1097-1102.
193. Lee, L.-T.; Cabane, B., Effects of surfactants on thermally collapsed poly(N-isopropylacrylamide) macromolecules. *Macromolecules* **1997,** *30* (21), 6559-6566.
194. Bharadwaj, S.; Kumar, P. B. S.; Komura, S.; Deshpande, A. P., Kosmotropic effect leads to LCST decrease in thermoresponsive polymer solutions. *J. Chem. Phys.* **2018,** *148* (8), 1-13.
195. Bloksma, M. M.; Bakker, D. J.; Weber, C.; Hoogenboom, R.; Schubert, U. S., The effect of hofmeister salts on the LCST transition of poly(2-oxazoline)s with varying hydrophilicity. *Macromol. Rapid Commun.* **2010,** *31* (8), 724-728.
196. Zhang, Y.; Furyk, S.; Sagle, L. B.; Cho, Y.; Bergbreiter, D. E.; Cremer, P. S., Effects of hofmeister anions on the LCST of PNIPAM as a function of molecular weight. *J. Phys. Chem. C Nanomater. Interfaces* **2007,** *111* (25), 8916-8924.
197. Kang, B.; Tang, H.; Zhao, Z.; Song, S., Hofmeister series: Insights of ion specificity from amphiphilic assembly and interface property. *ACS Omega* **2020,** *5* (12), 6229-6239.
198. Zhang, Y.; Furyk, S.; Bergbreiter, D. E.; Cremer, P. S., Specific ion effects on the water solubility of macromolecules: PNIPAM and the hofmeister series. *J. Am. Chem. Soc.* **2005,** *127* (41), 14505-14510.
199. Sang, Y.; Xie, K.; Mu, Y.; Lei, Y.; Zhang, B.; Xiong, S.; Chen, Y.; Qi, N., Salt ions and related parameters affect PEI-DNA particle size and transfection efficiency in Chinese hamster ovary cells. *Cytotechnology* **2015,** *67* (1), 67-74.
200. Jette, K. K.; Law, D.; Schmitt, E. A.; Kwon, G. S., Preparation and drug loading of poly(ethylene gycol)-block-poly(ε-caprolactone) micelles through the evaporation of a cosolvent azeotrope. *Pharm. Res.* **2004,** *21* (7), 1184-1191.
201. Adams, M. L.; Kwon, G. S., Relative aggregation state and hemolytic activity of amphotericin B encapsulated by poly(ethylene oxide)-block–poly(N-hexyl-l-aspartamide)-acyl conjugate micelles: effects of acyl chain length. *J. Control. Release* **2003,** *87* (1), 23-32.
202. Alexandridis, P.; Holzwarth, J. F.; Hatton, T. A., Micellization of poly(ethylene oxide)-poly(propylene oxide)-poly(ethylene oxide) triblock copolymers in aqueous solutions: thermodynamics of copolymer association. *Macromolecules* **1994,** *27* (9), 2414-2425.
203. Alexandridis, P.; Athanassiou, V.; Fukuda, S.; Hatton, T. A., Surface activity of poly(ethylene oxide)-block-poly(propylene oxide)-block-poly(ethylene oxide) copolymers. *Langmuir* **1994,** *10* (8), 2604-2612.
204. Kabanov, A. V.; Batrakova, E. V.; Alakhov, V. Y., Pluronic® block copolymers as novel polymer therapeutics for drug and gene delivery. *J. Control. Release* **2002,** *82* (2), 189-212.
205. Ranger, M.; Jones, M.-C.; Yessine, M.-A.; Leroux, J.-C., From well-defined diblock copolymers prepared by a versatile atom transfer radical polymerization method to supramolecular assemblies. *J. Polym. Sci. Part A: Polym. Chem.* **2001,** *39* (22), 3861-3874.

206. Hussein, Y. H. A.; Youssry, M., Polymeric micelles of biodegradable diblock copolymers: enhanced encapsulation of hydrophobic drugs. *Materials* **2018,** *11* (5), 688-714.
207. Li, Z.; Yuan, D.; Fan, X.; Tan, B. H.; He, C., Poly(ethylene glycol) conjugated poly(lactide)-based polyelectrolytes: Synthesis and formation of stable self-assemblies induced by stereocomplexation. *Langmuir* **2015,** *31* (8), 2321-2333.
208. Creutz, S.; van Stam, J.; De Schryver, F. C.; Jérôme, R., Dynamics of poly((dimethylamino)alkyl methacrylate-block-sodium methacrylate) micelles. Influence of hydrophobicity and molecular architecture on the exchange rate of copolymer molecules. *Macromolecules* **1998,** *31* (3), 681-689.
209. Yokoyama, M.; Fukushima, S.; Uehara, R.; Okamoto, K.; Kataoka, K.; Sakurai, Y.; Okano, T., Characterization of physical entrapment and chemical conjugation of adriamycin in polymeric micelles and their design for in vivo delivery to a solid tumor. *J. Control. Release* **1998,** *50* (1), 79-92.
210. Gunawan, C.; Lim, M.; Marquis, C. P.; Amal, R., Nanoparticle–protein corona complexes govern the biological fates and functions of nanoparticles. *J. Mater. Chem. B* **2014,** *2* (15), 2060-2083.
211. Nguyen, V. H.; Lee, B. J., Protein corona: a new approach for nanomedicine design. *Int. J. Nanomedicine* **2017,** *12*, 3137-3151.
212. Alexis, F.; Pridgen, E.; Molnar, L. K.; Farokhzad, O. C., Factors affecting the clearance and biodistribution of polymeric nanoparticles. *Mol. Pharm.* **2008,** *5* (4), 505-515.
213. Blanco, E.; Shen, H.; Ferrari, M., Principles of nanoparticle design for overcoming biological barriers to drug delivery. *Nat. Biotechnol.* **2015,** *33* (9), 941-951.
214. Walkey, C. D.; Olsen, J. B.; Song, F.; Liu, R.; Guo, H.; Olsen, D. W. H.; Cohen, Y.; Emili, A.; Chan, W. C. W., Protein corona fingerprinting predicts the cellular interaction of gold and silver nanoparticles. *ACS Nano* **2014,** *8* (3), 2439-2455.
215. Walkey, C. D.; Olsen, J. B.; Guo, H.; Emili, A.; Chan, W. C. W., Nanoparticle size and surface chemistry determine serum protein adsorption and macrophage uptake. *J. Am. Chem. Soc.* **2012,** *134* (4), 2139-2147.
216. Zagorovsky, K.; Chou, L. Y. T.; Chan, W. C. W., Controlling DNA–nanoparticle serum interactions. *Proc. Natl. Acad. Sci.* **2016,** *113* (48), 13600-13605.
217. Walkey, C. D.; Chan, W. C. W., Understanding and controlling the interaction of nanomaterials with proteins in a physiological environment. *Chem. Soc. Rev.* **2012,** *41* (7), 2780-2799.
218. Hossen, M. N.; Murphy, B.; García-Hevia, L.; Bhattacharya, R.; Mukherjee, P., Probing cellular processes using engineered nanoparticles. *Bioconjug. Chem.* **2018,** *29* (6), 1793-1808.
219. Yang, C.; Gao, S.; Dagnaes-Hansen, F.; Jakobsen, M.; Kjems, J., Impact of PEG chain length on the physical properties and bioactivity of PEGylated chitosan/siRNA nanoparticles in vitro and in vivo. *ACS Appl. Mater. Interfaces* **2017,** *9* (14), 12203-12216.
220. Knop, K.; Hoogenboom, R.; Fischer, D.; Schubert, U. S., Poly(ethylene glycol) in drug delivery: pros and cons as well as potential alternatives. *Angew. Chem. Int. Ed.* **2010,** *49* (36), 6288-6308.

221. Verhoef, J. J. F.; Anchordoquy, T. J., Questioning the use of PEGylation for drug delivery. *Drug Deliv. Transl. Res.* **2013,** *3* (6), 499-503.
222. Suk, J. S.; Xu, Q.; Kim, N.; Hanes, J.; Ensign, L. M., PEGylation as a strategy for improving nanoparticle-based drug and gene delivery. *Adv. Drug Deliv. Rev.* **2016,** *99*, 28-51.
223. Dos Santos, N.; Allen, C.; Doppen, A. M.; Anantha, M.; Cox, K. A.; Gallagher, R. C.; Karlsson, G.; Edwards, K.; Kenner, G.; Samuels, L.; Webb, M. S.; Bally, M. B., Influence of poly(ethylene glycol) grafting density and polymer length on liposomes: relating plasma circulation lifetimes to protein binding. *Biochim. Biophys. Acta* **2007,** *1768* (6), 1367-1377.
224. Abstiens, K.; Maslanka Figueroa, S.; Gregoritza, M.; Goepferich, A. M., Interaction of functionalized nanoparticles with serum proteins and its impact on colloidal stability and cargo leaching. *Soft Matter* **2019,** *15* (4), 709-720.
225. Cagliani, R.; Gatto, F.; Bardi, G., Protein adsorption: A feasible method for nanoparticle functionalization? *Materials* **2019,** *12* (12), 1991-2002.
226. Aggarwal, P.; Hall, J. B.; McLeland, C. B.; Dobrovolskaia, M. A.; McNeil, S. E., Nanoparticle interaction with plasma proteins as it relates to particle biodistribution, biocompatibility and therapeutic efficacy. *Adv. Drug Deliv. Rev.* **2009,** *61* (6), 428-437.
227. Alyautdin, R. N.; Tezikov, E. B.; Ramge, P.; Kharkevich, D. A.; Begley, D. J.; Kreuter, J., Significant entry of tubocurarine into the brain of rats by adsorption to polysorbate 80-coated polybutylcyanoacrylate nanoparticles: an in situ brain perfusion study. *J. Microencapsul.* **1998,** *15* (1), 67-74.
228. Goppert, T. M.; Muller, R. H., Polysorbate-stabilized solid lipid nanoparticles as colloidal carriers for intravenous targeting of drugs to the brain: comparison of plasma protein adsorption patterns. *J. Drug Target* **2005,** *13* (3), 179-187.
229. Caracciolo, G.; Cardarelli, F.; Pozzi, D.; Salomone, F.; Maccari, G.; Bardi, G.; Capriotti, A. L.; Cavaliere, C.; Papi, M.; Lagana, A., Selective targeting capability acquired with a protein corona adsorbed on the surface of 1,2-dioleoyl-3-trimethylammonium propane/DNA nanoparticles. *ACS Appl. Mater. Interfaces* **2013,** *5* (24), 13171-13179.
230. Fang, J.; Nakamura, H.; Maeda, H., The EPR effect: Unique features of tumor blood vessels for drug delivery, factors involved, and limitations and augmentation of the effect. *Adv. Drug Deliv. Rev.* **2011,** *63* (3), 136-151.
231. Peer, D.; Karp, J. M.; Hong, S.; Farokhzad, O. C.; Margalit, R.; Langer, R., Nanocarriers as an emerging platform for cancer therapy. *Nat. Nanotechnol.* **2007,** *2* (12), 751-760.
232. Félétou, M., *The Endothelium: Part 1: Multiple functions of the endothelial cells—Focus on endothelium-derived vasoactive mediators.* Morgan & Claypool Life Sciences: San Rafael (CA), 2011.
233. Aird, W. C., Phenotypic heterogeneity of the endothelium. *Circ. Res.* **2007,** *100* (2), 158-173.
234. Rajabi, M.; Mousa, S. A., The role of angiogenesis in cancer treatment. *Biomedicines* **2017,** *5* (2), 34-46.

235. Siemann, D. W., The unique characteristics of tumor vasculature and preclinical evidence for its selective disruption by Tumor-Vascular Disrupting Agents. *Cancer Treat. Rev.* **2011,** *37* (1), 63-74.
236. Kalyane, D.; Raval, N.; Maheshwari, R.; Tambe, V.; Kalia, K.; Tekade, R. K., Employment of enhanced permeability and retention effect (EPR): Nanoparticle-based precision tools for targeting of therapeutic and diagnostic agent in cancer. *Mater. Sci. Eng. C* **2019,** *98*, 1252-1276.
237. Leu, A. J.; Berk, D. A.; Lymboussaki, A.; Alitalo, K.; Jain, R. K., Absence of functional lymphatics within a murine sarcoma: a molecular and functional evaluation. *Cancer Res.* **2000,** *60* (16), 4324-4327.
238. Padera, T. P.; Kadambi, A.; di Tomaso, E.; Carreira, C. M.; Brown, E. B.; Boucher, Y.; Choi, N. C.; Mathisen, D.; Wain, J.; Mark, E. J.; Munn, L. L.; Jain, R. K., Lymphatic metastasis in the absence of functional intratumor lymphatics. *Science* **2002,** *296* (5574), 1883-1886.
239. Fang, J.; Nakamura, H.; Maeda, H., The EPR effect: Unique features of tumor blood vessels for drug delivery, factors involved, and limitations and augmentation of the effect. *Adv. Drug Deliv. Rev.* **2011,** *63* (3), 136-151.
240. Barenholz, Y., Doxil® — The first FDA-approved nano-drug: Lessons learned. *J. Control. Release* **2012,** *160* (2), 117-134.
241. Zhang, Y.-N.; Poon, W.; Tavares, A. J.; McGilvray, I. D.; Chan, W. C. W., Nanoparticle–liver interactions: Cellular uptake and hepatobiliary elimination. *J. Control. Release* **2016,** *240*, 332-348.
242. Li, C. J.; Miyamoto, Y.; Kojima, Y.; Maeda, H., Augmentation of tumour delivery of macromolecular drugs with reduced bone marrow delivery by elevating blood pressure. *Br. J. Cancer* **1993,** *67* (5), 975-980.
243. Torosean, S.; Flynn, B.; Axelsson, J.; Gunn, J.; Samkoe, K. S.; Hasan, T.; Doyley, M. M.; Pogue, B. W., Nanoparticle uptake in tumors is mediated by the interplay of vascular and collagen density with interstitial pressure. *Nanomedicine* **2013,** *9* (2), 151-158.
244. Mattheolabakis, G.; Mikelis, C. M., Nanoparticle delivery and tumor vascular normalization: The chicken or the egg? *Front. Oncol.* **2019,** *9*, 1227-1227.
245. Goel, S.; Wong, A. H.-K.; Jain, R. K., Vascular normalization as a therapeutic strategy for malignant and nonmalignant disease. *Cold Spring Harb. Perspect. Med.* **2012,** *2* (3), a006486.
246. Jiang, W.; Huang, Y.; An, Y.; Kim, B. Y. S., Remodeling tumor vasculature to enhance delivery of intermediate-sized nanoparticles. *ACS Nano* **2015,** *9* (9), 8689-8696.
247. Nel, A.; Ruoslahti, E.; Meng, H. New insights into “permeability” as in the enhanced permeability and retention effect of cancer nanotherapeutics. *ACS Nano* **2017,** *11* (10), 9567-9569.
248. Liu, X.; Jiang, J.; Meng, H., Transcytosis - An effective targeting strategy that is complementary to "EPR effect" for pancreatic cancer nano drug delivery. *Theranostics* **2019,** *9* (26), 8018-8025.
249. Dvorak, A. M.; Kohn, S.; Morgan, E. S.; Fox, P.; Nagy, J. A.; Dvorak, H. F., The vesiculo-vacuolar organelle (VVO): a distinct endothelial cell structure that

provides a transcellular pathway for macromolecular extravasation. *J. Leukoc. Biol.* **1996,** *59* (1), 100-115.
250. Feng, D.; Nagy, J. A.; Hipp, J.; Dvorak, H. F.; Dvorak, A. M., Vesiculo-vacuolar organelles and the regulation of venule permeability to macromolecules by vascular permeability factor, histamine, and serotonin. *J. Exp. Med.* **1996,** *183* (5), 1981-1986.
251. Pang, H.-B.; Braun, G. B.; Friman, T.; Aza-Blanc, P.; Ruidiaz, M. E.; Sugahara, K. N.; Teesalu, T.; Ruoslahti, E., An endocytosis pathway initiated through neuropilin-1 and regulated by nutrient availability. *Nat. Comm.* **2014,** *5* (1), 4904-4916.
252. Nichols, J. W.; Bae, Y. H., Odyssey of a cancer nanoparticle: from injection site to site of action. *Nano Today* **2012,** *7* (6), 606-618.
253. Woodcock, T., Plasma volume, tissue oedema, and the steady-state Starling principle. *BJA Education* **2016,** *17* (2), 74-78.
254. Hu, X.; Adamson, R. H.; Liu, B.; Curry, F. E.; Weinbaum, S., Starling forces that oppose filtration after tissue oncotic pressure is increased. *Am. J. Phys. Heart Circ. Physiol.* **2000,** *279* (4), 1724-1736.
255. Pluen, A.; Netti, P. A.; Jain, R. K.; Berk, D. A., Diffusion of macromolecules in agarose gels: comparison of linear and globular configurations. *Biophys. J.* **1999,** *77* (1), 542-552.
256. Ramanujan, S.; Pluen, A.; McKee, T. D.; Brown, E. B.; Boucher, Y.; Jain, R. K., Diffusion and convection in collagen gels: implications for transport in the tumor interstitium. *Biophys. J.* **2002,** *83* (3), 1650-1660.
257. Alexandrakis, G.; Brown, E. B.; Tong, R. T.; McKee, T. D.; Campbell, R. B.; Boucher, Y.; Jain, R. K., Two-photon fluorescence correlation microscopy reveals the two-phase nature of transport in tumors. *Nat. Med.* **2004,** *10* (2), 203-207.
258. Raeesi, V.; Chan, W. C., Improving nanoparticle diffusion through tumor collagen matrix by photo-thermal gold nanorods. *Nanoscale* **2016,** *8* (25), 12524-12530.
259. Pluen, A.; Boucher, Y.; Ramanujan, S.; McKee, T. D.; Gohongi, T.; di Tomaso, E.; Brown, E. B.; Izumi, Y.; Campbell, R. B.; Berk, D. A.; Jain, R. K., Role of tumor-host interactions in interstitial diffusion of macromolecules: cranial vs. subcutaneous tumors. *Proc. Natl. Acad. Sci.* **2001,** *98* (8), 4628-4633.
260. Chou, L. Y.; Ming, K.; Chan, W. C., Strategies for the intracellular delivery of nanoparticles. *Chem. Soc. Rev.* **2011,** *40* (1), 233-245.
261. Nelemans, L. C.; Gurevich, L., Drug delivery with polymeric nanocarriers-cellular uptake mechanisms. *Materials* **2020,** *13* (2), 366-387.
262. Conner, S. D.; Schmid, S. L., Regulated portals of entry into the cell. *Nature* **2003,** *422* (6927), 37-44.
263. Canton, I.; Battaglia, G., Endocytosis at the nanoscale. *Chem. Soc. Rev.* **2012,** *41* (7), 2718-2739.
264. Sahay, G.; Alakhova, D. Y.; Kabanov, A. V., Endocytosis of nanomedicines. *J. Control. Release* **2010,** *145* (3), 182-195.
265. Doherty, G. J.; McMahon, H. T., Mechanisms of endocytosis. *Ann. Rev. Biochem.* **2009,** *78* (1), 857-902.
266. Behzadi, S.; Serpooshan, V.; Tao, W.; Hamaly, M. A.; Alkawareek, M. Y.; Dreaden, E. C.; Brown, D.; Alkilany, A. M.; Farokhzad, O. C.; Mahmoudi, M.,

Cellular uptake of nanoparticles: journey inside the cell. *Chem. Soc. Rev.* **2017,** *46* (14), 4218-4244.
267. Foroozandeh, P.; Aziz, A. A., Insight into cellular uptake and intracellular trafficking of nanoparticles. *Nanoscale Res. Lett.* **2018,** *13* (1), 339-351.
268. Rejman, J.; Oberle, V.; Zuhorn, I. S.; Hoekstar, D., Size-dependent internalization of particles via the pathways of clathrin- and caveolae-mediated endocytosis. *Biochem. J.* **2004,** *377* (1), 159-169.
269. Panariti, A.; Miserocchi, G.; Rivolta, I., The effect of nanoparticle uptake on cellular behavior: disrupting or enabling functions? *Nanotechnol. Sci. Appl.* **2012,** *5*, 87-100.
270. Nishikawa, T.; Iwakiri, N.; Kaneko, Y.; Taguchi, A.; Fukushima, K.; Mori, H.; Morone, N.; Kadokawa, J.-i., Nitric oxide release in human aortic endothelial cells mediated by delivery of amphiphilic polysiloxane nanoparticles to caveolae. *Biomacromolecules* **2009,** *10* (8), 2074-2085.
271. Chithrani, B. D.; Chan, W. C. W., Elucidating the mechanism of cellular uptake and removal of protein-coated gold nanoparticles of different sizes and shapes. *Nano Lett.* **2007,** *7* (6), 1542-1550.
272. Jin, H.; Heller, D. A.; Sharma, R.; Strano, M. S., Size-dependent cellular uptake and expulsion of single-walled carbon nanotubes: Single particle tracking and a generic uptake model for nanoparticles. *ACS Nano* **2009,** *3* (1), 149-158.
273. Lu, F.; Wu, S.-H.; Hung, Y.; Mou, C.-Y., Size effect on cell uptake in well-suspended, uniform mesoporous silica nanoparticles. *Small* **2009,** *5* (12), 1408-1413.
274. Osaki, F.; Kanamori, T.; Sando, S.; Sera, T.; Aoyama, Y., A quantum dot conjugated sugar ball and its cellular uptake. On the size effects of endocytosis in the subviral region. *J. Am. Chem. Soc.* **2004,** *126* (21), 6520-6521.
275. Wang, S.-H.; Lee, C.-W.; Chiou, A.; Wei, P.-K., Size-dependent endocytosis of gold nanoparticles studied by three-dimensional mapping of plasmonic scattering images. *J. Nanobiotechnol.* **2010,** *8* (1), 33-46.
276. Gratton, S. E. A.; Ropp, P. A.; Pohlhaus, P. D.; Luft, J. C.; Madden, V. J.; Napier, M. E.; DeSimone, J. M., The effect of particle design on cellular internalization pathways. *Proc. Natl. Aca. Sci.* **2008,** *105* (33), 11613-11618.
277. Li, S.; Malmstadt, N., Deformation and poration of lipid bilayer membranes by cationic nanoparticles. *Soft Matter* **2013,** *9* (20), 4969-4976.
278. Dausend, J.; Musyanovych, A.; Dass, M.; Walther, P.; Schrezenmeier, H.; Landfester, K.; Mailänder, V., Uptake mechanism of oppositely charged fluorescent nanoparticles in HeLa cells. *Macromol. Biosci.* **2008,** *8* (12), 1135-1143.
279. Brandenberger, C.; Mühlfeld, C.; Ali, Z.; Lenz, A.-G.; Schmid, O.; Parak, W. J.; Gehr, P.; Rothen-Rutishauser, B., Quantitative evaluation of cellular uptake and trafficking of plain and polyethylene glycol-coated gold nanoparticles. *Small* **2010,** *6* (15), 1669-1678.
280. Li, Y.; Chen, X.; Gu, N., Computational investigation of interaction between nanoparticles and membranes: Hydrophobic/hydrophilic effect. *J. Phys. Chem. B* **2008,** *112* (51), 16647-16653.

281. Curtis, E. M.; Bahrami, A. H.; Weikl, T. R.; Hall, C. K., Modeling nanoparticle wrapping or translocation in bilayer membranes. *Nanoscale* **2015,** *7* (34), 14505-14514.
282. Wang, S.; Guo, H.; Li, Y.; Li, X., Penetration of nanoparticles across a lipid bilayer: effects of particle stiffness and surface hydrophobicity. *Nanoscale* **2019,** *11* (9), 4025-4034.
283. Zhang, R.; Qin, X.; Kong, F.; Chen, P.; Pan, G., Improving cellular uptake of therapeutic entities through interaction with components of cell membrane. *Drug Deliv.* **2019,** *26* (1), 328-342.
284. Vasir, J. K.; Labhasetwar, V., Targeted drug delivery in cancer therapy. *Technol. Cancer Res. Treat.* **2005,** *4* (4), 363-374.
285. Srinivasarao, M.; Low, P. S., Ligand-targeted drug delivery. *Chem. Rev.* **2017,** *117* (19), 12133-12164.
286. Narmani, A.; Rezvani, M.; Farhood, B.; Darkhor, P.; Mohammadnejad, J.; Amini, B.; Refahi, S.; Abdi Goushbolagh, N., Folic acid functionalized nanoparticles as pharmaceutical carriers in drug delivery systems. *Drug Dev. Res.* **2019,** *80* (4), 404-424.
287. Hami, Z.; Amini, M.; Ghazi-Khansari, M.; Rezayat, S. M.; Gilani, K., Doxorubicin-conjugated PLA-PEG-Folate based polymeric micelle for tumor-targeted delivery: synthesis and in vitro evaluation. *Daru* **2014,** *22* (1), 30-37.
288. Stella, B.; Arpicco, S.; Peracchia, M. T.; Desmaële, D.; Hoebeke, J.; Renoir, M.; D'Angelo, J.; Cattel, L.; Couvreur, P., Design of folic acid-conjugated nanoparticles for drug targeting. *J. Pharm. Sci.* **2000,** *89* (11), 1452-1464.
289. Kerdous, R.; Sureau, F.; Bour, A.; Bonneau, S., Release kinetics of an amphiphilic photosensitizer by block-polymer nanoparticles. *Int. J. Pharm.* **2015,** *495* (2), 750-760.
290. Till, U.; Gibot, L.; Mingotaud, A. F.; Ehrhart, J.; Wasungu, L.; Mingotaud, C.; Souchard, J. P.; Poinso, A.; Rols, M. P.; Violleau, F.; Vicendo, P., Drug release by direct jump from poly(ethylene-glycol-b-epsilon-caprolactone) nano-vector to cell membrane. *Molecules* **2016,** *21* (12), 1643-1658.
291. Xiao, L.; Xiong, X.; Sun, X.; Zhu, Y.; Yang, H.; Chen, H.; Gan, L.; Xu, H.; Yang, X., Role of cellular uptake in the reversal of multidrug resistance by PEG-b-PLA polymeric micelles. *Biomaterials* **2011,** *32* (22), 5148-5157.
292. Chen, H.; Kim, S.; Li, L.; Wang, S.; Park, K.; Cheng, J.-X., Release of hydrophobic molecules from polymer micelles into cell membranes revealed by Förster resonance energy transfer imaging. *Proc. Natl. Aca. Sci.* **2008,** *105* (18), 6596-6601.
293. Kiss, A. L.; Botos, E., Endocytosis via caveolae: alternative pathway with distinct cellular compartments to avoid lysosomal degradation? *J. Cell Mol. Med.* **2009,** *13* (7), 1228-1237.
294. Parton, R. G.; Richards, A. A., Lipid rafts and caveolae as portals for endocytosis: new insights and common mechanisms. *Traffic* **2003,** *4* (11), 724-738.
295. Pelkmans, L.; Fava, E.; Grabner, H.; Hannus, M.; Habermann, B.; Krausz, E.; Zerial, M., Genome-wide analysis of human kinases in clathrin- and caveolae/raft-mediated endocytosis. *Nature* **2005,** *436* (7047), 78-86.

296. Vermeulen, L. M. P.; De Smedt, S. C.; Remaut, K.; Braeckmans, K., The proton sponge hypothesis: Fable or fact? *Eur. J. Pharm. Biopharm.* **2018,** *129*, 184-190.
297. Curtis, K. A.; Miller, D.; Millard, P.; Basu, S.; Horkay, F.; Chandran, P. L., Unusual salt and pH induced changes in polyethylenimine solutions. *PLoS One* **2016,** *11* (9), e0158147.
298. Benjaminsen, R. V.; Mattebjerg, M. A.; Henriksen, J. R.; Moghimi, S. M.; Andresen, T. L., The possible "proton sponge " effect of polyethylenimine (PEI) does not include change in lysosomal pH. *Mol. Ther.* **2013,** *21* (1), 149-157.
299. Sun, C.; Tang, T.; Uludag, H.; Cuervo, J. E., Molecular dynamics simulations of DNA/PEI complexes: effect of PEI branching and protonation state. *Biophys. J.* **2011,** *100* (11), 2754-2763.
300. van de Wetering, P.; Moret, E. E.; Schuurmans-Nieuwenbroek, N. M.; van Steenbergen, M. J.; Hennink, W. E., Structure-activity relationships of water-soluble cationic methacrylate/methacrylamide polymers for nonviral gene delivery. *Bioconjug. Chem.* **1999,** *10* (4), 589-597.
301. Haensler, J.; Szoka, F. C., Jr., Polyamidoamine cascade polymers mediate efficient transfection of cells in culture. *Bioconjug. Chem.* **1993,** *4* (5), 372-379.
302. Giguère, G.; Zhu, X. X., Functional star polymers with a cholic acid core and their thermosensitive properties. *Biomacromolecules* **2010,** *11* (1), 201-206.
303. Giguère, G.; Zhu, X. X., Synthesis and aggregation properties of anionic star-shaped polymers with cholic acid cores and polyacrylate arms. *J. Polym. Sci. Part A: Polym. Chem.* **2007,** *45* (17), 4173-4178.
304. Washington, K. E.; Kularatne, R. N.; Biewer, M. C.; Stefan, M. C., Combination loading of doxorubicin and resveratrol in polymeric micelles for increased loading efficiency and efficacy. *ACS Biomater. Sci. Eng.* **2018,** *4* (3), 997-1004.
305. Feng, H.; Chu, D.; Li, Z.; Guo, Z.; Jin, L.; Fan, B.; Zhang, J.; Li, J., A DOX-loaded polymer micelle for effectively inhibiting cancer cells. *RSC Advances* **2018,** *8* (46), 25949-25954.
306. Cunningham, A. J.; Zhu, X. X., Polymers made of bile acids: from soft to hard biomaterials. *Can. J. Chem.* **2016,** *94* (8), 659-666.
307. Cunningham, A. J.; Robinson, M.; Banquy, X.; Leblond, J.; Zhu, X. X., Bile acid-based drug delivery systems for enhanced doxorubicin encapsulation: Comparing hydrophobic and ionic interactions in drug loading and release. *Mol. Pharm.* **2018,** *15* (3), 1266-1276.
308. Cunningham, A. J.; Gibson, V. P.; Banquy, X.; Zhu, X. X.; Leblond J., Cholic acid-based mixed micelles as siRNA delivery agents for gene therapy. *Int. J. Pharm.* **2020,** *578*, 119078.

Chapter 2. Polymers made of bile acids: From soft to hard biomaterials.*

Abstract

Bile acids are gaining increasing importance as building blocks in the development of novel polymeric materials. This is evidenced by the growing number of publications advocating the advantages of their incorporation in the design and construction of materials. Composed of a rigid steroid backbone, functional groups with potential towards diverse reactions, and a biocompatible framework, there are various ways in which these molecules can be utilized to afford biomaterials via distinct architectures. Soft materials utilize the intrinsic capacity of bile acids to self-assemble and have seen a range of applications most notably in the field of drug delivery. On the other hand, there is also the possibility of including bile acids in the polymer backbone which has been used in the preparation of elastomers. This review discusses a selection of materials that can be prepared using bile acids and the advantages afforded by these molecules. Focus will be on the development of soft and hard materials, where soft materials are described as being held by weak intermolecular interactions, whereas hard materials are mechanically stronger with bile acids covalently incorporated in the polymer network.

* Published as a review: A. J. Cunningham, X. X. Zhu., *Can J. Chem.* **2016**, *94(8)*, 659-666.

2.1 Introduction

Ubiquitous to all animals, bile acids represent an important class of molecules with various functionalities ranging from the absorption of vital nutrients and vitamins to the well-being of the organism through preservation of homeostasis of key cellular functions.[1-4] Indeed, recently bile acids have been the focus of extensive research, where novel roles for these steroid-based molecules are being unravelled.[1, 5-7] Once thought to simply act as solubilizers of lipids and vitamins for their absorption through intestinal cells, growing evidence points towards their involvement in signalling pathways and their role in regulating homeostasis.[1, 8-11] Notwithstanding their physiological importance, bile acids are rapidly gaining impetus as frameworks for the development of novel materials with considerable importance in the pharmacological, biochemical, and nanotechnological fields.[2, 12-13] Although they have found potential applications in the treatment of liver diseases,[14-15] and as antifungal[16] and antiviral agents,[17] the present review will provide an account of the use of bile acids as platforms for the preparation of soft and hard materials. Central to this idea, we will begin with a glance of the physicochemical properties of bile acids, followed by examples of their exploitation for the development of soft materials such as self-healing gels and nanoparticles for drug delivery, and in their development of hard materials such as elastomers and dental resins.

Primary bile acids are synthesized from cholesterol inside the liver and play vital roles in digestion and absorption of dietary lipids and fats by the formation of cylindrical micelles.[3-4] Bile acids exist as two isomers (Figure 2.1), the 5α-cholanic acid possessing trans-orientation between rings A and B, and the 5β-cholanic acid possessing cis-orientation. The cis-orientation allows the formation of a cavity with a convex β-face and a concave α-face.[18] Most bile acids have their hydroxyl groups positioned in the α-face and their methyl groups in the β-face thereby creating facial amphiphilicity and providing detergent properties; hence their use as emulsifiers in the digestion of fats and lipids. Amphiphilic derivatives of bile acids may be used to self-assemble into more elaborate structures. Moreover, the rigid steroidal backbone of bile acids confers tough mechanical properties and the biocompatibility of these molecules also renders the parent material biocompatible. They are rather abundant and easily obtainable, which are all desirable traits in the realm of material sciences.

Bile acids offer the possibility of reactions at their hydroxyl groups as well as the carboxylic acid group serving as promising platforms for various designs and architectures. The hydroxyl groups on the steroid ring can be functionalized in various ways; for example, cross-linkable groups can be attached to yield a bile acid-based cross-linked network where the steroid core provides rigidity. The hydroxyl groups can also serve as initiators for different polymerizations; i.e. ring-opening and ionic polymerizations which both utilize hydroxyl groups as initiators. Actually, hydrophobic and hydrophilic polymers have been polymerized onto bile acids thereby tuning their hydrophobicity as an attempt to achieve diverse supramolecular arrangements. They can also be used as repeating units in the polymer backbone or as pendant molecules on the polymer chain. This has been seen mostly for the preparation of hard materials where mechanical strength was a necessity, e.g., for the preparation of dental resins and shape-memory polymers. In a nutshell, their inherent amphiphilicity, biocompatibility, rigid steroidal backbone, and low critical aggregation concentration (CAC) allow for the conception of biomaterials in different settings, as will be assessed in the following paragraphs.

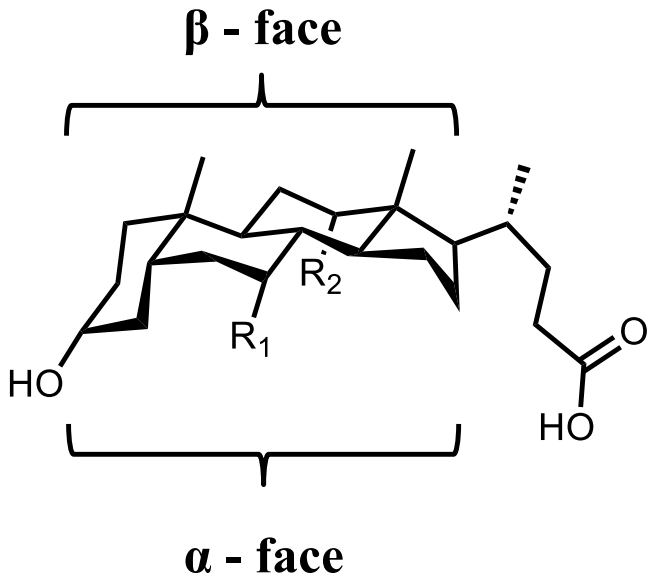

Bile acid	Abbreviation	R_1	R_2
Cholic acid	CA	OH	OH
Deoxycholic acid	DCA	H	OH
Chenodeoxycholic acid	CDCA	OH	H
Lithocholic acid	LCA	H	H

Figure 2.1 Chemical structure of bile acids in the cis-orientation.

2.2 Soft Materials

2.2.1 Self-assembled systems.

In this review, soft materials are defined as these that can form self-assembled structures or that are held by weak intermolecular forces, such as hydrogen bonding. There exist various examples of the use of bile acids for the development of soft materials in recent literature. One approach is to use bile acids as a template onto which polymers can be grown. Ring-opening polymerization has been a method of choice, where the hydroxyl groups at positions C-3, C-7, and C-12 can be used as initiating points in the presence of DL-lactide, ε-caprolactone, or other cyclic ester monomers.[19-25] Zhuo et al. exploited the hydroxyl groups of cholic acid to prepare a three arm-star shaped polylactide with

potential applications in drug delivery and as scaffolds for promoting cell adhesion and proliferation. However, high polydispersity and uneven chain lengths are shortcomings of ring-opening polymerization in the present context.[26] Therefore, one method to circumvent this issue is the use of anionic polymerizations which has been shown to yield well-defined polymers with tuneable sizes and low polydispersity.

We have extensively studied the use of anionic polymerization for the synthesis of bile acid-based polymers and their self-assembly into a range of nanostructures. Giguère et al. showed that a cholic acid derivative can be synthesized to bear four hydroxyl groups on the concave side which were further used as initiators in the anionic polymerization of various epoxide monomers for the preparation of poly(ethylene glycol) (PEG) or poly(allyl glycidyl ether) (PAGE) giving rise to a bile acid with four polymer chains branching from cholic acid (Figure 2.2).[27-28] Investigation into the aggregation behaviour of these derivatized bile acids demonstrated the array of accessible nanoparticle aggregates. PEGylated bile acids were studied first to understand the effect of the hydrophilic polymer on the self-assembly of bile acid derivatives.[28] Notable observations included increases in the critical aggregation concentration (CAC) with increasing PEG chain length; from 9 to 19 milimolal due to the increase in the hydrophilicity. Moreover, changes in the aggregate structures were observed. Figure 2.3 shows the freeze-fracture TEM images of sodium cholate, CA-$(PEG_5)_4$, and CA-$(PEG_{15})_4$. The pure salt form of cholic acid forms cylindrical micelles, whereas PEGylated cholic acids form spherical aggregates with sizes ranging from 100 to 130 nm. As a measure of comparison, primary aggregates of bile acid salts determined by DLS shows a D_h of 2 - 3.4 nm.[29] Knowing that hydrogen bonding may play a role in the formation of the large aggregates and that the relative position of the hydroxyl groups on the concave faces of cholic acid are extended by the PEG chains, it is expected that the aggregation mechanism will be different from that of the bile salts leading to the different structures observed.

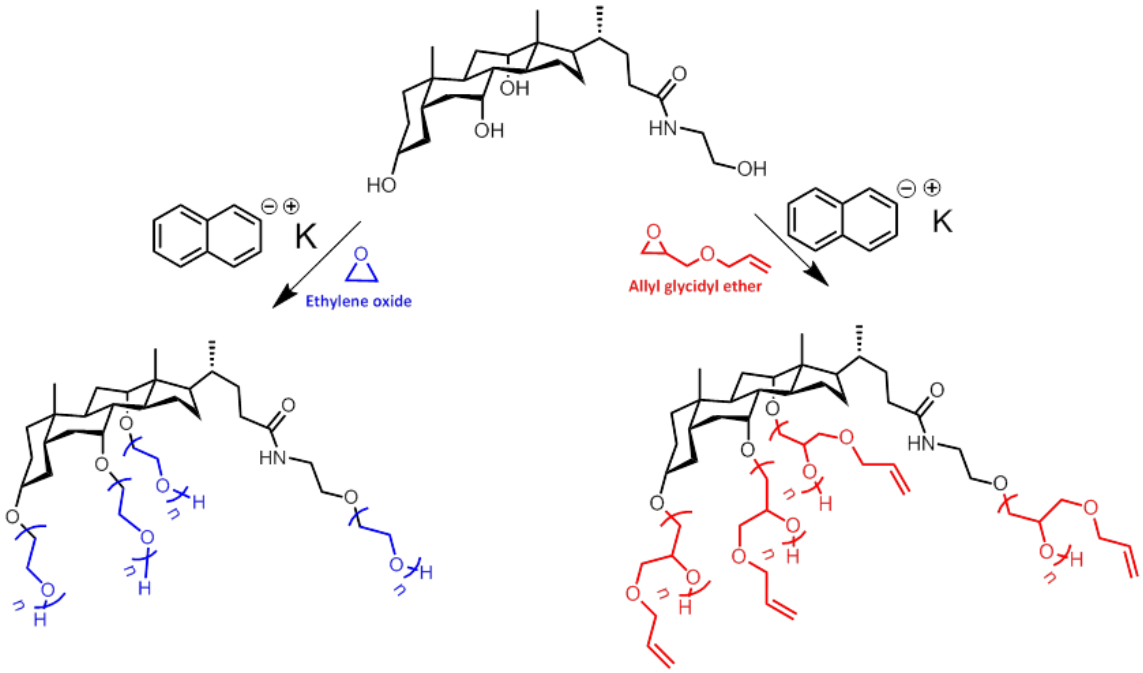

Figure 2.2 Polymerization of allyl glycidyl ether (left) and ethylene oxide (right) on the surface of cholic acid.

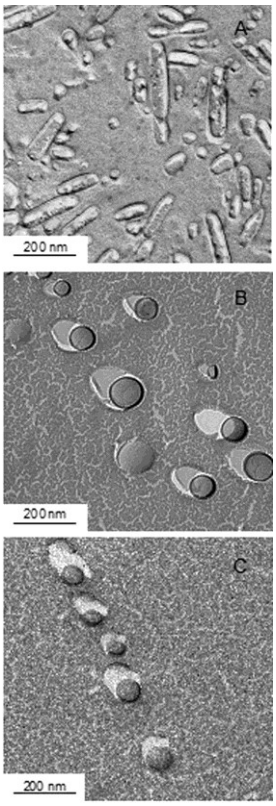

Figure 2.3 TEM images of aggregates of sodium cholate at 0.040 molal (A), CA-$(PEG_5)_4$ at 0.025 molal (B), and CA-$(PEG_{15})_4$ at 0.020 molal (C).[28] (Reprinted with permission from © Copyright 2009 American chemical society)

The self-assembly process of bile acid-based polymers is described in the work of Despa et al.[30] Using computer simulations and known experimental values, the aggregation phenomenon for cholic acid and cholic acid-based polymers was compared and elucidated. The convex structure of the bile acids induces the formation of an internal cavity (Figure 2.4 a). In conjunction with the facial amphiphilicity, this arrangement allows the entrapment of water molecules at the interfaces and weakens the hydrophobic attraction between the monomers leading to the observed hollow-core micelles. Now, the attachment of PEG chains on the hydroxyl groups of the bile acids generates a steric repulsion between the individual polymer chains which favours a further reduction in the micelle size (Figure 2.4 b). Moreover, the authors observed a correlation between the PEG lengths and the micellar properties; the longer the PEG chains the higher the CMC, but

also the smaller the internal cavities. Finally, a model was proposed; the driving force for the self-assembly depends on the facial polarization between the amphiphiles.

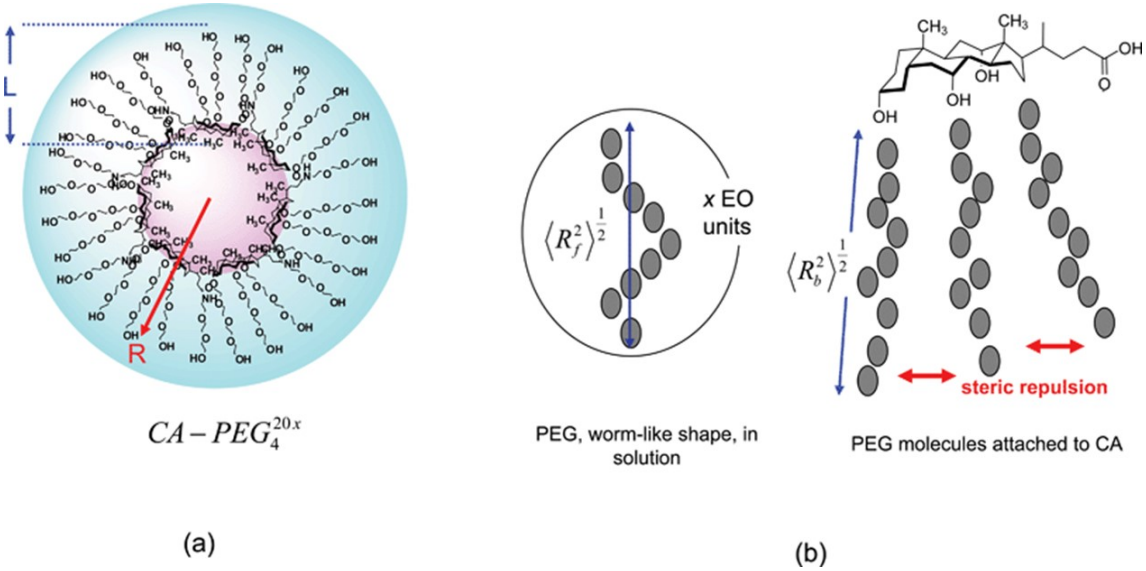

Figure 2.4 (a) The convex structure of the bile acids induces the formation of an internal cavity lined with the hydrophobic face of the bile acids, and colloidally stabilized in an aqueous environment by the hydrophilic PEG; (b) Attaching the PEG chains on the hydroxyl groups causes a steric repulsion between adjacent PEG chains.[30] (Reprinted with permission from © Copyright -2010 Royal Society of Chemistry)

Other examples of the tuning of the aggregation process of polymer-derivatized bile acids can be drawn from the literature. Giguère et al. reported on the aggregation and thermosensitivity of star polymers derived from cholic acid offering alternatives to the existing thermosensitive polymers.[27] Cholic acid derived with PAGE were functionalized with amines or carboxylic acids yielding amphiphilic polymers where the CAC varied with chain length and functionalization, and the thermosensitivity was tuned from 15 to 48 °C simply by varying the amount of protonated amines or by acetylation. Li et al. prepared thermosensitive cholic acid derived with PAGE-b-PEG block copolymers to form four amphiphilic block copolymer branches.[31] Dynamic light scattering (DLS) and UV-visible spectroscopy studies showed that the polymers formed aggregates of different sizes depending on the temperature. Cholic acid-based polymers with a shorter PEG chain typically formed micelles with a hydrodynamic diameter (D_h) of ca. 70 nm at low temperatures (1 to 10 °C). The D_h increased to 130 – 140 nm as the temperature rose to

25 °C with a broad transition. On the other hand, cholic acid with longer PEG chains typically formed micelles with a small diameter of 15 nm. Upon heating, micellar clusters were observed with a D_h around 1000 nm before finally decreasing to 700 – 800 nm. The cloud point of the cholic acid-based block copolymers could be tuned from 13 to 55 °C simply by varying the PEG chain length. These thermoresponsive properties of the cholic acid-based block copolymers demonstrate the potential nanostructures that can be obtained from bile acid derivatives and the propensity to tune their aggregation from a synthetic standpoint.

2.2.2 Drug delivery systems.

Stemming from the aggregation studies, research into the use of bile acids as drug delivery vehicles has seen the light of day, as one prominent advantage of using bile acids in drug delivery strategies is the micelles formed by bile acids are typically less densely packed and smaller than micelles prepared using other surfactants.[30] As a result, the internal reservoir formed upon self-assembly may be used to encapsulate the hydrophobic drug and potentially lead to high drug loading. Le Dévédec et al.[32] studied the aggregation behaviour of three different bile acids functionalized with PEG, i.e. lithocholic acid (LCA), deoxycholic acid (DCA), and cholic acid (CA), and their encapsulation efficiencies toward the hydrophobic drug ibuprofen. The three different bile acids used in their study present varying numbers of hydroxyl groups which permits different numbers of PEG chains to extend from the steroid core; two for LCA, three for DCA, and four for CA. By varying the numbers of PEG arms and their relative length, the hydrophobicity of the system was varied and the impact of this parameter on the drug loading efficiency was determined and optimized. Results showed that the CA with four arms formed more stable micelles than DCA and LCA and the micelles had a lower size dispersity, but were characterized with lower loading presumably due to the smaller internal reservoir; 2.8 mg/mL for CA vs. 6.1 mg/mL for LCA. Similarly, PEGylated bile acids were used as encapsulating agents to increase the bioavailability of hydrophobic antifungal drugs, such as itraconazole, as self-emulsifying drug delivery systems (SEDDS).[33] Results indicate high drug loading was achieved with a shorter PEG chain (drug encapsulation of 35 % (w/w) and drug loading efficiencies above 89 %). Not a large difference was observed

between CA, DCA, and LCA of similar chain length. Impressively, when compared to the commercially available itraconazole formulation or to itraconazole-loaded polymeric micelles, *in vivo* results show that both *per os* and *i.v.* administration of the bile acid-based SEDDS gave similar area under the time-concentration curve (AUC), plasma clearance (CL_p), and terminal half-life ($t_{1/2}$) albeit at a lower concentration; 2.5 vs. 5 mg/kg for *i.v.* administration and 12.5 vs. 15 mg/kg for *per os* administration. Moreover, biocompatibility experiments show that these bile acid derivatives are non-cytotoxic with higher $IC_{50\%}$ than the natural bile acid counterparts.

Others have also explored the use of bile acids as templates for the design of drug delivery systems. Lam and coworkers opted for a bile acid-based linear-dendritic system for the encapsulation of therapeutic molecules.[34-35] Using PEG as the linear block and an elegant synthetic method inspired from peptide synthesis to prepare cholic acid dendrimers, the drug delivery system was able to form micellar particles and encapsulate a range of therapeutics. By varying the amount of cholic acid and PEG chain length, micelles from 10 to 150 nm were prepared with very low polydispersity. Once again, high loading for these bile acid-based drug delivery systems were obtained with 36.5 % (w/w) for paclitaxel, and 14.8 % (w/w) for doxorubicin (DOX). In addition, hydrophilic drugs were also encapsulated. Indeed, due to the amphiphilic properties of bile acids, core-inversible micelles were prepared for the loading of congo red, a hydrophilic therapeutic molecule with loading values up to 12.7 % (w/w).[36] At last, these encouraging results demonstrate the high potential that bile acids possess towards drug delivery vehicles.

2.2.3 Thermoresponsive polymers and hydrogels.

Bile acids can also be used as pendant chains in block copolymers thereby tuning the properties of these materials toward engaging, novel functionalities and properties. Thermoresponsive water-soluble polymers that undergo a phase transition in water such as a cloud point (CP) or a lower critical solution temperature transition (LCST) present compelling aspects for their use in the fields of drug delivery, tissue engineering, sensors, and catalysis.[37-40] However, the tuning of the LCST presents one hurdle for their successful implementation. Many different strategies have been designed to tune the LCST for a specific application, with the use of bile acids as pendant chains as a potential candidate.[41-44] Their biocompatibility and presence of functional groups for further

functionalization renders them ideal candidates as building blocks in the preparation of polymer-based biomaterials. Indeed, in our group we have prepared and modified various acrylamide-based block copolymers with cholic acids as pendant chains to study its effect on the tuning of the LCST.[45-49]

Bile acids have the property of associating with β-cyclodextrin (β-CD), due to the compatibility of the size and shape of bile acids with the cavity of β-CD.[50-55] This reversible association allows the tuning of the thermoresponsive properties via the addition of a supramolecular host. Jia et al. showed that the block copolymer of *N*-isopropylacrylamide (iPA), (*N,N'*-dimethylacrylamide) (DMA), and a cholic acid-based methacrylate monomer (CA) had thermoresponsive properties with a CP at 22 °C depending on the monomer ratio (Figure 2.5).[42] The addition of β-CD induced an increase in the CP by rendering CA more hydrophilic; an increase from 22 to 31.3 °C was observed with an increasing [β-CD]/[CA] of 0 to 10. This association was shown to be reversible with the addition of potassium 1-adamantylcarboxylate (K-Ada) which has a higher association constant with β-CD than CA. This strategy was used to prepare a biocompatible, autonomous, self-healable supramolecular hydrogel via reversible host-guest interactions.[41] Two DMA-based block copolymers, one containing CA and the other containing β-CD as pendant chains, associated into a hydrogel where the strength of the hydrogel was shown to depend on both the ratio [β-CD]/[CA] and polymer concentrations. Interestingly, the healing time was observed to occur in less than one minute *in situ* with no observable weak points, due to the dynamic complexation between CA and β-CD. In addition, 97 % recovery was measured without necessitating external treatment.

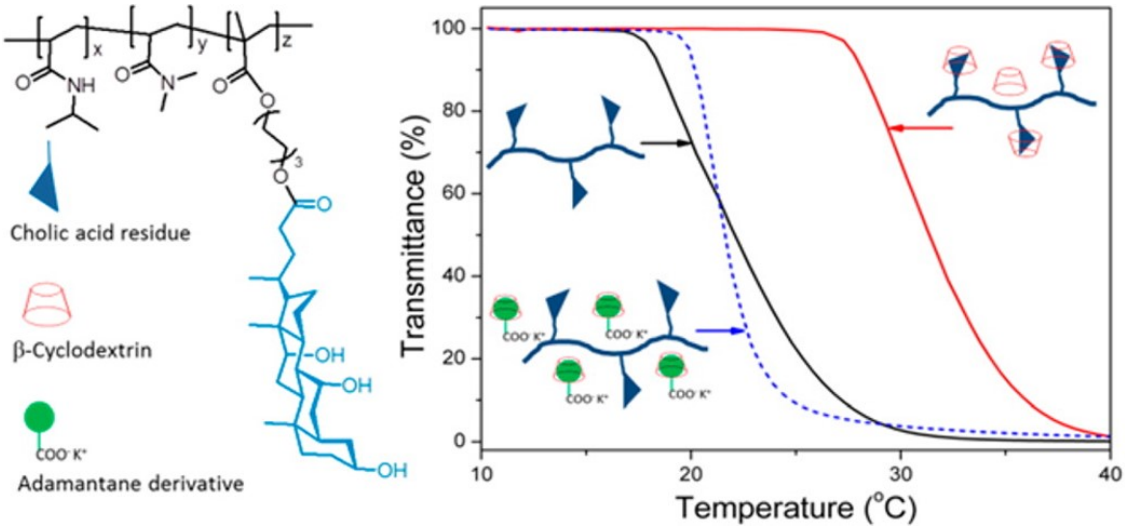

Figure 2.5 Copolymers of *N*-isopropylacrylamide (iPA), (*N,N'*-dimethylacrylamide) (DMA), and a cholic acid-based methacrylate monomer (CA) formed thermoresponsive polymers with tuneable properties via the addition of cyclodextrin and potassium 1-adamantylcarboxylate.[42] (Reprinted with permission from © Copyright 2014 American Chemical Society)

Similarly, a series of *N*-isopropylacrylamide-based random copolymers containing CA-based methacrylate monomers were able to form vesicles driven by the inherent amphiphilic properties of CA which associated to form hydrogels through hydrogen bonding between their hydrophilic surfaces.[56] Varying the CA content allowed the tuning of the CP with the formation of a hydrogel occurring in a time frame of 30 sec. above the CP. The formation of aggregates resulting from the presence of bile acids as pendant chains have been previously studied with potential drug and gene delivery applications.[43-44, 56-59] In a report of Pal et al., random copolymers of 2-(metharcyloyloxy)-ethyl cholate (MAECA) with either polyethylene glycol methyl ether methacrylate (PEGMA) or *N,N*-dimethylaminoethyl methacrylate (DMAEMA) were prepared for thermo and both pH- and thermo-responsiveness, respectively. The system had a range of tunable CP resulting from varying CA content in the random copolymers allowing the tuning of the LCST via both pH and temperature. Interestingly, spherical micelles were obtained from these random copolymers.

In an analogous strategy, Jia et al. prepared a block copolymer with pendant CA and oligo(ethylene glycol)s repeated in the polymer backbone.[60] Synthesized via a norbornene monomer, their block copolymer displayed aggregation, thermo- and pH-sensitive properties as well as potential towards drug encapsulation. High loading values were obtained with Nile Red as a model hydrophobic molecule. The system shows pH-responsiveness where the CA units become deprotonated at higher pH. In a previous report, Jia et al. showed the encapsulation of paclitaxel (PTX) in a similar system with 1 g/L of loaded PTX.[43] Moreover, very low IC_{50} were measured pointing to promising antitumor activity of the PTX-loaded micelles; 27.4 ng/mL.

Under the definition of soft materials in this paper, another example that merits attention is the formation of bile acid-based supramolecular hydrogels. The group of Maitra et al. has significantly contributed to the understanding and preparation of these hydrogels.[61-63] In the late 1950s, it was observed that a helical macromolecule was obtained from sodium-deoxycholate which further aggregated into a matrix of high viscosity and gel-like properties.[64] When the pH is lowered, some of the deoxycholate anions is protonated and instead of precipitating, the uncharged carboxyl groups point inwards of the helical structure and forms hydrogen bonds with other deoxycholates thereby reducing the repulsion between two protonated deoxycholates. This event leads to the formation of helical structures which grow in all directions ultimately giving rise to the observed gel. Since these early studies, the bile acid-based gelation process has been optimized. Of notable consideration, metal-cholate hybrid hydrogels has been the subject of recent research efforts as they hold enormous potential in various applications from sensing to medical implants.[65-67] Typically, doping trivalent lanthanides (Ln(III)) in the presence of sodium cholate afforded the hydrogel. The Ln(III) complexed to the carboxylate ions and caused the cholate moieties to come together. Due to their amphiphilicity, the hydrophobic faces of the cholates associated in the aqueous medium yielding the nano-fibrous network.[66] These gels were characterized with viscoelastic properties similar to soft solids and had advantageous luminescent properties arising from the presence of the lanthanides in the gels.

2.3 Hard Materials

Hard materials are defined here as being composed of bile acids held through covalent bonds in the polymer backbone or network. Compared to the previous section, there are limited accounts for the use of bile acids with this architecture. Nonetheless, they present interesting properties which merit further attention.

2.3.1 Dental Resins and biocompatible materials.

In the previous section, examples of soft materials arising from the repeating of bile acids as pendant chains on the polymer backbone was presented, however hard materials can also be obtained from this architecture depending on the post-polymerization processing of the polymers. A notable configuration is the crosslinking of methacrylate monomers derived from bile acids to produce a crosslinked network.[68] The advantages of the use of bile acids for this architecture type are the hard steroidal backbone of bile acids which provides strong mechanical properties and the biocompatibility of the bile acids which is extended in the crosslinked network. This becomes interesting especially in the development of constituents for dental composites. Plagued by issues of biocompatibility and shortcomings in their shrinkage and incompletion during polymerization, traditional monomers in dental composites may one day be replaced by the promising bile acid-based monomers. Pioneers in the field, Gauthier et al. showed that di-, tri-, and tetra-methacrylate derivatives of bile acids are less cytotoxic than the commercial dental monomers.[69] Indeed, over the entire range of solubility the bile acid monomers did not affect cell viability and had considerably higher IC_{50} (half maximal inhibitory concentration) than the commercial monomers. In another report, the authors showed that these monomers presented superior features over commercial monomers towards dental composites.[70] They showed lower polymerization shrinkage and improved high-temperature mechanical properties than the commercial monomers.

In one report, a cholic acid pendant polymer was prepared via free-radical polymerization of a methacrylate-functionalized cholic acid. The linear polymers crystallized into fibrils with the hydrophobic core forming the wick of the fibrils covered by the hydrophilic pendant carboxylic acid moieties.[71] These fibrils enabled the formation of hydroxyapatite on the amphiphilic surface thereby serving as a platform for crystallization in a process similar to the biomineralization intrinsic to animals and plants.

In this manner, bile acids may also serve in the preparation of hard tissues like bones, cartilage, and teeth with the advantage of being biocompatible.

2.3.2 Polyesters, polyamides, and polyurethanes.

Another architecture available is the use of bile acids as repeating units in the main chain of the polymer. Polycondensation was performed in the presence of p-toluenesulfonic acid as a catalyst and high temperatures by Ahlheim and Hallensleben.[72] The resulting polymers were branched, with low molecular weights due to the presence of more than one hydroxyl group. Other strategies used linear polycondensation using lipase as catalysts or a combination of coupling agents such as (*N,N*-diisopropylcarbodiimide) and catalyst such as *N,N*-(dimethylamino)pyridine, both yielding reasonably high molecular weight polymers (20-60 kDa).[73-74] Gautrot et al. demonstrated the use of second generation Grubbs' catalyst in the ring-opening polymerization (ROP) of cyclic cholic acid monomers yielding high (M_n above 100 kDa) molecular weight polymers.[75-78] The resulting polymers had elastomeric properties and were degradable with rates in the order of several months in phosphate-buffered saline solution at 37 °C. Alternatively, these polymers may be synthesized by the use of lipase in the ROP of the macrocyclic monomers.[79] Due to the presence of a glass-transition temperature (T_g) and elastomeric properties, these polymers were shown to have shape memory properties driven by chain entanglements. Remarkably, the T_g was tuneable allowing to reach temperatures near that of the body and high recovery ratio (> 94 %) were obtained. Such characteristics may be useful in the biomedical field for the design of stents and self-tightening knots for sutures (Figure 2.6). In a similar report, Shao et al. showed how norbornene-based copolymers with cholic acid pendant groups displayed quadrupole shape memory effect.[80] The T_g of the block copolymer was tuned from -58 to 176 °C with a broad T_g range (20 °C). By utilizing the broad T_g, a quadrupole shape memory effect was observed with shape recovery ratios higher than 94 %. Furthermore, using biological compounds such as cholic and cinnamic acid a triple and quadrupole shape memory polymer was obtained with recovery ratio in the range of 75 to 99 %.[81]

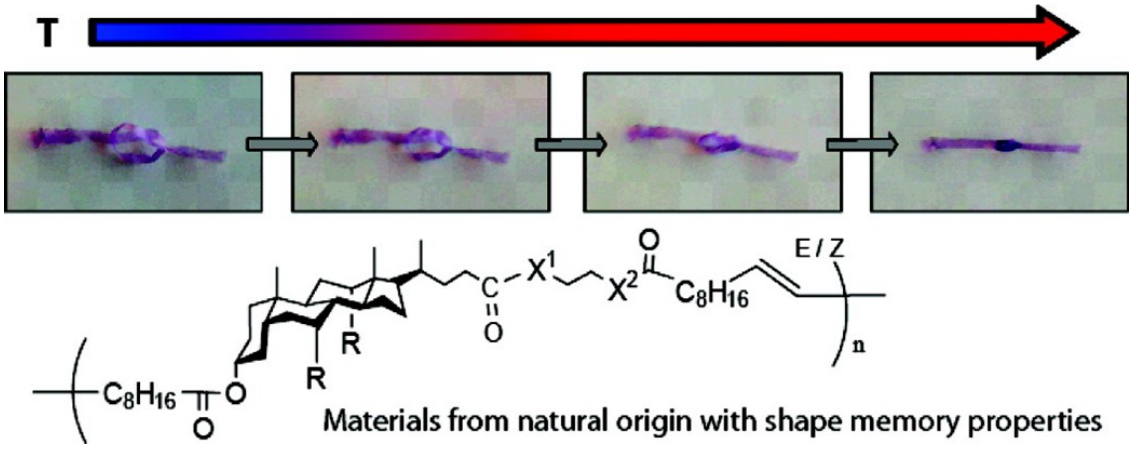

Figure 2.6 A thread of bile acid-based polyester was stretched to 200% of its original length below its transition temperature and tied into a loose knot. Upon warming to room temperature, the shape recovery process triggers the tightening of the knot.[77] (Reprinted with permission from © Copyright 2009 American Chemical Society)

Click chemistry was also used to prepare rigid polyamides and polyesters based on bile acids. Heterofunctional precursors were used in a copper(I)-catalyzed azide-alkyne cycloaddition for the successful preparation of high molecular weight polymers, 25 kDa.[82] The presence of bile acids with different linkers repeated in the backbone of the polymers led to a range of polymers with interesting properties. Li et al. prepared various main chain poly(bile acid)s using different bile acid monomers. Using long flexible alkyl chains, amide groups, phenyl groups, and sterically hindered structures as linkers on the bile acid monomers, the molecular weight and properties of the resulting polymers were tuned.[83] Interestingly, the T_g of the polymers was tuned from 110 to 240 °C via the linkers used while retaining biocompatibility, with promising elastomeric properties. By careful choice of linkers in the synthesis of the polymers, properties such as the T_g, thermosensitivity, crystallinity, and degradation can be optimized. For example, polyesters were synthesized using deoxycholic acid and oligo(ethylene glycol)s (OEG) of different lengths via polycondensation to tune the aforementioned properties toward biomedical applications.[84] Increasing the length of the OEGs in the polyesters increased the hydrolytic degradation rate of the polyesters while providing water solubility and increased crystallinity. More recently, polyurethanes based on derivatives of cholic and lithocholic acids were prepared and demonstrated good mechanical properties.[85] These

examples truly demonstrate the versatility in the chemical structure that can be obtained when using bile acids repeated in the polymer backbone and the resulting range in properties and performances in the polymers.

2.3.3 Surface modifications.

Bile acids have also been used for surface modification of polymers. In the first example, a self-assembled monolayer (SAM) film was prepared by chemical immobilization of oligo(p-phenylene-ethynylene) (OPE) covalently modified with cholic acids.[86] The purpose was to use cholic acid as a pH sensor in organic solvents. In a polar aprotic solvent like acetone, cholic acid derivatives form pockets that can encapsulate ions and reside on top of the SAM thereby quenching the fluorescence of OPE. In this strategy, cholic acid can sense the presence of ions in acetone. In another report, Hu et al. modified poly(vinylidene fluoride) (PVDF) microfiltration membranes with cholic acid thereby increasing its hydrophilicity.[87] The functionalization of the PVDF membrane improves its surface properties allowing the permeation of water without affecting its mechanical properties. In an elegant exploitation of the facial amphiphilicity of bile acids, the hydrophobic face of the cholic acid serves to adsorb the molecule on the material's surface whereas the hydrophilic face provides the anti-fouling properties. These two examples demonstrate the potential of bile acids towards surface functionalization. Not only bile acids are versatile in the sense that they can be chemically and physically adsorbed to a desired surface, but they may also serve either as sensing molecules or simply modify the surface chemistry as seen in the above examples. For sensing purposes, bile acids have the advantage of forming reversible pockets in different solvents which can be utilized to encapsulate hydrophobic or hydrophilic molecules depending on the environment (Figure 2.7).[88-90]

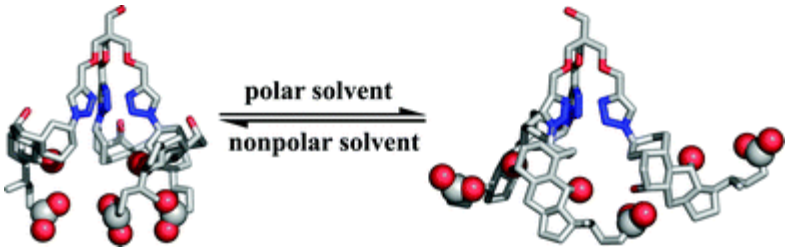

Figure 2.7 Reversible pockets are formed in different solvents and allow the entrapment of various molecules.[88] The CA trimer can adopt different conformations depending on the solvent polarity. In a nonpolar solvent, the hydroxyl groups of the CA trimers face each other and interact via H-bonding with the hydrophobic steroid backbone pointing outwards. In a polar solvent, the hydroxyl groups of CA point outward and form H-bonds with water, while the hydrophobic steroid backbone point inward and interact via hydrophobic interactions. (Reprinted with permission from © Copyright 2011 Royal Society of Chemistry)

2.4 Conclusion

Bile acids possess key properties that make them interesting building blocks in the preparation of novel materials for diverse applications. The biocompatibility of these natural compounds may be extended in the materials which they compose, making them easily applicable in the biomedical field. Moreover, the steroidal backbone of these molecules imparts strong mechanical properties to the materials that they compose while the functional groups, both hydroxyl and carboxylic acid groups, of the bile acids allows for a variety of chemical modifications facilitating their use in the construction of novel materials. This was apparent through the different types of structures that utilize bile acids in their architecture. Either acting as a template onto which polymers are grown or modified with acrylate functionalities, the various synthetic strategies permitted the preparation of soft and hard materials. From self-assembled structures to polymer networks it seems that the materials design is only limited by the imagination of the researchers. These interesting biological molecules opened the door to high performance, novel materials with versatile properties for use in various areas.

2.5 Acknowledgements

Financial support from NSERC, FQRNT, Canada Research Chair program and the Camille-Sandorfy scholarship (for AJC) is gratefully acknowledged.

2.6 References

1. Thomas, C.; Pellicciari, R.; Pruzanski, M.; Auwerx, J.; Schoonjans, K., Targeting bile-acid signaling for metabolic diseases. *Nat. Rev.* **2008,** *7*, 678-693.
2. Enhsen, A.; Kramer, W.; Wess, G., Bile acids in drug discovery. *Drug Discov. Today* **1998,** *3*, 409-418.
3. Nair, P. P.; Kritchevsky, D., *The bile acids. Chemistry, Physiology, and Metabolism*. Plenum Press: New York, 1973; Vol. 2.
4. Danilson, H.; Sjovall, J., *New Comprehensive Biochemistry, Vol. 12: Sterols and bile acids*. Elsevier: Amsterdam, 1985.
5. Devlin, A. S.; Fischbach, M. A., A biosynthetic pathway for a prominent class of microbiota-derived bile acids. *Nat. Chem. Biol.* **2015,** *11* (9), 685-690.
6. Li, T.; Chiang, J. Y. L., Bile acid signaling in liver metabolism and diseases. *J. Lipids* **2012,** *2012* (9), 3-9.
7. Sayin, Sama I.; Wahlström, A.; Felin, J.; Jäntti, S.; Marschall, H.-U.; Bamberg, K.; Angelin, B.; Hyötyläinen, T.; Orešič, M.; Bäckhed, F., Gut microbiota regulates bile acid metabolism by reducing the levels of tauro-beta-muricholic acid, a naturally occurring FXR antagonist. *Cell Metab.* **2013,** *17* (2), 225-235.
8. Kawamata, Y.; Fujii, R.; Hosoya, M.; Harada, M.; Yoshida, H.; Miwa, M.; Fukusumi, S.; Habata, Y.; Itoh, T.; Shintani, Y.; Hinuma, S.; Fujisawa, Y.; Fujino, M., A G Protein-coupled receptor responsive to bile acids. *J. Biol. Chem.* **2003,** *278* (11), 9435-9440.
9. Watanabe, M.; Houten, S. M.; Mataki, C.; Christoffolete, M. A.; Kim, B. W.; Sato, H.; Messaddeq, N.; Harney, J. W.; Ezaki, O.; Kodama, T.; Schoonjans, K.; Bianco, A. C.; Auwerx, J., Bile acids induce energy expenditure by promoting intracellular thyroid hormone activation. *Nature* **2006,** *439* (7075), 484-489.
10. Makishima, M.; Lu, T. T.; Xie, W.; Whitfield, G. K.; Domoto, H.; Evans, R. M.; Haussler, M. R.; Mangelsdorf, D. J., Vitamin D receptor as an intestinal bile acid sensor. *Science* **2002,** *296* (5571), 1313-1316.
11. Talukdar, S.; Bhatnagar, S.; Dridi, S.; Hillgartner, F. B., Chenodeoxycholic acid suppresses the activation of acetyl-coenzyme A carboxylase-α gene transcription by the liver X receptor agonist T0-901317. *J. Lipid Res.* **2007,** *48* (12), 2647-2663.
12. Zhu, X. X.; Nichifor, M., Polymeric materials containing bile acids. *Acc. Chem. Res.* **2002,** *35*, 539-546.
13. Virtanen, E.; Kolehmainen, E., Use of bile acids in pharmacological and supramolecular applications. *Eur. J. Org. Chem.* **2004,** *2004* (16), 3385-3399.
14. Hofmann, A. F., Bile acids as drugs: principles, mechanisms of action and formulations. *Ital. J. Gastroenterol.* **1995,** *27* (2), 106-113.
15. Li, T. G.; Chiang, J. Y. L., Regulation of bile acid and cholesterol metabolism by PPARs. *PPAR Res.* **2009**, *15*, 1-16.

16. Berlati, F.; Ceschel, G.; Clerici, C.; Pellicciari, R.; Roda, A.; Ronchi, C. The use of bile acids as antiviral agents. International Patent WO1994000126A1, January 6, 1994.
17. Marples, B. A.; Stretton, R. J. Use of steroidal compounds as anti-fungal agents. UK Patent GB2243550A, November 15, 1990.
18. Li, Y.; Dias, J. R., Dimeric and oligomeric steroids. *Chem. Rev.* **1997,** *97* (1), 283-304.
19. Zou, T.; Cheng, S. X.; Zhang, X. Z.; Zhuo, R. X., Novel cholic acid functionalized star oligo/poly(DL-lactide)s for biomedical applications. *J. Biomed. Mater. Res. B Appl. Biomater.* **2007,** *82* (2), 400-407.
20. Zou, T.; Li, S. L.; Cheng, S. X.; Zhang, X. Z.; Zhuo, R. X., Fabrication and in vitro drug release of drug-loaded star oligo/poly(DL-lactide) microspheres made by novel ultrasonic-dispersion method. *J. Biomed. Mater. Res. A* **2007,** *83* (3), 696-702.
21. Wan, T.; Liu, Y.; Yu, J.-Q.; Chen, S.; Li, F.; Zhang, X.-Z.; Cheng, S.-X.; Zhuo, R.-X., Synthesis and characterization of star oligo/poly(2,2-dimethyltrimethylene carbonate)s containing cholic acid moieties. *J. Polym. Sci. Part A: Polym. Chem.* **2006,** *44* (23), 6688-6696.
22. Fu, H.-L.; Yu, L.; Zhang, H.; Zhang, X.-Z.; Cheng, S.-X.; Zhuo, R.-X., Synthesis of novel cholic acid functionalized branched oligo/poly(ε-caprolactone)s for biomedical applications. *J. Biomed. Mat. Res. Part A* **2007,** *81* (1), 186-194.
23. Fu, H.-L.; Cheng, S.-X.; Zhang, X.-Z.; Zhuo, R.-X., Dendrimer/DNA complexes encapsulated in a water soluble polymer and supported on fast degrading star poly(dl-lactide) for localized gene delivery. *J. Control. Release* **2007,** *124* (3), 181-188.
24. Zou, T.; Li, S.-L.; Hu, Z.-Y.; Cheng, S.-X.; Zhuo, R.-X., Synthesis and properties of star oligo/poly(trimethylene carbonate)s with cholic acid moieties as cores. *J. Biomater. Sci. Polym. Ed.* **2007,** *18* (5), 519-530.
25. Zhang, H.; Tong, S.-Y.; Zhang, X.-Z.; Cheng, S.-X.; Zhuo, R.-X.; Li, H., Novel solvent-free methods for fabrication of nano- and microsphere drug delivery systems from functional biodegradable polymers. *J. Phys. Chem. C* **2007,** *111* (34), 12681-12685.
26. Zhang, J.; Zhu, X.X., Biomaterials made of bile acids. *Sci. China, Ser B: Chem.* **2009,** *52* (7), 849-861.
27. Giguere, G.; Zhu, X. X., Functional star polymers with a cholic acid core and their thermosensitive properties. *Biomacromolecules* **2010,** *11* (1), 201-206.
28. Luo, J.; Giguere, G.; Zhu, X. X., Asymmetric poly(ethylene glycol) star polymers with a cholic acid core and their aggregation properties. *Biomacromolecules* **2009,** *10* (4), 900-906.
29. Mazer, N. A.; Carey, M. C.; Kwasnick, R. F.; Benedek, G. B., Quasielastic light scattering studies of aqueous biliary lipid systems: Size, shape, and thermodynamics of bile salt micelles. *Biochemistry* **1979,** *18* (14), 3064-3075.
30. Despa, F.; Luo, J. T.; Li, J.; Duan, Y.; Lam, K. S., Cholic acid micelles--controlling the size of the aqueous cavity by PEGylation. *Phys. Chem. Chem. Phys.* **2010,** *12* (7), 1589-1594.

31. Li, C.; Lavigueur, C.; Zhu, X. X., Aggregation and thermoresponsive properties of new star block copolymers with a cholic acid core. *Langmuir* **2011,** *27* (17), 11174-11179.
32. Le Devedec, F.; Fuentealba, D.; Strandman, S.; Bohne, C.; Zhu, X. X., Aggregation behavior of pegylated bile acid derivatives. *Langmuir* **2012,** *28* (37), 13431-13440.
33. Le Devedec, F.; Strandman, S.; Hildgen, P.; Leclair, G.; Zhu, X. X., PEGylated bile acids for use in drug delivery systems: enhanced solubility and bioavailability of itraconazole. *Mol. Pharm.* **2013,** *10* (8), 3057-3066.
34. Li, Y.; Xiao, K.; Luo, J.; Xiao, W.; Lee, J. S.; Gonik, A. M.; Kato, J.; Dong, T. A.; Lam, K. S., Well-defined, reversible disulfide cross-linked micelles for on-demand paclitaxel delivery. *Biomaterials* **2011,** *32* (27), 6633-6645.
35. Xiao, K.; Luo, J.; Li, Y.; Lee, J. S.; Fung, G.; Lam, K. S., PEG-oligocholic acid telodendrimer micelles for the targeted delivery of doxorubicin to B-cell lymphoma. *J. Control. Release* **2011,** *155* (2), 272-281.
36. Huang, W.; Shi, C.; Shao, Y.; Lam, K. S.; Luo, J., The core-inversible micelles for hydrophilic drug delivery. *Chem. Comm.* **2013,** *49* (59), 6674-6676.
37. Ganta, S.; Devalapally, H.; Shahiwala, A.; Amiji, M., A review of stimuli-responsive nanocarriers for drug and gene delivery. *J. Control. Release* **2008,** *126* (3), 187-204.
38. Alarcon, C.; de las, H.; Pennadam, S.; Alexander, C., Stimuli responsive polymers for biomedical applications. *Chem. Soc. Rev.* **2005,** *34*, 276-285.
39. Schmaljohann, D., Thermo- and pH-responsive polymers in drug delivery. *Adv. Drug Delivery Rev.* **2006,** *58* (15), 1655-1670.
40. Weber, C.; Hoogenboom, R.; Schubert, U. S., Temperature responsive bio-compatible polymers based on poly(ethylene oxide) and poly(2-oxazoline)s. *Prog. Polym. Sci.* **2012,** *37* (5), 686-714.
41. Jia, Y.-G.; Zhu, X. X., Self-healing supramolecular hydrogel made of polymers bearing cholic acid and β-cyclodextrin pendants. *Chem. Mater.* **2015,** *27* (1), 387-393.
42. Jia, Y. G.; Zhu, X. X., Thermoresponsiveness of copolymers bearing cholic acid pendants induced by complexation with beta-cyclodextrin. *Langmuir* **2014,** *30* (39), 11770-11775.
43. Shao, Y.; Jia, Y. G.; Shi, C.; Luo, J.; Zhu, X. X., Block and random copolymers bearing cholic acid and oligo(ethylene glycol) pendant groups: aggregation, thermosensitivity, and drug loading. *Biomacromolecules* **2014,** *15* (5), 1837-1844.
44. Pal, S.; Ghosh Roy, S.; De, P., Synthesis via RAFT polymerization of thermo- and pH-responsive random copolymers containing cholic acid moieties and their self-assembly in water. *Polym. Chem.* **2014,** *5* (4), 1275-1284.
45. Zhang, Y. H.; Zhu, X. X., Polymers made from cholic acid derivatives: Selected properties. *Macromol. Chem. Phys.* **1996,** *197* (10), 3473-3482.
46. Hao, J.; Li, H.; Zhu, X. X., Synthesis of a comb-shaped cholic acid-containing polymer by atom transfer radical polymerization. *Biomacromolecules* **2006,** *7* (3), 995-998.

47. Liu, H.; Avoce, D.; Song, Z.; Zhu, X. X., N-Isopropylacrylamide copolymers with acrylamide and methacrylamide derivatives of cholic acid: Synthesis and characterization. *Macromol. Rapid Comm.* **2001,** *22* (9), 675-680.
48. Avoce, D.; Liu, H. Y.; Zhu, X. X., N-Alkylacrylamide copolymers with derivatives of cholic acid: Synthesis and thermosensitivity. *Polymer* **2003,** *44* (4), 1081-1087.
49. Benrebouh, A.; Avoce, D.; Zhu, X. X., Thermo- and pH-sensitive polymers containing cholic acid derivatives. *Polymer* **2001,** *42* (9), 4031-4038.
50. Cabrer, P. R.; Alvarez-Parrilla, E.; Al-Soufi, W.; Meijide, F.; Nunez, E. R.; Tato, J. V., Complexation of bile salts by natural cyclodextrins. *Supramol. Chem.* **2003,** *15* (1), 33-43.
51. Cabrer, P. R.; Alvarez-Parrilla, E.; Meijide, F.; Seijas, J. A.; Nunez, E. R.; Tato, J. V., Complexation of sodium cholate and sodium deoxycholate by β-cyclodextrin and derivatives *Langmuir* **1999,** *15* (17), 5489-5495.
52. Chen, Y.; Li, F.; Liu, B. W.; Jiang, B. P.; Zhang, H. Y.; Wang, L. H.; Liu, Y., Thermodynamic origin of selective binding of β-cyclodextrin derivatives with chiral chromophoric substituents toward steroids. *J. Phys. Chem. B* **2010,** *114* (49), 16147-16155.
53. Liu, Y.; Zhao, Y. L.; Zhang, H. Y., Recognition-induced supramolecular porous nanosphere formation from cyclodextrin conjugated by cholic acid. *Langmuir* **2006,** *22* (7), 3434-3438.
54. Tan, Z. J.; Zhu, X. X.; Brown, G. R., Formation of inclusion complexes of cyclodextrins with bile salt anions as determined by NMR titration studies. *Langmuir* **1994,** *10* (4), 1034-1039.
55. Yim, C. T.; Zhu, X. X.; Brown, G. R., Kinetics of inclusion reactions of β-cyclodextrin with several dihydroxycholate ions studied by NMR spectroscopy. *J. Phys. Chem. B* **1999,** *103* (3), 597-602.
56. Wang, X.; Duan, Y.; Li, C.; Lu, C., Synthesis, self-assembly, and formation of polymer vesicle hydrogels of thermoresponsive copolymers. *J. Mater. Sci.* **2015,** *50*, 3541-3548.
57. Xiong, Y.; Qi, J.; Yao, P., Amphiphilic cholic-acid-modified dextran sulfate and its application for the controlled delivery of superoxide dismutase. *Macromol. Biosci.* **2012,** *12* (4), 515-524.
58. Zhang, K.; Yu, A.; Wang, D.; Yang, W.; Li, J.; Zhang, X.; Wang, Y., Solvent-controlled self-assembly of amphiphilic cholic acid-modified PAMAM dendrimers. *Mater. Lett.* **2011,** *65* (2), 293-295.
59. Xu, F. J.; Zhu, Y.; Chai, M. Y.; Liu, F. S., Comparison of ethanolamine/ethylenediamine-functionalized poly(glycidyl methacrylate) for efficient gene delivery. *Acta Biomater.* **2011,** *7* (8), 3131-40.
60. Jia, Y. G.; Zhu, X. X., Thermo- and pH-responsive copolymers bearing cholic acid and oligo(ethylene glycol) pendants: Self-assembly and pH-controlled release. *ACS Appl. Mater. Interfaces* **2015,** *7* (44), 24649-2465.
61. Maitra, U.; Mukhopadhyay, S.; Sarkar, A.; Rao, P.; Indi, S. S., Hydrophobic pockets in a nonpolymeric aqueous gel: Observation of such a gelation process by color change. *Angew. Chem. Int. Ed.* **2001,** *40* (12), 2281-2283.

62. Sangeetha, N. M.; Balasubramanian, R.; Maitra, U.; Ghosh, S.; Raju, A. R., Novel cationic and neutral analogues of bile acids: Synthesis and preliminary study of their aggregation properties. *Langmuir* **2002,** *18* (19), 7154-7157.
63. Maitra, U.; Babu, P., First synthesis of phosphonobile acids and preliminary studies on their aggregation properties. *Steroids* **2003,** *68* (5), 459-63.
64. Blow, D. M.; Rich, A., Studies on the formation of helical deoxycholate complexes. *J. Am. Chem. Soc.* **1960,** *82* (14), 3566-3571.
65. Kandanelli, R.; Sarkar, A.; Maitra, U., Tb3+ sensitization in a deoxycholate organogel matrix, and selective quenching of luminescence by an aromatic nitro derivative. *Dalton Trans.* **2013,** *42* (43), 15381-15386.
66. Banerjee, S.; Kandanelli, R.; Bhowmik, S.; Maitra, U., Self-organization of multiple components in a steroidal hydrogel matrix: design, construction and studies on novel tunable luminescent gels and xerogels. *Soft Matter* **2011,** *7* (18), 8207-8215.
67. Chakrabarty, A.; Maitra, U.; Das, A. D., Metal cholate hydrogels: versatile supramolecular systems for nanoparticle embedded soft hybrid materials. *J. Mater. Chem.* **2012,** *22* (35), 18268-18274.
68. Zhu, X. X.; Moskova, M.; Denike, J. K., Preparation and characterization of copolymers of new monomers from bile acid derivatives with methacrylic monomers and selective hydrolysis of the homopolymers. *Polymer* **1996,** *37* (3), 493-498.
69. Gauthier, M. A.; Simard, P.; Zhang, Z.; Zhu, X. X., Bile acids as constituents for dental composites: in vitro cytotoxicity of (meth)acrylate and other ester derivatives of bile acids. *J. R. Soc. Interface* **2007,** *4* (17), 1145-1150.
70. Gauthier, M. A.; Zhang, Z.; Zhu, X. X., New dental composites containing multimethacrylate derivatives of bile acids: a comparative study with commercial monomers. *ACS Appl. Mater. Interfaces* **2009,** *1* (4), 824-832.
71. Zhang, X.; Li, Z.; Zhu, X. X., Biomimetic mineralization induced by fibrils of polymers. *Biomacromolecules* **2008,** *9* (9), 2309-2314.
72. Ahlheim, M.; Hallensleben, M. L., Kondensation polymerisation von gallensauren. *Makromol. Chem. Rapid Commun.* **1988,** *9*, 299-302.
73. Noll, O.; Ritter, H., Enzyme in polymer chemistry, 9. Polymerizable oligoesters from cholic acid via lipase catalyzed condensation reaction. *Macromol. Rapid Comm.* **1996,** *17*, 553-557.
74. Zuluaga, F.; Valderruten, N. E.; Wagener, K. B., The ambient temperature synthesis and characterization of bile acid polymers. *Polym. Bull.* **1999,** *42*, 41-46.
75. Gautrot, J. E.; Zhu, X. X., Main-chain bile acid based degradable elastomers synthesized by entropy-driven ring-opening metathesis polymerization. *Angew. Chem. Int. Ed.* **2006,** *45* (41), 6872-6874.
76. Gautrot, J. E.; Zhu, X. X., High molecular weight bile acid and ricinoleic acid-based copolyesters via entropy-driven ring-opening metathesis polymerisation. *Chem. Commun.* **2008,** *14*, 1674-1676.
77. Gautrot, J. E.; Zhu, X. X., Shape memory polymers based on naturally-occurring bile acids. *Macromolecules* **2009,** *42* (19), 7324-7331.
78. Thérien-Aubin, H.; Gautrot, J. E.; Shao, Y.; Zhang, J.; Zhu, X. X., Shape memory properties of main chain bile acids polymers. *Polymer* **2010,** *51* (1), 22-25.

79. Strandman, S.; Tsai, I. H.; Lortie, R.; Zhu, X. X., Ring-opening polymerization of bile acid macrocycles by Candida antarctica lipase B. *Polym. Chem.* **2013,** *4* (16), 4312-4316.
80. Shao, Y.; Lavigueur, C.; Zhu, X. X., Multishape memory effect of norbornene-based copolymers with cholic acid pendant groups. *Macromolecules* **2012,** *45* (4), 1924-1930.
81. Wang, K.; Jia, Y.-G.; Zhu, X. X., Biocompound-based multiple shape memory polymers reinforced by photo-cross-linking. *ACS Biomater. Sci. Eng.* **2015,** *1* (9), 855-863.
82. Ivanysenko, O.; Strandman, S.; Zhu, X. X., Triazole-linked polyamides and polyesters derived from cholic acid. *Polym. Chem.* **2012,** *3*, 1962-1965.
83. Li, S.; Malmstadt, N., Deformation and poration of lipid bilayer membranes by cationic nanoparticles. *Soft Matter* **2013,** *9* (20), 4969-4976.
84. Stanciu, M.; Nichifor, M., New degradable polyesters from deoxycholic acid and oligo(ethylene glycol)s. *Polym. Int.* **2013,** *62*, 1236-1242.
85. Levaray, N.; Zhu, X. X., Polyurethanes made from bile acids. *Chin. J. Polym. Sci.* **2016,** *34*, 616-622.
86. Cui, H.; He, G.; Wang, H.; Sun, X.; Liu, T.; Ding, L.; Fang, Y., Fabrication of a novel cholic acid modified OPE-based fluorescent film and its sensing performances to inorganic acids in acetone. *ACS Appl. Mater. Interfaces* **2012,** *4* (12), 6935-6941.
87. Hu, M. X.; Li, J. N.; Zhang, S. L.; Li, L.; Xu, Z. K., Hydrophilic modification of PVDF microfiltration membranes by adsorption of facial amphiphile cholic acid. *Colloids Surf. B* **2014,** *123* (1), 809-813.
88. Zhang, Z.; Liu, J.; Luo, Q.; Zhang, J.; Xu, J.; Zhu, X. X., Construction of a tunable metallohydrolase center on an invertible molecular pocket. *Org. Biomol. Chem.* **2011,** *9* (24), 8220-8223.
89. Zhang, J.; Junk, M. J. N.; Luo, J.; Hinderberger, D.; Zhu, X. X., 1,2,3-Triazole-containing molecular pockets derived from cholic acid: The influence of structure on host−guest coordination properties. *Langmuir* **2010,** *26* (16), 13415-13421.
90. Zhang, J.; Luo, J.; Zhu, X. X.; Junk, M. J. N.; Hinderberger, D., Molecular pockets derived from cholic acid as chemosensors for metal ions. *Langmuir* **2010,** *26* (4), 2958-2962.

Chapter 3. Thermoresponsive properties of star-shaped amphiphilic block copolymers based on cholic acid*

Abstract

Block copolymers having stimuli-responsive properties are gaining impetus in the design of drug and gene delivery systems for therapeutic purposes. Thermoresponsive polymers are particularly interesting due to the ease of control over their solution behavior in aqueous media. The fine tuning of the lower critical solution temperature (LCST) of such polymers is necessary to achieve a successful drug delivery. In this work, the thermoresponsive properties of block copolymers based on a bile acid are studied in aqueous media to determine the factors affecting the LCST. Poly(allyl glycidyl ether) (PAGE) and poly(ethylene glycol) (PEG) blocks were grafted from a cholic acid (CA) core to yield star-shaped block copolymers with 4 arms. The PAGE block was further functionalized to bear pendant amine groups. The effects of PEG length and of the amine groups on the LCST behavior in water at various salt concentrations were examined. A shorter PEG chain of 21 repeat units shows a LCST of 16 °C, whereas a longer PEG of 41 repeat units failed to show thermoresponsiveness up to 80 °C and at concentrations up to 50 mg/mL. Functionalizing the allyl groups increased the LCST of the polymers. A salting-out effect was observed by a decrease in LCST and the presence of salt also promoted precipitation of the nanoparticles.

* Submitted for publication as an article: A.J. Cunningham, X. Feng, H. Zhang, X. Banquy, J. Leblond Chain, X. X. Zhu

Contributions of authors other than supervisors:
Alexander J. Cunningham: Experimental design, conducting experiments, data analysis, manuscript writing.
Xiantao Feng: Helped in conducting experiments.
Hu Zhang: Helped in experimental design.

3.1 Introduction

Block copolymers represent an important class of nanomaterials with promising properties for biomedical applications. The literature describes examples of polymers tailored for a specific purpose in the biomedical field, i.e., controlled drug delivery,[1-3] scaffold for tissue engineering,[4-6] diagnostics,[7-9] medical devices,[10-11] and implants.[12-13] In response to a stimulus, such polymers are characterized by changes in their shape, structure, or solubility.[14-17] Polymers that possess a lower critical solution temperature (LCST) respond to variations in temperature by undergoing a sol-gel transition at a critical temperature.[18-19] The LCST behavior is a result of entropic effects.[18, 20] Above the LCST, the enthalpic contribution of hydrogen bonding between water and polymer chains is less than the entropic gain from the release of ordered water molecules surrounding the polymer which leads to the collapse of the polymers and loss of solubility.[18, 21] The polymers were shown to undergo coil-to-globule transitions,[22-24] aggregation stages that cause changes in solubility. The polymers possessing an LCST are versatile in the design of drug delivery systems; examples include injectable hydrogels,[21, 25] nanogels,[26-27] core-shell nanodevices,[28] and thermo-sensitive liposomes.[29] The common advantage in these examples is the creation of a drug depot that could be readily internalized by cells. Above the LCST, either exogenously or endogenously triggered, the polymer changes from a soluble micellar dispersion to an insoluble aggregate that accumulate at the target site and releases the loaded therapeutic compound over time acting as a slow drug release device. For therapeutic compounds like siRNA that do not cross the lipid membranes on their own, the presence of a LCST may severely hinder drug delivery, preventing the aggregated siRNA/polymer complex to enter the cell.[30] Therefore, control over the LCST behavior of drug delivery systems is warranted.

The factors that can affect the transition temperature are classified as either intrinsic or extrinsic. These factors include pH[31-32] and salt concentration[33-35] as intrinsic factors and surfactants[36-37] and co-solvents[38] as extrinsic factors since they all affect the polymer-solvent interactions. For example, the presence of salt has been discovered to promote a systematic decrease in the LCST.[33] The salts affect the hydration shell around the polymers and lower the critical temperature needed to cause aggregation of the polymers.[33] Moreover, in the case of poly(N-isopropylacrylamide) (PNIPAM), anions are

thought to bind directly to the amide groups on the polymer backbone and further destabilize the hydrogen bonding between the amide groups and water.[35] Studying the LCST behavior under various conditions is necessary and important to tailor the biomedical applications of the polymers; for example, tumoral environments were discovered to contain higher salt concentrations.[39]

Bile acids are a class of steroid-based endogenous molecules that act as surfactants for the solubilization of lipids in the intestine of various animals. Recently, they have been the focus of research efforts as starting materials in the design of drug delivery systems.[40-42] Bile acids are characterized by an intrinsic ability to self-assemble into micellar particles and can be further functionalized to tune their aggregation behavior. Poly(ethylene glycol) (PEG) and poly(allyl glycidyl ether) (PAGE) have been added onto a core of cholic acid (CA, a bile acid) to significantly improve the bioavailability of Itraconazole, a commonly prescribed hydrophobic antifungal drug.[42] Moreover, CA-based drug delivery systems have been designed for the encapsulation and delivery of various hydrophobic active pharmaceutical ingredients.[41] The allyl groups of PAGE can be further functionalized via click chemistry to include amines as pendant groups, since the introduction of amines can facilitate the ionic complexation needed in gene delivery.[30] In response to the requirements for such a polyplex system, we have designed and prepared star-shaped CA-(PAGE-*b*-PEG)$_4$ copolymers since it is constructed from biocompatible starting material, i.e., cholic acid, a naturally occurring compound in the body, and PEG which is an FDA-approved excipient in drug formulations.[43-44] The block copolymer chains extend from the cholic acid core as four branches in a star-shaped architecture. Branched polymers have been shown in several reports to favor higher siRNA loading over linear polymers.[45-46] Indeed, we have previously demonstrated that the amine functionalized CA-(PAGE-*b*-PEG)$_4$ (CA-(PAGE-NH$_2$-*b*-PEG)$_4$) allowed a high loading of siRNA even at low molar equivalents.[30] Some of these CA-based block copolymers are characterized with an LCST behavior especially under physiological conditions in the presence of electrolytes, their thermoresponsive properties have yet to be thoroughly examined.[47] To the best of our knowledge, there are few reports that describe the implication of adding amine groups to polymers on their solution stability and thermoresponsive properties. Thermoresponsiveness is often described as a desirable

trait in numerous applications, but in the case of gene delivery it can present a hurdle to the transfection process. It is customary to study the transfection potential of a delivery system in vitro in conditions and time frames that do not mimic those encountered in the blood circulation. As a result, the impact of salt concentrations on the solution stability of amine-functionalized polymers is often overlooked. To explore the potential use of CA-based amphiphilic block copolymers for drug and gene delivery,[40, 42] the present study examines the thermoresponsive properties of the CA-based block copolymers in aqueous solutions under different conditions. The PAGE and PEG blocks are sequentially polymerized on CA to afford a star-shaped block copolymer with four pendant arms (CA-(PAGE-*b*-PEG)$_4$). The effects of PEG length, the presence of amine groups and salt concentrations on the LCST behavior have been studied.

3.2 Experimental Section

3.2.1 Chemicals and reagents.

All chemicals and reagents were purchased from Sigma Aldrich and used without further purification, unless stated otherwise. For the anionic polymerization, dimethyl sulfoxide (DMSO) and allyl glycidyl ether (AGE) were dried over calcium hydride overnight and distilled prior to use. Ethylene oxide gas was passed through a column of calcium hydride before condensing. Methanol was dried with magnesium sulfate and filtered before use. Tetrahydrofuran (THF) was dried with sodium under reflux and distilled prior to use. Azobisisobutyronitrile (AIBN) was used without further purification.

3.2.2 Anionic polymerization of CA-(PAGE-*b*-PEG)$_4$.

CA-(PAGE-*b*-PEG)$_4$ were synthesized via anionic polymerization using an ethanolamine derivative of cholic acid (CA) as initiator. The ethanolamine derivative of CA, i.e. 5β-cholanoamide, was synthesized according to a previous publication (Scheme 1).[48] This initiator is used in the anionic polymerization of AGE followed by the anionic polymerization of ethylene oxide to afford a star-shaped CA-(PAGE-*b*-PEG)$_4$ with 4-arms composed of hydrophobic PAGE and hydrophilic PEG blocks. The protocol that was followed is the same as that previously published.[30, 40] The purified polymers were characterized by ^{1}H-NMR and SEC.

3.2.3 Functionalization of CA-(PAGE-*b*-PEG)$_4$.

The pendant allyl groups of CA-(PAGE-*b*-PEG)$_4$ were functionalized using click chemistry to afford pendant primary (CA-(PAGE-NH$_2$-*b*-PEG)$_4$) (Scheme 1). For the CA-(PAGE-NH$_2$-*b*-PEG)$_4$ synthesis, CA-(PAGE-*b*-PEG)$_4$ (2 g, 0.15 mmol) was dissolved in dry methanol (25 mL). AIBN (0.8 g, 4.6 mmol, 30 eq) was added to the methanol solution followed by cysteamine hydrochloride (4.2 g, 36.8 mmol, 240 eq). The reaction was initiated by immersing in an oil bath at 75 °C under reflux and argon atmosphere. The reaction proceeded overnight and was stopped by cooling to room temperature. Water was added to the methanol and the mixture was dialyzed for 48 h using regenerated cellulose (MWCO 3.5 kDa) to remove unreacted cysteamine hydrochloride. The polymers were freeze-dried and stored at 4 °C. The functionalized polymers were characterized by ^{1}H-NMR spectroscopy.

3.2.4 Characterization methods.

The molar mass of the polymers was determined by size exclusion chromatography (SEC) with dimethylformamide (DMF) as eluent on a Breeze system from Waters equipped with a 717 plus autosampler, a 1525 Binary HPLC pump, and a 2410 refractive index detector and two consecutive Polar Gel M and Polar Gel L columns (Agilent Technologies, USA) with a flow rate of 0.7 mL/min and at 50 °C. Poly(methyl methacrylate) (PMMA) standards were used for calibration. All samples were filtered on a PTFE 0.2 μm filters prior to injection. HPLC grade DMF was degassed with N_2 for 30 min before use. The ^{1}H-NMR spectra were recorded using a Bruker AV400 spectrometer operating at 400 MHz. The samples were dissolved in DMSO-d_6 and ran with 24 scans and a relaxation delay of 10 s. Dynamic light scattering (DLS) measurements were performed on a Malvern Zetasizer NanoZS instrument equipped with a He-Ne laser with a wavelength of 633 nm, and at a scattering angle of 173.5°. Intensity-averaged hydrodynamic diameters of the dispersions were obtained using the non-negative least-squares (NNLS) algorithm. Disposable cuvettes were used, and the samples were filtered using 0.45 μm nylon filters prior to measurements. The samples were measured in triplicates and the average value is reported. The values for viscosity, refractive index and dielectric constant were those pre-set in the instrument for the respective solution. To study the effect of temperature, the micelle size was measured from 1 to 60 °C measuring

at each 1 °C increment and with a 2 min equilibration at each temperature point. The average of triplicate values is reported. The critical micellar concentration was obtained using a previously published protocol.[49] Briefly, a stock solution of pyrene in acetone (10^{-6} M) was prepared and added to a series of vials. Then, acetone was removed by rotary evaporation. Block copolymer aqueous solutions with concentrations varying from 10^{-6} to 0.1 mg/mL were prepared by dissolving the polymer into deionized water and then added to the vials containing pyrene. The solutions were stirred for 24 h to allow equilibration of the micelles and pyrene encapsulation. Then, the fluorescence spectra of pyrene were recorded using a Cary Eclipse fluorescence spectrometer (Agilent Technologies, USA). The excitation wavelength was set to 340 nm and the fluorescence recorded between 350 to 470 nm with a band width of 5 nm for both excitation and emission. From the pyrene fluorescence spectrum, the peak intensities at 373 and 383 nm (I_1 and I_3, respectively) were recorded and plotted as the ratio I_3/I_1 vs. block copolymer concentration. From this graph, two lines were fitted for each of the two slopes in the curve and the CMC was obtained by calculating the intersection of these two lines. Cloud points of the polymer samples at various concentrations were measured using UV-Vis spectroscopy. The polymers were dissolved in the solution and the absorbance measured with varying temperature at a heating rate of 0.5 °C/min. The absorbance (A) values were correlated to the percentage of transmission (T) according to the following equation:

$$T = 10^{(2-A)} \text{ x } 100\%$$

3.3 Results and discussion

3.3.1 Polymer synthesis and characterization.

To study the influence of the polymer architecture on the LCST properties of the CA-based block copolymers, the length of the different blocks was varied, and their physico-chemical properties were examined under different conditions. Once the star-shaped block copolymers were synthesized, the pendant allyl groups of PAGE were functionalized via a thiol-ene click reaction (Scheme 3.1) to afford CA-[(PAGE-NH_2)-*b*-PEG]$_4$. Cysteamine hydrochloride was coupled to the allyl groups affording a primary amine group. The SEC chromatograms show polymers of narrow molecular weight distributions and an increase in the molecular weight when extending the PAGE blocks

with PEG (Figures 3.1 and S3.1). The molecular weights obtained relative to PMMA standards are shown in Table 3.1.

The ^{1}H-NMR spectra of the polymers are shown in Figures 3.2 and S3.2. The NMR signals at 0.58, 0.81 and 0.92 ppm correspond to the methyl groups on positions 18, 19 and 21 of the cholic acid core, respectively. The signals at 5.1-5.28 and 5.8-5.95 ppm (peaks c and b, respectively) correspond to the methylene (=CH_2) and methine (-CH=) protons of the pendant allyl groups of the PAGE block, respectively. The signals at 3.35-3.60 ppm (peak a) correspond to the methylene protons of the PAGE main chain. Setting the integral region of the peak at 0.58 ppm and measuring the integral region of the peaks at 3.35-3.60 ppm, the number of repeating units of the PAGE block was calculated (Table 3.1). Upon chain extension of the PAGE blocks with PEG, the integral region at 3.35-3.60 ppm (peak a for methylene protons on PEG) increases significantly. The spin-lattice relaxation times (T_1) of the nuclei in polymer chain ends are known to be longer than those from the nuclei in the polymer backbone.[50] Hence, to minimize its impact on the measured molecular weight, the integral region of the methine proton at 5.8-5.95 ppm (peak b) of the PAGE pendant groups was used as reference to calculate the integral region of the methylene peaks at 3.35-3.60 ppm (peak a) of both PAGE and PEG backbone and the molecular weights calculated are shown in Table 3.1. To ensure that all four hydroxyl groups reacted to give rise to a 4-arm star-shaped block copolymer, the terminal hydroxyl groups of the PEG chain of the polymers were reacted with trifluoroacetic anhydride which causes a downfield chemical shift change in the terminal methylene protons to 4.45-4.60 ppm (peak i) (Figure 3.2). Measuring the integral region of this peak and comparing it to the integral region of the methine proton from the PAGE allyl group at 5.8-5.95 ppm (peak b), the results show that 4-armed star-shaped block copolymers were successfully synthesized.

Upon functionalization, the methylene (=CH_2) and methine (-CH=) peaks (peaks c and b, respectively) of the pendant allyl group of PAGE disappear and new peaks corresponding to the methylene groups of thioethaneamine (-S-CH_2-CH_2-NH_2) groups appear. For both CA-[(AGE-NH_2)$_7$-*b*-EG$_{21}$]$_4$ and CA-[(AGE-NH_2)$_9$-*b*-EG$_{41}$]$_4$, the peaks at 2.70-2.82 ppm (peaks d) corresponds to the methylene protons adjacent to the thioether (-S-C$\underline{H}_2$-), whereas the peaks at 2.92-3.0 ppm (peaks f, -C$\underline{H}_2$-NH_2) corresponds to the

methylene protons adjacent to the amino group. Setting the integral region of the methylene peaks at 3.35-3.60 ppm (peaks a) from the PAGE and PEG backbone as reference, the integral region of the thioethaneamine groups (peaks d, e, and f) was calculated and the results show close to 100% functionalization.

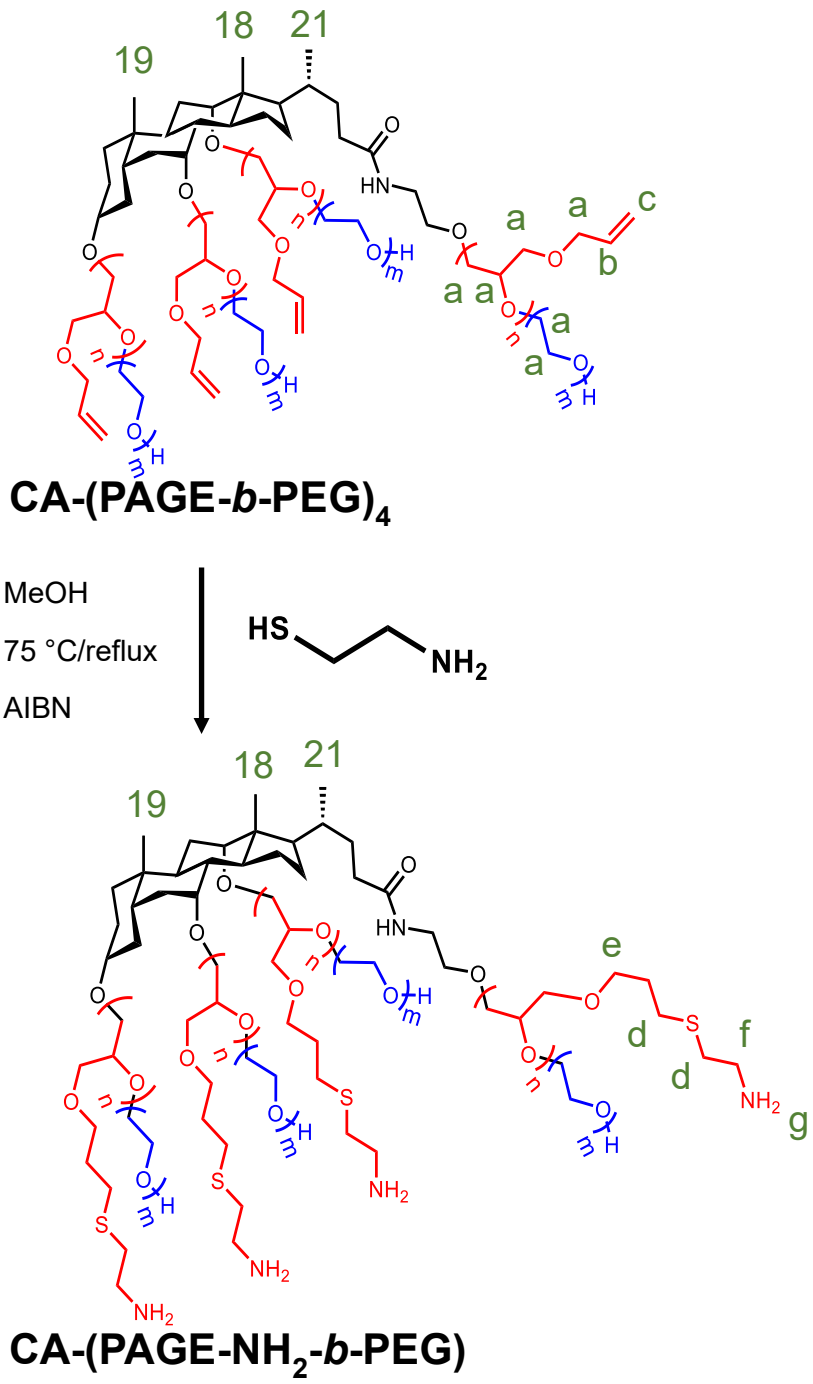

Scheme 3.1. Structure of the star-shaped block copolymers based on cholic acid made by anionic polymerization and the post-polymerization functionalization of the PAGE block through thiol-ene reactions. Certain groups are numbered to facilitate the discussion

related to the attribution of characteristic proton signals in the NMR spectrum in Figure 3.2.

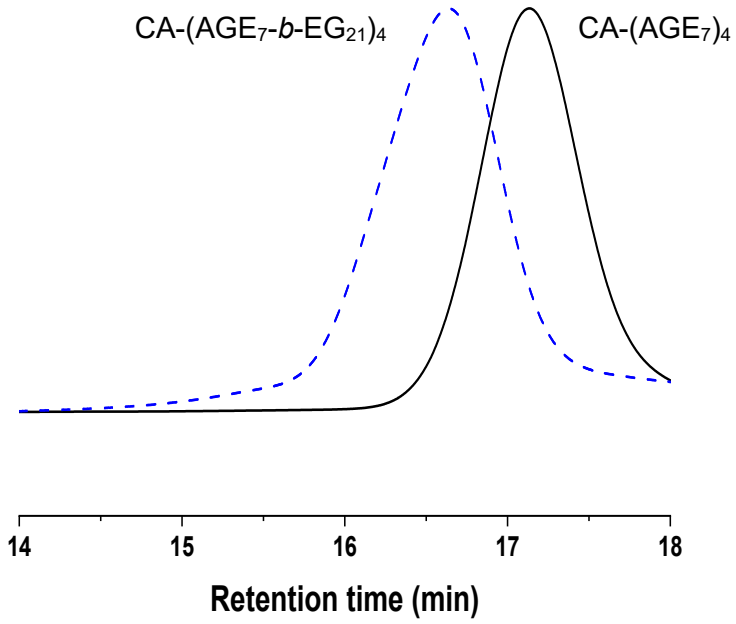

Figure 3.1. SEC chromatograms for CA-$(AGE_7)_4$ homopolymer and the corresponding CA-$(AGE_7$-*b*-$EG_{21})_4$ block copolymer obtained at 30 °C using DMF as eluent and calibrated with PMMA standards.

Table 3.1 Characteristics of the polymer samples obtained from the anionic polymerization as studied by SEC and ^{1}H-NMR.

Polymer	Molecular Weight (M_n, g/mol)		Đ
	^{1}H-NMR	SEC	
CA-$(AGE_7)_4$	3,600	3,700	1.29
CA-$(AGE_7$-*b*-$EG_{21})_4$	7,300	9,000	1.19
CA-$(AGE_9)_4$	4,100	5,500	1.19
CA-$(AGE_9$-*b*-$EG_{41})_4$	11,800	16,100	1.18

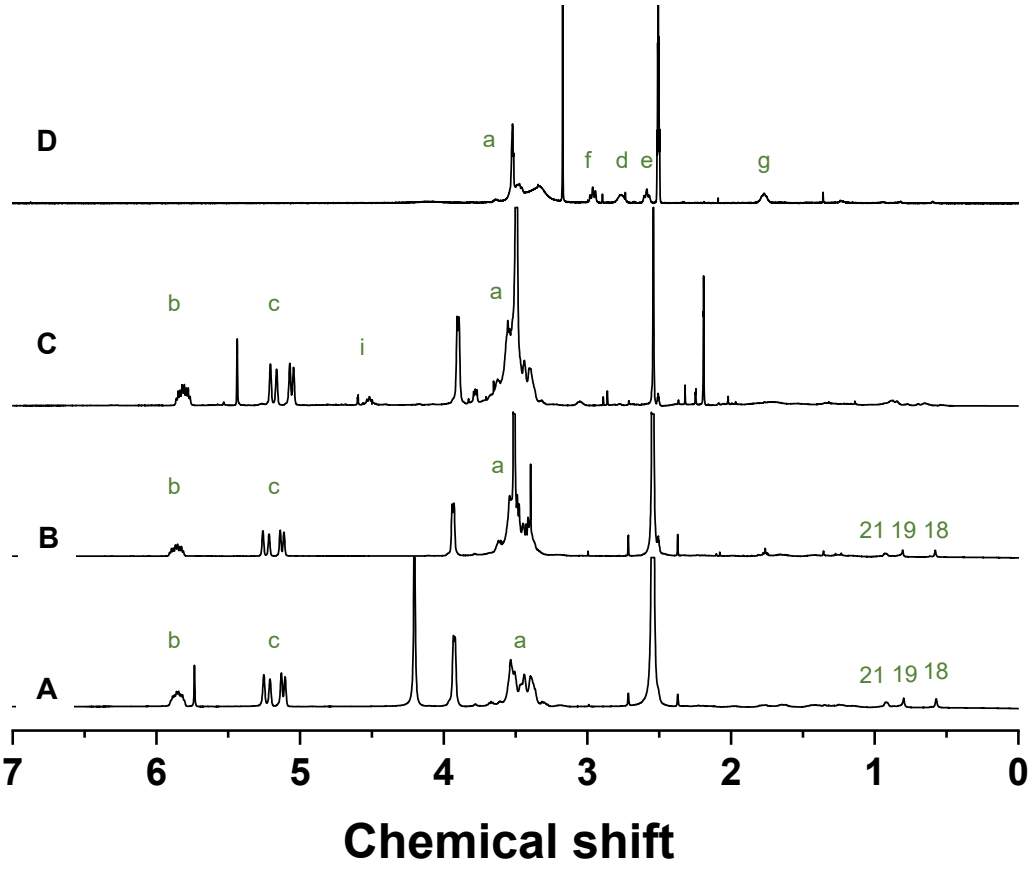

Figure 3.2. ^{1}H-NMR spectra of (A) homopolymer CA-(PAGE$_7$)$_4$, (B) block copolymer CA(PAGE$_7$-*b*-PEG$_{21}$)$_4$, (C) CA-(AGE$_7$-*b*-EG$_{21}$-CF$_3$)$_4$ and (D) CA-((AGE-NH$_2$)$_7$-*b*-EG$_{21}$)$_4$ in DMSO-d$_6$. The characteristic peaks in the spectra are numbered as shown in the structures in Scheme 1.

3.3.2 Aggregation properties.

Due to the amphiphilic nature of the star-shaped block copolymers, both CA-(AGE$_7$-*b*-EG$_{21}$)$_4$ and CA-(AGE$_9$-*b*-EG$_{41}$)$_4$ are expected to self-assemble in an aqueous environment above their critical aggregation concentration (CAC). To determine the CAC, a fluorescence technique using pyrene as a reporter probe was used.[51-52] The vibronic fine structure intensity of pyrene monomer displays solvent polarity dependency and plotting the ratio of I_3/I_1 in varying concentration of polymer allows the determination of the CAC value.[52] The results are shown in Figure 3.3. The CAC for CA-(AGE$_7$-*b*-EG$_{21}$)$_4$ is 2 μg/mL whereas that of CA-(AGE$_9$-*b*-EG$_{41}$)$_4$ is 19 μg/mL. The two polymers have a similar length for the hydrophobic block but vary greatly in their hydrophilic block. It was previously observed that there exist an linear relationship between the length of the

hydrophilic block and the CMC value, where the longer the hydrophilic block the higher the CAC value.[53-54] Therefore, it is not surprising that the CAC value increases from 2 to 19 µg/mL when the length of the hydrophilic block increases from CA-(AGE$_7$-*b*-EG$_{21}$)$_4$ to CA-(AGE$_9$-*b*-EG$_{41}$)$_4$. For CA-[(AGE-NH$_2$)$_9$-*b*-EG$_{41}$]$_4$, no change in the ratio I_3/I_1 was observed for concentrations up to 0.1 mg/mL indicating that no micelles form below this concentration (data not shown). Coupling cysteamine to the pendant allyl groups of PAGE increases the hydrophilicity of the PAGE block thereby disrupting the hydrophobic interaction between the polymer and preventing its aggregation at relatively low concentrations.

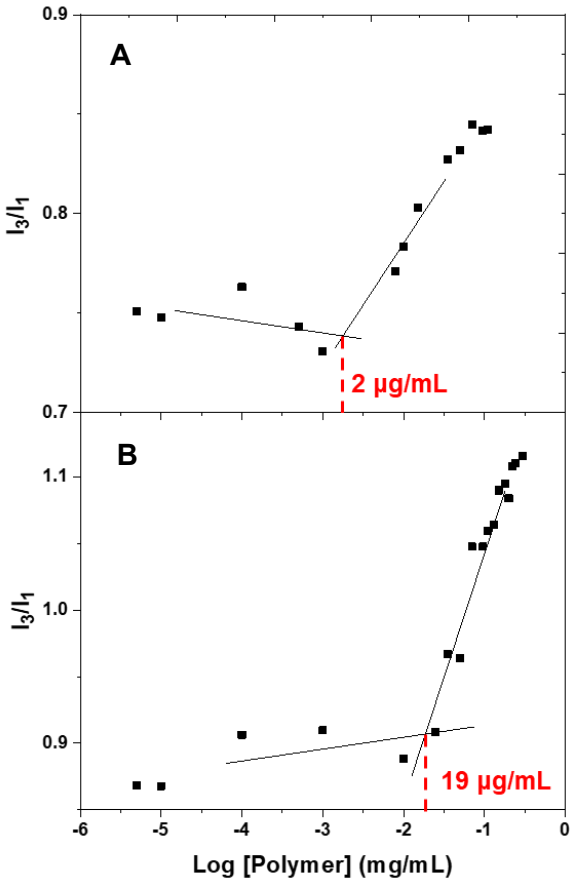

Figure 3.3. Fluorescence intensity ratio (I_3/I_1) of pyrene in the presence of varying concentration of (A) CA-(AGE$_7$-*b*-EG$_{21}$)$_4$ and (B) CA-(AGE$_9$-*b*-EG$_{41}$)$_4$. The intercept shown in the data gives the critical micellar concentration of the amphiphilic copolymers.

The micellar size of the amphiphilic star-shaped block copolymers was measured by using DLS (Figure 3.4). The results show a monomodal micelle population of 16 nm for CA-(AGE$_9$-*b*-EG$_{41}$)$_4$ with a low size dispersity of 0.09, whereas CA-(AGE$_7$-*b*-EG$_{21}$)$_4$ presents a bimodal population with one population of 84 nm and another of 541 nm and a size dispersity of 0.30. We have previously studied the shape of the nanoparticles under TEM for a similar system and the results demonstrate that spherical micellar aggregates with a dense core were obtained for CA-(PAGE-*b*-PEG)$_4$.[40] The difference in the micellar size for these two systems is a result of the steric stabilization afforded by the PEG chains. The longer PEG chains minimize micellar aggregation and the DLS shows one micelle population for CA-(AGE$_9$-*b*-EG$_{41}$)$_4$, whereas the shorter PEG of CA-(AGE$_7$-*b*-EG$_{21}$)$_4$ is not as successful in preventing micellar aggregation and a bimodal population with much larger diameters is observed. A similar conclusion was previously reported.[55] It was shown that the PEG chains reduced micellar aggregation through steric repulsion and that a PEG chain of 16 repeating unit failed to prevent micellar aggregation with a reported micelle size > 2 μm, whereas a PEG chain of 45 and 113 repeating units reduced the micelle size significantly to 750 and 250 nm, respectively.[55]

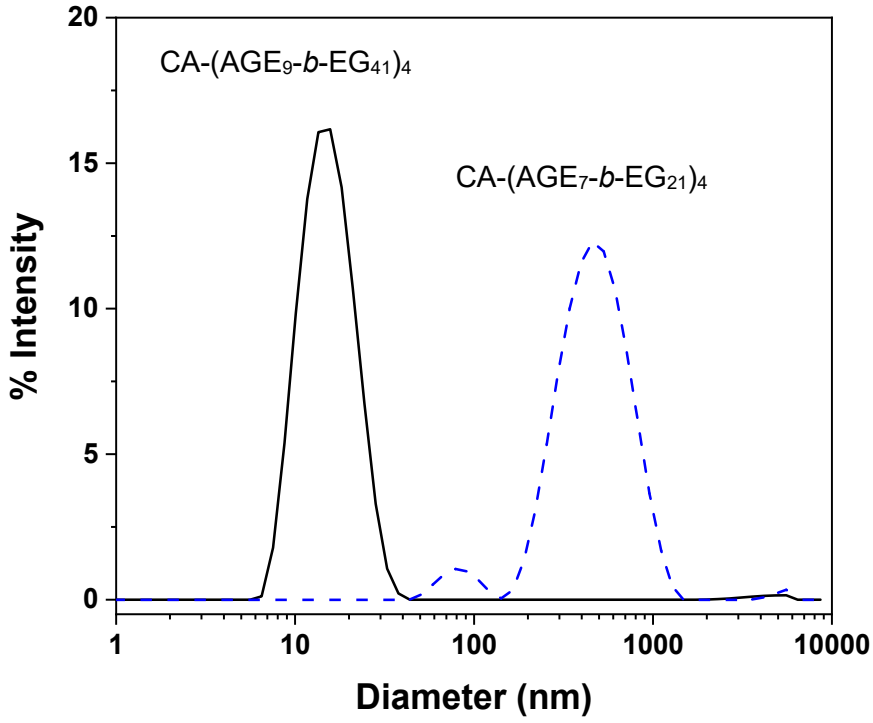

Figure 3.4. DLS data showing the intensity size distribution of CA-(PAGE-*b*-PEG)$_4$ samples obtained in deionized water at a concentration of 1 mg/mL. Samples were filtered with 0.45 μm nylon filters prior to measurement.

3.3.3 Thermosensitive properties.

PEG is a neutral, water-soluble, and biocompatible polymer that has been used extensively in the design of drug delivery systems. PEG has been previously observed to possess thermoresponsive properties displaying an LCST above 100 °C.[56-58] At elevated temperatures, PEG suffers from dehydration causing aggregation of the block copolymer micelles and precipitation.[57] In order to implement PEG as a hydrophilic block in the design of bile acid-based star block copolymers for use in drug and gene delivery systems, it is necessary to fully characterize the thermoresponsive properties of CA-(PAGE-*b*-PEG)$_4$. To this end, the cloud points of CA-(AGE$_7$-*b*-EG$_{21}$)$_4$ and CA-(AGE$_9$-*b*-EG$_{41}$)$_4$ were measured at different concentrations. Figure 3.5 clearly shows the cloud points by the temperature dependence of the transmittance of CA-(AGE$_7$-*b*-EG$_{21}$)$_4$ at different polymer concentrations. These measurements were carried out in triplicates at each concentration (Figure S3.3) with the average values of the cloud points reported in Figure

3.5. Lowering the concentration from 50 to 5 mg/mL causes a decrease in the cloud point from 24 to 16 °C, but the cloud point increases to 39 °C when the concentration is lowered further to 1 mg/mL. A partial phase diagram for CA-(AGE$_7$-*b*-EG$_{21}$)$_4$ can be constructed as shown in Figure 3.5. The PEG chains for the CA-(AGE$_7$-*b*-EG$_{21}$)$_4$ are short and dehydrate at lower temperatures when the concentration is increased from 1 to 50 mg/mL. This instability can result from insufficient steric stabilization due to the short PEG length which worsen with increasing polymer concentration causing the micelles to associate into micellar clusters.[59] Interestingly, the cloud point increases when the concentration is further lowered from 5 to 1 mg/mL. This is believed to arise from a kinetics effect. Measuring the cloud point by turbidimetry is affected by the kinetics of the aggregation process and is sensitive only to macroscopic phase separation phenomena, i.e., the formation of polymer aggregates, and at low concentration of polymers this process may be slow or even difficult and occur at higher temperatures, which can facilitate the aggregation at very low concentrations.[60-62] In contrast, the CA-(AGE$_9$-*b*-EG$_{41}$)$_4$ nanoparticles with longer PEG chains does not exhibit a cloud point up to 80 °C even for concentrations as high as 50 mg/mL (Figure S3.4). The longer PEG chains are more hydrophilic and are expected to possess higher cloud points.

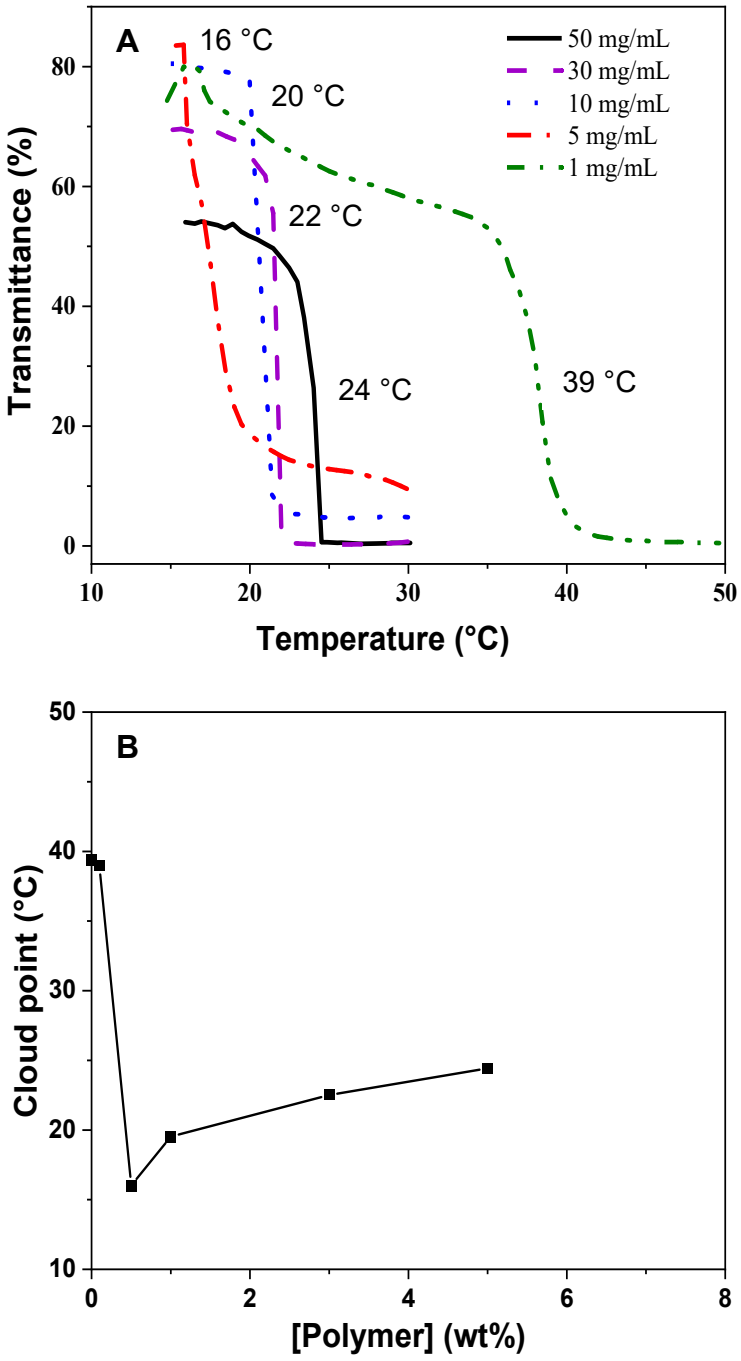

Figure 3.5. (A) light transmittance at λ = 500 nm for CA-(AGE$_7$-*b*-EG$_{21}$)$_4$ as a function of temperature obtained at different polymer concentrations with a heating rate of 1 °C/min and (B) partial phase diagram obtained for CA-(AGE$_7$-*b*-EG$_{21}$)$_4$.

To further characterize the thermoresponsive properties of CA-(AGE$_7$-*b*-EG$_{21}$)$_4$, the size of the nanoparticles measured by DLS as a function of temperature is reported in Figure 3.6. The initial micelle size at 1 °C is 79 nm and the size increases with increasing temperature to reach > 1500 nm at 36 °C. The cloud point can be obtained by fitting two linear regressions tangent to the curve as depicted in Figure 6 and calculating the intersection of those two lines. The calculated cloud point is 32 °C, lower than 39 °C obtained from the turbidity measurements. This discrepancy in the measured cloud points by different techniques has been reported in the literature.[18] DLS measurements typically provide lower and more accurate cloud point measurements than other techniques as they measure the onset of particle aggregation even before they reach a critical size that would yield clouding of the solution and a change in transmittance.[18]

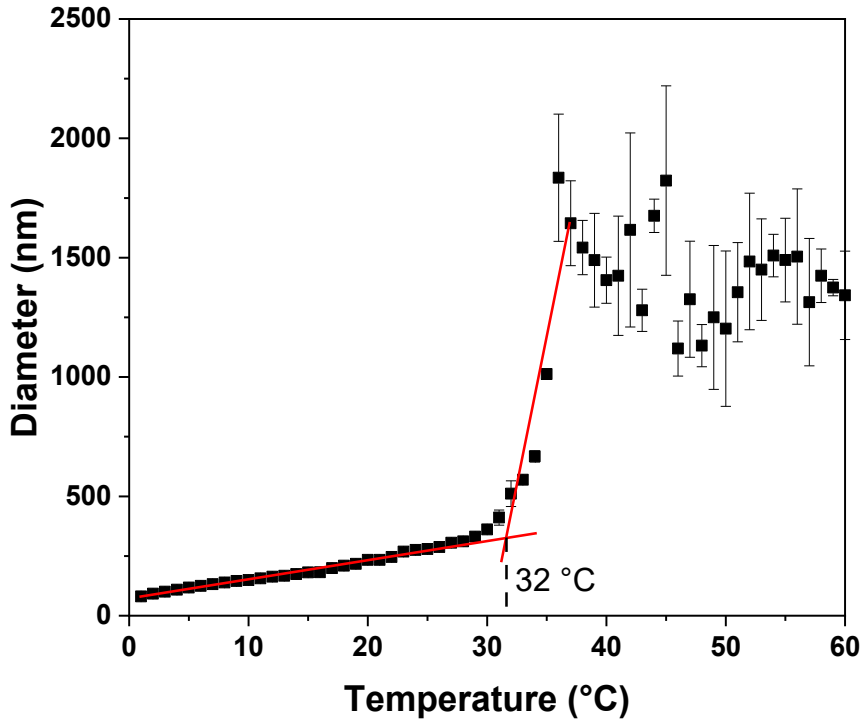

Figure 3.6. DLS temperature trend for CA-(AGE$_7$-*b*-EG$_{21}$)$_4$ obtained at a concentration of 1 mg/mL and sample equilibrated for 2 min at each temperature point. Triplicate values were obtained for each temperature point and the average value is reported.

Next, the thermoresponsive properties of the functionalized CA-[(PAGE-NH$_2$)-*b*-PEG]$_4$ was studied. It shows a cloud point at 75 °C (Figure 3.7) which is significantly higher than

that of the non-functionalized CA-(AGE_7-*b*-EG_{21})$_4$ at 16 °C and can result from the more extensive hydrogen bonding with water due to the presence of the pendant amine groups. The hydrogen bonds must be broken to elicit aggregation of the micellar nanoparticles. Similarly, DLS was used to measure particle size as a function of temperature but no cloud point was observed up to 60 °C (Figure S3.5). Unsurprisingly, no cloud point was observed for CA-[(AGE-NH_2)$_9$-*b*-EG_{41}]$_4$ at temperatures up to 80 °C (Figure 3.7A). The longer PEG chain length and higher hydrophilicity imparted by functionalization of the allyl groups of PAGE with pendant amine groups raises the cloud point even higher.

The presence of salt is known to decrease the cloud point of thermoresponsive polymers in a phenomenon known as the salting-out effect.[63-65] Since such polymers may be exposed to the high salt concentrations present *in vivo*, the thermoresponsive properties of CA-[(AGE-NH_2)$_7$-*b*-EG_{21}]$_4$ was studied in varying NaCl concentration from 10 to 200 mM (Figure 3.7B). It precipitated at all salt concentrations tested and did not show a cloud point between 15 and 80 °C indicating that its cloud point is below 15 °C. The change in the cloud point is highly consistent with other reports of a large shift in the cloud point as a function of salt concentration.[33] The amine groups of CA-[(PAGE-NH_2)-*b*-PEG]$_4$ block copolymers influence the solubility of the nanoparticle and can lead to precipitation in the presence of NaCl. The amine groups on CA-[(PAGE-NH_2)-*b*-PEG]$_4$ are necessary for the ionic complexation with siRNA in gene therapy. In the presence of salt, however, these block copolymers may lose their colloidal stability due to a salting-out effect. Although amine-functionalized polymers have been extensively studied as potential gene delivery vectors, to the best of our knowledge, there are few reports on the study of the salt effect on the colloidal stability of these systems. It is necessary to examine the influence of the type and the number of amine groups on the solution stability of such polymers and their thermoresponsive properties under various conditions. Moreover, we have previously demonstrated the advantage of adding co-surfactants to stabilize the CA-[(PAGE-NH_2)-*b*-PEG]$_4$ in salt solutions.[30] Lipids were added as co-surfactants and increased the T_{cp} of CA-[(PAGE-NH_2)-*b*-PEG]$_4$ to temperatures higher than the physiological temperature.[30] Additional studies examining different types of co-surfactants, the length of PEG blocks and their combined effect on the thermoresponsive properties would aide in improving

the solution stability of amine-functionalized polymers in salt solutions for *in vivo* gene therapy.

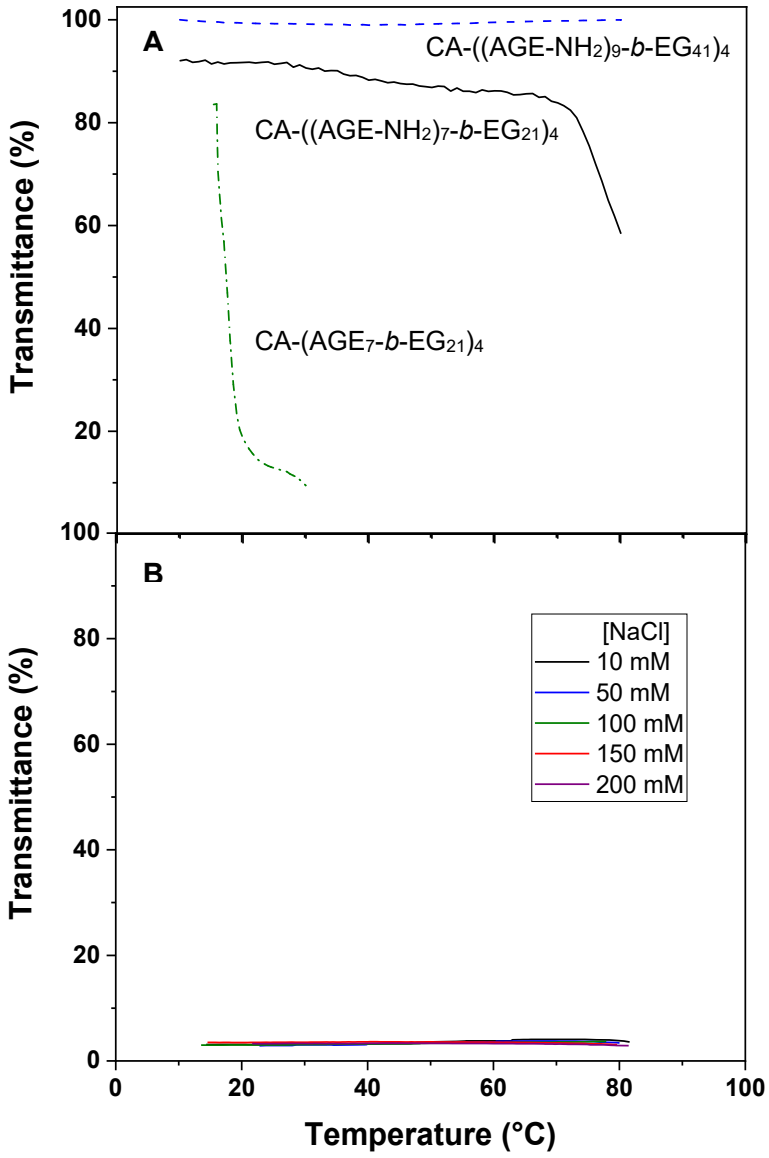

Figure 3.7. (A) Light transmittance as a function of temperature for CA-((AGE-NH_2)$_7$-*b*-EG_{21})$_4$ and CA-((PAGE-NH_2)$_9$-*b*-PEG_{41})$_4$. The sample concentration was 5 mg/mL with a scan rate of 1 °C/min. (B) Transmittance as a function of temperature for CA-((AGE-NH_2)$_7$-*b*-EG_{21})$_4$ at NaCl concentrations varying from 10 to 200 mM. The sample concentration was 25 mg/mL with a scan rate of 1 °C/min.

3.4 Conclusions

Star-shaped block copolymers based on cholic acid in the form CA-(PAGE-*b*-PEG)$_4$ were synthesized via successive anionic polymerization of AGE and EO monomers. The PAGE blocks were further functionalized via thiol-ene click chemistry to afford pendant amine groups repeated along the PAGE block. Both CA-(AGE$_7$-*b*-EG$_{21}$)$_4$ and CA-(AGE$_9$-*b*-EG$_{41}$)$_4$ formed micelles with CMC values of 2 and 19 μg/mL, respectively. CA-(AGE$_9$-*b*-EG$_{41}$)$_4$ with longer PEG blocks has a higher CMC value due its higher hydrophilicity. CA-(AGE$_9$-*b*-EG$_{41}$)$_4$ formed micelles of 15 nm with a monomodal population and low dispersity, whereas the CA-(AGE$_7$-*b*-EG$_{21}$)$_4$ with a shorter PEG chain formed a bimodal population of micelles with 84 and 541 nm in diameters. No micellar clustering was observed for the polymers with a longer PEG chain at 41 repeating units, while the shorter PEG chains (21 repeating units) showed micellar clustering at a certain critical temperature. CA-(AGE$_7$-*b*-EG$_{21}$)$_4$ showed a cloud point of 16 °C, which increased to 75 °C when the PAGE groups were functionalized with pendant amine groups. This increase in cloud point is a result of increased hydrogen bonding between the amine groups of functionalized PAGE and water that needs to be broken to induce a change in solubility. In the presence of varying NaCl concentration from 10 to 200 mM, CA-[(AGE-NH$_2$)$_7$-*b*-EG$_{21}$]$_4$ formed precipitates and no cloud points were observed between 15 and 80 °C. Neither CA-(AGE$_9$-*b*-EG$_{41}$)$_4$ nor CA-[(AGE-NH$_2$)$_9$-*b*-EG$_{41}$]$_4$ displayed thermoresponsive properties up to 80 °C due to the longer PEG chains and higher hydrophilicity. To further characterize the thermoresponsive behavior of these star-shaped block copolymers, the length of the PEG block and amount of amine groups repeated in the PAGE block need to be studied to understand the relationship between the cloud point and salt concentration. Moreover, the addition of lipids as co-surfactants is being investigated to improve the solution stability of these amine-functionalized star-shaped block copolymers.

3.5 Acknowledgments

Financial support from NSERC of Canada is gratefully acknowledged. AC and XXZ are members of CQMF funded by FRQNT and GRSTB funded by FRSQ. AC thanks the Camille Sandorfy, Charron Lam, and GRSTB Ph.D. scholarships.

3.6 Supporting Information

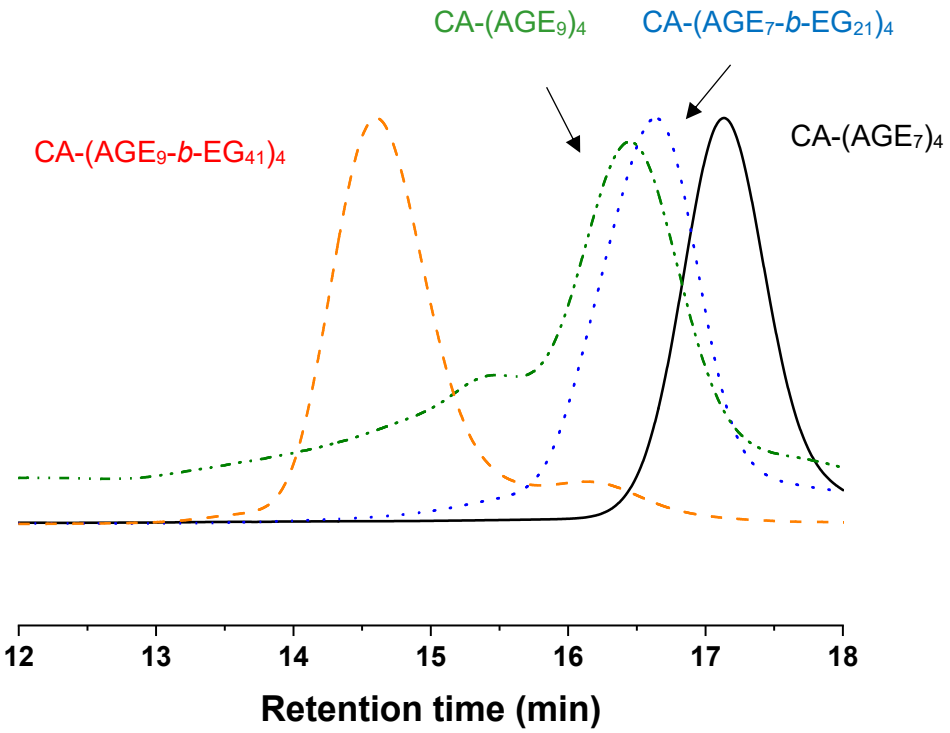

Figure S3.1. SEC chromatograms of CA-$(AGE_7)_4$ and CA-$(AGE_9)_4$ homopolymers and their corresponding CA-$(AGE_7$-*b*-$EG_{21})_4$ and CA-$(AGE_9$-*b*-$EG_{41})_4$ block copolymers. The traces were obtained at 30 °C using DMF as eluent. The molecular weights shown in Table 1 are relative to PMMA standards.

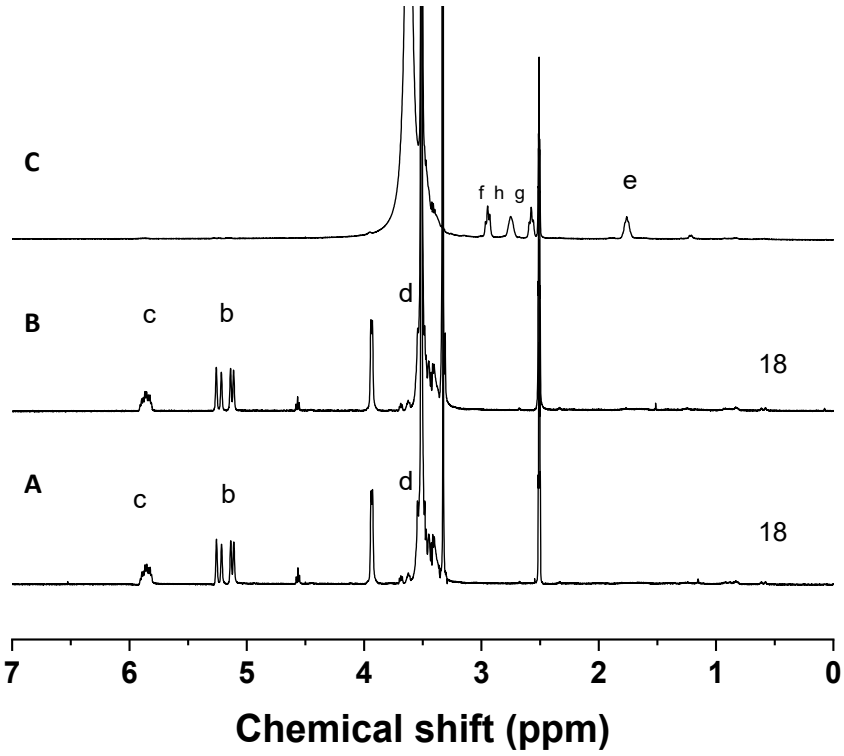

Figure S3.2. ^{1}H-NMR spectra of (A) homopolymer CA-$(AGE_9)_4$, (B) block copolymer CA-$(AGE_9$-*b*-$EG_{41})_4$ and (C) CA-$((AGE\text{-}NH_2)_9$-*b*-$EG_{41})_4$ in DMSO-d_6. The characteristic peaks in the spectra were numbered according to the structures shown in Scheme 1.

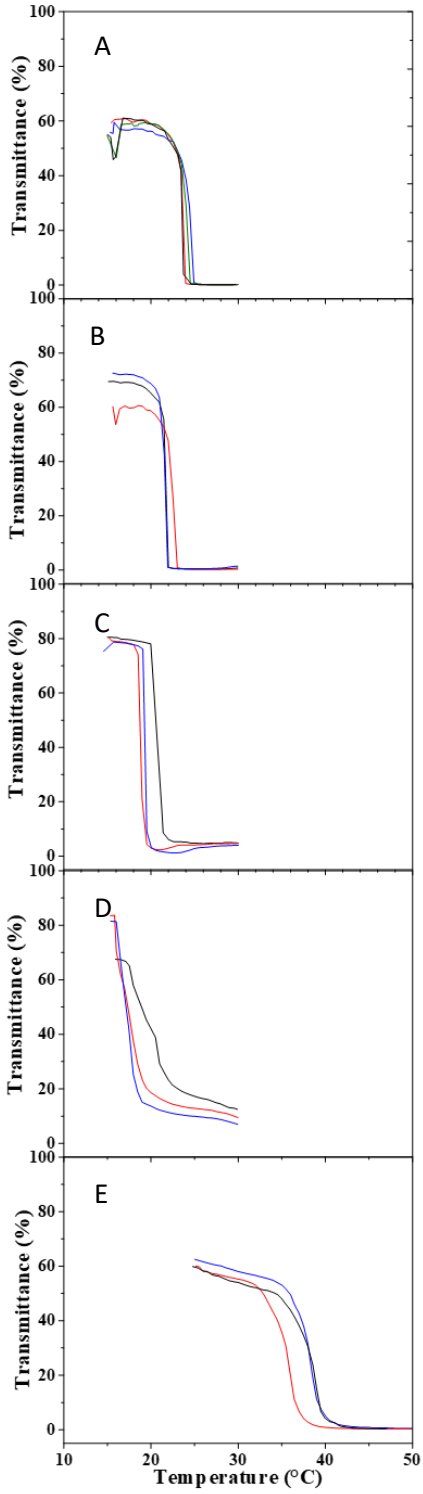

Figure S3.3. Transmittance variation as a function of temperature for CA-(AGE$_7$-*b*-EG$_{21}$)$_4$ at concentrations of (A) 50, (B) 30, (C) 10, (D) 5, and (E) 1 mg/mL with a scan rate of 1 °C/min, triplicate measurements for each sample.

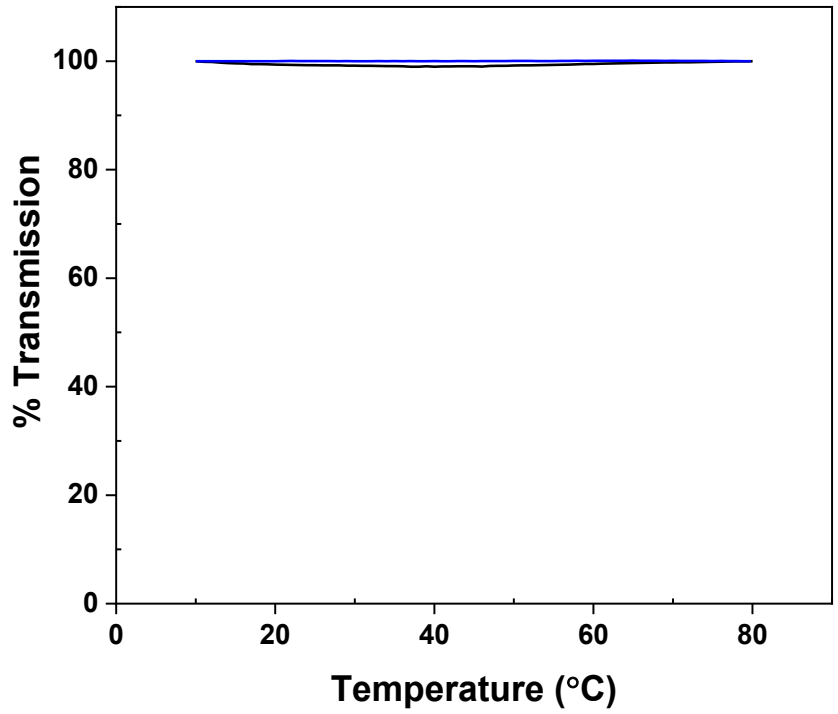

Figure S3.4. Light transmittance as a function of temperature for CA-$(AGE_9$-*b*-$EG_{41})_4$ (λ = 500 nm). The sample concentration was 50 mg/mL with a scan rate of 1 °C/min.

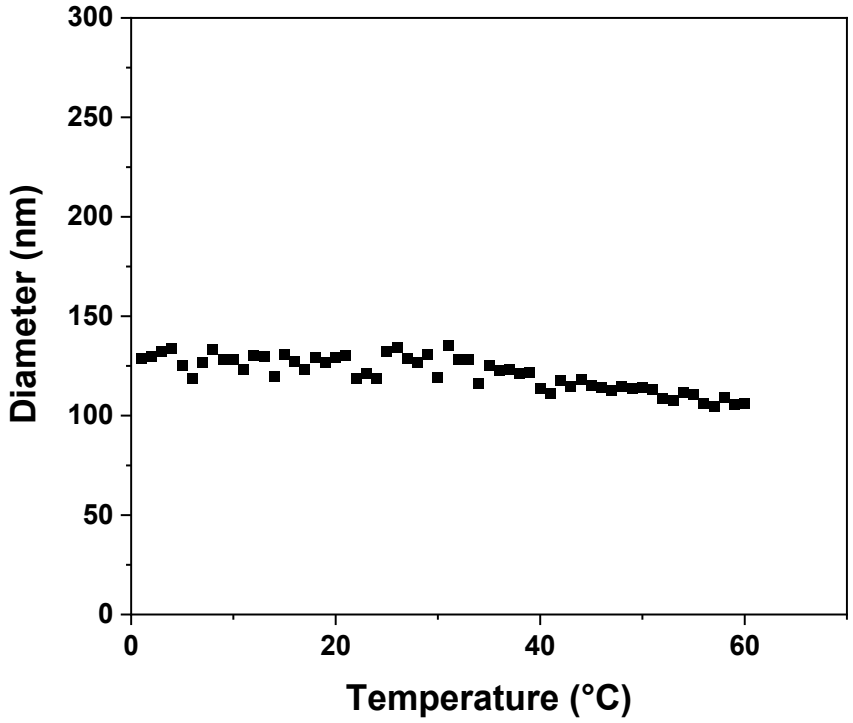

Figure S3.5. DLS temperature trend for CA-((AGE-NH_2)$_7$-*b*-EG_{21})$_4$ obtained at a concentration of 1 mg/mL and sample equilibrated for 2 min at each temperature point. Triplicate values were obtained for each temperature point and the average value is reported.

3.7 References

1. Liechty, W. B.; Kryscio, D. R.; Slaughter, B. V.; Peppas, N. A., Polymers for drug delivery systems. *Annu. Rev. Chem. Biomol. Eng.* **2010,** *1*, 149-173.
2. Uhrich, K. E.; Cannizzaro, S. M.; Langer, R. S.; Shakesheff, K. M., Polymeric systems for controlled drug release. *Chem. Rev.* **1999,** *99* (11), 3181-3198.
3. Goldberg, M.; Langer, R.; Jia, X., Nanostructured materials for applications in drug delivery and tissue engineering. *J. Biomater. Sci. Polym. Ed.* **2007,** *18* (3), 241-268.
4. Stratton, S.; Shelke, N. B.; Hoshino, K.; Rudraiah, S.; Kumbar, S. G., Bioactive polymeric scaffolds for tissue engineering. *Bioact. Mater.* **2016,** *1* (2), 93-108.
5. Liu, X.; Ma, P. X., Polymeric scaffolds for bone tissue engineering. *Ann. Biomed. Eng.* **2004,** *32* (3), 477-486.
6. Place, E. S.; George, J. H.; Williams, C. K.; Stevens, M. M., Synthetic polymer scaffolds for tissue engineering. *Chem. Soc. Rev.* **2009,** *38* (4), 1139-1151.
7. Perkins, A. C., Polymer diagnostics: the next generation of image contrast agents. *J. Drug Target* **1998,** *6* (2), 79-84.
8. Parisi, O. I.; Scrivano, L.; Sinicropi, M. S.; Picci, N.; Puoci, F., Engineered polymer-based nanomaterials for diagnostic, therapeutic and theranostic applications. *Mini Rev. Med. Chem.* **2016,** *16* (9), 754-761.
9. Piletsky, S. A.; Turner, N. W.; Laitenberger, P., Molecularly imprinted polymers in clinical diagnostics—Future potential and existing problems. *Med. Eng. Phys.* **2006,** *28* (10), 971-977.
10. Bernard, M.; Jubeli, E.; Pungente, M. D.; Yagoubi, N., Biocompatibility of polymer-based biomaterials and medical devices – regulations, in vitro screening and risk-management. *Biomater. Sci.* **2018,** *6* (8), 2025-2053.
11. Angelova, N.; Hunkeler, D., Rationalizing the design of polymeric biomaterials. *Trends Biotechnol.* **1999,** *17* (10), 409-421.
12. Dang, T. T.; Nikkhah, M.; Memic, A.; Khademhosseini, A., Chapter 19 - Polymeric biomaterials for implantable prostheses. In *Natural and Synthetic Biomedical Polymers*, Kumbar, S. G.; Laurencin, C. T.; Deng, M., Eds. Elsevier: Oxford, 2014; pp 309-331.
13. Teo, A. J. T.; Mishra, A.; Park, I.; Kim, Y.-J.; Park, W.-T.; Yoon, Y.-J., Polymeric biomaterials for medical implants and devices. *ACS Biomater. Sci. Eng.* **2016,** *2* (4), 454-472.
14. Narayanaswamy, R.; Torchilin, V. P., Hydrogels and their applications in targeted drug delivery. *Molecules* **2019,** *24* (3), 603-621.
15. Kamaly, N.; Yameen, B.; Wu, J.; Farokhzad, O. C., Degradable controlled-release polymers and polymeric nanoparticles: Mechanisms of controlling drug release. *Chem. Rev.* **2016,** *116* (4), 2602-2663.
16. Wei, M.; Gao, Y.; Li, X.; Serpe, M. J., Stimuli-responsive polymers and their applications. *Polym. Chem.* **2017,** *8* (1), 127-143.
17. Stuart, M. A. C.; Huck, W. T. S.; Genzer, J.; Müller, M.; Ober, C.; Stamm, M.; Sukhorukov, G. B.; Szleifer, I.; Tsukruk, V. V.; Urban, M.; Winnik, F.; Zauscher, S.; Luzinov, I.; Minko, S., Emerging applications of stimuli-responsive polymer materials. *Nat. Mater.* **2010,** *9* (2), 101-113.

18. Zhang, Q.; Weber, C.; Schubert, U. S.; Hoogenboom, R., Thermoresponsive polymers with lower critical solution temperature: from fundamental aspects and measuring techniques to recommended turbidimetry conditions. *Mater. Horiz.* **2017,** *4* (2), 109-116.
19. Parmar, I. A.; Shedge, A. S.; Badiger, M. V.; Wadgaonkar, P. P.; Lele, A. K., Thermo-reversible sol–gel transition of aqueous solutions of patchy polymers. *RSC Advances* **2017,** *7* (9), 5101-5110.
20. Lessard, D. G.; Ousalem, M.; Zhu, X. X., Effect of the molecular weight on the lower critical solution temperature of poly(N,N-diethylacrylamide) in aqueous solutions. *Can. J. Chem.* **2001,** *79* (12), 1870-1874.
21. Klouda, L.; Mikos, A. G., Thermoresponsive hydrogels in biomedical applications. *Eur. J. Pharm. Biopharm.* **2008,** *68* (1), 34-45.
22. Wang, X.; Wu, C., Light-scattering study of coil-to-globule transition of a poly(N-isopropylacrylamide) chain in deuterated water. *Macromolecules* **1999,** *32* (13), 4299-4301.
23. Chu, B.; Wu, C., Coil-globule transition: Self-assembly of a single polymer chain. *Macromol. Symp.* **1996,** *106* (1), 421-423.
24. Wang, X.; Qiu, X.; Wu, C., Comparison of the coil-to-globule and the globule-to-coil transitions of a single poly(N-isopropylacrylamide) homopolymer chain in water. *Macromolecules* **1998,** *31* (9), 2972-2976.
25. Ron, E. S.; Bromberg, L. E., Temperature-responsive gels and thermogelling polymer matrices for protein and peptide delivery. *Adv. Drug Deliv. Rev.* **1998,** *31* (3), 197-221.
26. Gandhi, S. S.; Yan, H.; Kim, C., Thermoresponsive gelatin nanogels. *ACS Macro Lett.* **2014,** *3* (11), 1210-1214.
27. Wu, H. Q.; Wang, C. C., Biodegradable smart nanogels: A new platform for targeting drug delivery and biomedical diagnostics. *Langmuir* **2016,** *32* (25), 6211-6225.
28. Zhang, J. L.; Srivastava, R. S.; Misra, R. D. K., Core−shell magnetite nanoparticles surface encapsulated with smart stimuli-responsive polymer: Synthesis, characterization, and LCST of viable drug-targeting delivery system. *Langmuir* **2007,** *23* (11), 6342-6351.
29. Wang, J.; Ayano, E.; Maitani, Y.; Kanazawa, H., Tunable surface properties of temperature-responsive polymer-modified liposomes induce faster cellular uptake. *ACS Omega* **2017,** *2* (1), 316-325.
30. Cunningham, A. J.; Gibson, V. P.; Banquy, X.; Zhu, X. X.; Jeanne, L. C., Cholic acid-based mixed micelles as siRNA delivery agents for gene therapy. *Int. J. Pharm.* **2020,** *578*, 119078.
31. Tamaki, M.; Kojima, C., pH-Switchable LCST/UCST-type thermosensitive behaviors of phenylalanine-modified zwitterionic dendrimers. *RSC Advances* **2020,** *10* (18), 10452-10460.
32. Pei, Y.; Chen, J.; Yang, L.; Shi, L.; Tao, Q.; Hui, B.; Li, J., The effect of pH on the LCST of poly(N-isopropylacrylamide) and poly(N-isopropylacrylamide-co-acrylic acid). *J. Biomater. Sci. Polym. Ed.* **2004,** *15* (5), 585-594.

33. Freitag, R.; Garret-Flaudy, F., Salt effects on the thermoprecipitation of poly-(N-isopropylacrylamide) oligomers from aqueous solution. *Langmuir* **2002,** *18* (9), 3434-3440.
34. Liu, X.; Cheng, F.; Liu, H.; Chen, Y., Unusual salt effect on the lower critical solution temperature of hyperbranched thermoresponsive polymers. *Soft Matter* **2008,** *4* (10), 1991-1994.
35. Du, H.; Wickramasinghe, R.; Qian, X., Effects of salt on the lower critical solution temperature of poly (N-isopropylacrylamide). *J. Phys. Chem. B* **2010,** *114* (49), 16594-16604.
36. Lee, S. B.; Song, S. C.; Jin, J. I.; Sohn, Y. S., Surfactant effect on the lower critical solution temperature of poly(organophosphazenes) with methoxy-poly(ethylene glycol) and amino acid esters as side groups. *Colloid Polym. Sci.* **2000,** *278* (11), 1097-1102.
37. Lee, L.-T.; Cabane, B., Effects of surfactants on thermally collapsed poly(N-isopropylacrylamide) macromolecules. *Macromolecules* **1997,** *30* (21), 6559-6566.
38. Bharadwaj, S.; Kumar, P. B. S.; Komura, S.; Deshpande, A. P., Kosmotropic effect leads to LCST decrease in thermoresponsive polymer solutions. *J. Chem. Phys.* **2018,** *148* (8), 084903.
39. Amara, S.; Tiriveedhi, V., Inflammatory role of high salt level in tumor microenvironment. *Int. J. Oncol.* **2017,** *50* (5), 1477-1481.
40. Cunningham, A. J.; Robinson, M.; Banquy, X.; Leblond, J.; Zhu, X. X., Bile acid-based drug delivery systems for enhanced doxorubicin encapsulation: Comparing hydrophobic and ionic interactions in drug loading and release. *Mol. Pharm.* **2018,** *15* (3), 1266-1276.
41. Cunningham, A. J.; Zhu, X. X., Polymers made of bile acids: from soft to hard biomaterials. *Can. J. Chem.* **2016,** *94* (8), 659-666.
42. Le Dévédec, F.; Strandman, S.; Hildgen, P.; Leclair, G.; Zhu, X. X., PEGylated bile acids for use in drug delivery systems: Enhanced solubility and bioavailability of itraconazole. *Mol. Pharm.* **2013,** *10* (8), 3057-3066.
43. Strickley, R. G., Solubilizing excipients in oral and injectable formulations. *Pharm. Res.* **2004,** *21* (2), 201-230.
44. D'souza, A. A.; Shegokar, R., Polyethylene glycol (PEG): a versatile polymer for pharmaceutical applications. *Expert Opin. Drug Deliv.* **2016,** *13* (9), 1257-1275.
45. Boeckle, S.; von Gersdorff, K.; van der Piepen, S.; Culmsee, C.; Wagner, E.; Ogris, M., Purification of polyethylenimine polyplexes highlights the role of free polycations in gene transfer. *J. Gene Med.* **2004,** *6* (10), 1102-1111.
46. Scholz, C.; Wagner, E., Therapeutic plasmid DNA versus siRNA delivery: common and different tasks for synthetic carriers. *J. Control. Release* **2012,** *161* (2), 554-565.
47. Li, C.; Lavigueur, C.; Zhu, X. X., Aggregation and thermoresponsive properties of new star block copolymers with a cholic acid core. *Langmuir* **2011,** *27* (17), 11174-11179.
48. Luo, J.; Giguère, G.; Zhu, X. X., Asymmetric poly(ethylene glycol) star polymers with a cholic acid core and their aggregation properties. *Biomacromolecules* **2009,** *10* (4), 900-906.

49. Topel, Ö.; Çakır, B. A.; Budama, L.; Hoda, N., Determination of critical micelle concentration of polybutadiene-block-poly(ethyleneoxide) diblock copolymer by fluorescence spectroscopy and dynamic light scattering. *J. Mol. Liq.* **2013,** *177*, 40-43.
50. Chen, D.; Gao, L.-f.; Li, X.-h.; Tu, Y.-f., Precise molecular weight determination and structure characterization of end-functionalized polymers: An NMR approach via combination of one-dimensional and two-dimensional techniques. *Chin. J. Polym. Sci.* **2017,** *35* (5), 681-692.
51. Aguiar, J.; Carpena, P.; Molina-Bolívar, J. A.; Carnero Ruiz, C., On the determination of the critical micelle concentration by the pyrene 1:3 ratio method. *J. Colloid Interface Sci.* **2003,** *258* (1), 116-122.
52. Kalyanasundaram, K.; Thomas, J. K., Environmental effects on vibronic band intensities in pyrene monomer fluorescence and their application in studies of micellar systems. *J. Am. Chem. Soc.* **1977,** *99* (7), 2039-2044.
53. Astafieva, I.; Khougaz, K.; Eisenberg, A., Micellization in block polyelectrolyte solutions. 2. Fluorescence study of the critical micelle concentration as a function of soluble block length and salt concentration. *Macromolecules* **1995,** *28* (21), 7127-7134.
54. Kabanov, A. V.; Batrakova, E. V.; Alakhov, V. Y., Pluronic® block copolymers as novel polymer therapeutics for drug and gene delivery. *J. Control. Release* **2002,** *82* (2), 189-212.
55. Thevenot, J.; Troutier, A.-L.; David, L.; Delair, T.; Ladavière, C., Steric stabilization of lipid/polymer particle assemblies by poly(ethylene glycol)-lipids. *Biomacromolecules* **2007,** *8* (11), 3651-3660.
56. Saeki, S.; Kuwahara, N.; Nakata, M.; Kaneko, M., Upper and lower critical solution temperatures in poly (ethylene glycol) solutions. *Polymer* **1976,** *17* (8), 685-689.
57. Cui, Q.; Wu, F.; Wang, E., Thermosensitive behavior of poly(ethylene glycol)-based block copolymer (PEG-b-PADMO) controlled via self-assembled microstructure. *J. Phys. Chem. B* **2011,** *115* (19), 5913-5922.
58. Bae, Y. C.; Lambert, S. M.; Soane, D. S.; Prausnitz, J. M., Cloud-point curves of polymer solutions from thermooptical measurements. *Macromolecules* **1991,** *24* (15), 4403-4407.
59. Li, C.; Lavigueur, C.; Zhu, X. X., Aggregation and thermoresponsive properties of new star block copolymers with a cholic acid core. *Langmuir* **2011,** *27* (17), 11174-11179.
60. Boutris, C.; Chatzi, E. G.; Kiparissides, C., Characterization of the LCST behaviour of aqueous poly(N-isopropylacrylamide) solutions by thermal and cloud point techniques. *Polymer* **1997,** *38* (10), 2567-2570.
61. Mannella, G. A.; Carrubba, V. L.; Brucato, V., Measurement of cloud point temperature in polymer solutions. *Rev. Sci. Instrum.* **2013,** *84* (7), 075118.
62. Philipp, M.; Aleksandrova, R.; Müller, U.; Ostermeyer, M.; Sanctuary, R.; Müller-Buschbaum, P.; Krüger, J. K., Molecular versus macroscopic perspective on the demixing transition of aqueous PNIPAM solutions by studying the dual character of the refractive index. *Soft Matter* **2014,** *10* (37), 7297-7305.

63. Pandit, N.; Trygstad, T.; Croy, S.; Bohorquez, M.; Koch, C., Effect of salts on the micellization, clouding, and solubilization behavior of pluronic F127 solutions. *J. Colloid Interface Sci.* **2000,** *222* (2), 213-220.
64. Nishida, K.; Morita, H.; Katayama, Y.; Inoue, R.; Kanaya, T.; Sadakane, K.; Seto, H., Salting-out and salting-in effects of amphiphilic salt on cloud point of aqueous methylcellulose. *Process Biochem.* **2017,** *59*, 52-57.
65. Curbelo, F.; Garnica, A.; Neto, E., Salinity effect in cloud point phenomena by nonionic surfactants used in enhanced oil recovery tests. *Petrol. Sci. Tech.* **2013,** *31* (15), 1544-1552.

Chapter 4. Bile acid-based drug delivery systems for enhanced doxorubicin encapsulation: Comparing hydrophobic and ionic interactions in drug loading and release*

Abstract

Doxorubicin (Dox) is a drug of choice in the design of drug delivery systems directed towards breast cancers but is often limited by loading and control over its release from polymer micelles. Bile acid-based block copolymers present certain advantages over traditional polymer-based systems for drug delivery purposes since they can enable a higher drug loading via the formation of a reservoir through their aggregation process. In this study, hydrophobic and electrostatic interactions are compared for their influence on Dox loading inside cholic acid-based block copolymers. Poly(allyl glycidyl ether) (PAGE) and poly(ethylene glycol) (PEG) were grafted from the cholic acid (CA) core yielding a star-shaped block copolymer with 4 arms (CA-(PAGE-*b*-PEG)$_4$) and then loaded with Dox via a nanoprecipitation technique. The interaction of CA-(PAGE-*b*-PEG)$_4$ with Dox was modulated either through covalent modification of the PAGE block to afford electrostatic binding or *via* hydrophobic interaction between the micelle core and Dox. A high Dox loading of 14 wt % was achieved via electrostatic as opposed to hydrophobic interactions with or without oleic acid as a cosurfactant. The electrostatic interactions confer a pH responsiveness to the system. 50% of the loaded Dox was released at pH 5 in comparison to 12% at pH 7.4. The nanoparticles with Dox loaded via hydrophobic interactions, did not show such a pH responsiveness. The systems with Dox loaded via electrostatic interactions showed the lowest IC_{50} and highest cellular internalization indicating the pre-eminence of this interaction in Dox loading. The blank formulations are biocompatible and did not show cytotoxicity up to 0.17 mg/mL. The new

* Published as an article: A.J. Cunningham, M. Robinson, X. Banquy, J. Leblond-Chain, X.X. Zhu, *Mol. Pharm.*, **2018**, *15*, 1266-1276.

Contributions of authors other than supervisors:
Alexander J. Cunningham: Experimental design, conducting experiments, data analysis, manuscript writing.
Mattieu Robinson: Helped in experimental design.

functionalized star block copolymers based on cholic acid show great potential as drug delivery carriers.

4.1 Introduction

Breast cancer is the second most prevalent and deadly form of cancer in women. It is currently treated with a combination of surgery and chemotherapy.[1] Over the course of chemotherapy, not only will the patient suffer greatly from adverse effects, but the cancer often develops resistance mechanisms limiting the therapeutic outcome of the treatment.[2] A common strategy to diminish the side effects inherent to chemotherapy is the encapsulation of the cytotoxic molecules into a drug delivery system. Doxorubicin (Dox) is currently used for breast cancer treatment but is characterized with severe toxicity due to its off-target effects. Over the past decades, a great deal of research effort has been directed at encapsulating chemotherapeutics in drug delivery systems to increase their safety and transport efficiency to the cancer tissues. Toward this end, polymer-based micelles have attracted much attention with several formulations reaching clinical trials.[3,4]

Polymer-based micelles of a core-shell structure are typically aggregates of polymer chains with a hydrophobic core and hydrophilic corona. They are often the preferred platform for antitumor drug formulations due to their unique core-shell structure, tunable size and shape, ease of synthesis and freedom in design and structure.[5,6] Much research work has focused on the loading of therapeutically relevant molecules with hydrophobic character inside the core of these micelles.[7-10] For these systems, the drug loading level is greatly influenced by the hydrophobic interaction of the core-forming block and the drug.[11] Unfortunately, these formulations are often plagued with a low drug loading and instability in vivo.[12-14] Strategies to circumvent this limitation include adjustment of the hydrophobic-hydrophilic balance,[15-17] improvement of the polymer-drug interactions,[18-21] cross-linking,[22-25] or conjugation of the drug to the polymer via covalent bonding.[15,26-29] However, these strategies are often met with challenges, particularly slow, insufficient release. For example, release of a drug conjugated to the polymer necessitates the cleavage of a covalent bond, which may slow down the release. Non-covalent interactions such as ionic interactions and hydrogen bonding may also favor drug loading.[30-38] Dox bears a positive charge at physiological pH and is composed of aromatic rings favoring non-covalent interactions via aromatic stacking. Many reports demonstrate the superiority of

ionic interactions offering higher drug loading and better stability, and stimuli-sensitive release in response to the environmental pH.[30,32-34] Despite recent advancements in polymer-based systems, achieving high drug loading and improving tissue biodistribution remain limiting factors.[6,15,39] In an effort to address the first issue, we intend to study the interaction and forces that govern Dox loading in the context of bile acid-based polymer micelles.

We have previously shown the advantage of using bile acids in the design of drug delivery systems.[40-42] Micelles formed by bile acid-based polymers are less densely packed than linear polymers of similar structure,[43] creating an internal reservoir that may hold a larger amount of hydrophobic therapeutic molecules. We have studied the loading of hydrophobic itraconazole in bile acid-based nanoparticles.[41] These formulations reached high loading contents (35 wt %) and high encapsulation efficiencies (>89 %) as well as improved bioavailability and pharmacokinetics of the drug. Dox presents a different challenge with different interaction forces. Therefore, we modified the design of the copolymer based on cholic acid. Hydrophobic poly(allyl glycidyl ether) (PAGE) and hydrophilic poly(ethylene glycol) (PEG) blocks were attached sequentially via anionic polymerization onto a cholic acid (CA) core to yield a star-shaped copolymer of 4 arms, CA-(PAGE-*b*-PEG)$_4$ (Scheme 1). The star-shaped polymers based on bile acids have demonstrated their advantages in biocompatibility and drug loading.[44] The allyl groups of PAGE can be functionalized post-polymerization. Incorporating COOH moieties in the polymer backbone can facilitate Dox loading via electrostatic interactions and improve the stability of the complex. The different interactions between Dox and the polymer aggregates (hydrophobic, intrinsic electrostatic, and extrinsic electrostatic) are studied to compare their impact on drug loading, stability, drug release, and in vitro cytotoxicity of the new formulations.

4.2 Materials and Methods

4.2.1 Materials

All chemical reagents were purchased from Sigma-Aldrich and used without further purification unless stated otherwise. For the anionic polymerization, dimethyl sulfoxide (DMSO) and allyl glycidyl ether (AGE) was dried overnight with calcium hydride and distilled immediately prior to use. Ethylene oxide gas was passed through a column of

calcium hydride and condensed with dry ice and acetone for quantification before adding to the reaction vessel. Tetrahydrofuran (THF) was dried using sodium under reflux, and methanol was dried using magnesium sulphate. Doxorubicin hydrochloride was purchased from Tecoland.

4.2.2 Synthesis of CA-(PAGE-*b*-PEG)$_4$ via anionic polymerization

The synthesis and functionalization of the polymers are shown in Scheme 1. For the anionic polymerizations, all glassware was flame-dried under vacuum and purged three times with argon before use. The ethanolamine derivative of cholic acid with four hydroxyl groups was synthesized according to a previous method.[45,46] For anionic polymerization, 5β-cholanoamide (1.66 mmol, 0.75 g) was dissolved in 40 mL of dry DMSO. A potassium naphthalenide solution in THF was added (0.44 mol/L, 1.66 mmol, 1 eq., 3.74 mL) dropwise using a canula under high pressure. AGE was distilled and added (7.6 g, 66.4 mmol, 40 eq.) dropwise using a canula under high pressure. The anionic polymerization was initiated by immersing in an oil bath at 40 °C and allowed to proceed for 24 h to allow the consumption of all the AGE monomers. Then, dry ethylene oxide (17 mL, 332.2 mmol, 200 eq.) chilled in dry ice/acetone was introduced into the flask and polymerized for another 24 h. The reaction was stopped by quenching the reaction with concentrated hydrochloric acid. The DMSO solution was extracted with hexane (3 x 10 mL) to remove the naphthalenide. Distilled water was added to the DMSO solution and the mixture was dialyzed against distilled water (48 h) through a membrane with 3,500 Da molecular weight cut-off (MWCO) to remove all unreacted monomers.

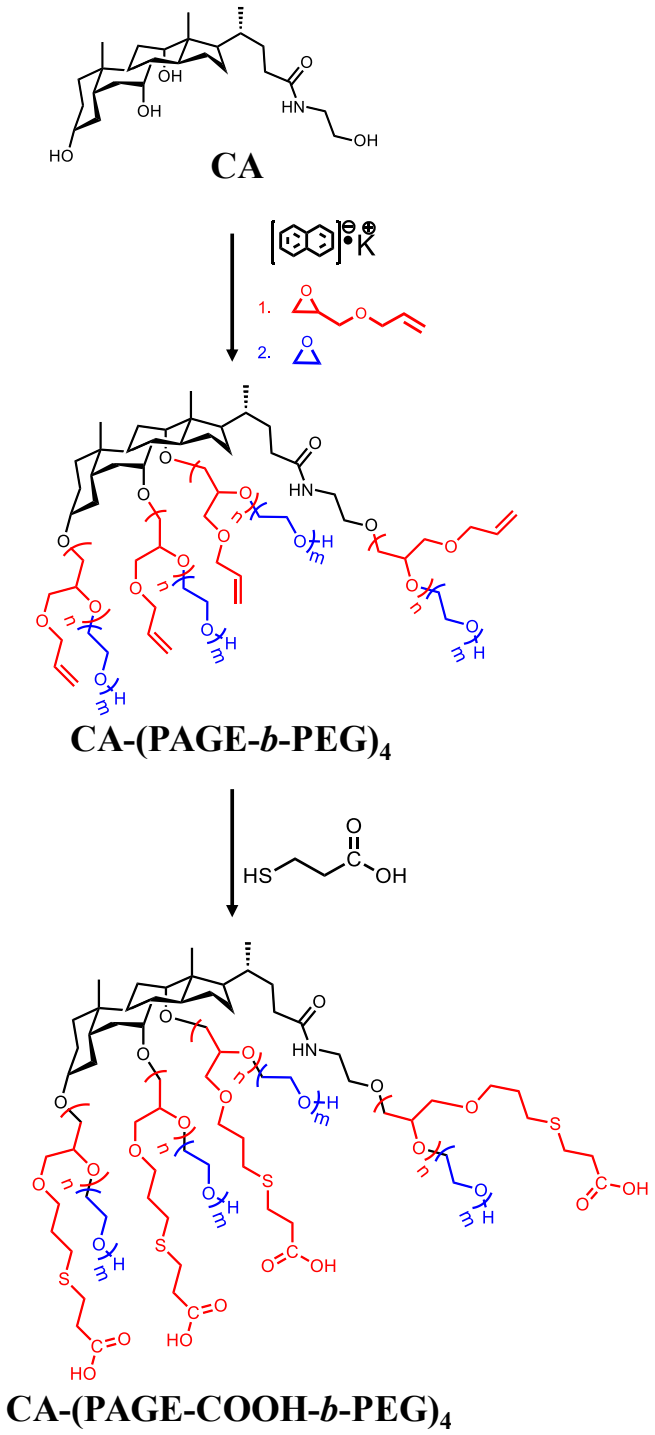

Scheme 4.1. Synthesis of cholic acid-based star polymers via anionic polymerization and the functionalization of the PAGE block through thiol-ene reactions.

4.2.3 Functionalization of CA-(PAGE-*b*-PEG)$_4$ to CA-(PAGE-COOH-*b*-PEG)$_4$

The purified and dried CA-(PAGE-*b*-PEG)$_4$ polymers (2 g, 0.14 mmol) were dissolved in dry methanol (20 mL). Azobisisobutyronitrile (0.5 g, 3.2 mmol), and 3-mercaptopropionic acid (9.0 g, 84.4 mmol) were dissolved in the solution which was refluxed at 70 °C overnight. The reaction was stopped by cooling and methanol was removed. Finally, distilled water was added to dissolve product and remaining reactants and the solution was dialyzed against distilled water for 48 h and dried to yield CA-(PAGE-COOH-*b*-PEG)$_4$.

4.2.4 Characterization methods

The molar mass of the polymers was determined by size exclusion chromatography (SEC) running on THF as eluent on a Breeze system from Waters equipped with a 717 plus autosampler, a 1525 Binary HPLC pump, and a 2410 refractive index detector and three consecutive styragel columns with a flow rate of 1.0 mL/min and at 30 °C. Polystyrene standards were used for calibration. All samples were filtered on a PTFE 0.2 μm filters prior to injection. ^{1}H-NMR spectra were recorded on a Bruker AV400 spectrometer operating at 400 MHz and samples were dissolved in d_6-DMSO. Dynamic light scattering (DLS) measurements were performed on a Malvern Zetasizer NanoZS instrument equipped with a He-Ne laser with a wavelength of 633 nm, and at a scattering angle of 173.5°. Intensity-averaged hydrodynamic diameters of the dispersions were obtained using the non-negative least-squares algorithm (NNLS). Disposable cuvettes were used, and the samples were filtered using 0.45 μm Nylon filters prior to measurements. Sample concentration used was 1 mg/mL for both blank and loaded micelles and samples were run at room temperature. Dox concentration was determined by recording the fluorescence spectra on a Cary eclipse fluorescence spectrophotometer with excitation and emission wavelengths of 485 and 590 nm, respectively, and a bandwidth of 5 nm. The transmission electron microscope (TEM) images were obtained on a FEI Tecnai 12 at 80kV and equipped with an AMT XR80C CCD camera system. TEM samples were prepared by drop-casting blank micelles on a carbon-coated copper grid (300 mesh, Carbon Type-B, Ted Pella Inc.).

4.2.5 Doxorubicin loading and release

The encapsulation of Dox into the micelles is illustrated in Fig. 4.1. Different strategies of encapsulation were selected. The first loading method (for CA-(PAGE-*b*-PEG)$_4$) used TEA to remove the charge on Dox and the other two (for CA-(PAGE-*b*-PEG)$_4$ with OA and CA-(PAGE-COOH-*b*-PEG)$_4$) did not use TEA, i.e. the charged form of Dox was used. The charge was removed from Dox for the CA-(PAGE-*b*-PEG)$_4$ system to optimize the loading so that only hydrophobic interactions would contribute. The salt form of Dox (Dox-HCl) is more aqueous soluble and would lead to lower loading because of its lower hydrophobicity. The other two systems used the charged form of Dox so that electrostatic interactions between Dox and the polymer would occur and drive the loading. It is necessary to use a different loading method because the uncharged form of Dox would not be loaded with electrostatic interactions. Therefore, to compare hydrophobic and electrostatic interactions, these need to be isolated using different loading methods. Briefly, for the CA-(PAGE-COOH-*b*-PEG)$_4$ sample, the copolymers (10 mg) were dissolved in methanol (1 mL) along with Dox (2 mg) with gentle stirring. The solution was added dropwise into 10 mL PBS buffer (pH 7.4, 10 mM) over a period of 10 min using a syringe pump. The resulting PBS solution was stirred gently for 10 min before purification via dialysis (MWCO 6,000-8,000 Da) against 1 L PBS (pH 7.4, 10 mM) for 24 h, changing the outer media twice. Samples of the outer media were taken before replenishment to quantify the amount of Dox released. The same procedure was repeated for the CA-(PAGE-*b*-PEG)$_4$ + OA sample, with a slight modification by using 10 mg of copolymer and 0.126 mg of OA. For the CA-(PAGE-*b*-PEG)$_4$ system, the same procedure was followed by using 10 mg of CA-(PAGE-*b*-PEG)$_4$ alone and Dox which was reacted overnight with 1.5 eq TEA prior to the nanoprecipitation. Dox loading was measured by quantifying the amount of Dox released during the purification and subtracting this value from the amount of Dox in the feed. The quantification was achieved by taking 1 mL of the outer water, mixing with 1 mL DMSO, measuring the fluorescence intensity on a Cary fluorescence spectrometer (excitation 485 nm, emission 590 nm), and comparing with a calibration curve for Dox in DMSO/PBS (1:1 Vol.).

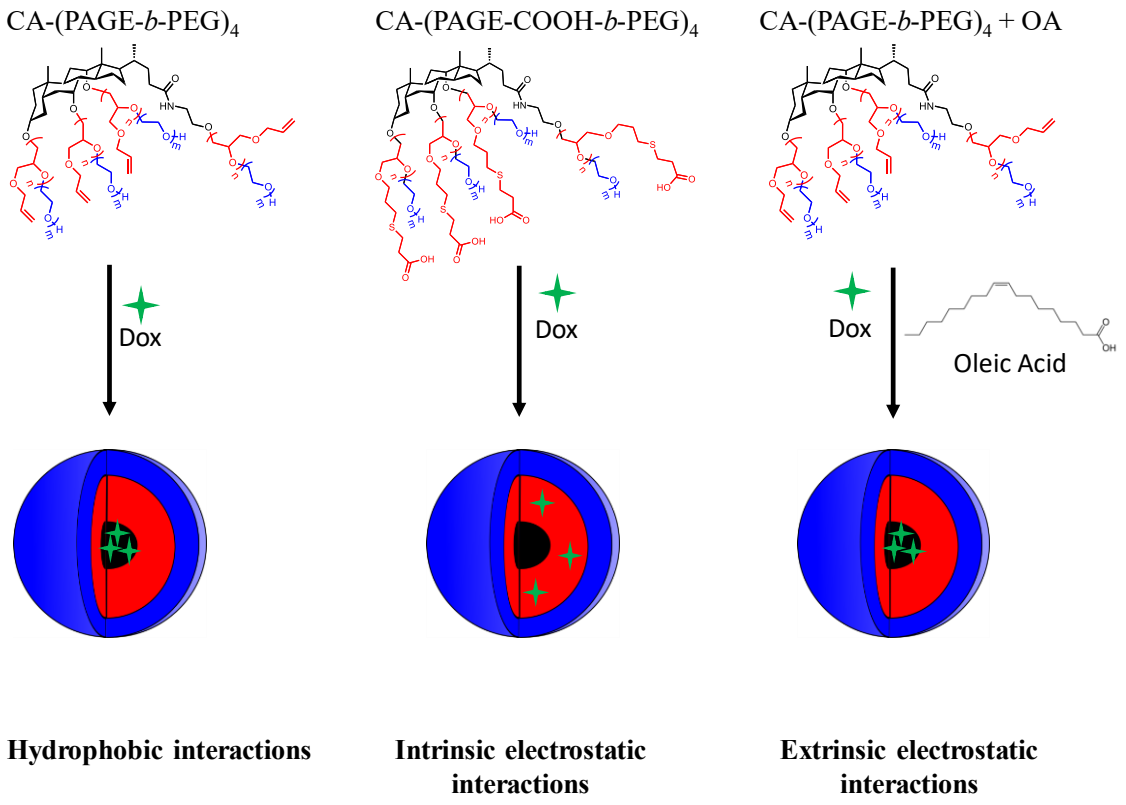

Figure 4.1 Formulations based on different drug-polymer interactions. For CA-(PAGE-*b*-PEG)$_4$, Dox is loaded via hydrophobic interactions between the drug and the core of the micelle composed of cholic acid and hydrophobic PAGE. For CA-(PAGE-COOH-*b*-PEG)$_4$, Dox is loaded via intrinsic electrostatic interactions between the drug and the pendant COOH groups. For CA-(PAGE-*b*-PEG)$_4$ + OA, the electrostatic interactions are perceived as extrinsic because they appear on OA only. The hydrophobicity of the OA aliphatic chains may drive the loading of Dox more toward the hydrophobic core.

$$DLC\ (wt\%) = \frac{weight\ of\ loaded\ drug}{weight\ of\ copolymer}\ \text{x}\ 100\%$$

$$EE\ (wt\%) = \frac{weight\ of\ loaded\ drug}{weight\ of\ drug\ in\ feed}\ \text{x}\ 100\%$$

The Dox release from the different formulations was determined with a dialysis method at different pH. Briefly, 2 mL of the drug-loaded formulations were placed in a dialysis bag (MWCO 6,000-8,000 Da) and dialyzed against 225 mL of the appropriate buffer at 37 °C; PBS pH 7.4 or acetate buffer pH 5 10 mM for the experiments conducted at pH 7.4 and 5, respectively. 1 mL of the outer media was taken at regular intervals and replenished with fresh buffer. The amount of Dox released was quantified by fluorescence spectroscopy with the appropriate calibration curve. All experiments were conducted in triplicates and the results are presented as average values.

4.2.6 In vitro cytotoxicity assay

HeLa cells were grown in Dulbecco's Modified Eagle's Medium (DMEM) medium supplemented with 10% Fetal Bovine Serum (FBS). MTT assay was used to determine the cytotoxicity of the blank formulations and the IC_{50} for free Dox and all three Dox-loaded formulations. MTT assay was conducted according to manufacturer's protocol. HeLa cells were plated on a 96-well plate at a seeding density of 5,000 cells per well in 200 µL DMEM and allowed to adhere overnight (37 °C, 5% CO_2, 12 h). 40 µL of the formulation to be tested was added to each well. The plates were incubated for 48 h (37 °C, 5% CO_2). Medium was removed and replaced with 100 µL of fresh medium. 10 µL of MTT solution (5 mg/mL) was added to each well and incubated (37 °C, 5% CO_2) for 4 h. DMEM medium was carefully removed from each well and replaced with DMSO. MTT crystals were dissolved, and the absorbance was read at 590 nm using a plate reader. Cytotoxicity is reported as compared to absorbance measured for control (untreated cells). To calculate the IC_{50}, a linear regression was extrapolated by drawing a straight line through the inflection in the viability curve. The IC_{50} value was obtained by setting y = 50% from the linear equation obtained and solving for x.

4.2.7 Fluorescence activated cell sorting (FACS) assay

HeLa cells were grown in DMEM medium supplemented with 10% FBS. Cells were seeded in a 24-well plate at a seeding density of 5 x 10^4 cells/well and allowed to adhere overnight (37 °C, 5% CO_2). The cells were washed with PBS and replenished with fresh medium. Free Dox and Dox-loaded formulations were added to the cells to yield a final concentration of 1 and 10 µM Dox in 550 µL DMEM. After 1 h incubation, the cells were washed with PBS, trypsinized (100 µL of 0.25 % Trypsin/EDTA), and suspended in

FACS buffer (400 μL, 95% PBS, 5% FBS, 1 mM EDTA). The cells were observed on a FACScalibur flow cytometer (BD Biosciences, San Jose, CA, USA). Dox concentration internalized in the cells was calculated with respect to control samples (untreated cells). The experiment was done in triplicates.

4.3 Results and Discussion

4.3.1 Drug formulation

To study the interactions driving the Dox loading, three formulations were prepared (Figure 4.1). The first is composed of CA-(PAGE-*b*-PEG)$_4$ alone, in which only hydrophobic interactions are present to ensure Dox loading inside the core of the micelles. The hydrophobicity is conferred from the hydrophobic face of the cholic acid and the hydrophobic PAGE block, while the hydrophilic PEG block promotes micelle formation and stability in the aqueous environment. Numerous studies point toward the use of PEG chain length of about 2,000 g/mol as the optimal chain length for successful drug delivery.[47] Our previous results showed that the ratio of PAGE/PEG controls the hydrophobicity/hydrophilicity of the system and affects the micelle aggregation.[48] When the PAGE block is too long compared to the PEG block (a PAGE/PEG ratio of 0.7 or greater), the hydrophobicity of the individual polymer chains causes the micelles to aggregate into species with large diameters. A block length of 19 for PAGE and of 30 for PEG (ratio of 0.63) should be appropriate for the polymer to maintain micellar stability and maximize Dox loading. The second formulation is composed of functionalized PAGE blocks bearing carboxylic acid groups (CA-(PAGE-COOH-*b*-PEG)$_4$). Here, electrostatic interactions between the NH_2 groups of Dox and the COOH groups attached on PAGE drives the loading of Dox into the middle block in addition to the hydrophobic core. In this situation, the electrostatic interactions may be tuned by varying the PAGE block length. The third formulation is composed of CA-(PAGE-*b*-PEG)$_4$ supplemented with oleic acid (OA). OA is used to mimic the carboxylic acid content on the CA-(PAGE-COOH-*b*-PEG)$_4$ formulation. The carboxylic acid groups of OA can complex electrostatically to Dox and the aliphatic chain of OA imparts an enhanced hydrophobicity thereby increasing Dox loading while reducing its premature release at physiological pH.[49] Here the electrostatic interactions are extrinsic to the system; the COOH group of

OA and the increased hydrophobicity imparted by OA drive the loading of Dox inside the nanoparticles.

4.3.2 Polymer synthesis and characterization

The star-shaped block copolymers were synthesized as shown in Scheme 1. An ethanolamine derivative of CA with four hydroxyl groups was used as initiator for the anionic polymerization of allyl glycidyl ether (AGE), followed by the addition of ethylene glycol (EG) to afford a star-shaped CA-(PAGE-*b*-PEG)$_4$ with 4-arms composed of hydrophobic PAGE and hydrophilic PEG blocks. The copolymer obtained was analyzed by SEC and ^{1}H-NMR (Figures 4.S1 and 4.S2). The SEC traces show monomodal, narrow distributions and an increase in Mn when going from CA-(PAGE)$_4$ to CA-(PAGE-*b*-PEG)$_4$. The NMR signals at 0.58, 0.81, and 0.92 ppm were assigned to the 18-CH_3, 19-CH_3, and 21-CH_3 groups, respectively, on the cholic acid backbone. These peaks were used as reference for the analysis of the peaks at 5.79-5.92 and 3.35-3.60 ppm, which correspond respectively to the CH_2 protons on the PAGE block and on both PAGE and PEG. The block copolymer was determined to be CA-(AGE$_{19}$-b-EG$_{30}$)$_4$ with 19 monomer units of AGE and 30 monomer units of EG (Table 4.1). The presence of four arms was confirmed by reacting the polymers with trifluoroacetic anhydride and by the appearance of the methylene protons at 4.5 ppm, corresponding to protons of the PEG terminal CH_2 unit coupled with the trifluoroacetic group. Then, the allyl side chains from the PAGE block were functionalized with mercaptopropionic acid with close to 100% functionalization as confirmed by ^{1}H-NMR (Figure 4.S2).

Table 4.1. SEC and ^{1}H-NMR results for the anionic polymerization of CA with AGE and EG monomers.

	Molecular Weight (M_n, g/mol)		
Polymer	^{1}H-NMR	SEC	Đ
CA-(PAGE$_{19}$)$_4$	9,100	3,900	1.10
CA-(PAGE$_{19}$-*b*-PEG$_{30}$)$_4$	14,400	8,400	1.13

The critical micellar concentration (CMC) of the bile acid derivative in water was measured with fluorescence spectroscopy using pyrene as a probe.[50] Pyrene fluorescence is measured with increasing concentration of the block copolymers and the CMC is calculated from a plot of the excitation intensity ratio I_{383}/I_{373} as a function of polymer concentration. The CMC for CA-(PAGE-*b*-PEG)$_4$ is determined to be 20 μg/mL (Figure 4.S3), comparable to typical polymer-based micellar systems found in the literature.[43,51-53]

Particle size and distribution were analyzed with dynamic light scattering (DLS) and transmission electron microscopy (TEM), before and after Dox loading. The DLS results show that CA-(PAGE-*b*-PEG)$_4$ forms larger aggregates (d = 62 ± 18 nm) than (CA-(PAGE-*b*-PEG)$_4$ with OA, and CA-(PAGE-COOH-*b*-PEG)$_4$) (Figure 4.2). CA-(PAGE-*b*-PEG)$_4$ mixed with OA, a surfactant, forms mixed micelles smaller in diameter (27 ± 10 nm). The negatively charged COOH moieties may induce an electrostatic repulsion between individual polymer chains leading to smaller micelles. These results are corroborated with the TEM images showing spherical aggregates with a dense core (Figure 4.3). Bile acid-based micelles have a hydrophobic β-face that drives the micellization process. This micellization is affected by the presence of polymer chains on the surface of the bile acids. In the case of CA-(PEG)$_4$, the literature shows that the length of the PEG blocks controls the size of the cavity formed during micellization.[43] The size of the cavity is governed by steric repulsion between individual PEG chains; the longer the PEG chains, the stronger the repulsion which results in a smaller cavity and a smaller micelle. The current system should be expected to behave similarly, i.e., the electrostatic repulsion between the individual polymer chains governs the cavity size. The micelles obtained with the CA-(PAGE-COOH-*b*-PEG)$_4$ are smaller than those obtained with CA-(PAGE-*b*-PEG)$_4$ because the electrostatic repulsion between the individual polymer chains is stronger than the steric repulsion which leads to a smaller micelle. However, the hydrophobic β-face of cholic acid causes micellization of the star-shaped block copolymers and leads to the appearance of a dense core as shown in the TEM images (Fig. 4.3).

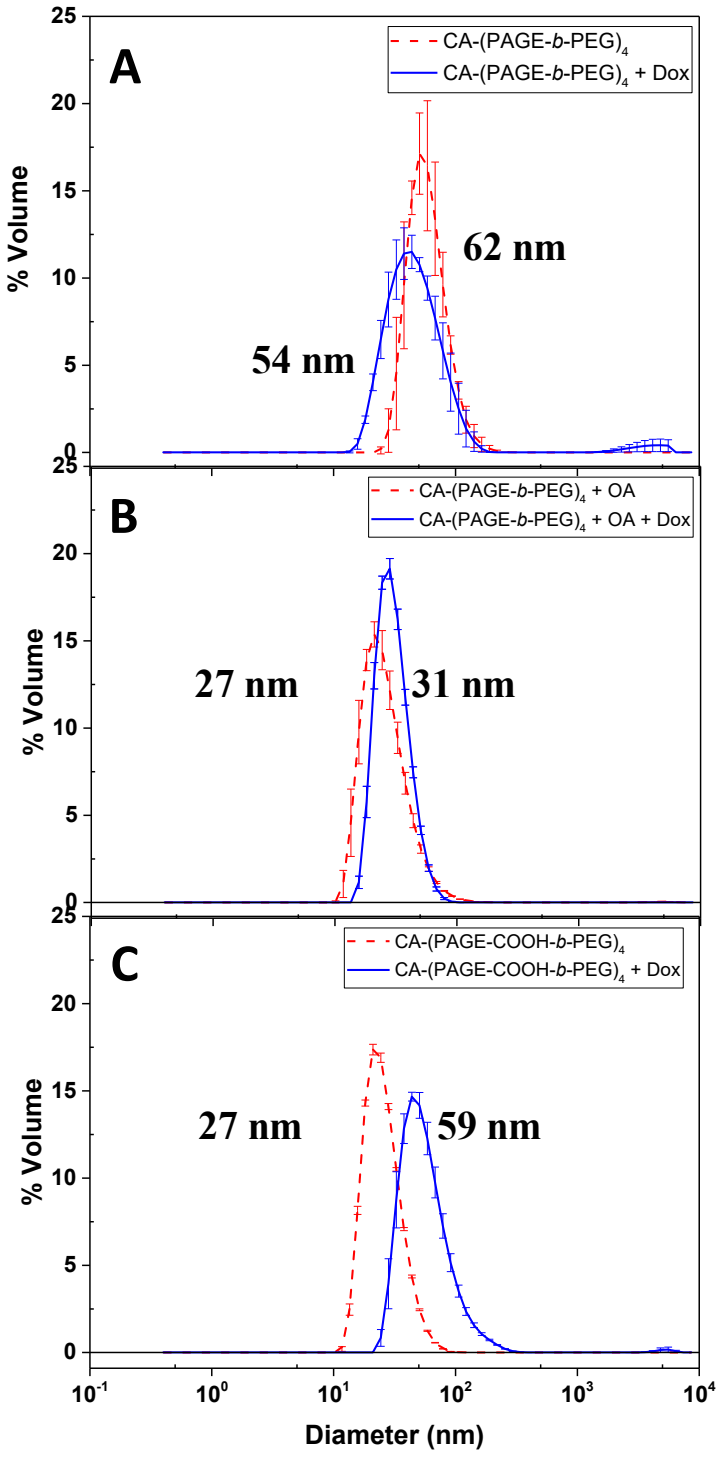

Figure 4.2 The volume-size distribution of (A) CA-(PAGE-*b*-PEG)$_4$ with and without Dox, (B) CA-(PAGE-*b*-PEG)$_4$ + OA with and without Dox, and (C) CA-(PAGE-COOH-*b*-PEG)$_4$ with and without Dox as determined by DLS. Blank micelles and

formulations are obtained at 1 mg/mL and filtered with 0.45 μm PES filters prior to DLS measurements.

Table 2 shows the zeta potentials measured for the nanoparticles. The CA-(PAGE-*b*-PEG)$_4$ micelles have a zeta potential close to neutral with a value of -3.9 ± 0.4 mV, whereas the presence of the negatively charged COOH moieties lead to larger negative values, -9.2 ± 0.7 mV for CA-(PAGE-*b*-PEG)$_4$ with OA and -17.2 ± 0.1 mV for the CA-(PAGE-COOH-*b*-PEG)$_4$ micelles where the COOH groups in the middle block are more exposed to the surface.

Table 4.2. Aggregate size and Dox-loading of the formulations based on star-shaped block copolymers.

Drug formulation	Diameter blank micelle and Dox-loaded micelle (nm)		Micelle dispersity from DLS	Zeta potential (mV)	DLC‡ (wt %)	EE† (%)
	DLS	TEM				
CA-(PAGE-*b*-PEG)$_4$	62 ± 18	57 ± 29	0.2	-3.9 ± 0.4	10	50
CA-(PAGE-*b*-PEG)$_4$ + Dox	54 ± 27	29 ± 7	0.2	-0.29 ± 0.06		
CA-(PAGE-*b*-PEG)$_4$ + OA	27 ± 14	26 ± 7	0.1	-9.2 ± 0.7	11.6	58
CA-(PAGE-*b*-PEG)$_4$ + OA + Dox	31 ± 10	34 ± 14	0.3	-5.4 ± 0.2		
CA-(PAGE-COOH-*b*-PEG)$_4$	27 ± 10	28 ± 11	0.2	-17.2 ± 0.09	14	72
CA-(PAGE-COOH-*b*-PEG)$_4$ + Dox	59 ± 32	40 ± 11	0.1	-17.4 ± 0.9		

* All samples were examined at a 1 mg/mL concentration in 10 mM PBS at 7.4 pH with 154 mM NaCl.
‡ Drug loading content.
† Encapsulation efficiency.

4.3.3 Doxorubicin loading and release

We hypothesize that electrostatic interactions enhance the loading of Dox in comparison to Dox via hydrophobic interaction. To study these interaction forces, the three different formulations were loaded with equal amount of Dox but using different loading procedure. The encapsulation efficiencies and drug loading contents are listed in

Table 4.1. The CA-(PAGE-*b*-PEG)$_4$ aggregates showed drug loading content of 10 wt% and an encapsulation efficiency of 50%. Adding OA to the formulation enabled a higher drug loading and encapsulation efficiency, 11.6 wt% and 58%, respectively, most likely due to an increased hydrophobicity of the Dox complex.[49] Functionalizing the bile acid-based polymers with pendant COOH moieties resulted in an improvement of the drug loading to 14 wt% and loading efficiency to 72%.

In the case of CA-(PAGE-*b*-PEG)$_4$ and CA-(PAGE-*b*-PEG)$_4$ with OA, there is no significant change in the micellar sizes for both CA-(PAGE-*b*-PEG)$_4$ and CA-(PAGE-*b*-PEG)$_4$ with OA systems before and after Dox loading. The decrease in micelle size observed for CA-(PAGE-*b*-PEG)$_4$ falls within the error of the instrument and this small decrease observed with the DLS is not significant. A similar observation was made previously for bile acid-based systems;[54] there are no appreciable changes in micelle sizes when the Dox loading is carried out using hydrophobic interactions. TEM images in Figure 4.3 show that upon Dox loading, both CA-(PAGE-*b*-PEG)$_4$ and CA-(PAGE-*b*-PEG)$_4$ with OA retain their spherical shape. In contrast, the Dox-loaded CA-(PAGE-COOH-*b*-PEG)$_4$ micelles showed the formation of aggregates larger in size (Figure 4.2) and the spherical micelles changed to vesicular-shaped polymersomes (Figure 4.3).

Zeta potential measurements showed a slight increase in the surface charge of the micelles upon Dox loading when compared to the blank micelles (Table 4.1) due to the presence of positively charged Dox loaded in the reservoir of the polymersome and adsorbed on the surface of the micelles. Dox has amphiphilic properties and has been shown to be distributed at the core-shell interface with its anthracycline ring inserted in the hydrophobic core and the amine exposed at the surface.[55] Moreover, Dox has a pKa of 9.53, therefore at pH 7.4 of PBS, the amine is positively charged. For the case of CA-(PAGE-*b*-PEG)$_4$ system there was a significant change upon Dox loading where the zeta potential increased from -3.9 to -0.29. Here, we believe that Dox is found in the core and at the interface of the PAGE and PEG blocks, which causes the zeta potential of the micellar surface to increase (become more positive). In the case of CA-(PAGE-COOH-*b*-PEG)$_4$, there is substantially more negative charges from the polymer chain than there is from Dox; considering the molar equivalence of both and Dox loading there is 76 negative charges per polymer for 3.71 positive charges contributed from Dox. Therefore, even after

loading, the surface charge of the micelles remains highly negatively charged due to the presence of the high number of negative charges and this is what is observed in the zeta potential experiment.

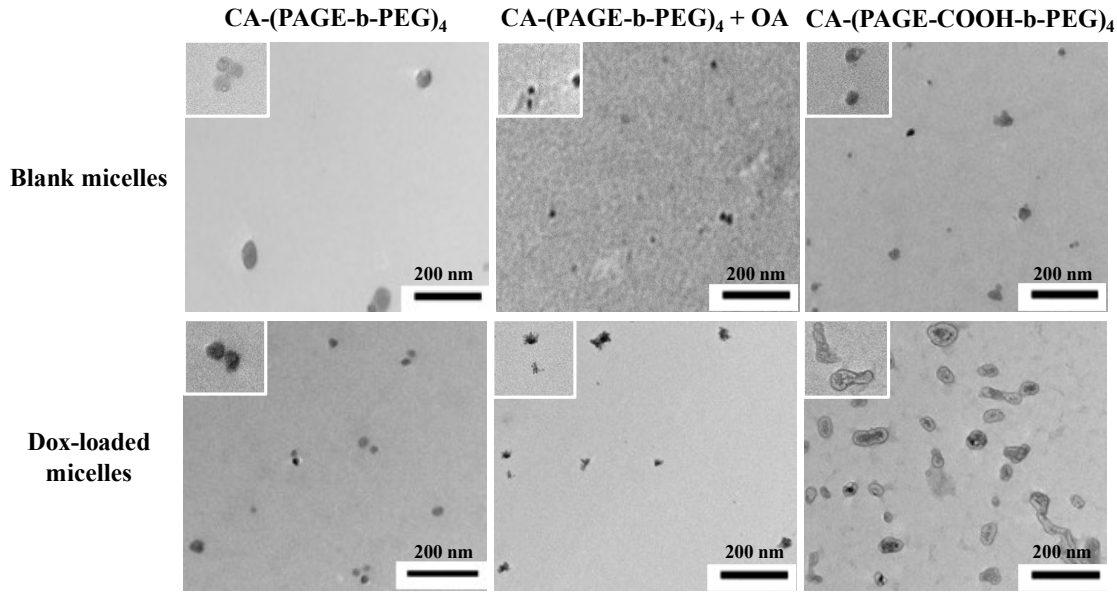

Figure 4.3 Transmission electron micrograph images of the micelles formed: (top) blank formulations and (bottom) Dox-loaded formulations (1 mg/mL samples).

In vitro Dox release profiles at 37 °C were obtained at two different pH values, mimicking the endosomal pH at 5 encountered by the nanoparticles upon cellular entry and the physiological pH at 7.4 sensed by the nanoparticles during transport. The objective of this experiment is to compare the release kinetics of the different formulations to assess the impact of the interaction forces on the release profile. Moreover, the presence of the COOH moieties in the CA-(PAGE-COOH-*b*-PEG)$_4$ formulation bestows pH-responsiveness to the system, an advantage compared to hydrophobic entrapment alone. The results shown in Figure 4.4 compare the Dox release profiles at both pH values for all three formulations. As a control, free Dox was loaded in the dialysis bag and its release was monitored over time. The declivity observed for free Dox at pH 7.4 can be explained by the possible degradation of the drug as reported previously.[56,57] At pH 5 the free Dox is more stable.[58] The degradation of Dox was also observed for the CA-(PAGE-*b*-PEG)$_4$

with OA formulation at pH 7.4, but not for the other two formulations for which the quantity of Dox released was small so that the degradation was not measured at an appreciable amount.

All formulations show a biphasic release with an initial burst release within the first 8 h, followed by a slower, continuous release. The CA-(PAGE-*b*-PEG)$_4$ formulation should be pH-irresponsive but shows an increase in the release from 7.2 to 23% when the pH changes from 7.4 to 5. The higher solubility of Dox at pH 5 facilitates its release.[59] For the CA-(PAGE-*b*-PEG)$_4$ with OA formulation, the release increased from 24 to 35% when pH varies from 7.4 to 5 (Table 4.3). In this case, Dox interacts electrostatically with the negative COOH moieties on the OA and the long aliphatic chain of OA provides a higher hydrophobicity for Dox to remain in the core.[49] At pH 5, the COOH groups are partially protonated weakening their electrostatic interaction with Dox, while the core remains hydrophobic and keeps the drug inside. Therefore, lowering the pH does not significantly impact the release of Dox from the core of the micelle.[60] OA and the CA-(PAGE-*b*-PEG)$_4$ forms mixed micelles that have a higher hydrophobic core. We believe that the system with OA imparts enough hydrophobicity to Dox through its long aliphatic chain that after protonation the hydrophobic interaction between Dox and OA maintains Dox in the hydrophobic core. Moreover, not all of the carboxylic acid groups of OA are exposed to the surface (as can be seen in the zeta potential results) such that at low pH not all are deprotonated and this maintains the Dox in the micelles. Finally, the CA-(PAGE-COOH-*b*-PEG)$_4$ formulation shows the highest difference between the two pHs, with a change in release from 16 to 51% when the pH changed from 7.4 to 5. For the CA-(PAGE-COOH-*b*-PEG)$_4$ system, the carboxylic acid groups are more exposed to the surface and are more easily protonated and this breaks its interaction with Dox causing a higher release at pH 5. This demonstrates the pH responsiveness of the formulation. The COOH groups on the polymer protonate at pH 5, thereby disrupting the electrostatic interaction between the polymer and the drug helping with its release. Moreover, this formulation shows a more stable drug loading at physiological pH than the other two formulations.

Table 4.3. The maximum amount of Dox released in response to pH change.

	Dox release	
Drug formulation	pH 7.4[1]	pH 5[2]
CA-(PAGE-*b*-PEG)$_4$	7.2	23.0
CA-(PAGE-*b*-PEG)$_4$ + OA	24.2	35.5
CA-(PAGE-COOH-*b*-PEG)$_4$	16.3	51.5

[1]Maximum Dox released at pH 7.4 and [2]maximum Dox released at pH 5, the values at 48 h were used. This value gives a measure of the pH responsiveness of the system.

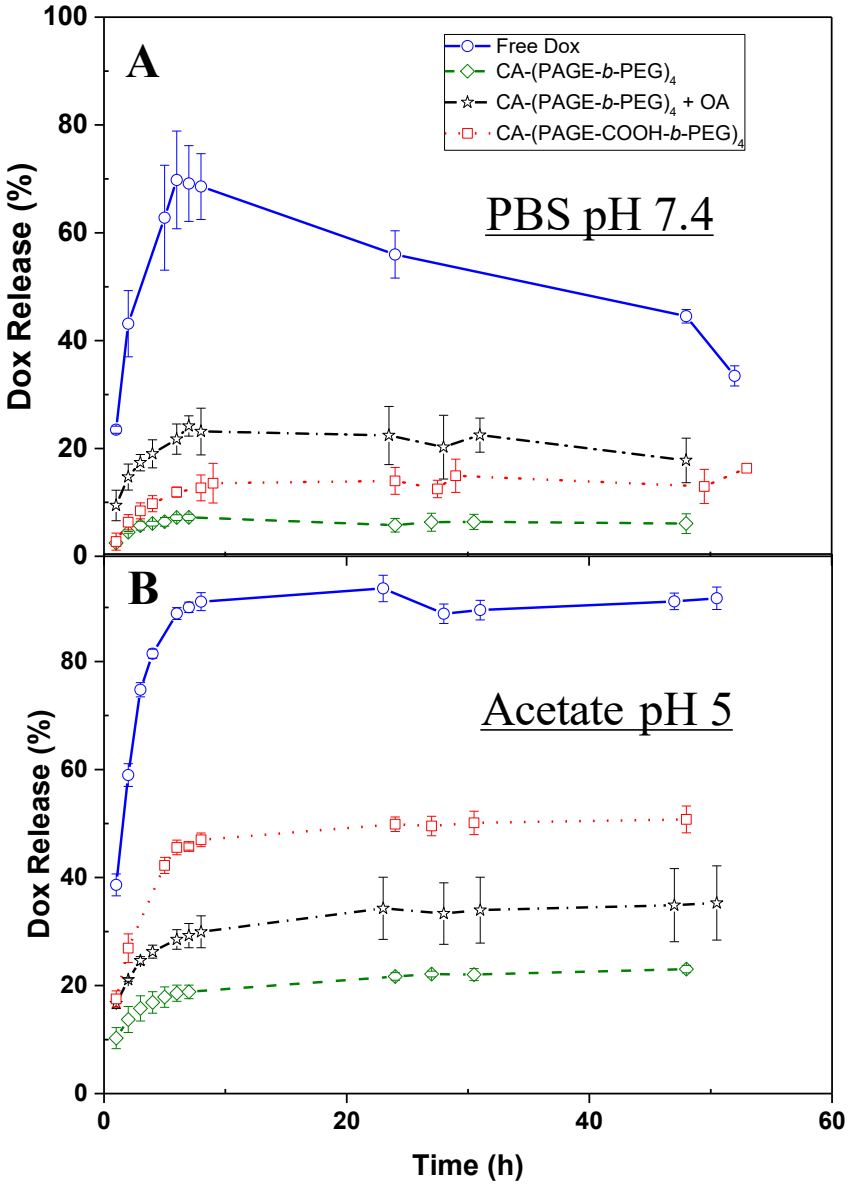

Figure 4.4 Cumulative release of Doxorubicin from formulations at 37 °C (A) in PBS buffer at pH 7.4 and (B) in acetate buffer at pH 5. Results show pH-responsiveness for the CA-(PAGE-COOH-*b*-PEG)$_4$ formulation but not for the other two formulations.

4.3.4 In vitro cytotoxicity

The toxicity of the blank formulations was tested in HeLa cells and the results are presented in Figure 4.S6. All the formulations are non-toxic up to 0.17 mg/mL with over 80% cell viability, consistent with the previous reports on bile acid micelles.[44] To determine the efficiency of the new bile acid-based drug delivery system, the IC_{50} of the

different formulations were obtained on HeLa cells and compared with that of free Dox. The IC_{50} of free Dox is 2 μM, in agreement with values reported in the literature.[22,61] The CA-(PAGE-*b*-PEG)$_4$ formulation has an IC_{50} of 13 μM which is ca. 6 times higher than that of free Dox. For the CA-(PAGE-*b*-PEG)$_4$ with OA formulation, no IC_{50} was observed at the concentrations tested. Finally, for the CA-(PAGE-COOH-*b*-PEG)$_4$ formulation, the IC_{50} obtained is 11 μM, comparable to that of the CA-(PAGE-*b*-PEG)$_4$ formulation.

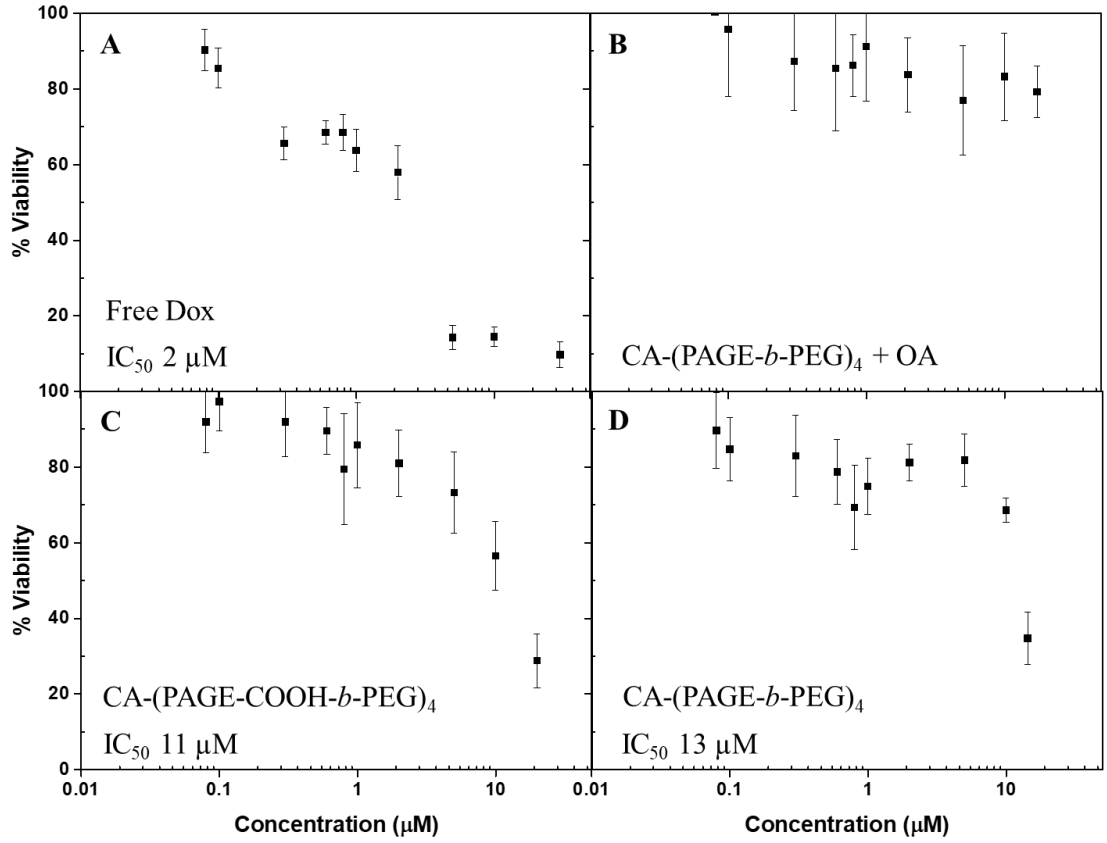

Figure 4.5 In vitro cytotoxicity obtained on HeLa cells after 48 h incubation of (A) free Dox compared with the three blank formulations: (B) CA-(PAGE-*b*-PEG)$_4$ with OA, (C) CA-(PAGE-COOH-*b*-PEG)$_4$, and (D) CA-(PAGE-*b*-PEG)$_4$. The results are presented as mean ± S.D.

To clarify these results, cellular entry for the formulation was studied and compared with that of free Dox using flow cytometry (Figure 4.6). Free Dox is readily internalized inside the cell but Dox in aggregates of both CA-(PAGE-*b*-PEG)$_4$ and CA-(PAGE-COOH-*b*-PEG)$_4$ is less readily internalized. Although previous reports indicate the

advantage of spherical over vesicular-shaped nanoparticles for cellular entry, the negative charge of the nanoparticles had a greater impact.[62,63] Presumably, the negative charge of CA-(PAGE-COOH-*b*-PEG)$_4$ may interact with extracellular proteins to facilitate membrane interaction and internalization, and consequently slightly lower the IC_{50}.[63] The higher IC_{50} observed may be a result of cellular entry. Therefore, the pH responsiveness of the CA-(PAGE-COOH-*b*-PEG)$_4$ formulation does not bring an advantage over the neutral, non-responsive system. The pH-responsiveness was unfavorable due to kinetics of Dox release; Dox release was not sufficiently rapid to promote endosomal escape and cellular uptake was the determining factor for lowering of the IC_{50}. Surprisingly, the formulation with OA showed even less cellular entry than the other two formulations. The presence of OA affected the cellular entry hence increasing further the IC_{50}, probably due to its impact on the structure of the micelles or the surface properties. The TEM images shows that the micelles prepared from OA are much smaller than those of the other two formulations but are also dense and irregular in shape. Reports demonstrated the advantage of smaller nanoparticles for cellular entry, but also the effect of particle shape on cellular entry.[62,63] It is believed that the irregular shape of the Dox-loaded nanoparticles caused by the presence of the OA reduced the cellular internalization process observed via FACS. The proposed drug delivery systems achieve a higher stability avoiding unspecific uptake of Dox, but further studies are necessary to improve the specific nanoparticle internalization in cancer cells and optimize the pH-responsiveness to enable adequate endosomal escape.

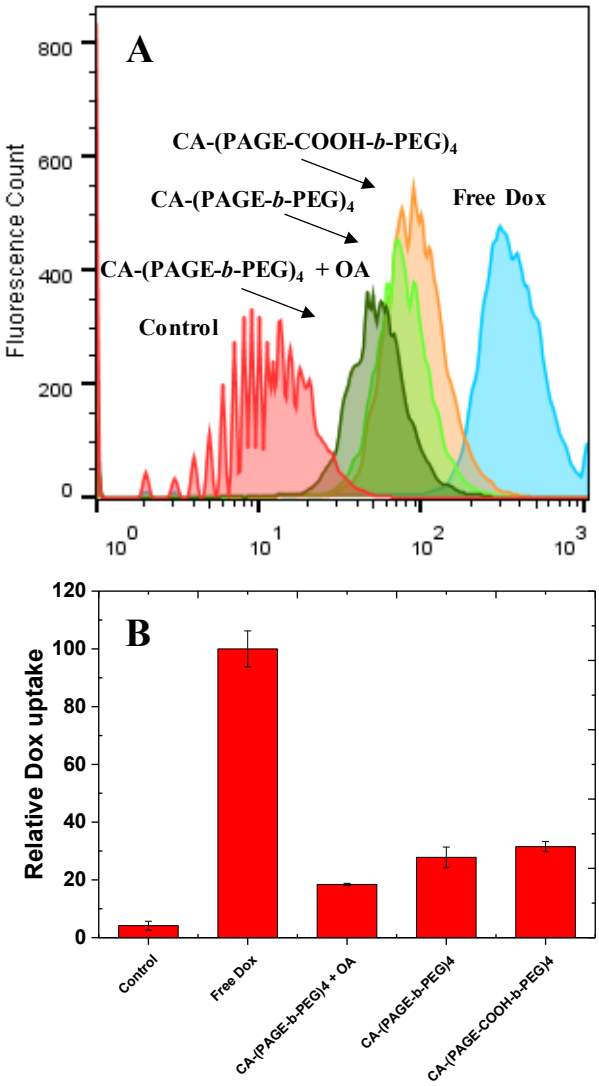

Figure 4.6 Flow cytometry uptake profiles for formulations of free Dox and with CA-(PAGE-*b*-PEG)$_4$, CA-(PAGE-*b*-PEG)$_4$ with OA, and CA-(PAGE-COOH-*b*-PEG)$_4$. Experiment was performed in triplicates with HeLa cells with 2 h incubation; non-treated HeLa cells were used as control.

4.4 Conclusion

Cholic acid-based micelles formed stable micellar aggregates with high Dox loading. Electrostatic interactions in the case of the CA-(PAGE-COOH-*b*-PEG)$_4$ formulation led to higher loading than the CA-(PAGE-*b*-PEG)$_4$ formulation based on hydrophobic interaction. The loading of Dox via electrostatic interactions confers pH-responsiveness to the drug delivery system in the context of drug release in vitro, lowering

the pH from 7.4 to 5 led to an increase in Dox release from 12 to 50%. In previous report, we have used OA to increase loading of hydrophobic itraconazole for CA-$(PEG)_4$.[44] However, in the present formulation, OA did not provide an advantage for Dox loading when compared to loading via electrostatic interaction in CA-(PAGE-COOH-*b*-$PEG)_4$. We believe that part of the negative charges on OA may be buried in the core of the micelle and less accessible for electrostatic binding with Dox. Moreover, the new nanoparticles are non-toxic with over 80% cell viability at concentrations up to 0.17 mg/mL. IC_{50} values for both CA-(PAGE-*b*-$PEG)_4$ and CA-(PAGE-COOH-*b*-$PEG)_4$ formulations are higher than that for free Dox and this has been linked to lower cellular internalization of the Dox-loaded micellar aggregates. The CA-(PAGE-*b*-$PEG)_4$ formulation with OA did not show an IC_{50} at the measured concentration range and had lower cellular internalization than the other two formulations. Cholic acid-based drug delivery systems present advantages of higher Dox loading and pH-responsiveness in release but does not show pH-responsiveness for drug delivery inside the cells due to difficulties in cellular entry. The proposed system can be used to alleviate side effects caused by premature release of Dox during systemic administration. As can be seen, the Dox is more stable and does not release significantly from the CA-(PAGE-COOH-*b*-$PEG)_4$ system at pH 7.4 but releases 50% of Dox at pH 5. Therefore, the system can be used to release Dox at the tumor site since tumor micro-environments are known to be more acidic than the healthy tissues. Challenges related to cellular entry need to be further addressed to achieve an overall successful drug delivery platform. To achieve higher cellular internalization and increased efficiency, the addition of targeting ligand on the surface of the nanoparticle is currently being tested. Further studies are underway to determine the efficiency of the new bile acid-based drug delivery system on drug resistant cancer cell lines and cytotoxic drugs with poor cellular entry.

4.5 Acknowledgements

Financial support from NSERC of Canada is gratefully acknowledged. AC and XXZ are members of CSACS funded by FRQNT and GRSTB funded by FRSQ. AC thanks the Camille Sandorfy, Charron Lam, and GRSTB Ph.D. scholarships. The authors thank Mrs. Mouna Rabeb-Derbali and Dr. Wilms E. Baille for their technical support.

4.6 Supporting Information

4.6.1 Critical micellization concentration (CMC) determination

The CMC was determined according to a previously published protocol.[50] Briefly, pyrene was dissolved in methanol to give a final concentration of 10^{-6} M in 5 mL PBS, followed by the evaporation of methanol. A stock solution at 8 mg/mL of copolymer micelles was prepared via a nanoprecipitation method. This stock solution was diluted with buffer solution to obtain a series of solutions with copolymer concentrations ranging from 10^{-4} to 8 mg/mL and added to the vials containing pyrene. The solutions were stirred for 48 h to allow the pyrene to equilibrate. Fluorescence spectra were recorded on a Cary Eclipse fluorescence spectrometer (Agilent). The emission wavelength was set to 335 nm with a band width of 2.5 for both excitation and emission. The I_3/I_1 ratio was obtained from the ratio of fluorescence intensity at 383 nm (I_3) and 373 nm (I_1).

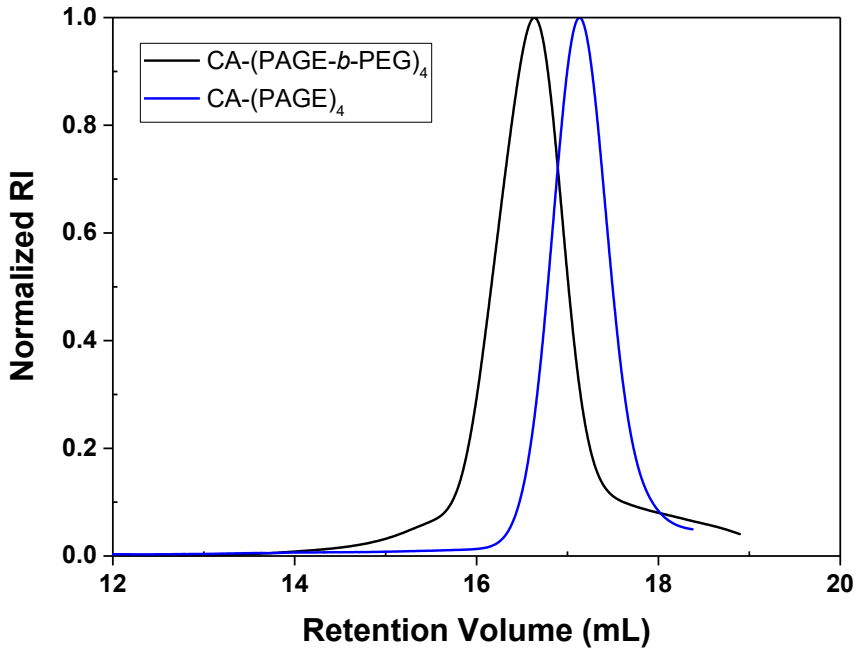

Figure 4.S1 SEC traces of homopolymer CA-$(PAGE)_4$ and block copolymer CA-$(PAGE\text{-}b\text{-}PEG)_4$. THF was used as eluent with a flow rate of 1 mL/min at 35 °C and analyzed with a calibration curve based on PS standards. Figure shows increase in molecular weight following polymerization of PEG and narrow dispersity.

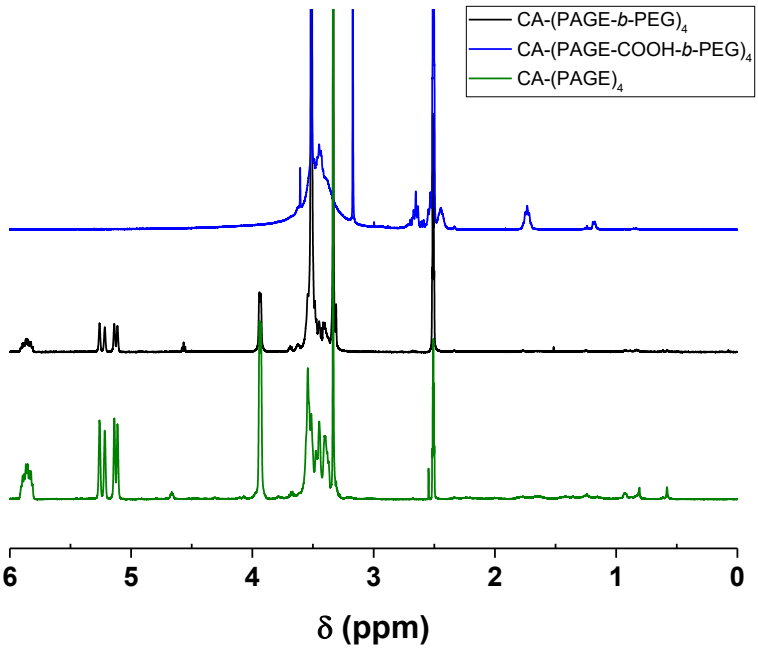

Figure 4.S2 ^{1}H NMR spectra of homopolymer CA-(PAGE)$_4$, and block copolymers CA-(PAGE-*b*-PEG)$_4$ and CA-(PAGE-COOH-*b*-PEG)$_4$ in d_6-DMSO. The disappearance of the methine and methylene peaks at 5.8 – 6.0 ppm and 5.1 – 5.3 ppm of pendant allyl group on PAGE backbone testifies to the successful functionalization.

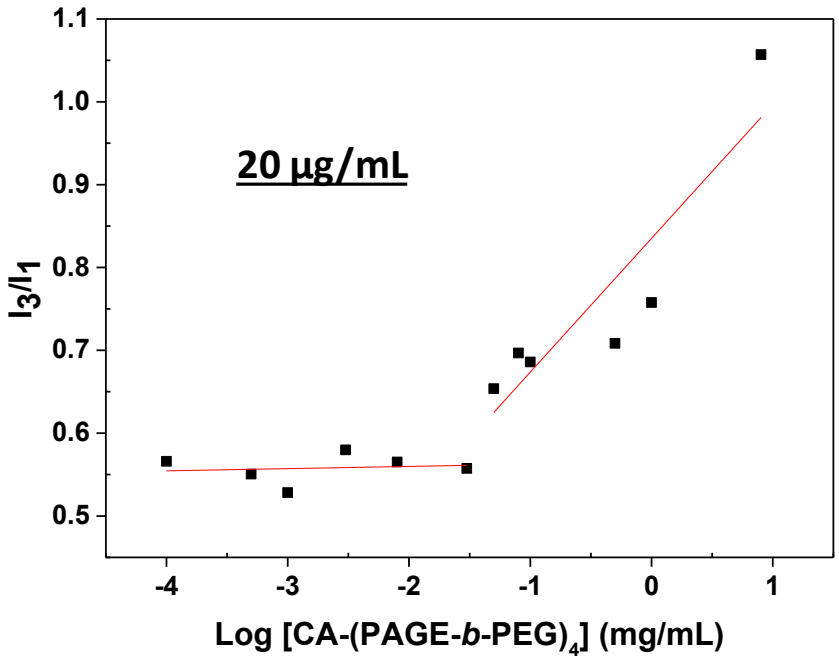

Figure 4.S3 Critical micellar concentration measured by fluorescence spectroscopy using pyrene as a probe. The ratio I_3/I_1 (obtained from fluorescence spectra) is plotted as a function of CA-(PAGE-*b*-PEG)$_4$ concentration. CMC is obtained by the intercept of the two linear regressions. In this case, CMC = 20 µg/mL.

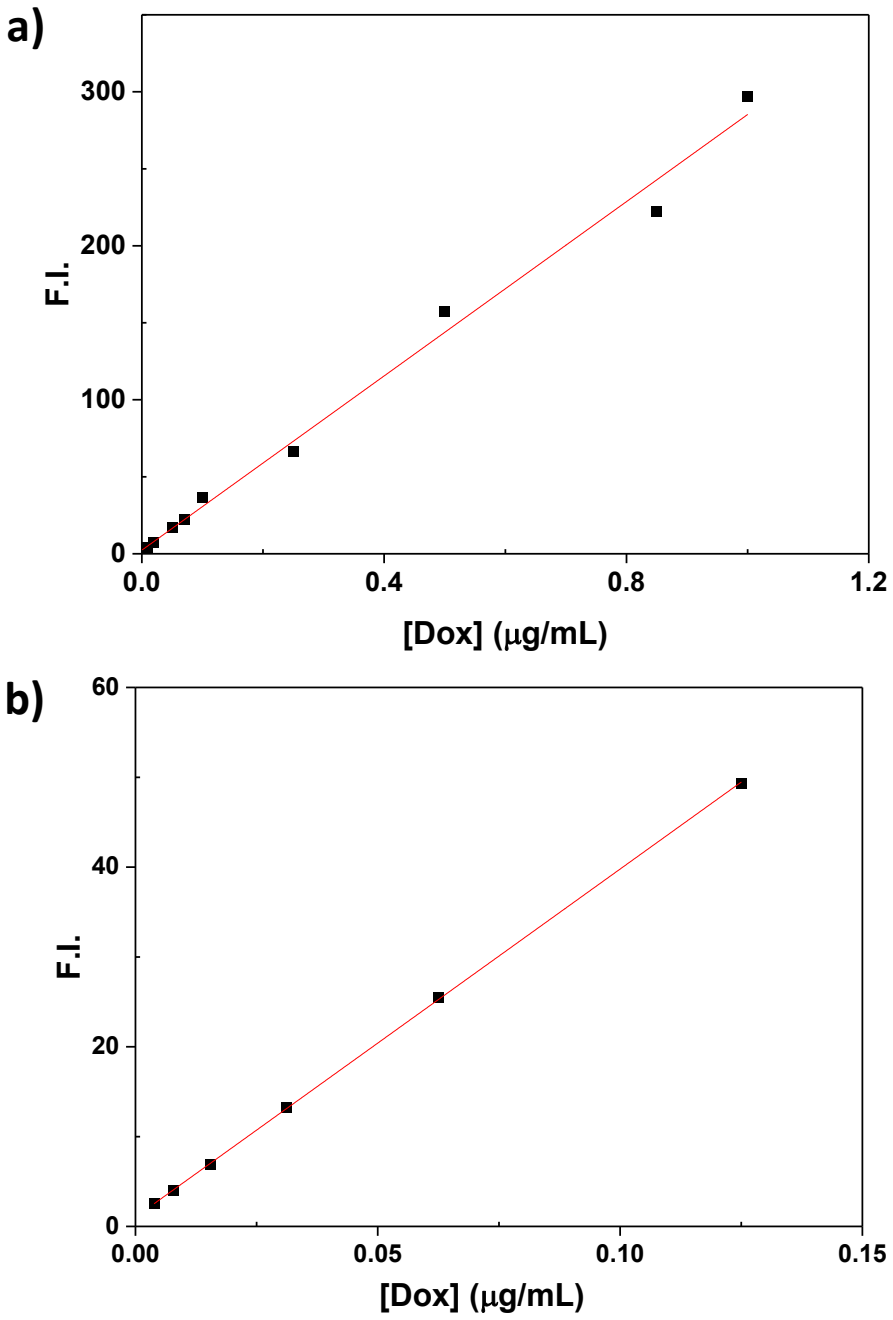

Figure 4.S4 Dox calibration curves for release experiment. Calibration curve was obtained by measuring fluorescence intensity of Dox in (a) 1/1 DMSO/PBS (pH 7.4) solution and (b) 1/1 DMSO/Acetate (pH 5) solution.

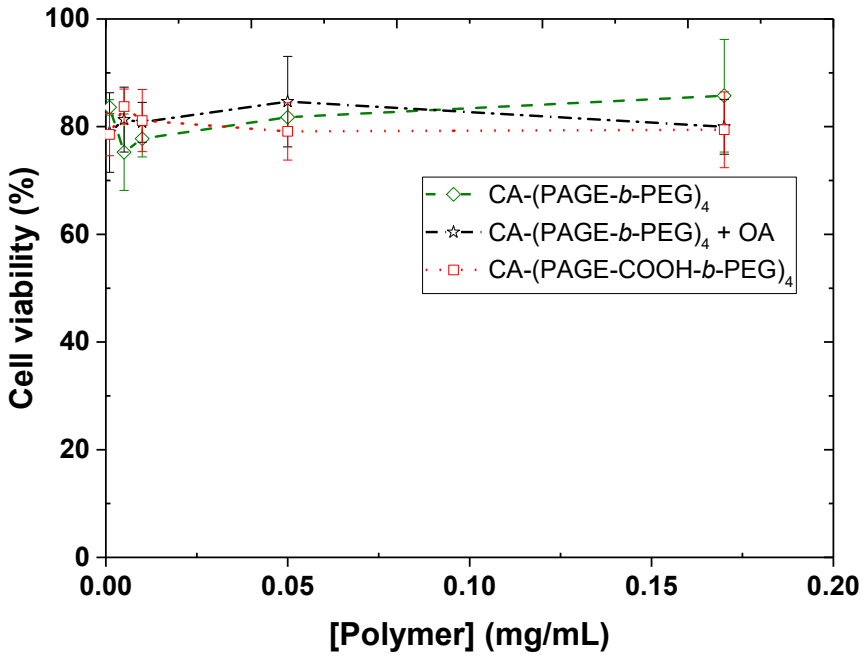

Figure 4.S5 In vitro cytotoxicity of blank formulations was tested in HeLa cells using the MTT assay with a 48 h incubation. The results are expressed as mean ± S.D. Results show the formulations are non-toxic up to 0.17 mg/mL.

4.7 References

1. Global Burden of Disease Cancer, C. Global, regional, and national cancer incidence, mortality, years of life lost, years lived with disability, and disability-adjusted life-years for 32 cancer groups, 1990 to 2015: A systematic analysis for the global burden of disease study. *JAMA Oncology* **2017,** *3*, (4), 524-548.
2. Gonzalez-Angulo, A. M.; Morales-Vasquez, F.; Hortobagyi, G. N. Overview of resistance to systemic therapy in patients with breast cancer. *Adv. Exp. Med. Biol.* **2007,** *608*, 1-22.
3. Cabral, H.; Kataoka, K. Progress of drug-loaded polymeric micelles into clinical studies. *J. Control. Release* **2014,** *190*, 465-476.
4. Gong, J.; Chen, M.; Zheng, Y.; Wang, S.; Wang, Y. Polymeric micelles drug delivery system in oncology. *J. Control. Release* **2012,** *159*, (3), 312-323.
5. Chan, J. M.; Valencia, P. M.; Zhang, L.; Langer, R.; Farokhzad, O. C., Polymeric nanoparticles for drug delivery. In *Cancer Nanotechnology: Methods and Protocols*, Grobmyer, S. R.; Moudgil, B. M., Eds. Humana Press: Totowa, NJ, 2010; pp 163-175.
6. Kataoka, K.; Harada, A.; Nagasaki, Y. Block copolymer micelles for drug delivery: design, characterization and biological significance. *Adv. Drug Deliv. Rev.* **2001,** *47*, (1), 113-131.
7. Kim, D. W.; Kim, S. Y.; Kim, H. K.; Kim, S. W.; Shin, S. W.; Kim, J. S.; Park, K.; Lee, M. Y.; Heo, D. S. Multicenter phase II trial of Genexol-PM, a novel

Cremophor-free, polymeric micelle formulation of paclitaxel, with cisplatin in patients with advanced non-small-cell lung cancer. *Ann. Oncol.* **2007,** *18*, (12), 2009-2014.
8. Lee, K. S.; Chung, H. C.; Im, S. A.; Park, Y. H.; Kim, C. S.; Kim, S.-B.; Rha, S. Y.; Lee, M. Y.; Ro, J. Multicenter phase II trial of Genexol-PM, a Cremophor-free, polymeric micelle formulation of paclitaxel, in patients with metastatic breast cancer. *Breast Cancer Res. Tr.* **2008,** *108*, (2), 241-250.
9. Hamaguchi, T.; Matsumura, Y.; Suzuki, M.; Shimizu, K.; Goda, R.; Nakamura, I.; Nakatomi, I.; Yokoyama, M.; Kataoka, K.; Kakizoe, T. NK105, a paclitaxel-incorporating micellar nanoparticle formulation, can extend in vivo antitumour activity and reduce the neurotoxicity of paclitaxel. *Br. J. Cancer* **2005,** *92*, (7), 1240-1246.
10. Alexander, S.; Cosgrove, T.; Prescott, S. W.; Castle, T. C. Flurbiprofen encapsulation using pluronic triblock copolymers. *Langmuir* **2011,** *27*, (13), 8054-8060.
11. Varshosaz, J.; Hasanzadeh, F.; Eslamdoost, M. Optimization of self-assembling properties of fatty acids grafted to methoxy poly(ethylene glycol) as nanocarriers for etoposide. *Acta Pharm.* **2012,** *62*, (1), 31-44.
12. Wang, X.; Wu, G.; Lu, C.; Zhao, W.; Wang, Y.; Fan, Y.; Gao, H.; Ma, J. A novel delivery system of doxorubicin with high load and pH-responsive release from the nanoparticles of poly (α,β-aspartic acid) derivative. *Eur. J. Pharm. Sci.* **2012,** *47*, (1), 256-264.
13. Shen, Y.; Jin, E.; Zhang, B.; Murphy, C. J.; Sui, M.; Zhao, J.; Wang, J.; Tang, J.; Fan, M.; Van Kirk, E.; Murdoch, W. J. Prodrugs forming high drug loading multifunctional nanocapsules for intracellular cancer drug delivery. *J. Am. Chem. Soc.* **2010,** *132*, (12), 4259-4265.
14. Zhang, Y.; Ren, T.; Gou, J.; Zhang, L.; Tao, X.; Tian, B.; Tian, P.; Yu, D.; Song, J.; Liu, X.; Chao, Y.; Xiao, W.; Tang, X. Strategies for improving the payload of small molecular drugs in polymeric micelles. *J. Control. Release* **2017,** *261* (10), 352-366.
15. Ke, X.; Ng, V. W. L.; Ono, R. J.; Chan, J. M. W.; Krishnamurthy, S.; Wang, Y.; Hedrick, J. L.; Yang, Y. Y. Role of non-covalent and covalent interactions in cargo loading capacity and stability of polymeric micelles. *J. Control. Release* **2014,** *193* (10), 9-26.
16. Gadelle, F.; Koros, W. J.; Schechter, R. S. Solubilization of aromatic solutes in block copolymers. *Macromolecules* **1995,** *28*, (14), 4883-4892.
17. Soliman, G. M.; Sharma, R.; Choi, A. O.; Varshney, S. K.; Winnik, F. M.; Kakkar, A. K.; Maysinger, D. Tailoring the efficacy of nimodipine drug delivery using nanocarriers based on A2B miktoarm star polymers. *Biomaterials* **2010,** *31*, (32), 8382-8392.
18. Letchford, K.; Liggins, R.; Burt, H. Solubilization of hydrophobic drugs by methoxy poly(ethylene glycol)-block-polycaprolactone diblock copolymer micelles: theoretical and experimental data and correlations. *J. Pharm. Sci.* **2008,** *97* (3), 1179-1190.

19. Sharma, A.; Soliman, G. M.; Al-Hajaj, N.; Sharma, R.; Maysinger, D.; Kakkar, A. Design and evaluation of multifunctional nanocarriers for selective delivery of coenzyme Q10 to mitochondria. *Biomacromolecules* **2012,** *13* (1), 239-252.
20. Yan, J.; Ye, Z.; Chen, M.; Liu, Z.; Xiao, Y.; Zhang, Y.; Zhou, Y.; Tan, W.; Lang, M. Fine tuning micellar core-forming block of poly(ethylene glycol)-block-poly(ε-caprolactone) amphiphilic copolymers based on chemical modification for the solubilization and delivery of doxorubicin. *Biomacromolecules* **2011,** *12* (7), 2562-2572.
21. LeDevedec, F.; Houdaihed, L.; Allen, C. Anionic polymerization of an amphiphilic copolymer for preparation of block copolymer micelles stabilized by π-π stacking interactions. *J. Vis. Exp.* **2016,** *116*, e54422.
22. Chen, W.; Meng, F.; Cheng, R.; Deng, C.; Feijen, J.; Zhong, Z. Facile construction of dual-bioresponsive biodegradable micelles with superior extracellular stability and activated intracellular drug release. *J. Control. Release* **2015,** *210*, 125-133.
23. Shuai, X.; Merdan, T.; Schaper, A. K.; Xi, F.; Kissel, T. Core-cross-linked polymeric micelles as paclitaxel carriers. *Bioconjugate Chem.* **2004,** *15* (3), 441-448.
24. Wu, Y.; Chen, W.; Meng, F.; Wang, Z.; Cheng, R.; Deng, C.; Liu, H.; Zhong, Z. Core-crosslinked pH-sensitive degradable micelles: A promising approach to resolve the extracellular stability versus intracellular drug release dilemma. *J. Control. Release* **2012,** *164* (3), 338-345.
25. Lin, W.; Kim, D. pH-Sensitive micelles with cross-linked cores formed from polyaspartamide derivatives for drug delivery. *Langmuir* **2011,** *27* (19), 12090-12097.
26. Zhong, Y.; Goltsche, K.; Cheng, L.; Xie, F.; Meng, F.; Deng, C.; Zhong, Z.; Haag, R. Hyaluronic acid-shelled acid-activatable paclitaxel prodrug micelles effectively target and treat CD44-overexpressing human breast tumor xenografts in vivo. *Biomaterials* **2016,** *84*, 250-261.
27. Yin, S.; Huai, J.; Chen, X.; Yang, Y.; Zhang, X.; Gan, Y.; Wang, G.; Gu, X.; Li, J. Intracellular delivery and antitumor effects of a redox-responsive polymeric paclitaxel conjugate based on hyaluronic acid. *Acta Biomater.* **2015,** *26* (15), 274-285.
28. Xu, R.; Fisher, M.; Juliano, R. L. Targeted albumin-based nanoparticles for delivery of amphipathic drugs. *Bioconjug .Chem.* **2011,** *22* (5), 870-878.
29. Prabaharan, M.; Grailer, J. J.; Pilla, S.; Steeber, D. A.; Gong, S. Amphiphilic multi-arm-block copolymer conjugated with doxorubicin via pH-sensitive hydrazone bond for tumor-targeted drug delivery. *Biomaterials* **2009,** *30* (29), 5757-5766.
30. Lv, S.; Song, W.; Tang, Z.; Li, M.; Yu, H.; Hong, H.; Chen, X. Charge-conversional PEG-polypeptide polyionic complex nanoparticles from simple blending of a pair of oppositely charged block copolymers as an intelligent vehicle for efficient antitumor drug delivery. *Mol. Pharm.* **2014,** *11* (5), 1562-1574.
31. Wang, C. H.; Wang, W. T.; Hsiue, G. H. Development of polyion complex micelles for encapsulating and delivering amphotericin B. *Biomaterials* **2009,** *30* (19), 3352-3358.

32. Eckman, A. M.; Tsakalozou, E.; Kang, N. Y.; Ponta, A.; Bae, Y. Drug release patterns and cytotoxicity of PEG-poly(aspartate) block copolymer micelles in cancer cells. *Pharm. Res.* **2012,** *29* (7), 1755-1767.
33. Xu, H.; Yang, D.; Cai, C.; Gou, J.; Zhang, Y.; Wang, L.; Zhong, H.; Tang, X. Dual-responsive mPEG-PLGA-PGlu hybrid-core nanoparticles with a high drug loading to reverse the multidrug resistance of breast cancer: an in vitro and in vivo evaluation. *Acta Biomater.* **2015,** *16*, 156-168.
34. Xu, H.; Cai, C.; Gou, J.; Sui, B.; Jin, J.; Xu, H.; Zhang, Y.; Wang, L.; Zhai, Y.; Tang, X. Self-assembled monomethoxy (polyethylene glycol)-b-p(D,L-lactic-co-glycolic acid)-b-p(L-glutamic acid) hybrid-core nanoparticles for intracellular pH-triggered release of doxorubicin. *J. Biomed. Nanotechnol.* **2015,** *11* (8), 1354-1369.
35. Yang, C.; Tan, J. P. K.; Cheng, W.; Attia, A. B. E.; Ting, C. T. Y.; Nelson, A.; Hedrick, J. L.; Yang, Y.-Y. Supramolecular nanostructures designed for high cargo loading capacity and kinetic stability. *Nano Today* **2010,** *5* (6), 515-523.
36. Yang, C.; Ebrahim Attia, A. B.; Tan, J. P. K.; Ke, X.; Gao, S.; Hedrick, J. L.; Yang, Y.-Y. The role of non-covalent interactions in anticancer drug loading and kinetic stability of polymeric micelles. *Biomaterials* **2012,** *33* (10), 2971-2979.
37. Su, W.; Luo, X.-h.; Wang, H.-f.; Li, L.; Feng, J.; Zhang, X.-Z.; Zhuo, R. Hyperbranched polycarbonate-based multimolecular micelle with enhanced stability and loading efficiency. *Macromol. Rapid Comm.* **2011,** *32* (4), 390-396.
38. Kim, S. H.; Tan, J. P. K.; Nederberg, F.; Fukushima, K.; Colson, J.; Yang, C.; Nelson, A.; Yang, Y.-Y.; Hedrick, J. L. Hydrogen bonding-enhanced micelle assemblies for drug delivery. *Biomaterials* **2010,** *31* (31), 8063-8071.
39. Tsoi, K. M.; MacParland, S. A.; Ma, X.-Z.; Spetzler, V. N.; Echeverri, J.; Ouyang, B.; Fadel, S. M.; Sykes, E. A.; Goldaracena, N.; Kaths, J. M.; Conneely, J. B.; Alman, B. A.; Selzner, M.; Ostrowski, M. A.; Adeyi, O. A.; Zilman, A.; McGilvray, I. D.; Chan, W. C. W. Mechanism of hard-nanomaterial clearance by the liver. *Nat. Mater.* **2016,** *15* (11), 1212-1221.
40. Le Dévédec, F.; Fuentealba, D.; Strandman, S.; Bohne, C.; Zhu, X. X. Aggregation behavior of Pegylated bile acid derivatives. *Langmuir* **2012,** *28* (37), 13431-13440.
41. Le Devedec, F.; Strandman, S.; Baille, W. E.; Zhu, X. X. Functional star block copolymers with a cholane core: Thermo-responsiveness and aggregation behavior. *Polymer* **2013,** *54* (15), 3898-3903.
42. Shao, Y.; Jia, Y.-G.; Shi, C.; Luo, J.; Zhu, X. X. Block and random copolymers bearing cholic acid and oligo(ethylene glycol) pendant groups: Aggregation, thermosensitivity, and drug loading. *Biomacromolecules* **2014,** *15* (5), 1837-1844.
43. Despa, F.; Luo, J. T.; Li, J.; Duan, Y.; Lam, K. S. Cholic acid micelles-controlling the size of the aqueous cavity by PEGylation. *Phys. Chem. Chem. Phys.* **2010,** *12* (7), 1589-1594.
44. Le Dévédec, F.; Strandman, S.; Hildgen, P.; Leclair, G.; Zhu, X. X. Pegylated bile acids for use in drug delivery systems enhanced solubility and bioavailability of itraconazole. *Mol. Pharm.* **2013,** *10*, 3057-3066.

45. Juo, J.; Giguère, G.; Zhu, X. X. Asymmetric poly(ethylene glycol) star polymers with a cholic acid core and their aggregation properties. *Biomacromolecules* **2009,** *10* (8), 900-906.
46. Gouin, S.; Zhu, X. X. Synthesis of 3 alpha- and 3 beta-dimers from selected bile acids. *Steroids* **1996,** *61* (11), 664-669.
47. Knop, K.; Hoogenboom, R.; Fischer, D.; Schubert, U. S. Poly(ethylene glycol) in drug delivery: pros and cons as well as potential alternatives. *Angew. Chem. Int. Ed.* **2010,** *49* (36), 6288-6308.
48. Li, C.; Lavigueur, C.; Zhu, X. X. Aggregation and thermoresponsive properties of new star block copolymers with a cholic acid core. *Langmuir* **2011,** *27* (17), 11174-11179.
49. Zhang, X.; Sun, X.; Li, J.; Zhang, X.; Gong, T.; Zhang, Z. Lipid nanoemulsions loaded with doxorubicin-oleic acid ionic complex: characterization, in vitro and in vivo studies. *Die Pharmazie* **2011,** *66* (7), 496-505.
50. Topel, Ö.; Çakır, B. A.; Budama, L.; Hoda, N. Determination of critical micelle concentration of polybutadiene-block-poly(ethyleneoxide) diblock copolymer by fluorescence spectroscopy and dynamic light scattering. *J. Mol. Liq.* **2013,** *177*, 40-43.
51. Allen, C.; Maysinger, D.; Eisenberg, A. Nano-engineering block copolymer aggregates for drug delivery. *Colloid Surf. B Biointerfaces* **1999,** *16* (1), 3-27.
52. Shao, Y.; Shi, C.; Xu, G.; Guo, D.; Luo, J. Photo and redox dual responsive reversibly cross-linked nanocarrier for efficient tumor-targeted drug delivery. *ACS Appl. Mater. Interfaces* **2014,** *6* (13), 10381-10392.
53. Li, Y.; Xiao, K.; Luo, J.; Xiao, W.; Lee, J. S.; Gonik, A. M.; Kato, J.; Dong, T. A.; Lam, K. S. Well-defined, reversible disulfide cross-linked micelles for on-demand paclitaxel delivery. *Biomaterials* **2011,** *32* (27), 6633-6645.
54. Xiao, K.; Luo, J.; Li, Y.; Lee, J. S.; Fung, G.; Lam, K. S. PEG-oligocholic acid telodendrimer micelles for the targeted delivery of doxorubicin to B-cell lymphoma. *J. Control. Release* **2011,** *155* (2), 272-281.
55. Wang, J.; Xing, X.; Fang, X.; Zhou, C.; Huang, F.; Wu, Z.; Lou, J.; Liang, W. Cationic amphiphilic drugs self-assemble to the core-shell interface of PEGylated phospholipid micelles and stabilize micellar structure. *Philos. Trans. Royal Soc. A* **2013,** *371*, 20120309.
56. Janssen, M. J. H.; Crommelin, D. J. A.; Storm, G.; Hulshoff, A. Doxorubicin decomposition on storage. Effect of pH, type of buffer and liposome encapsulation. *Int. J. Pharm.* **1985,** *23* (1), 1-11.
57. Wu, D. C.; Ofner, C. M. Adsorption and degradation of doxorubicin from aqueous solution in polypropylene containers. *AAPS Pharm. Sci. Tech.* **2013,** *14* (1), 74-77.
58. Zutshi, A. Physicochemical characterization and stability of doxorubicin in aqueous solutions. Doctoral dissertation, University of Florida, Fl, 1994.
59. Fritze, A.; Hens, F.; Kimpfler, A.; Schubert, R.; Peschka-Süss, R. Remote loading of doxorubicin into liposomes driven by a transmembrane phosphate gradient. *Biomembranes* **2006,** *1758* (10), 1633-1640.
60. Thorat, N. D.; Bohara, R. A.; Noor, M. R.; Dhamecha, D.; Soulimane, T.; Tofail, S. A. M. Effective cancer theranostics with polymer encapsulated

superparamagnetic nanoparticles: Combined effects of magnetic hyperthermia and controlled drug release. *ACS Biomater. Sci. Eng.* **2017,** *3* (7), 1332-1340.
61. Plourde, K.; Derbali, R. M.; Desrosiers, A.; Dubath, C.; Vallée-Bélisle, A.; Leblond, J. Aptamer-based liposomes improve specific drug loading and release. *J. Control. Release* **2017,** *251*, 82-91.
62. Salatin, S.; Maleki Dizaj, S.; Yari Khosroushahi, A. Effect of the surface modification, size, and shape on cellular uptake of nanoparticles. *Cell Biol. Int.* **2015,** *39* (8), 881-890.
63. Zhao, J.; Lu, H.; Wong, S.; Lu, M.; Xiao, P.; Stenzel, M. H. Influence of nanoparticle shapes on cellular uptake of paclitaxel loaded nanoparticles in 2D and 3D cancer models. *Polym. Chem.* **2017,** *8* (21), 3317-3326.

Chapter 5. Cholic acid-based mixed micelles as siRNA delivery agents for gene therapy*

Abstract

Gene therapy is a promising tool for the treatment of various cancers but is hindered by the physico-chemical properties of siRNA and needs a suitable vector for the delivery of siRNA to the target tissue. Bile acid-based block copolymers offers certain advantages for the loading and delivery of siRNA since they can efficiently complex siRNA and bile acids are biocompatible endogenous molecules. In this study, we demonstrate the use of lipids as co-surfactants for the preparation of mixed micelles to improve the siRNA delivery of cholic acid-based block copolymers. Poly(allyl glycidyl ether) (PAGE) and poly(ethylene glycol) (PEG) were polymerized on the surface of cholic acid to afford a star-shaped block copolymer with four arms (CA-PAGE-*b*-PEG)$_4$. The allyl groups of PAGE were functionalized to bear primary or tertiary amines and folic acid was grafted onto the PEG chain end to increase cell uptake. (CA-PAGE-*b*-PEG)$_4$ functionalized with either primary or tertiary amines show high siRNA complexation with close to 100% complexation at N/P ratio of 8. Uniform aggregates with diameters between 181 and 188 nm were obtained. DOPE, DSPE-PEG$_{2k}$, and DSPE-PEG$_{5k}$ lipids were added as co-surfactants to help stabilize the nanoparticles in the cell culture media. Mixed micelles had high siRNA loading with close to 100% functionalization at N/P ratio of 16 and diameters ranging from 153 to 221 nm. The presence of lipids in the mixed micelles improved cell uptake with a concomitant siRNA transfection in HeLa and HeLa-GFP model cells, respectively.

* Published as an article: A.J. Cunningham, V. Passos Gibson, X. Banquy, X.X. Zhu, J. Leblond-Chain, *Int. J. Pharm.*, **2020**, *578*, 119078.

Contributions of authors other than supervisors:
Alexander J. Cunningham: Experimental design, carrying out experiments, data analysis, writing manuscript.
Victor Passos Gibson: Helped in carrying out experiments.

5.1 Introduction

In recent years, a great deal of effort has been directed towards the development and optimization of nanoparticles for gene delivery. Gene delivery offers a formulation challenge due to the hydrophilicity, large size, and numerous negative charges on the siRNA. Nevertheless, a vast array of publications describing gene delivery systems has flooded the scientific literature with many reaching clinical trials but very few currently used in the clinic. The two most thoroughly studied non-viral systems are lipid- and polymer-based nanoparticles, both characterized by their own limitations. Polymers have the advantage of low immunogenicity, ease of synthesis with a lower production cost, and versatility [1-3], but they are mainly limited by their cytotoxicity and low transfection potential. The cytotoxicity arises from the high number of positive charges needed to complex the gene product, whereas the low transfection potential is a result of low endosomal escape once internalized inside the cell [4-5]. Polyethyleneimine (PEI) has been extensively studied for its high transfection potential. There exists a balance in PEI between high transfection and good biocompatibility governed by the length of the polymer that is directly linked to the number of positive charges, where 25 kDa is considered the gold standard [4-6]. Interestingly, reports have demonstrated that branched PEI was more efficient than linear PEI in complexing siRNA with lower N/P ratios needed to complex the siRNA [5, 7-8]. It is believed that the branched structure of PEI allows more flexibility and folding options in a 3-dimensional space to complex the siRNA that is thought to be more rigid and less amenable to folding and rearrangement [5]. Cholic acid-modified PEI have been shown to increase the transfection potential of low molecular weight PEI [9-11]. Indeed, adding amphiphilic bile acids drove the formation of polyplexes of low molecular weight PEI with siRNA and improved gene delivery. Furthermore, different reports have demonstrated the advantage of using branched polymers. For example, a branched histidine/lysine peptide was shown to effectively inhibit protein expression by 80% [12]. Dendrimers, hyperbranched structures, are also gaining importance in the field of siRNA delivery [13-14].

To further improve the transfection efficiency of polymer-based siRNA delivery systems while minimizing the cytotoxic effects, we demonstrate the use of cholic acid-

based star-shaped block copolymers. Cholic acid (CA) is an endogenous compound serving in the emulsification of fats and lipids for their uptake through the intestinal cell wall. Moreover, cholic acid has four hydroxyl groups that can serve as initiators for polymerization yielding a star shaped structure. Recent reports have demonstrated its potential as a drug delivery system due to its inherent capacity to form micelles and its low cytotoxicity [15]. PEG-functionalized CA has been successfully used in the loading of itraconazole showing high loading content (35 %) [16]. In another report, CA-based diblock copolymers showed high loading content (14 %) of Doxorubicin via electrostatic interaction with minimal cytotoxicity [17]. In this report, CA was grafted with four chains of poly(allyl glycidyl ether) (PAGE) and poly(ethylene glycol) (PEG) blocks via anionic polymerization to form a star-shaped block copolymer with 4-arms, CA-(PAGE-*b*-PEG)$_4$. The allyl groups of PAGE were functionalized to bear amine groups promoting the siRNA complexation. Primary and tertiary amine were studied for their propensity for siRNA complexation. It was previously reported that primary amines show permanent positive charge under various pH conditions and this high positive charge leads to stronger binding and hence better siRNA complexation but can also give rise to inefficient release of the siRNA in the cytosol along with a high cytotoxicity [18-21]. Tertiary amines show a lower surface potential, therefore a lower complexation strength which can be beneficial for cytosolic release and lower cytotoxicity [22-23]. Tertiary amines have a lower pK_a and can protonate in the endosome to help in endosomal escape [24-25]. Based on the studies of branched PEI, the star-shaped architecture is believed to promote a higher complexation with siRNA due to the arrangement of the arms around the rigid siRNA molecules. To further stabilize the CA-based block copolymer formulations and promote a higher cell uptake, lipids like 1,2-dioleoyl-sn-glycero-3-phosphoethanolamine (DOPE), PEGylated 1,2-Distearoyl-sn-Glycero-3-Phosphoethanolamine with PEG 2,000 g/mol (DSPE-PEG$_{2k}$) and PEG 5,000 g/mol (DSPE-PEG$_{5k}$) were added to form mixed micelles. Adding lipids to polymers in mixed micelles is proposed to help in the stability of the carrier system and loading of active pharmaceutical ingredients [26-29]. DOPE, a neutral lipid, is known to promote endosomal escape [30], whereas DSPE-PEG has been shown to have good stabilization potential and is currently used for the formulation of the FDA-approved Doxil® [31]. Finally, to improve the cell uptake of the siRNA-loaded NP, folic acid (FA)

was coupled as an active targeting ligand to the terminal hydroxyl groups of the PEG chains of the tertiary-amine functionalized block copolymer. Folate receptors are over-expressed on the surface of various cancer cell lines whereas in healthy cells they are restricted to cells of the lung, kidneys, placenta, and choroid plexus with lower expressions [32-34]. Therefore, as demonstrated in the literature, coupling FA to the surface of NP has the potential to increase their uptake in cancer cells over healthy cells [32, 34]. In this report, the potential of the CA-based block copolymers toward siRNA delivery is measured in the absence and presence of the lipids as co-surfactants and the transfection is compared in the presence and absence of FA.

5.2 Materials and Methods

5.2.1 Materials

All chemical reagents were purchased from Sigma-Aldrich and used without further purification unless stated otherwise. For the anionic polymerization, dimethyl sulfoxide (DMSO) and allyl glycidyl ether (AGE) were dried overnight with calcium hydride and distilled immediately prior to use. Ethylene oxide in the gaseous state was passed through a column of calcium hydride and condensed with dry ice and acetone for quantification by volume before adding to the reaction vessel. Tetrahydrofuran (THF) was dried with sodium under reflux, and methanol was dried using magnesium sulfate. siRNA GFP duplex (target sequence 5'-GCA AGC TGA CCC TGA AGT TC–3') was purchased from Dhermacon (Lafayette, CO, United States) and negative control was purchased from Alpha DNA (Montreal, QC, Canada) Sense strand: UAGCGACUAAACACAUCAAUU and antisense strand: UUGAUGUGUUUAGUCGUAAUU. The fluorescently tagged siRNA used for quantifying cell uptake with flow cytometry was the negative siRNA tagged with Alexa Fluor 488 purchased from Qiagen (Toronto, ON, Canada). The siRNA used for cell uptake was tagged with Cy5 and was obtained from Dhermacon (Lafayette, CO, United States) Sense Strand: 5'-Cy5-UAGCGACUAAACACAUCAAUU-3' Antisense strand: 5'-UUGAUGUGUUUAGUCGCUAUU-3' with the 5'-Cy5 modification on the sense strand.

5.2.2 Synthesis of CA-(PAGE-*b*-PEG)$_4$ via anionic polymerization

The synthesis and functionalization of the polymers are depicted in Scheme 1. The ethanolamine derivative of cholic acid with four hydroxyl groups was synthesized according to a previous method [35-36]. For anionic polymerization, the glassware was flame-dried under vacuum and purged three times with argon before use. Briefly, 5β-cholanoamide (1.1 mmol, 0.5 g) was dissolved in 40 mL of dry DMSO. A potassium naphthalenide solution in THF was added (0.4 mol/L, 1.1 mmol, 1 eq., 3.2 mL) dropwise using a canula under high pressure. AGE was distilled and added (5.1 g, 44.3 mmol, 40 eq.) dropwise using a canula under high pressure. The anionic polymerization was initiated by immersing in an oil bath at 40 °C and allowed to proceed for 24 h to allow the consumption of all the AGE monomers. Then, dry ethylene oxide (6.6 mL, 132.9 mmol, 120 eq.) was chilled in dry ice/acetone to condense into a liquid for accurate measuring and was introduced into the flask. The mixture was polymerized for 24 h. The reaction was quenched by addition of concentrated hydrochloric acid (1 mL). The DMSO solution was extracted with hexane (3 x 10 mL) to remove the naphthalenide. Distilled water was added to the DMSO solution and the mixture was dialyzed against distilled water (48 h) through a regenerated cellulose membrane (MWCO 3,500 Da) (Fisher Scientific, Ottawa, ON, Canada) to remove all unreacted monomers. The polymer was then lyophilized and stored at 4 °C.

5.2.3 Functionalization of CA-(PAGE-*b*-PEG)$_4$ by addition of amine groups

For the preparation of CA-(PAGE-NH_2-*b*-PEG)$_4$ (or ABP-NH_2) containing primary amine groups, the purified and dried polymers of CA-(PAGE-*b*-PEG)$_4$ (2 g, 0.3 mmol) were dissolved in dry methanol (MeOH) (25 mL). 2,2′-Azobis(2-methylpropionitrile) (AIBN) (1.6 g, 9.7 mmol) was dissolved in MeOH. Cysteamine hydrochloride (8.8 g, 77.6 mmol) was dissolved in MeOH and the reaction was started by immersion in an oil bath at 75 ºC under reflux and Ar atmosphere. The reaction proceeded for 12 h, was cooled to room temperature and purified by dialysis against distilled water (48 h, MWCO 3,500 Da) to remove all unreacted cysteamine. A similar protocol was followed for the synthesis of CA-(PAGE-$N(Et)_2$-*b*-PEG)$_4$ (or ABP-NEt_2), however THF was used rather MeOH due to the limited solubility of 2-diethylaminoethanethiol HCl in

MeOH. CA-(PAGE-*b*-PEG)$_4$ (1 g, 0.08 mmol) was dissolved in dry THF. AIBN (0.4 g, 2.2 mmol) and 2-diethylaminoethanethiol HCl (3.8 g, 22.4 mmol) were dissolved in THF. The reaction was started by immersion in an oil bath at 75 ºC under reflux and Ar atmosphere. The reaction proceeded for 12 h and was cooled to room temperature. The reaction was purified by dialysis against distilled water (48 h, MWCO 3,500 Da) to remove all unreacted 2-diethylaminoethanethiol. The polymer was then lyophilized and stored at 4 °C.

5.2.4 Folic acid conjugation to CA-(PAGE-NEt$_2$-*b*-PEG)$_4$

In a round bottom flask, CA-(PAGE-NEt$_2$-*b*-PEG)$_4$ (1 g, 0.07 mmol) was dissolved in 15 mL dry DMF. Folic acid (FA) (7.8 mg, 0.07 mmol), N,N′-dicyclohexylcarbodiimide (DCC) (14 mg, 0.07 mmol), and 4-(dimethylamino)pyridine (DMAP) (8 mg, 0.07 mmol) were dissolved in DMF. The mixture was stirred in an oil bath at 30 ºC for 48 h. Then, the reaction was cooled to room temperature and filtered. The product was purified by dialysis against distilled water (48 h, MWCO 3,500) to remove all unreacted FA. The polymer (ABP-NEt$_2$-FA) was then lyophilized and stored at 4 °C.

5.2.5 Characterization methods

The molar mass of the polymers was determined by size exclusion chromatography (SEC) running on DMF as eluent on a Breeze system from Waters equipped with a 717 plus autosampler, a 1525 Binary HPLC pump, and a 2410 refractive index detector and two consecutive Polar Gel M and Polar Gel L columns (Agilent technologies, Santa Clara, CA, United States) with a flow rate of 0.7 mL/min and at 50 °C. Polymethyl methacrylate (PMMA) standards were used for calibration. All samples were filtered on a nylon 0.2 µm filters prior to injection. ^{1}H-NMR spectra were recorded on a Bruker AV400 spectrometer operating at 400 MHz and samples were dissolved in d$_6$-DMSO. Dynamic light scattering (DLS) measurements were performed on a Malvern Zetasizer NanoZS instrument equipped with a He-Ne laser with a wavelength of 633 nm, and at a scattering angle of 173.5°. Intensity-averaged hydrodynamic diameters of the dispersions were obtained using the non-negative least-squares algorithm (NNLS). Disposable micro-cuvettes were used, and the samples (0.5 mg/mL) were filtered using 0.45 µm nylon filters prior to

measurements. Samples were run at 37 ºC in the appropriate solvent (5 % Dextrose or DMEM). When using DMEM cell culture media, the parameters for running the DLS measurements were obtained from a previous publication: viscosity 0.94 cP, refractive index 1.345, dielectric constant 77.5896.[26] Lower critical solution temperatures (LCST) of the polymer samples (1 mg/mL) were analyzed by following the temperature trend of the polymer with DLS. The sequence was set at a starting temperature of 20 ºC and an end temperature of 60 ºC with a 1 ºC temperature interval. The sample equilibrated at each temperature interval for 120 s and 3 measurements were obtained for each interval. The general-purpose analysis model was used. The zeta potential was obtained on the same Malvern Zetasizer NanoZS instrument. The samples (0.03 mg/mL in distilled water) were run at 37 ºC using the Smoluchowski approximation and monomodal analysis model. Differential scanning calorimetry (DSC) was performed on a DSC Q1000 (TA instruments) at a heating rate of 10 °C/min. The temperature and heat flow were calibrated with indium before each measurement.

5.2.6 siRNA encapsulation

A stock solution of siRNA scrambled (AlphaDNA, Montreal, QC, Canada) was prepared in 5% dextrose (Dex) (160 nM). Stock solutions of polymer were prepared in 5% Dex at appropriate conditions to afford nitrogen of polymer /phosphate of siRNA (N/P) ratios ranging from 1 to 32 (using 42 phosphate groups for siRNA). 250 µL of siRNA solution was mixed with 250 µL of polymer solution and briefly vortexed. The complex was incubated for 30 min at room temperature. Then, an aliquot of 100 µL was added to a 96 well plate and 40 µL of 4X SYBR Gold fluorescent dye (Thermo Scientific, Waltham, MA, United States) was added to the aliquot and the fluorescence was measured using a Safire microplate reader (Tecan, Seestrasse, Switzerland) (λ_{ex} = 495 nm, λ_{em} = 537 nm). Three aliquots of each N/P ratio were measured as triplicates. To quantify the amount of siRNA loaded, a calibration curve was constructed. siRNA with concentrations ranging from 0 to 120 nM were added to a plate reader (100 µL) and 40 µL of 4X SYBR Gold was added to these solutions. The fluorescence of the SYBR Gold was measured and plotted into a calibration curve. The siRNA encapsulation efficiency (EE) was calculated from the siRNA concentrations using the following formula:

$$EE = \frac{[siRNA]\ in\ feed - [siRNA]\ measured\ with\ SYBR\ Gold}{[siRNA]\ in\ feed} * 100\ \%$$

5.2.7 Cytotoxicity

HeLa-GFP cells (Cell Biolabs Inc, San Diego, CA USA) and HeLa cells (CCL-2TM, ATCC®) were cultured in Dulbecco's Minimum Essential Medium (DMEM) supplemented with 10% fetal bovine serum (FBS) (Gibco, Burlington, ON, Canada). The cells were maintained in an incubator at 37 ºC and a 5% CO_2 atmosphere. MTS assay (Sigma Aldrich, Oakville, ON, Canada) was used to determine the cytotoxicity of the blank formulations and the siRNA-loaded formulations. MTS assay (Abcam ab197010, Toronto, ON, Canada) was conducted according to manufacturer's protocol. HeLa cells were plated on a 96-well plate at a seeding density of 5,000 cells per well in 200 µL DMEM and allowed to adhere overnight (37 °C, 5% CO_2, 12 h). 40 µL of the formulation to be tested was added to each well. The plates were incubated for 48 h (37 °C, 5% CO_2). 10 µL of MTS solution was added to each well and incubated (37 °C, 5% CO_2) for 30, 60 and 120 min, respectively. The absorbance was read at 490 nm using a plate reader (Tecan, Seestrasse, Switzerland) at each time point. Cytotoxicity is reported as compared to absorbance measured for control (untreated cells).

5.2.8 Transfection of siRNA-loaded nanoparticles

To assess the silencing capabilities of the siRNA-loaded nanoparticles, a HeLa-GFP cell line was used. HeLa-GFP cells (Cell Biolabs Inc, San Diego, CA USA) were cultured in Dulbecco's Minimum Essential Medium (DMEM) supplemented with 10% fetal bovine serum (FBS) (Gibco, Burlington, ON, Canada). The cells were maintained in an incubator at 37 ºC and a 5% CO_2 atmosphere. HeLa-GFP cells were placed in a 12-well plate at a seeding density of 40,000 cells/well in 1 mL DMEM/FBS and allowed to adhere overnight (37 °C, 5% CO_2). The following day, the cells were rinsed with PBS and 1 mL of Opti-MEM was added to the wells. The siRNA-loaded formulations were prepared in 5% Dex as described above using the corresponding N/P for the polymer being assayed and either 20, 40 or 60 nM siRNA. The complex was vortexed and incubated for 30 min. Then, the formulations were added to the cells, centrifuged (800 rpm, 5 min) and incubated for 4 h. After the incubation period, the cells were washed with PBS and fresh

DMEM/FBS (1 mL) was added. The cells were incubated for 48 h. After this incubation period, the cells were washed with PBS, trypsinized, and suspended in FACS buffer (95 % 1X PBS, 5 % FBS, 0.1% sodium azide) for analysis using a FACSCalibur® flow cytometer (BD Biosciences, San Jose, CA, USA). GFP expression was measured for each triplicate sample using FlowJo software and taking the mean fluorescence intensity of the cell population (minimum 10 000 events). The GFP expression was calculated taking untreated samples as control samples and using this control as a relative measure to calculate the % GFP expression in the siRNA treated samples. A positive control included Lipofectamine RNAiMAX® (Thermo Scientific) according to the manufacturer's protocol and a negative control included HeLa cells not expressing the GFP protein. All experiments were conducted in triplicates.

5.2.9 Cell uptake

HeLa cells were grown in DMEM medium supplemented with 10% FBS. Cells were seeded in a 12-well plate at a seeding density of 100,000 cells/well and allowed to adhere overnight (37 °C, 5% CO_2). The following day, the cells were rinsed with PBS and DMEM/FBS was replaced with Opti-MEM (1 mL). The formulations were prepared as above, but using siRNA labeled with Alexa488 fluorophore (60 nM, Qiagen, Toronto, ON, Canada) with the appropriate N/P ratio. After the corresponding incubation time (2, 4, and 24 h), the cells were washed with PBS, trypsinized (100 µL of 0.25 % Trypsin/EDTA), and suspended in FACS buffer (400 µL, 95 % PBS, 5 % FBS, 1 mM EDTA). The cells were observed on a FACScalibur flow cytometer (BD Biosciences, San Jose, CA, USA). Untreated HeLa cells were used as negative control and the % cell uptake were calculated using Lipofectamine RNAiMAX® (Thermo Scientific) as positive control. The experiment was done in triplicate.

For the fluorescence microscopy, the same procedure was followed with the exception of a fixed 4 h incubation time for the siRNA-labeled formulations and a siRNA labeled with Cy5.5 (Dhermacon, Lafeyette, CO, United States). Alternatively, 100 nM of LysoTracker® Green (Thermo Scientific) was added 30 min prior to imaging for the colocalization of siRNA and lysosomes. Imaging of HeLa cells was performed using an Olympus IX81 fluorescent microscope equipped with a Plan Apo N 40X silicone objective (Olympus Canada Inc., Toronto, ON, Canada) and a 12 bits Retiga-2000R CCD

camera (QImaging, Surry, BC, Canada). The images were obtained and analyzed using MetaMorph Advanced software 7.8.9 (Molecular Devices, San Jose, CA, USA). The Cy5 channel (λ_{ex} = 649 nm, λ_{em} = 666 nm) and the green channel (λ_{ex} = 504 nm, λ_{em} = 666 nm) were used. All fluorescent images were exported keeping the scaling and grey level range constant. The experiment was done in triplicate.

5.3 Results

5.3.1 Polymer synthesis and characterization

Star-shaped block copolymers bearing pendant amine groups were prepared via anionic polymerization followed by post-synthesis modifications according to Scheme 5.1. An ethanolamine derivative of cholic acid was obtained via a condensation reaction according to a previously published protocol [35-36]. This cholic acid derivative was used as an initiator in the anionic polymerization of allyl glycidyl ether (AGE), followed by the polymerization of ethylene oxide (EG) to afford a four-branched block copolymer CA-(PAGE-*b*-PEG)$_4$.

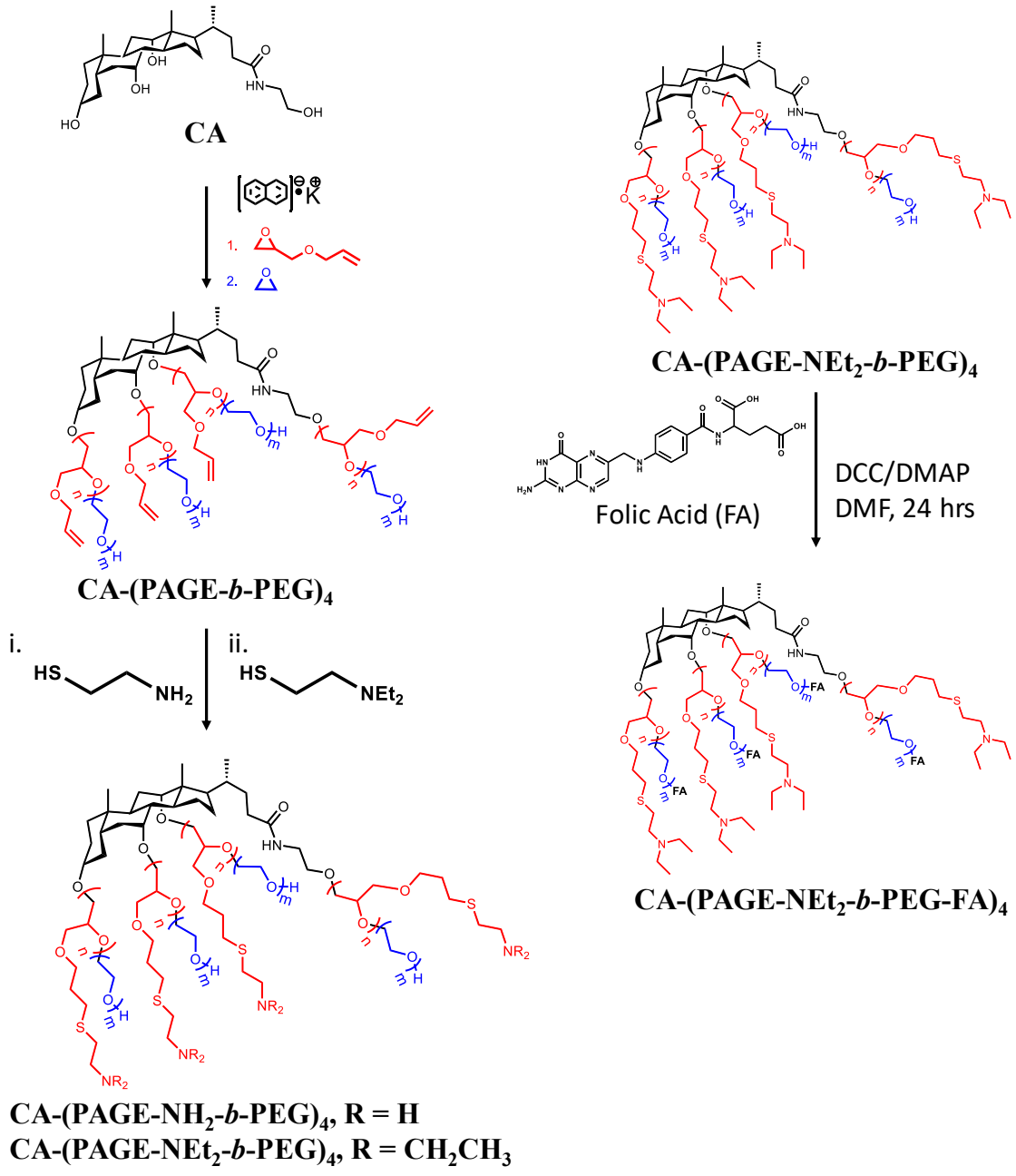

Scheme 5.1. Synthesis and functionalization of cholic acid-based nanoparticles.

The copolymers obtained were analyzed using SEC and ^{1}HNMR spectroscopy (Table 5.1). Two polymers present similar length of PAGE and variable PEG length to study the effect of the latter on the siRNA encapsulation efficiency. The SEC traces show an increase in the Mn when the PEG block was added on CA-(PAGE)$_4$ to form CA-(PAGE-*b*-PEG)$_4$ and a monomodal distribution with a low dispersity index (Figure 5.S1).

In the ^{1}HNMR spectrum (Figure 5.S2), the molar ratio of both polymers was calculated based on the methine peak (5.79-5.92 ppm) of PAGE and methylene peak (3.35-3.60 ppm) of PAGE and PEG, using the methyl proton (0.58 ppm) of cholic acid skeleton as reference. According to the ^{1}HNMR integration, the two polymers possess the following architecture: CA-(AGE$_6$-*b*-EG$_{17}$)$_4$ and CA-(AGE$_8$-*b*-EG$_{49}$)$_4$ (Table 1). PAGE blocks were further functionalized with primary and tertiary amine groups through thiol-ene reactions, in order to promote electrostatic interactions with siRNA, and study their potential towards transfection while minimizing the cytotoxicity of the polymers. The purified polymers were therefore reacted with a thiol-containing aliphatic amine (primary and tertiary amine) via thiol-ene reaction (Scheme 5.1) and the complete functionalization was confirmed by ^{1}HNMR (Figure 5.S3 and 5.S4). Upon functionalization, the allyl peaks (5.79-5.92 ppm) disappear, and new peaks appear (2.5-3 ppm) corresponding to the 2-(diethylamino)ethanethiol moiety. Using the reference peak at 0.58 ppm corresponding to the methyl protons on the CA steroid skeleton, ^{1}HNMR results show close to 100 % functionalization for the coupling of diethylaminomethyl and cysteamine. FA was coupled using a Steglich esterification following a previously published procedure [37]. The purified polymers were analyzed by ^{1}HNMR and UV-Vis spectroscopy. ^{1}HNMR (Figure 5.S5) shows the appearance of characteristic aromatic peaks for FA between 6.6-8.2 ppm. The functionalization ratio was calculated based on the FA methine peaks (region 7.7 ppm) as compared to the cholic acid reference peak (0.58 ppm). The results indicate that 62 % of the polymers were functionalized. Although UV-Vis spectroscopy cannot be used to quantify the amount of FA present on the polymers due to differences in the molar absorption coefficient of free FA and polymer-bound FA (data not shown), the UV-Vis spectrum corroborates the successful presence of FA on purified polymers (Figure 5.S6).

Table 5.1. ^{1}H-NMR and SEC characterization of CA-(PAGE-*b*-PEG)$_4$ polymers.

	Molecular weight (g/mol)		
Polymer	^{1}HNMR	SEC	Đ
CA-(AGE$_6$)$_4$	3,000	3,000	1.09
CA-(AGE$_6$-*b*-EG$_{17}$)$_4$	6,200	5,000	1.13
CA-(AGE$_8$)$_4$	4,300	5,500	1.19
CA-(AGE$_8$-*b*-EG$_{49}$)$_4$	13,000	16,200	1.18

Đ: polydispersity

5.3.2 siRNA encapsulation

Amine-functionalized polymers have the potential to encapsulate siRNA via electrostatic interaction between positively charged amines on the polymer backbone and negatively charged phosphate groups of the phosphodiester linkages of siRNA. Two parameters were investigated for siRNA loading: the impact of the PEG length and the nature of amino groups. Two polymers with different PEG lengths were investigated: 49 repeating units (long PEG), since a large body of evidence points toward a PEG length of 2,000 g/mol as the optimal length for drug delivery purposes[39-41] and 17 units (short PEG), to determine if lowering the PEG length could promote higher siRNA loading by providing a lower shielding of the surface charge. Primary amines were also compared to tertiary amines on the long PEG copolymer. The results are summarized in Figure 5.1.

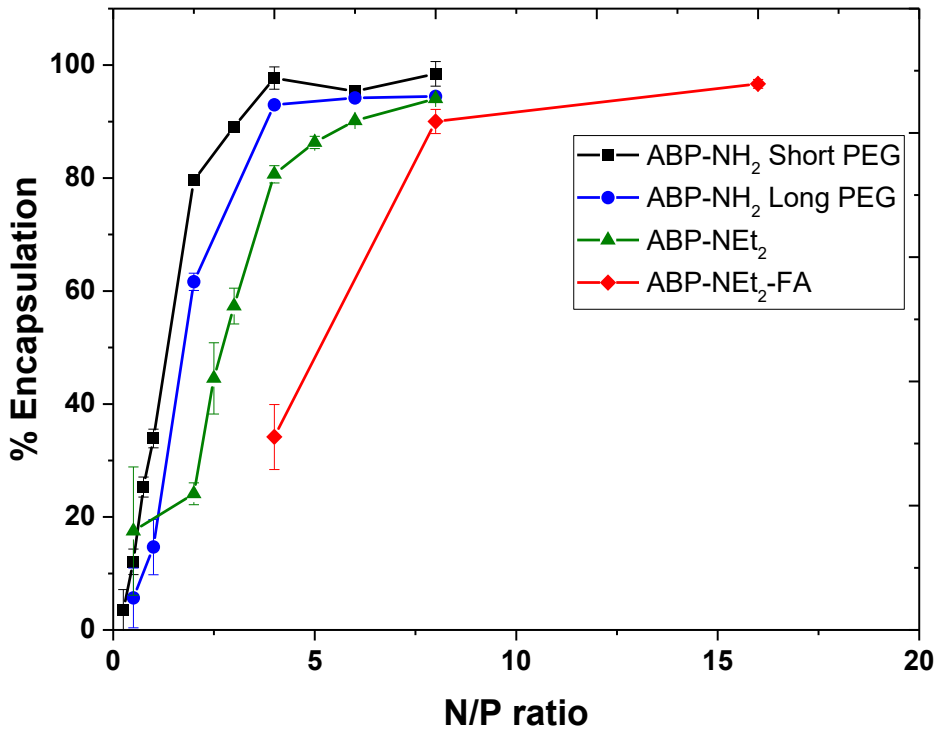

Figure 5.1 siRNA loading of CA-(PAGE-NH_2-*b*-PEG)$_4$ (ABP-NH_2) with short PEG, ABP-NH_2 with long PEG, CA-(PAGE-NEt_2-*b*-PEG)$_4$ (ABP-NEt_2), and CA-(PAGE-NEt_2-*b*-PEG-FA)$_4$ (ABP-NEt_2-FA). Samples were loaded with 60 nM siRNA and %

encapsulation was calculated using SYBR Gold fluorescence assay (n = 3). N/P ratio is the ratio of amine over phosphate groups. At a ratio of 1.3, there are equimolar amounts of siRNA and polymers.

The results show that a longer PEG chain (49 units) was less efficient than a shorter PEG (17 units) at complexing siRNA (61 ± 2 % vs. 79 ± 1 % encapsulation at a N/P = 2, for ABP-NH_2). Nevertheless, both polymers were able to fully complex siRNA at N/P = 4. Only the formulation with longer PEG (CA-(AGE_8-*b*-EG_{49})$_4$) was further characterized for gene delivery since this PEG chain length is optimal for drug delivery per the literature results on PEG 2,000 g/mol as optimal length.[39-41] Keeping the longer PEG chains constant, polymers bearing primary amines were compared to polymers functionalized with tertiary amines. CA-(PAGE-NEt_2-*b*-PEG)$_4$ (ABP-NEt_2) tertiary amine polymers demonstrated a lower ability to complex siRNA than ABP-NH_2, primary amine functionalized polymers, with long PEG at the same N/P ratio. Tertiary amines have a lower pKa and a lower surface potential compared to primary amines, which leads to a lower siRNA complexation strength.[31,32] The maximum siRNA encapsulation is reached only at N/P = 8 with 94 % loading for ABP-NEt_2 compared to N/P = 4 for ABP-NH_2. Coupling of FA to the end of the PEG chains impaired siRNA association, probably because the carboxylic groups of FA are negatively charged at physiological pH (Scheme 5.1). The highest encapsulation efficiency was attained at a N/P of 16 with ≈ 96 % siRNA loading. As a negative control, unfunctionalized polymers (CA-(AGE_8-*b*-EG_{49})$_4$) loaded with siRNA did not show any encapsulation efficiency of siRNA (Figure 5.S4) corroborating the electrostatic interaction as the driving force for the siRNA loading.

5.3.3 Nanoparticle size and zeta potential

Blank and siRNA-loaded formulations were characterized by dynamic light scattering (DLS) and zeta potential (Table 5.2). Interestingly, the empty ABP-NH_2 with long PEG formulation did not show aggregation, whereas complexation with siRNA led to the formation of aggregates of 181 nm.

Table 5.2. DLS and zeta potential of empty and siRNA-loaded formulations in 5% Dextrose.

Formulation	N/P	Diameter (nm)	Micelle dispersity	Zeta potential (mV)
ABP-NH_2 (long PEG)		N/A	N/A	0.7 ± 0.1
ABP-NH_2 with siRNA	4	181 ± 44	0.10	18.1 ± 2.5
ABP-NEt_2		209 ± 49	0.24	15.2 ± 3.9
ABP-NEt_2 with siRNA	16	188 ± 57	0.35	10.4 ± 1.0
ABP-NEt_2-FA		239 ± 52	0.04	39.8 ± 2.0
ABP-NEt_2-FA with siRNA	16	188 ± 57	0.35	23.2 ± 1.7

Formulations were prepared at N/P ratio showing highest siRNA loading. Measurements were done in triplicates.

In the case of the tertiary amine, both ABP-NEt_2 and ABP-NEt_2-FA showed a slight decrease in size upon siRNA loading corresponding to a collapse of the nanoparticles around the siRNA structure, an observation previously reported.[42] Upon siRNA complexation, the polydispersity of the micelles reached 0.1 for ABP-NH_2 and increased from 0.24 to 0.35 for ABP-NEt_2 and 0.04 to 0.35 for ABP-NEt_2-FA. This increase in the polydispersity can result from a restructuring of the polymers around the siRNA as exemplified by the ABP-NH_2 formulation which do not form aggregates without siRNA but aggregates in the presence of siRNA. The ABP-NH_2 formulation did not show an appreciable change in zeta potential upon loading of siRNA with a variation within its standard deviation. However, both ABP-NEt_2 and ABP-NEt_2-FA showed a decrease in their zeta potential upon siRNA loading, which is expected due to the negative charge of siRNA. Similar hydrodynamic diameters and zeta potentials were recorded for the siRNA-loaded aggregates and allows for their comparison in cell uptake and internalization. The positive surface charge of the formulations is promising for cell uptake and transfection.

5.3.4 siRNA transfection in HeLa cells

siRNA transfection was assessed in HeLa-GFP cells to compare the primary amine polymers (ABP-NH_2) to the tertiary amine counterpart (ABP-NEt_2) (Figure 5.2).

Unfortunately, only a small decrease in GFP expression was observed at all N/P ratios tested. It has to be noted that ABP-NH_2 exhibited cell toxicity at N/P > 2, whereas the lower N/P of 2 did not elicit a knockdown of GFP expression. Although less toxic, the ABP-NEt_2 did not yield substantial GFP knockdown at all N/P ratio tested. Several strategies were used to improve transfection, by increasing the siRNA concentration up to 60 nM, by removing serum in the culture media and by adding chloroquine, but none of them improved the transfection efficiency of ABP-NEt_2, whereas commercial Lipofectamine was able to silence GFP to the extent of 51.2 % (Figure 5.S7).

To further investigate the limited transfection of the ABP-NEt_2 formulation, cell uptake was quantified in HeLa model cells using fluorescently labeled siRNA (Figure 5.2). The results show a low cell uptake after 2, 4, and 24 h incubation time with less than 5 % uptake even at the longer time points. To promote higher cell uptake, folic acid (FA) was conjugated to the end of the PEG chains of ABP-NEt_2 yielding ABP-NEt_2-FA. Unexpectedly, this approach did not improve the cell uptake in HeLa cells, since less than 5 % of the formulation was internalized in the cell after 24 h, whereas Lipofectamine was able to enter the cells (Figure 5.2).

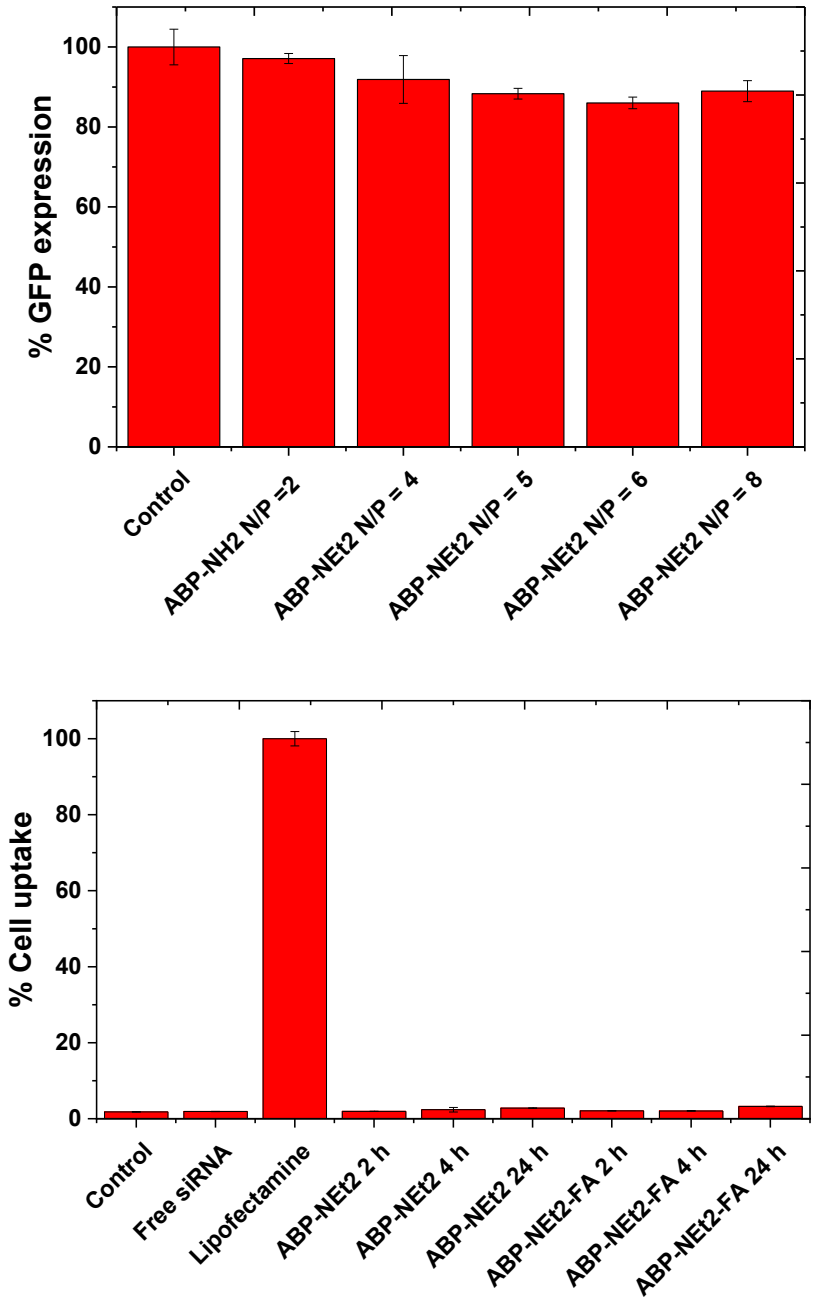

Figure 5.2 (top) siRNA transfection of ABP-NH_2 and ABP-NEt_2 in HeLa-GFP measured by flow cytometry of GFP fluorescence after 48 h incubation (n = 3). siRNA concentration was maintained at 30 nM and the N/P ratio varied. (bottom) Cell uptake of ABP-NEt_2 and ABP-NEt_2-FA in HeLa cells assessed by flow cytometry. 60 nM of Alexa488-labeled siRNA was complexed to the NP with a N/P ratio of 16. The results were obtained as triplicates.

To corroborate these results, the internalization was qualitatively monitored by fluorescence microscopy using Cy5-siRNA-loaded formulations (Figure 5.3). Lipofectamine used as a positive control show a large uptake with the cells appearing bright red, whereas the three formulations ABP-NH_2, ABP-NEt_2 and ABP-NEt_2-FA did not show an appreciable uptake. Only ABP-NEt_2-FA formulation showed a small uptake with a faint red appearing inside the cells. Interestingly, aggregates of approximately 1-2 μm appearing as bright red spots were seen in the microscopy images of all three formulations and were absent in the lipofectamine positive control. These aggregates could indicate a colloidal instability of the formulations in the cell culture media. To better understand this colloidal instability, the variation of the size of the ABP-NEt_2-FA nanoparticles were measured by DLS in different solutions as a function of temperature (Figure 5.S8). The results show that in 5% dextrose, ABP-NEt_2-FA do not show a LCST behavior, whereas in DMEM cell culture media, ABP-NEt_2-FA exhibits a LCST value of 37 °C. The presence of the LCST can be attributed to a salting-out effect on the polymer due to the high salt concentrations in DMEM.[43-45] In order to optimize the colloidal stability of ABP-NEt_2-FA, the addition of lipids as co-surfactants was investigated. DOPE, DSPE-PEG_{2k}, and DSPE-PEG_{5k} were added at a concentration of 10 wt%. The addition of the lipids shifted the LCST in DMEM to 42 °C for DOPE and DSPE-PEG_{5k} and 44 °C for DSPE-PEG_{2k}. Adding lipids as co-surfactant has the potential to provide colloidal stability of the ABP-NEt_2-FA formulation and optimize the siRNA delivery.[18-21]

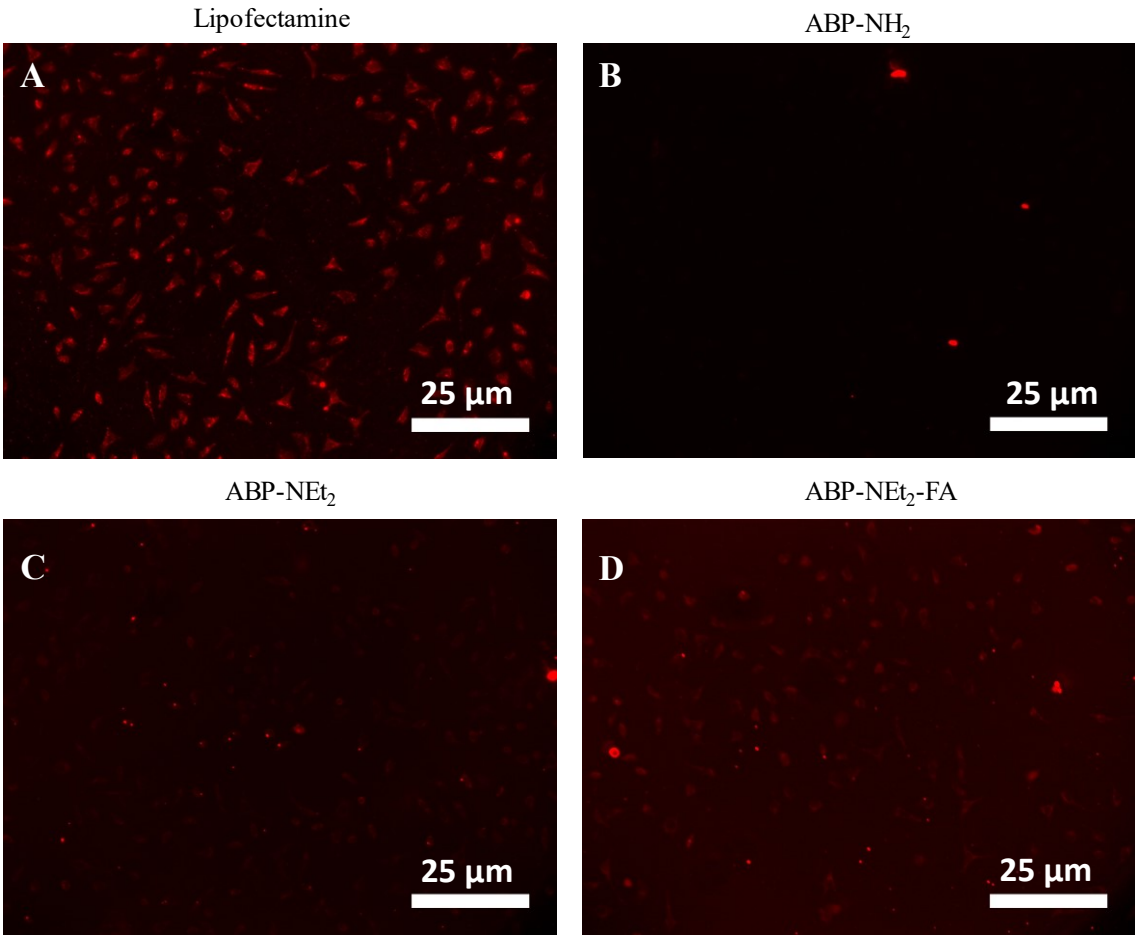

Figure 5.3 Fluorescence microscopy images for cell uptake of (A) lipofectamine used as a control and (B) ABP-NH_2, (C) ABP-NEt_2 and (D) ABP-NEt_2-FA in HeLa cells. 100 nM of Cy5-labeled siRNA was complexed to the NP with a N/P ratio of 16 for 30 min. The results were imaged at a 10X magnification and the same brightness level was applied to each image. The scale bars represent 25 µm in length.

5.3.5 siRNA encapsulation using lipid-polymer mixed micelles (LPM)

Since the ABP-NEt2-FA yielded better cell uptake compared to the other formulations (Figure 5.4), this formulation was further studied for stabilization with co-lipids. A series of three lipids were chosen to form LPMs namely DOPE, DSPE-PEG_{2k} and DSPE-PEG_{5k}. DOPE was chosen as it has been often used to improve transfection efficiency.[46] Also, DSPE lipids were tested as co-surfactants since they are used in the FDA-approved drug delivery system Doxil®.[47] To ascertain the formation of mixed micelles rather than separate aggregates of the polymer and lipids, the hydrodynamic

diameter of the ABP-NEt_2-FA was measured in the absence and presence of the lipids (Table 5.3). DSPE-PEG_{2k} and DSPE-PEG_{5k} alone at 0.1 mg/mL failed to form stable aggregates in 5% Dextrose using the co-evaporation method (data not shown). Whereas DOPE at a concentration of 0.1 mg/mL forms micelles with diameters of 188 ± 76 nm with a micelle dispersity of 0.19 (Figure 5.S9). To form the mixed micelles, ABP-NEt_2-FA was mixed with 10 wt% lipids using the co-evaporation method.[19,48] The mixed micelles showed a large increase in the micelle dispersity since ABP-NEt_2-FA micelles had a dispersity of 0.04 compared to 0.28 - 0.54 for mixed micelles. Interestingly, the size of the ABP-NEt_2-FA NP decreased substantially upon addition of the lipids to form the LPMs, an observation that was previously reported.[49] The surface zeta potential of ABP-NEt_2-FA with DOPE was higher than ABP-NEt_2-FA alone, 51.6 mV compared to 39.8 mV, due to the presence of positive charges on DOPE lipid. On the contrary, adding PEGylated lipids to the formulation lowered the surface zeta potential of ABP-NEt_2-FA (Table 5.3). The presence of the PEG chains masks the surface zeta potential and a trend is observed where the longer the PEG chains are, the lower the zeta potential.[50] To further corroborate the formation of mixed micelles, DSC thermograms of the mixed micelles were compared to ABP-NEt_2-FA, DOPE, DSPE-PEG_{2k}, and DSPE-PEG_{5k} alone (Figure 5.S10-5.S12). ABP-NEt_2-FA showed a melting temperature of 43 °C (Figure 5.S10). The lipids alone have a melting point of 115.4 °C for DOPE, 50.3 °C for DSPE-PEG_{2k}, and 57.7 °C for DSPE-PEG_{5k} (Figure 5.S11). When lipids are incorporated in the polymers to form mixed micelles, the melting points of the lipids disappeared (Figure 5.S12). Also, the DSC shows the appearance of a glass transition temperature at 25 °C for the ABP-NEt_2-FA with DOPE, 12 °C for ABP-NEt_2-FA with DSPE-PEG_{2k}, and 16 °C for ABP-NEt_2-FA with DSPE-PEG_{5k}. In the thermograms of the mixed micelles, only a subtle peak of a melting point can be observed between 45 and 51 °C which should correspond to the ABP-NEt_2-FA polymer chains that are free from interactions.

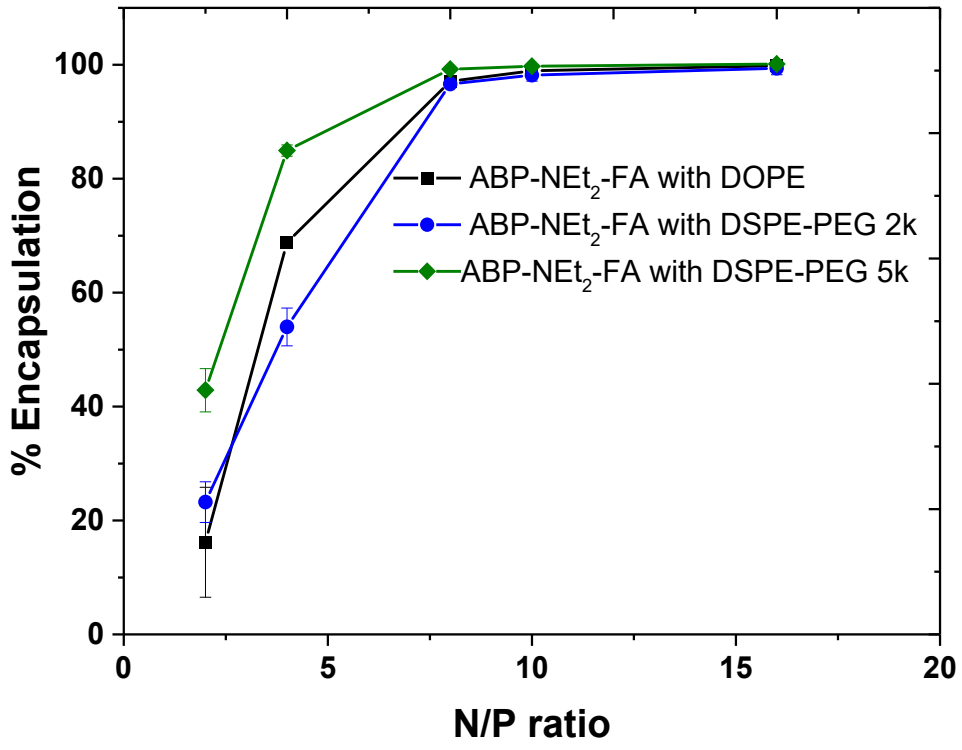

Figure 5.4 siRNA loading of ABP-NEt_2-FA with DOPE, DSPE-PEG_{2k} and DSPE-PEG_{5k}. Samples were loaded with 60 nM siRNA and % encapsulation was calculated against a standard curve. Samples were obtained in triplicates.

As shown in Figure 5.5, the presence of lipids improved the loading of siRNA for all three formulations compared to ABP-NEt_2-FA alone but yielded lower encapsulation capacity than the ABP-NEt_2 and ABP-NH_2 formulations. Nevertheless, all three formulations show close to 100% encapsulation at N/P of 8, similarly to ABP-NEt_2-FA. Size and zeta potential of the mixed micelles formulation before and after siRNA loading are presented in Table 5.3.

Table 5.3. DLS and zeta potential of empty and siRNA-loaded formulations in 5% Dextrose.

siRNA formulation	Diameter (nm)	Micelle dispersity	Zeta potential (mV)
ABP-NEt_2-FA	239 ± 52	0.04	39.8 ± 2.0
ABP-NEt_2-FA with siRNA	188 ± 57	0.35	23.2 ± 1.7
ABP-NEt_2-FA/DOPE	103 ± 55	0.28	51.6 ± 2.5
ABP-NEt_2-FA/DOPE with siRNA	221 ± 54	0.01	30.9 ± 2.6
ABP-NEt_2-FA/DSPE-PEG_{2k}	139 ± 62	0.38	32.9 ± 3.8
ABP-NEt_2-FA/DSPE-PEG_{2k} with siRNA	206 ± 64	0.13	19.5 ± 0.2
ABP-NEt_2-FA/DSPE-PEG_{5k}	121 ± 55	0.54	26.8 ± 1.5
ABP-NEt_2-FA/DSPE-PEG_{5k} with siRNA	153 ± 49	0.24	14.9 ± 1.6

Formulations were prepared at N/P ratio of 16. Measurements were done in triplicates.

Upon siRNA loading there is an increase in the micelle size with a concomitant decrease in the micelle dispersity. However, the micelle size of the siRNA-loaded mixed micelles is comparable to the ABP-NEt_2-FA with siRNA. Also, upon siRNA loading there is a decrease of the zeta potential, an observation that has been previously reported.[51] To ensure that the polymer and polymer-lipid mixed micelles were nontoxic and could be used as siRNA delivery systems, the cytotoxicity of each polymer as well as the blank micelles was measured in HeLa cells using the MTS assay (Figure 5.S13). ABP-NH_2 was quite toxic as low as 0.05 mg/mL and decreased cell viability to 32% at 1 mg/mL, which could explain the poor results of transfection (Figure 5.2). ABP-NEt_2 was less noxious to the cells, but followed the same trend, since only 48% of the cells were viable at 1 mg/mL. Interestingly, ABP-NEt_2-FA was much better tolerated up to 1 mg/mL. Although some reports show no significant difference in cytotoxicity upon FA conjugation,[57-58] in this report the FA improved the biocompatibility of the system; an observation that has been previously reported.[50] It is hypothesized that the folate ligand shields partially the interaction between the positive charges of the polymer and cell surface. Of the polymer-lipid mixed micelles, ABP-NEt_2-FA with DSPE-PEG_{2k} or DSPE-PEG_{5k} were well

tolerated with close to 100% cell viability up to 1 mg/mL, whereas ABP-NEt_2-FA with DOPE showed higher toxicity with 72% cell viability at 0.5 mg/mL.

5.3.6 siRNA transfection with lipid-polymer mixed micelles (LPM)

To determine the potential of the mixed micelles towards siRNA transfection, the cell uptake was observed using fluorescence microscopy (Figure 5.6). The results show a marked increase of the mixed micelles uptake in HeLa cells when compared to the micelles without lipids as cosurfactants. ABP-NEt_2-FA with DSPE-PEG_{2k} and ABP-NEt_2-FA with DSPE-PEG_{5k} both show higher uptake than the ABP-NEt_2-FA with DOPE. Moreover, the large aggregates seen in the previous formulation are absent in these images.

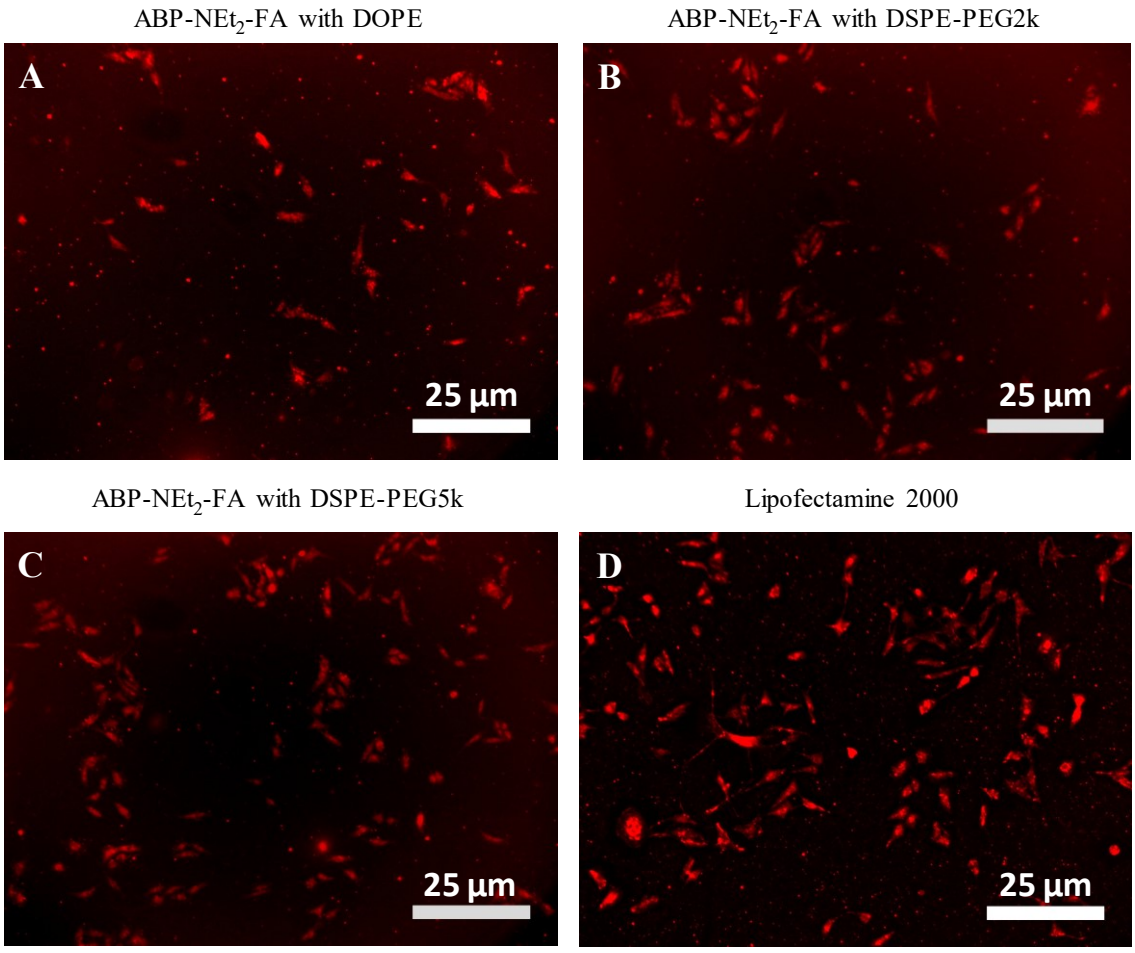

Figure 5.5 Fluorescence microscopy images for cell uptake (A) ABP-NEt_2-FA with DOPE, (B) ABP-NEt_2-FA with DSPE-PEG_{2k}, (C) ABP-NEt_2-FA with DSPE-PEG_{5k} and

(D) Lipofectamine 2000 in HeLa cells. 100 nM of Cy5-labeled siRNA was complexed to the NP with a N/P ratio of 16 for 30 min. The results were imaged at a 10X magnification and the same brightness level was applied to each image. The scale bars represent 25 μm in length.

These qualitative observations were confirmed by flow cytometry (Figure 5.7). When normalized to lipofectamine, mixed micelles exhibited 18-24% higher uptake than polymeric micelles, but still 5 times lower than lipofectamine. The presence of lipids likely aided in the stabilization of the nanoparticles in the culture medium by increasing the LCST thereby preventing aggregation, enabling cellular uptake. As compared to non-targeted micelles, the presence of FA significantly improved the uptake of the micelles (from 5% to 18-24%). This demonstrated the advantage of both components: lipids for improved stability and FA-conjugation for improved cell uptake.

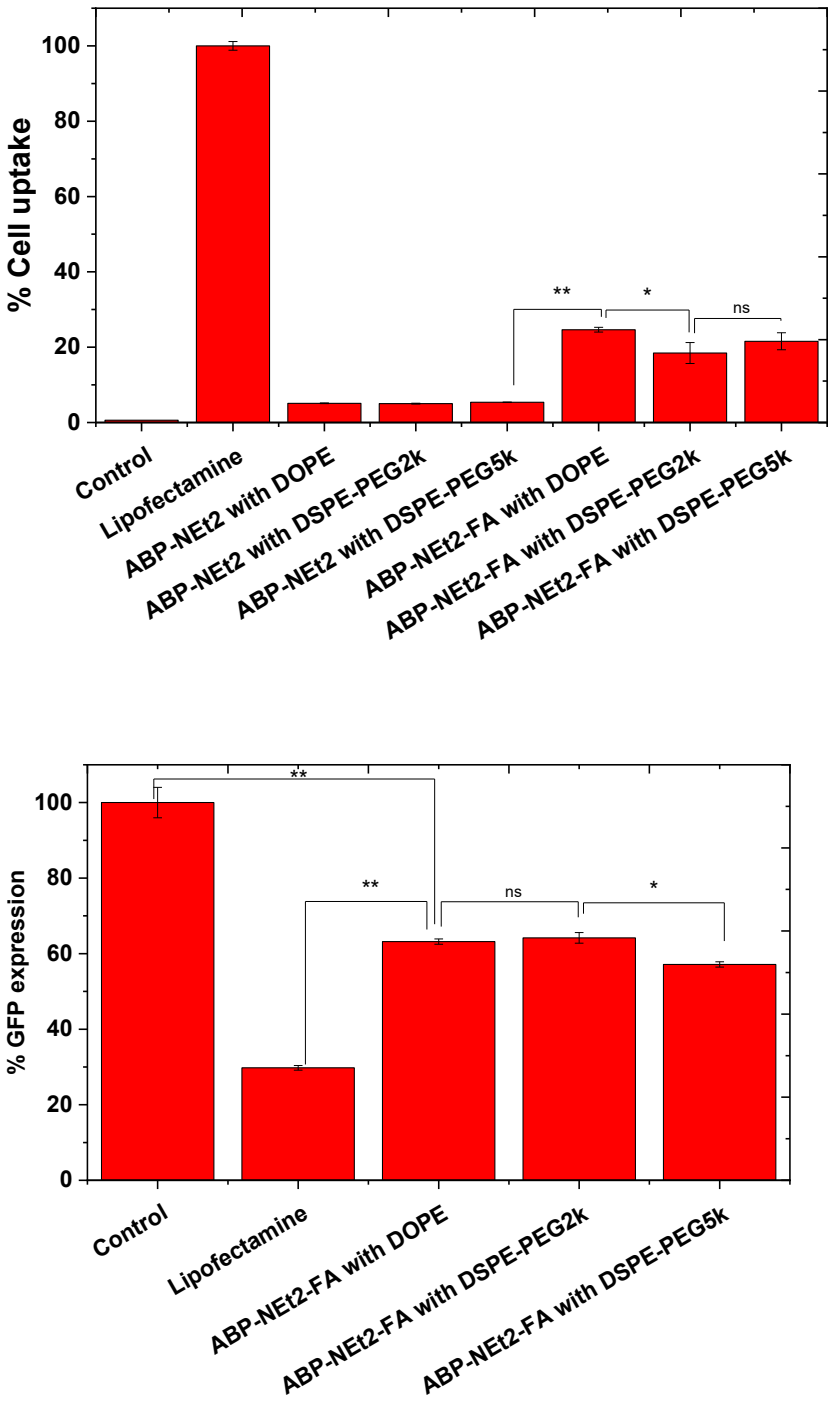

Figure 5.6 (top) Cell uptake of mixed micelles in HeLa cells assessed by flow cytometry. 60 nM of Alexa488-labeled siRNA was complexed to the NPs with a N/P ratio of 16. The results were obtained as triplicates. (bottom) siRNA transfection of mixed micelles in HeLa-GFP measured by flow cytometry of GFP fluorescence after 48

h incubation (n = 3). siRNA concentration was maintained at 60 nM and N/P of 16. Statistical analysis performed with Student's t test * = $p < 0.05$; ** = $p < 0.01$; ns = $p > 0.05$.

Although the uptake level did not reach Lipofectamine performance, this increase was enough to trigger significant siRNA transfection (Figure 5.7). ABP-NEt_2-FA mixed micelles reduced GFP expression to 57-65%, showing similar behavior for all three lipids, DOPE, DSPE-PEG_{2k} and DSPE-PEG_{5k}. Although not as efficient as lipofectamine, these results testify to an improvement in the formulation with the presence of the lipids as cosurfactant. The literature demonstrates the beneficial effect of DOPE in lipid-based delivery systems due to its fusogenic effect.[52-54] To determine the extent of lysosomal escape of the LPM, siRNA-loaded LPM and lysosomes colocalization was observed under fluorescence microscopy (Figure 5.S14). Both LysoTracker® green and siRNA labeled with Cy 5 were readily taken up by the cells after 4 h. For all three formulations of ABP-NEt_2-FA mixed micelles, strong colocalization was observed, confirming that internalization of LMP followed the endocytic pathway. This observation suggested that endosomal entrapment decreased the transfection efficiency and might explain the lower transfection observed for the mixed micelles when compared to lipofectamine (Figure 5.7).

The proposed BA-based block copolymers were developed for drug and gene delivery due to their highly biocompatible profile. In this study, the star-shaped BA-based block copolymers show a high siRNA complexation at low N/P ratio of 16 which is advantageous for gene delivery purposes because limited material is needed to deliver the siRNA, which decreases the potential toxic effects.[59] Adding co-lipids improved the loading and enabled transfection of the star-shaped block copolymers. An improvement to the proposed drug delivery system would be to optimize the choice of the lipid co-surfactant to increase the silencing activity to reach comparable levels to lipofectamine. In this perspective, pH-switchable lipids, which demonstrated quick endosomal escape and efficient cytoplasmic release of siRNA, could be used.[60] An advantage of the LPM system is the ease with which the platform can be tuned. The formulation can be optimized through the selection of lipids without the need to change the entire polymer structure. However, further studies are necessary to determine the stability of the polymer-lipid

mixed micelles in the presence of serum protein. Lipid-polymer hybrid nanoparticles are gaining importance because these systems combine the advantages of both polymers and lipids.[61] In one study, lipid-polymer hybrids enabled sustained long-term release of siRNA from nanoparticles which is an improvement to the transient release typically seen in nanoparticles made solely of lipids or polymers.[62] Another report used PEG-*b*-PLA-*b*-PEG polymer and DDAB lipid hybrid nanoparticles to improve the colloidal stability of DDAB in RPMI and promote gene silencing.[63] The advantage of using polymer-lipid hybrid nanoparticles in our system is that the polymer part confers lower cytotoxicity (Figure 5.S13) and high siRNA loading, whereas the lipid part promotes stability in the cell culture medium and high transfection.

5.4 Conclusion

Cholic acid-based block copolymers were obtained by anionic polymerization. The PAGE blocks may be functionalized to bear pendant primary or tertiary amine groups enabling siRNA loading. High loading was obtained for both primary and tertiary amines with close to 100% complexation at low N/P ratio. Folic acid can be grafted to the ends of the PEG chains for increased cell uptake in cancer cells. Unfortunately, the siRNA loaded micelles did not exhibit cell uptake or siRNA transfection. DLS temperature trends demonstrated that the nanoparticles were unstable in the DMEM cell culture media due to the presence of a LCST at 37 °C. DOPE, DSPE-PEG_{2k}, and DSPE-PEG_{5k} were used as co-surfactants to increase the colloidal stability of the ABP-NEt_2-FA NP. Adding these co-surfactants allowed to increase the LCST to 42 °C for DOPE and DSPE-PEG_{5k} and 44 °C for DSPE-PEG_{2k}. Although not as efficient, the presence of the lipids did not inhibit siRNA loading with close to 100% complexation at N/P ratio of 16. DSC results testify to the presence of mixed micelles with the disappearance of the melting endotherms of both ABP-NEt_2-FA polymers and corresponding lipids and the appearance of a glass transition temperatures for the mixed micelles. Finally, adding the mixed micelles showed an improved cell uptake. Although, not as efficient as lipofectamine, the mixed micelles showed siRNA knockdown of GFP expression. These results show that there is a great potential towards the use of cholic acid-based block copolymers for the delivery of siRNA in the form of mixed micelles. The star-shaped architecture of the cholic acid-based polymers enabled high siRNA loading but the presence of high salt concentrations in the

cell culture media led to colloidal instability, low cell uptake and low siRNA transfection. Fortunately, the presence of lipids as co-surfactants allowed to increase the LCST of the mixed micelles and provided colloidal stability in cell culture medium and promote siRNA transfection. Adding lipids to the polymer nanoparticles offers new opportunities in formulations of drug delivery systems. There are a large variety of modifications that can be added to improve polymer-based systems, such as adding targeting lipids to improve cell uptake, lipids as co-surfactants to improve colloidal stability, fusogenic lipids to increase endosomal release and even pH-sensitive lipids to promote drug release.

5.5 Acknowledgments

The financial support from NSERC of Canada in the form of Discovery grant to XXZ is gratefully acknowledged. AC and XXZ are members of CQMF funded by FRQNT of Quebec.

5.6 References

1. Xiang, Y.; Oo, N. N. L.; Lee, J. P.; Li, Z.; Loh, X. J., Recent development of synthetic nonviral systems for sustained gene delivery. *Drug Discov. Today* **2017,** *22* (9), 1318-1335.
2. Park, T. G.; Jeong, J. H.; Kim, S. W., Current status of polymeric gene delivery systems. *Adv. Drug Deliv. Rev.* **2006,** *58* (4), 467-486.
3. Oupicky, D., Utilizing polydrug and polymeric drug concepts in development of nucleic acid delivery vectors. *Nanomedicine* **2016,** *12* (2), 449-470.
4. Zhou, Z.; Liu, X.; Zhu, D.; Wang, Y.; Zhang, Z.; Zhou, X.; Qiu, N.; Chen, X.; Shen, Y., Nonviral cancer gene therapy: Delivery cascade and vector nanoproperty integration. *Adv. Drug Deliv. Rev.* **2017,** *115* (1), 115-154.
5. Scholz, C.; Wagner, E., Therapeutic plasmid DNA versus siRNA delivery: common and different tasks for synthetic carriers. *J. Control. Release* **2012,** *161* (2), 554-565.
6. Huh, S.-H.; Do, H.-J.; Lim, H.-Y.; Kim, D.-K.; Choi, S.-J.; Song, H.; Kim, N.-H.; Park, J.-K.; Chang, W.-K.; Chung, H.-M.; Kim, J.-H., Optimization of 25kDa linear polyethylenimine for efficient gene delivery. *Biologicals* **2007,** *35* (3), 165-171.
7. Kwok, A.; Hart, S. L., Comparative structural and functional studies of nanoparticle formulations for DNA and siRNA delivery. *Nanomedicine* **2011,** *7* (2), 210-219.
8. Boeckle, S.; von Gersdorff, K.; van der Piepen, S.; Culmsee, C.; Wagner, E.; Ogris, M., Purification of polyethylenimine polyplexes highlights the role of free polycations in gene transfer. *J. Gene Med.* **2004,** *6* (10), 1102-1111.

9. Dube, B.; Pandey, A.; Joshi, G.; Mulherkar, R.; Sawant, K., Cholic acid-modified polyethylenimine: in vitro and in vivo studies. *Int. J. Nanomedicine* **2018,** *13*, 83-85.
10. Kim, D.; Lee, D.; Jang, Y. L.; Chae, S. Y.; Choi, D.; Jeong, J. H.; Kim, S. H., Facial amphipathic deoxycholic acid-modified polyethyleneimine for efficient MMP-2 siRNA delivery in vascular smooth muscle cells. *Eur. J. Pharm. Biopharm.* **2012,** *81* (1), 14-23.
11. Weecharangsan, W.; Opanasopit, P.; Niyomtham, N.; Yingyongnarongkul, B. E.; Kewsuwan, P.; Lee, R. J., Synergistic inhibition of human carcinoma cell growth via co-delivery of p53 plasmid DNA and bcl-2 antisense oligodeoxyribonucleotide by cholic acid-modified polyethylenimine. *Anticancer Res.* **2017,** *37* (11), 6335-6340.
12. Leng, Q.; Scaria, P.; Zhu, J.; Ambulos, N.; Campbell, P.; Mixson, A. J., Highly branched HK peptides are effective carriers of siRNA. *J. Gene Med.* **2005,** *7* (7), 977-986.
13. Dzmitruk, V.; Apartsin, E.; Ihnatsyeu-Kachan, A.; Abashkin, V.; Shcharbin, D.; Bryszewska, M., Dendrimers show promise for siRNA and microRNA therapeutics. *Pharmaceutics* **2018,** *10* (3), 126-151.
14. Biswas, S.; Torchilin, V. P., Dendrimers for siRNA Delivery. *Pharmaceuticals* **2013,** *6* (2), 161-183.
15. Cunningham, A. J.; Zhu, X. X., Polymers made of bile acids: from soft to hard biomaterials. *Can. J. Chem.* **2016,** *94* (8), 659-666.
16. Le Dévédec, F.; Strandman, S.; Baille, W. E.; Zhu, X. X., Functional star block copolymers with a cholane core: Thermo-responsiveness and aggregation behavior. *Polymer* **2013,** *54* (15), 3898-3903.
17. Cunningham, A. J.; Robinson, M.; Banquy, X.; Leblond, J.; Zhu, X. X., Bile acid-based drug delivery systems for enhanced doxorubicin encapsulation: Comparing hydrophobic and ionic interactions in drug loading and release. *Mol. Pharm.* **2018,** *15* (3), 1266-1276.
18. Lin, Z.; Bao, M.; Yu, Z.; Xue, L.; Ju, C.; Zhang, C., The development of tertiary amine cationic lipids for safe and efficient siRNA delivery. *Biomater. Sci.* **2019,** *7* (7), 2777-2792.
19. Obata, Y.; Suzuki, D.; Takeoka, S., Evaluation of cationic assemblies constructed with amino acid based lipids for plasmid DNA delivery. *Bioconjug. Chem.* **2008,** *19* (5), 1055-1063.
20. Knudsen, K. B.; Northeved, H.; Kumar Ek, P.; Permin, A.; Gjetting, T.; Andresen, T. L.; Larsen, S.; Wegener, K. M.; Lykkesfeldt, J.; Jantzen, K.; Loft, S.; Møller, P.; Roursgaard, M., In vivo toxicity of cationic micelles and liposomes. *Nanomedicine* **2015,** *11* (2), 467-477.
21. Reschel, T.; Konak, C.; Oupicky, D.; Seymour, L. W.; Ulbrich, K., Physical properties and in vitro transfection efficiency of gene delivery vectors based on complexes of DNA with synthetic polycations. *J. Control. Release* **2002,** *81* (1), 201-217.
22. Whitehead, K. A.; Dorkin, J. R.; Vegas, A. J.; Chang, P. H.; Veiseh, O.; Matthews, J.; Fenton, O. S.; Zhang, Y.; Olejnik, K. T.; Yesilyurt, V.; Chen, D.; Barros, S.; Klebanov, B.; Novobrantseva, T.; Langer, R.; Anderson, D. G.,

Degradable lipid nanoparticles with predictable in vivo siRNA delivery activity. *Nat. Commun.* **2014,** *5*, 4277-4287.
23. Lu, Y.; Aimetti, A. A.; Langer, R.; Gu, Z., Bioresponsive materials. *Nat. Rev. Mater.* **2016,** *2* (16075), 1-17.
24. Mo, R.; Sun, Q.; Li, N.; Zhang, C., Intracellular delivery and antitumor effects of pH-sensitive liposomes based on zwitterionic oligopeptide lipids. *Biomaterials* **2013,** *34* (11), 2773-2786.
25. Habrant, D.; Peuziat, P.; Colombani, T.; Dallet, L.; Gehin, J.; Goudeau, E.; Evrard, B.; Lambert, O.; Haudebourg, T.; Pitard, B., Design of ionizable lipids to overcome the limiting step of endosomal escape: Application in the intracellular delivery of mRNA, DNA, and siRNA. *J. Med. Chem.* **2016,** *59* (7), 3046-3062.
26. Le Devedec, F.; Strandman, S.; Hildgen, P.; Leclair, G.; Zhu, X. X., PEGylated bile acids for use in drug delivery systems: enhanced solubility and bioavailability of itraconazole. *Mol. Pharm.* **2013,** *10* (8), 3057-3066.
27. Harmon, A. M.; Lash, M. H.; Tishbi, N.; Lent, D.; Mintzer, E. A.; Uhrich, K. E., Thermodynamic and physical interactions between novel polymeric surfactants and lipids: toward designing stable polymer-lipid complexes. *Langmuir* **2011,** *27* (15), 9131-9138.
28. Li, X.; Zhang, Y.; Fan, Y.; Zhou, Y.; Wang, X.; Fan, C.; Liu, Y.; Zhang, Q., Preparation and evaluation of novel mixed micelles as nanocarriers for intravenous delivery of propofol. *Nanoscale Res. Lett.* **2011,** *6* (1), 275-284.
29. Wu, H.; Zhu, L.; Torchilin, V. P., pH-sensitive poly(histidine)-PEG/DSPE-PEG co-polymer micelles for cytosolic drug delivery. *Biomaterials* **2013,** *34* (4), 1213-1222.
30. Hoekstra, D.; Rejman, J.; Wasungu, L.; Shi, F.; Zuhorn, I., Gene delivery by cationic lipids: in and out of an endosome. *Biochem. Soc. Trans.* **2007,** *35* (1), 68-71.
31. Li, J.; Wang, X.; Zhang, T.; Wang, C.; Huang, Z.; Luo, X.; Deng, Y., A review on phospholipids and their main applications in drug delivery systems. *Asian J. Pharm. Sci.* **2015,** *10* (2), 81-98.
32. Zwicke, G. L.; Mansoori, G. A.; Jeffery, C. J., Utilizing the folate receptor for active targeting of cancer nanotherapeutics. *Nano Rev.* **2012,** *3*, 18496-18507.
33. Parker, N.; Turk, M. J.; Westrick, E.; Lewis, J. D.; Low, P. S.; Leamon, C. P., Folate receptor expression in carcinomas and normal tissues determined by a quantitative radioligand binding assay. *Anal Biochem.* **2005,** *338* (2), 284-293.
34. Yoo, H. S.; Park, T. G., Folate-receptor-targeted delivery of doxorubicin nano-aggregates stabilized by doxorubicin-PEG-folate conjugate. *J. Control. Release* **2004,** *100* (2), 247-256.
35. Luo, J.; Giguère, G.; Zhu, X. X., Asymmetric poly(ethylene glycol) star polymers with a cholic acid core and their aggregation properties. *Biomacromolecules* **2009,** *10* (4), 900-906.
36. Gouin, S.; Zhu, X. X., Synthesis of 3 alpha- and 3 beta-dimers from selected bile acids. *Steroids* **1996,** *61* (11), 664-669.
37. Cao, Y.; He, J.; Liu, J.; Zhang, M.; Ni, P., Folate-conjugated polyphosphoester with reversible cross-linkage and reduction sensitivity for drug delivery. *ACS Appl. Mater. Interfaces* **2018,** *10* (9), 7811-7820.

38. Mo, R.; Sun, Q.; Li, N.; Zhang, C., Intracellular delivery and antitumor effects of pH-sensitive liposomes based on zwitterionic oligopeptide lipids. *Biomaterials* **2013,** *34* (11), 2773-2786.
39. Habrant, D.; Peuziat, P.; Colombani, T.; Dallet, L.; Gehin, J.; Goudeau, E.; Evrard, B.; Lambert, O.; Haudebourg, T.; Pitard, B., Design of ionizable lipids to overcome the limiting step of endosomal escape: Application in the intracellular delivery of mRNA, DNA, and siRNA. *J. Med. Chem.* **2016,** *59* (7), 3046-3062.
40. Zwicke, G. L.; Mansoori, G. A.; Jeffery, C. J., Utilizing the folate receptor for active targeting of cancer nanotherapeutics. *Nano Rev.* **2012,** *3*, 18496-18507.
41. Parker, N.; Turk, M. J.; Westrick, E.; Lewis, J. D.; Low, P. S.; Leamon, C. P., Folate receptor expression in carcinomas and normal tissues determined by a quantitative radioligand binding assay. *Anal Biochem.* **2005,** *338* (2), 284-293.
42. Yoo, H. S.; Park, T. G., Folate-receptor-targeted delivery of doxorubicin nano-aggregates stabilized by doxorubicin-PEG-folate conjugate. *J. Control. Release* **2004,** *100* (2), 247-256.
43. Cao, Y.; He, J.; Liu, J.; Zhang, M.; Ni, P., Folate-conjugated polyphosphoester with reversible cross-linkage and reduction sensitivity for drug delivery. *ACS Appl. Mater. Interfaces* **2018,** *10* (9), 7811-7820.
44. Knop, K.; Hoogenboom, R.; Fischer, D.; Schubert, U. S., Poly(ethylene glycol) in drug delivery: Pros and cons as well as potential alternatives. *Angew. Chem. Int. Ed.* **2010,** *49* (36), 6288-6308.
45. Jokerst, J. V.; Lobovkina, T.; Zare, R. N.; Gambhir, S. S., Nanoparticle PEGylation for imaging and therapy. *Nanomedicine* **2011,** *6* (4), 715-728.
46. Mishra, P.; Nayak, B.; Dey, R. K., PEGylation in anti-cancer therapy: An overview. *Asian J. Pharm. Sci.* **2016,** *11* (3), 337-348.
47. Katas, H.; Alpar, H. O., Development and characterisation of chitosan nanoparticles for siRNA delivery. *J. Control. Release* **2006,** *115* (2), 216-225.
48. Du, H.; Wickramasinghe, R.; Qian, X., Effects of salt on the lower critical solution temperature of poly (N-isopropylacrylamide). *J. Phys. Chem. B* **2010,** *114* (49), 16594-16604.
49. Freitag, R.; Garret-Flaudy, F., Salt effects on the thermoprecipitation of poly-(N-isopropylacrylamide) oligomers from aqueous solution. *Langmuir* **2002,** *18* (9), 3434-3440.
50. Liu, Y.-J.; Pallier, A.; Sun, J.; Rudiuk, S.; Baigl, D.; Piel, M.; Marie, E.; Tribet, C., Non-monotonous variation of the LCST of light-responsive, amphiphilic poly(NIPAM) derivatives. *Soft Matter* **2012,** *8* (32), 8446-8455.
51. Wasungu, L.; Hoekstra, D., Cationic lipids, lipoplexes and intracellular delivery of genes. *J. Control. Release* **2006,** *116* (2), 255-264.
52. Soundararajan, A.; Bao, A.; Phillips, W. T.; Perez, R., 3rd; Goins, B. A., [(186)Re]Liposomal doxorubicin (Doxil): in vitro stability, pharmacokinetics, imaging and biodistribution in a head and neck squamous cell carcinoma xenograft model. *Nucl. Med. Biol.* **2009,** *36* (5), 515-524.
53. Ciani, L.; Ristori, S.; Salvati, A.; Calamai, L.; Martini, G., DOTAP/DOPE and DC-Chol/DOPE lipoplexes for gene delivery: zeta potential measurements and electron spin resonance spectra. *Biochim. Biophys. Acta* **2004,** *1664* (1), 70-79.

54. Li, X.; Zhang, Y.; Fan, Y.; Zhou, Y.; Wang, X.; Fan, C.; Liu, Y.; Zhang, Q., Preparation and evaluation of novel mixed micelles as nanocarriers for intravenous delivery of propofol. *Nanoscale Res. Lett.* **2011,** *6* (1), 275-284.
55. Kumar, V.; Qin, J.; Jiang, Y.; Duncan, R. G.; Brigham, B.; Fishman, S.; Nair, J. K.; Akinc, A.; Barros, S. A.; Kasperkovitz, P. V., Shielding of lipid nanoparticles for siRNA delivery: Impact on physicochemical properties, cytokine induction, and efficacy. *Mol. Ther. Nucleic Acids* **2014,** *3* (210), 1-7.
56. Abdul Ghafoor Raja, M.; Katas, H.; Jing Wen, T., Stability, intracellular delivery, and release of siRNA from chitosan nanoparticles using different cross-linkers. *PLOS ONE* **2015,** *10* (6), e0128963.
57. Gjetting, T.; Arildsen, N. S.; Christensen, C. L.; Poulsen, T. T.; Roth, J. A.; Handlos, V. N.; Poulsen, H. S., In vitro and in vivo effects of polyethylene glycol (PEG)-modified lipid in DOTAP/cholesterol-mediated gene transfection. *Int. J. Nanomedicine* **2010,** *5*, 371-383.
58. Du, Z.; Munye, M. M.; Tagalakis, A. D.; Manunta, M. D. I.; Hart, S. L., The role of the helper lipid on the DNA transfection efficiency of lipopolyplex formulations. *Sci. Rep.* **2014,** *4* (7107), 1-6.
59. Mochizuki, S.; Kanegae, N.; Nishina, K.; Kamikawa, Y.; Koiwai, K.; Masunaga, H.; Sakurai, K., The role of the helper lipid dioleoylphosphatidylethanolamine (DOPE) for DNA transfection cooperating with a cationic lipid bearing ethylenediamine. *Biochim. Biophys. Acta Biomembr.* **2013,** *1828* (2), 412-418.
60. Hadinoto, K.; Sundaresan, A.; Cheow, W. S., Lipid–polymer hybrid nanoparticles as a new generation therapeutic delivery platform: A review. *Eur. J. Pharm. Biopharm.* **2013,** *85* (3), 427-443.
61. Shi, J.; Xu, Y.; Xu, X.; Zhu, X.; Pridgen, E.; Wu, J.; Votruba, A. R.; Swami, A.; Zetter, B. R.; Farokhzad, O. C., Hybrid lipid-polymer nanoparticles for sustained siRNA delivery and gene silencing. *Nanomedicine* **2014,** *10* (5), 897-900.
62. Monirinasab, H.; Asadi, H.; Rostamizadeh, K.; Esmaeilzadeh, A.; Khodaei, M.; Fathi, M., Novel lipid-polymer hybrid nanoparticles for siRNA delivery and IGF-1R gene silencing in breast cancer cells. *J. Drug Deliv. Sci. Tech.* **2018,** *48*, 96-105.

5.7 Supporting Information

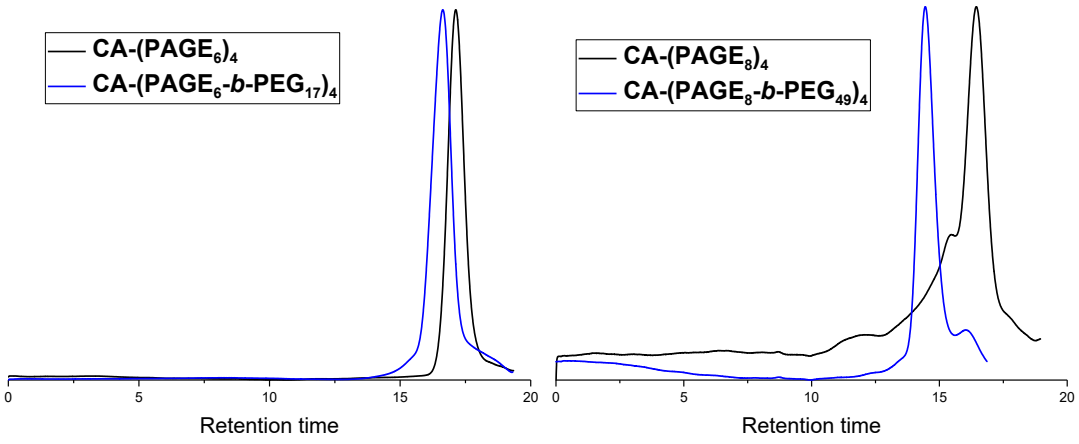

Figure 5.S1 SEC traces of CA-(PAGE)$_4$ homopolymers and CA-(PAGE-*b*-PEG)$_4$ block copolymers obtained in DMF. Flow rate was set to 0.7 mL/min at 50 °C and samples were analyzed with a calibration curve based on PMMA standards.

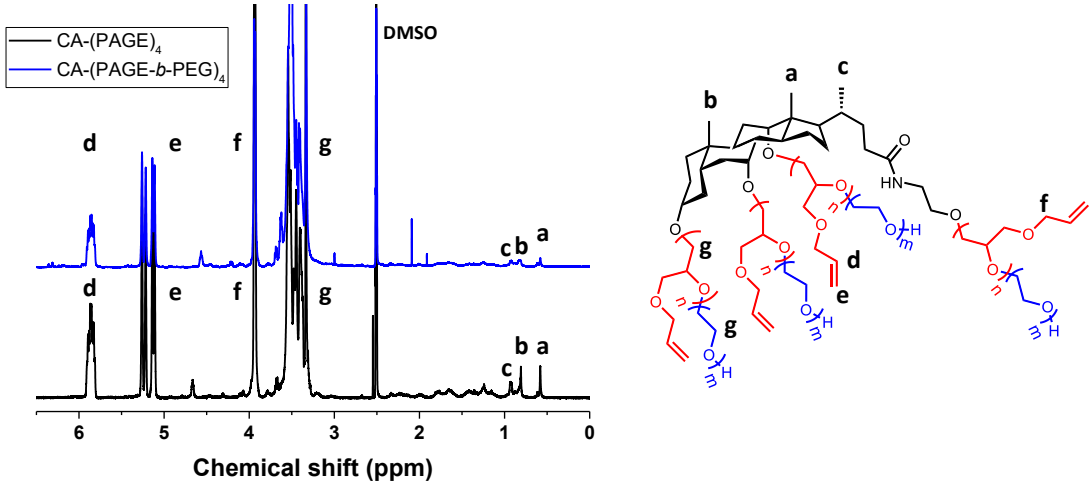

Figure 5.S2 ^{1}H-NMR spectrum of CA-(PAGE)$_4$ (bottom) and CA-(PAGE-*b*-PEG)$_4$ (top) obtained in d_6-DMSO.

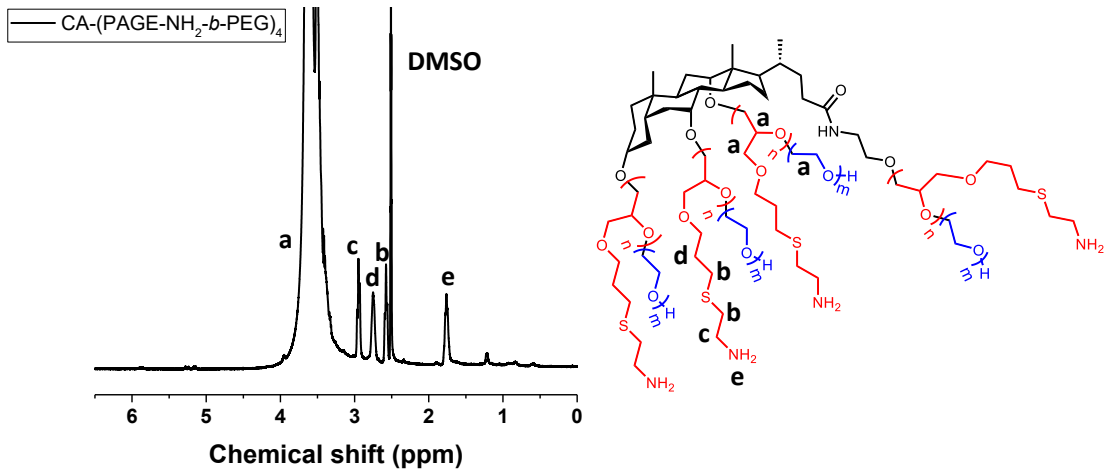

Figure 5.S3 ^{1}H-NMR spectrum of CA-(PAGE-NH_2-*b*-PEG)$_4$ (ABP-NH_2) obtained in d_6-DMSO.

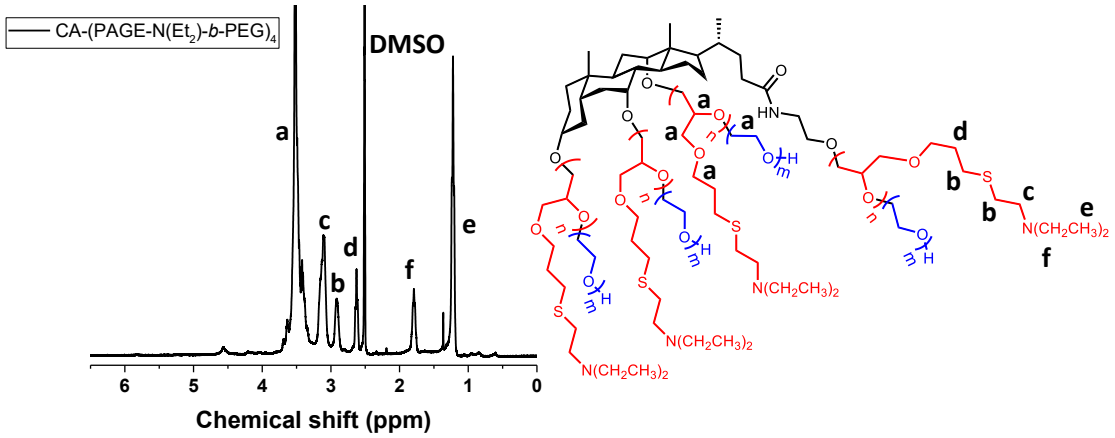

Figure 5.S4 ^{1}H-NMR spectrum of CA-(PAGE-NEt_2-*b*-PEG)$_4$ (ABP-NEt_2) obtained in d_6-DMSO.

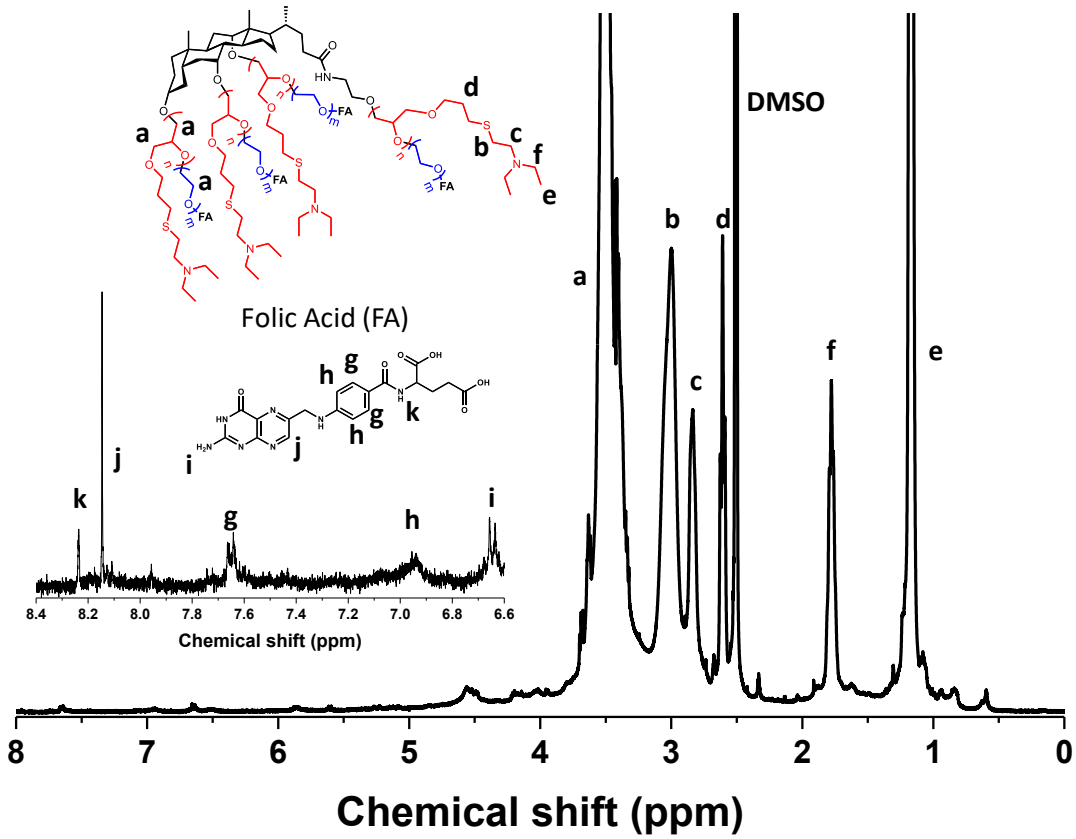

Figure 5.S5 ^{1}H-NMR spectrum of CA-(PAGE-NEt$_2$-*b*-PEG-FA)$_4$ (ABP-NEt$_2$-FA) obtained in d$_6$-DMSO.

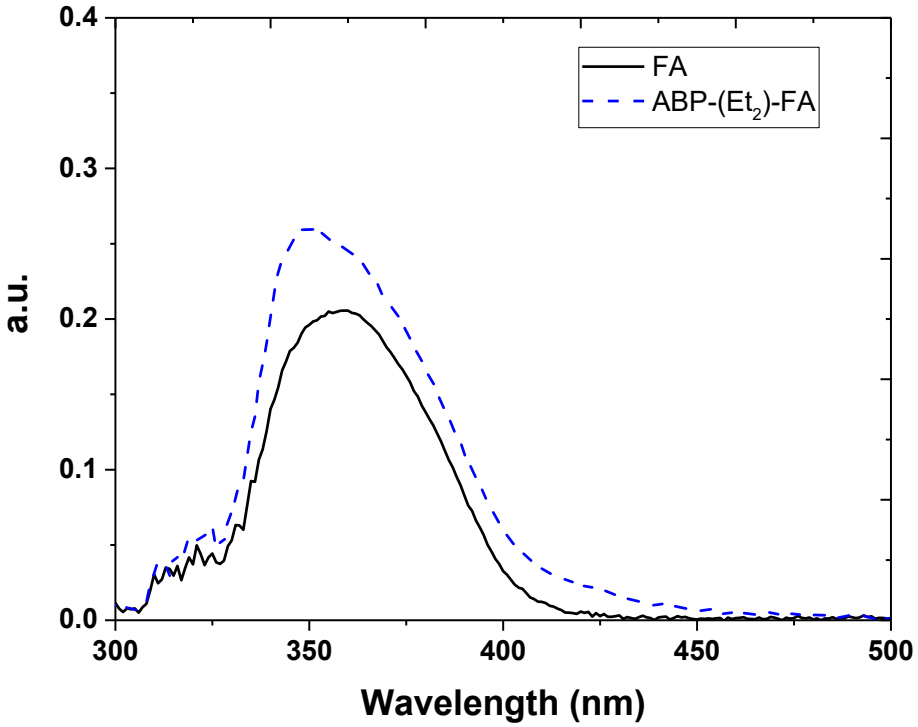

Figure 5.S6 UV-Vis spectrum of folic acid (FA) and ABP-NEt_2-FA polymers obtained in DMSO.

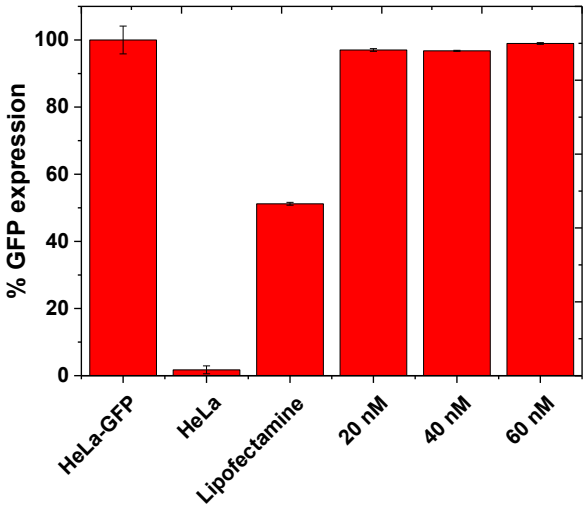

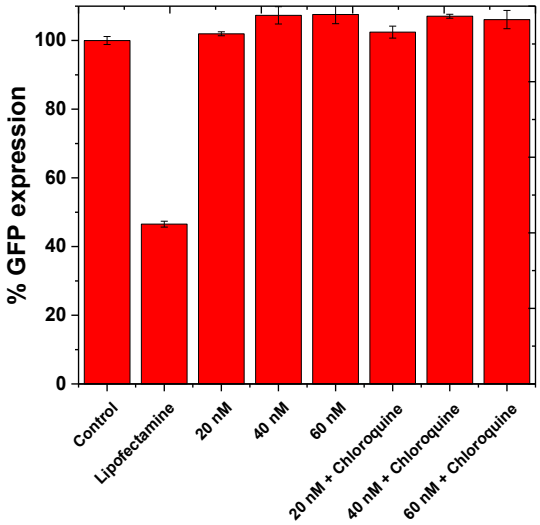

Figure 5.S7 siRNA transfection of ABP-NEt_2 in HeLa-GFP measured by flow cytometry of GFP fluorescence after 48 h incubation (n = 3). siRNA concentration was varied and siRNA formulation were added to cells in presence of serum (top) and absence of serum (bottom).

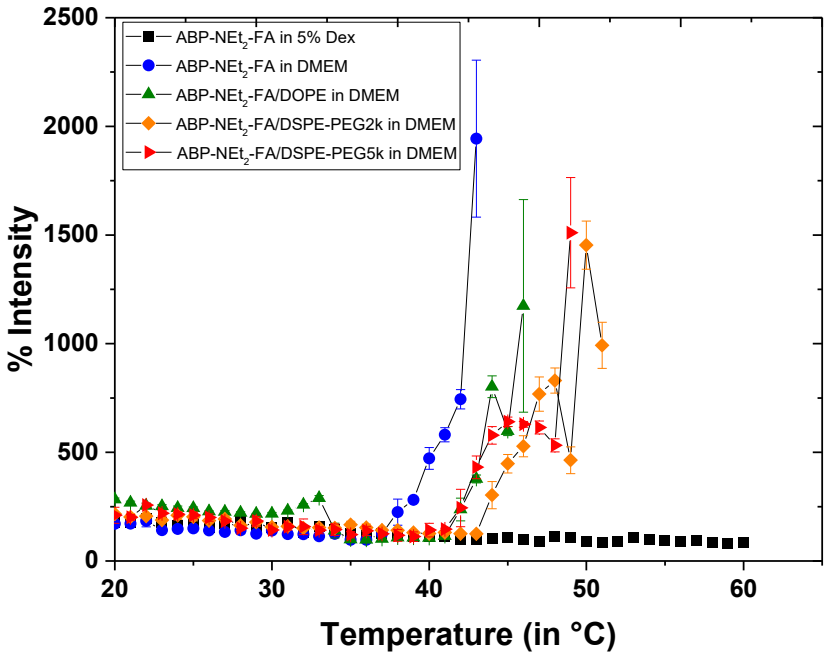

Figure 5.S8 DLS temperature trend for ABP-NEt_2-FA with and without lipids in 5% Dextrose vs. DMEM cell culture media.

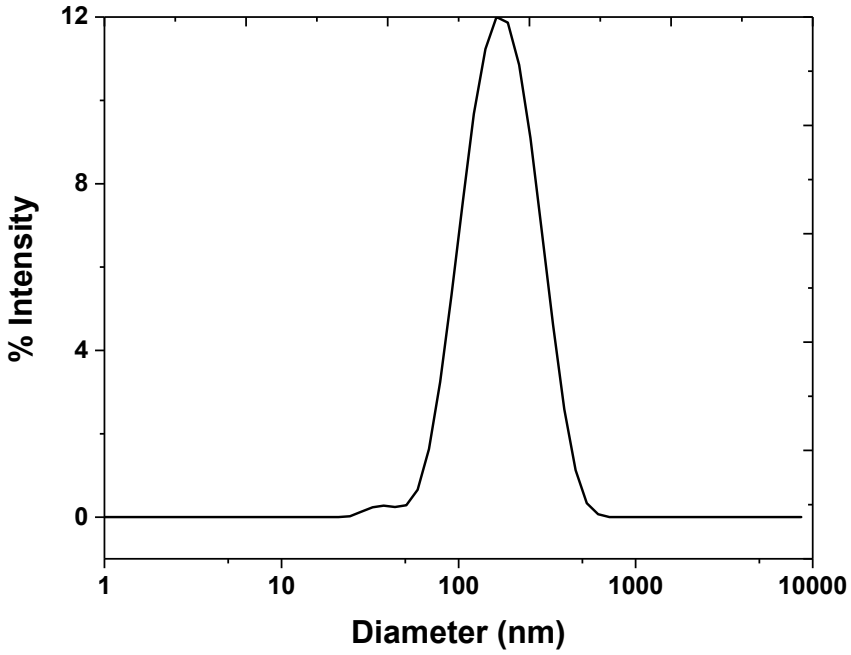

Figure 5.S9 DLS diagram of DOPE lipids at a concentration of 0.1 mg/mL prepared using the solvent evaporation technique and filtered using nylon 0.2 µm.

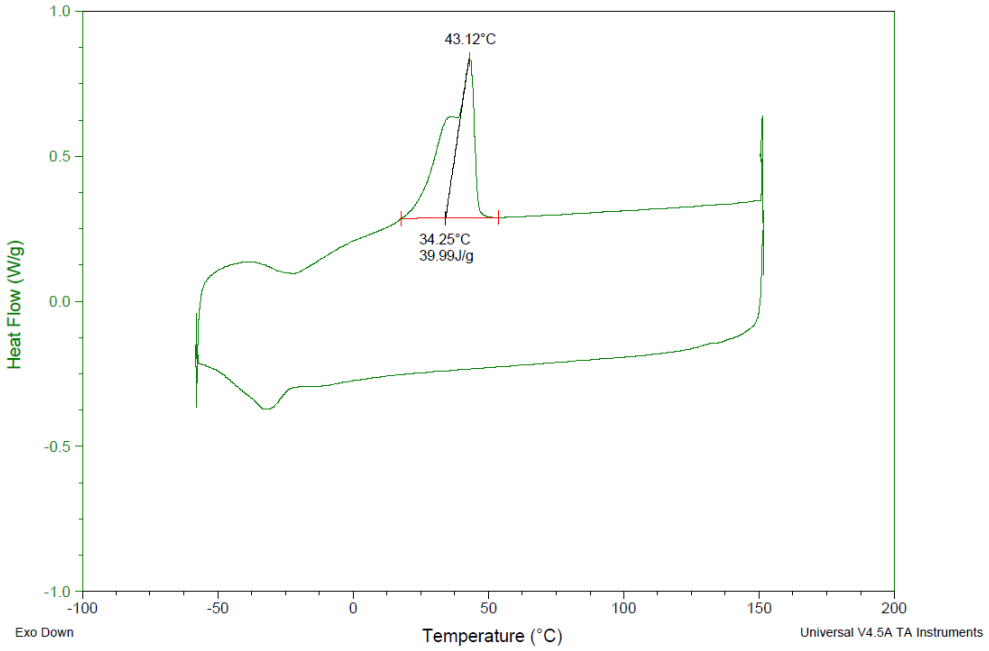

Figure 5.S10 DSC thermogram of ABP-NEt_2-FA obtained with a heating rate of 10 °C/min.

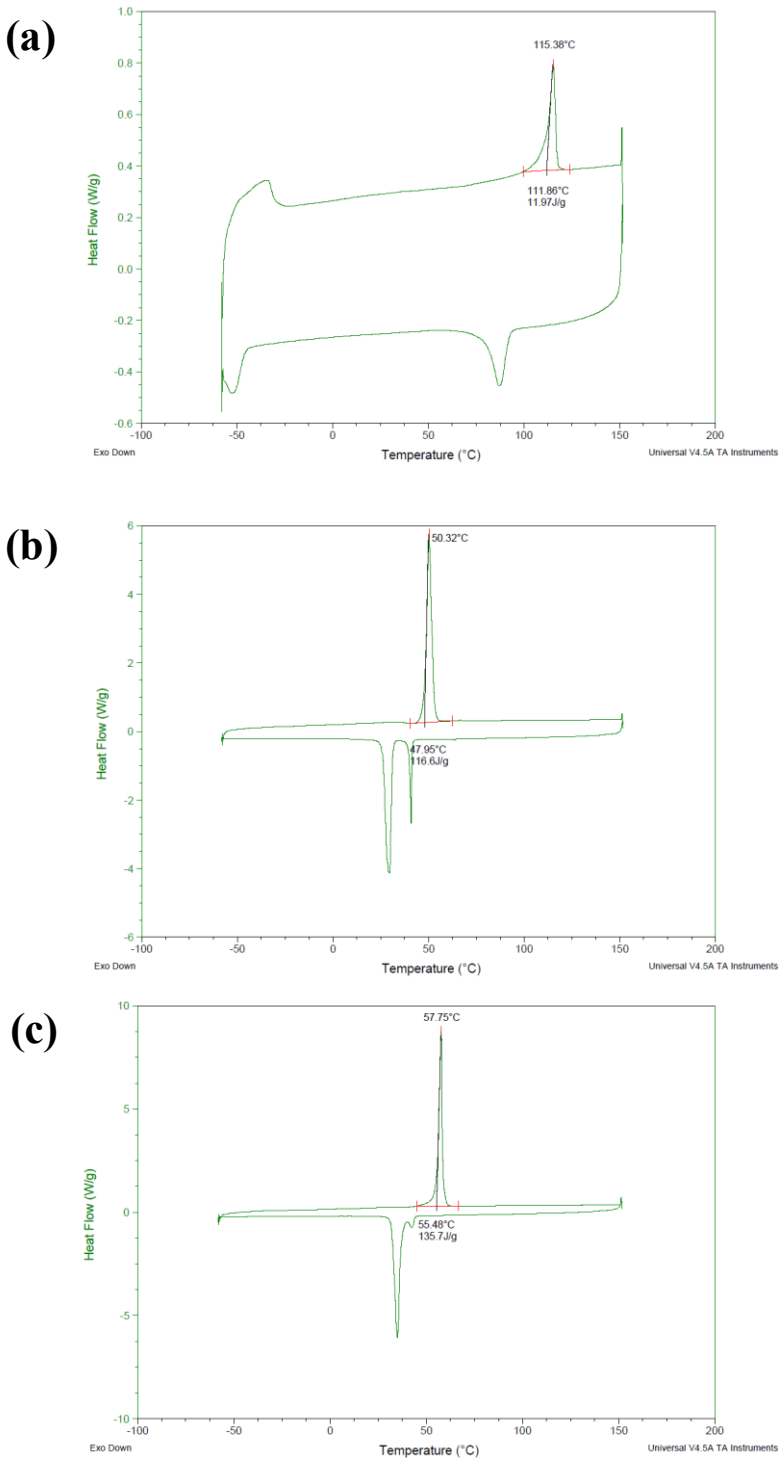

Figure 5.S11 DSC thermogram of DOPE (a), DSPE-PEG$_{2k}$ (b), and DSPE-PEG$_{5k}$ (c) obtained with a heating rate of 10 °C/min.

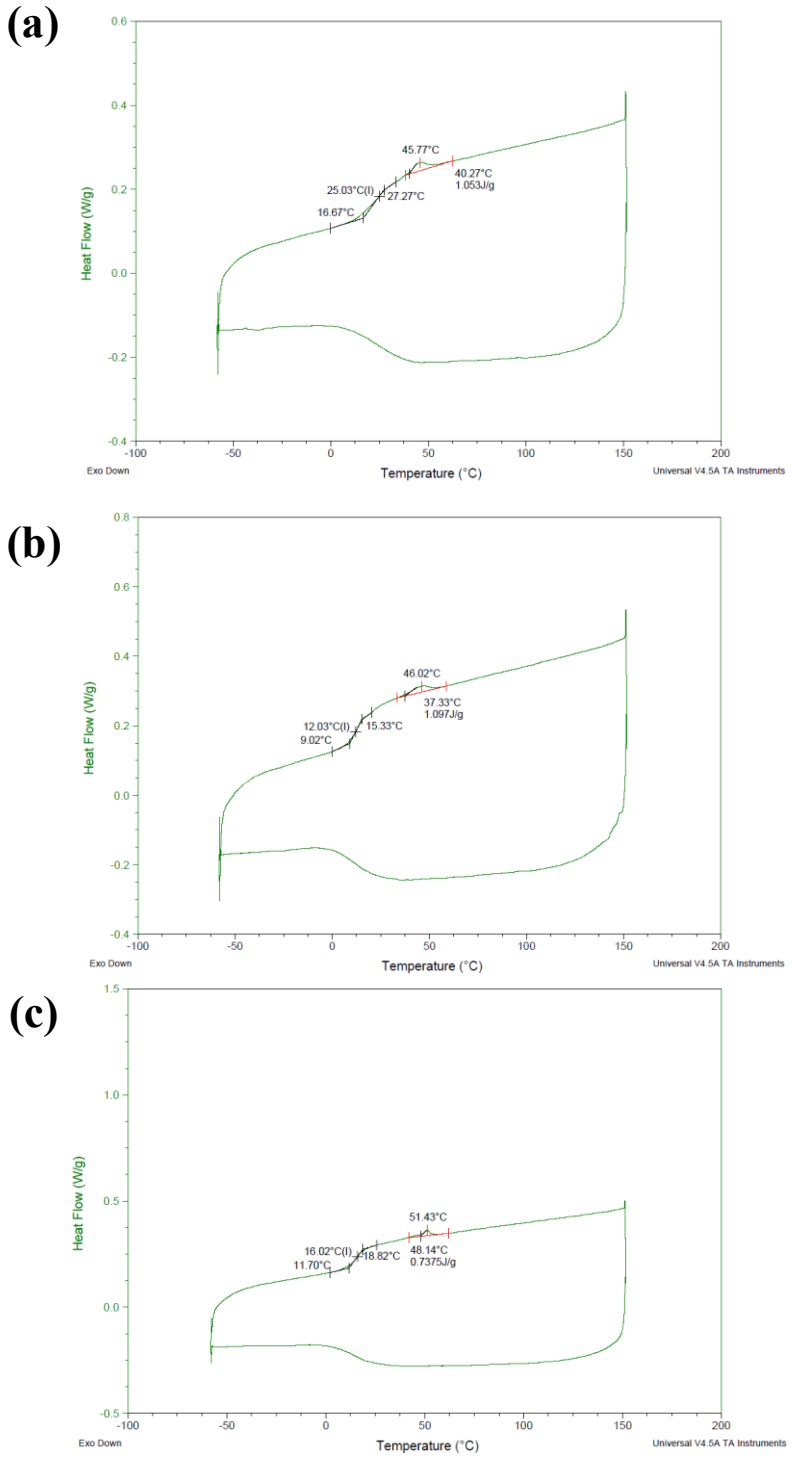

Figure 5.S12 DSC thermogram of mixed micelles formulation of ABP-NEt_2-FA with DOPE (a), ABP-NEt_2-FA with DSPE-PEG_{2k} (b), and ABP-NEt_2-FA with DSPE-PEG_{5k} (c) obtained with a heating rate of 10 °C/min.

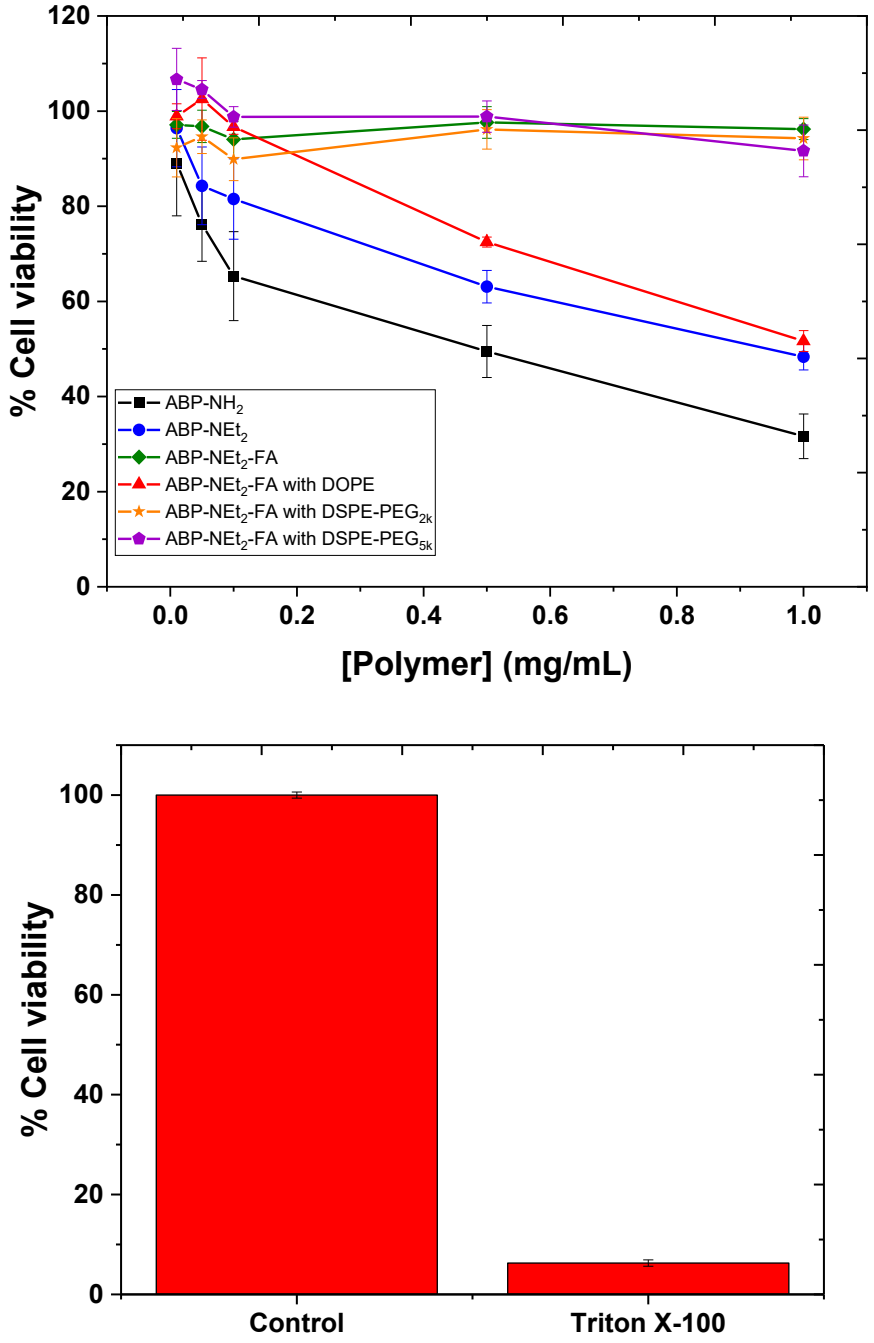

Figure 5.S13 HeLa cell viability in the presence of varying concentration of the ABP-NEt_2-FA in the presence and absence of lipids (top) and positive and negative control (bottom). Cell viability obtained using MTS assay and 48h incubation time. Cells were plated at 5,000 cells/well and sextuplet measurements were averaged for each concentration.

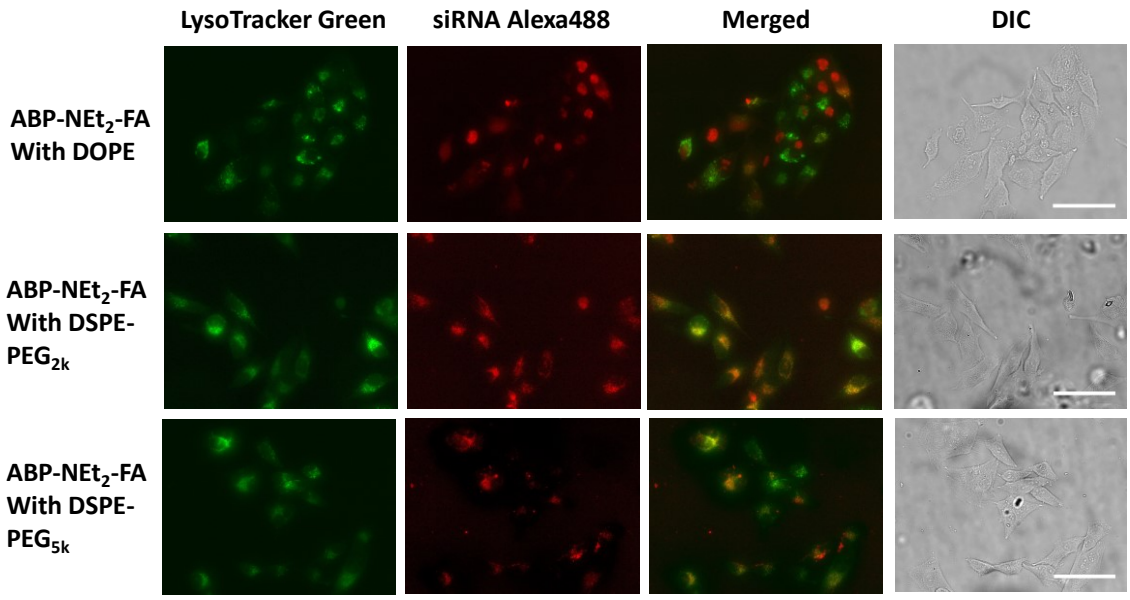

Figure 5.S14 Fluorescence microscopy images for cell uptake of ABP-NEt_2-FA with DOPE, ABP-NEt_2-FA with DSPE-PEG_{2k} and ABP-NEt_2-FA with DSPE-PEG_{5k} in HeLa cells. 100 nM of Cy5-labeled siRNA was complexed to the NP with a N/P ratio of 16 for 30 min. Cells were incubated with the nanoparticles for 4 h and 100 nM of LysoTracker® Green was added 30 min prior to imaging. The incubation medium was Opti-MEM®. The results were imaged at a 40X magnification and the scale bars represent 10 μm in length.

Chapter 6. Conclusions and perspectives

6.1 General conclusions

Conventional active pharmaceutical ingredients (API) are characterized by their intrinsic physico-chemical properties, i.e., molecular weight, chemical stability, and lipid/aqueous solubility, which influences their performance. These properties are intimately linked to the structure of these compounds and cannot be tuned without alterations to their structure. Unfortunately, the structure of these APIs also governs their biological response, and its modification would impact its efficacy. Therefore, drug delivery systems have been designed to improve the physico-chemical properties of these APIs without affecting their efficacy. Indeed, as covered in this thesis, multiple strategies employing bile acid-based polymers as starting materials have been investigated for the development of drug delivery systems. A successful delivery system possesses certain key properties, namely provides a high loading capacity,[1] composed of biocompatible materials,[2-3] possesses low toxicity,[4] and achieves high cell uptake.[5-6] The objective of this thesis is to design a drug delivery system using bile acid-based block copolymers to meet such needs. This bile acid-based drug delivery system was developed to promote a high loading of Dox and siRNA using biocompatible polymers, to promote a high cell uptake and to offer controlled release of Dox. It was hypothesized that using cholic acid as a core forming block would greatly improve the loading of hydrophobic therapeutic compounds. Also, the star-shaped structure of the cholic acid-based block copolymers would improve the loading of siRNA. In terms of biocompatibility, the use of biocompatible PAGE and PEG polymers would yield a drug delivery system with low cytotoxicity. Finally, to ensure high cell uptake, functionalizing the ends of the PEG chains with folic acid would increase the cell uptake.

In Chapter 3, the self-assembly of cholic acid-based star shaped block copolymers and its thermoresponsive properties was investigated. Then, in Chapter 4, these star-shaped block copolymers were functionalized to bear pendant carboxylic acid groups for the loading and release of Dox. Finally, in Chapter 5, the star-shaped block copolymers

were functionalized with pendant amine groups and their potential towards siRNA loading and delivery was studied in vitro. The results presented in this thesis demonstrate the feasibility of using cholic acid-based star-shaped block copolymers in the design of drug delivery systems and offer insights into key parameters controlling their loading and solution stability which can be extended to other polymer-based systems. In terms of drug delivery, it was discovered that the cholic acid-based micelles offer high drug and gene loading. However, one major hurdle that needs to be addressed is the low cell uptake. The strategies developed herein will greatly aid in the development of drug delivery systems by providing solutions to drug delivery systems with low colloidal stability in the cellular environment.

6.1.1 Cholic acid-based block copolymers for increased loading of a therapeutic compound

CA-(PAGE-*b*-PEG)$_4$ can be successfully loaded with a high amount of hydrophobic therapeutic compounds. Functionalizing the allyl groups to bear pendant carboxylic acids for electrostatic interaction with Dox afforded a loading of 14 wt%. Table 6.1 compiles the loading capacity of different polymer-based drug delivery systems. The type of interaction between the drug and polymer greatly influences the loading capacity where stronger interactions lead to higher drug loading. Hydrophobic and π-π stacking gave rise to the lowest drug loading. Interestingly, for CA-(PAGE-*b*-PEG)$_4$, hydrophobic interactions gave rise to a Dox loading as high as 10 wt% due to the formation of a bile acid core with a larger reservoir than typically observed with linear block copolymers. The Dox loading by CA-(PAGE-COOH-*b*-PEG)$_4$ is driven by electrostatic interactions and shows a similar level as observed in the literature for comparable systems. Poly(ethylene glycol)-*b*-poly(N-2-hydroxyethyl)-aspartamide showed an exceptionally high loading of 49 wt%, but this system was composed of a methacrylic acid block of 180 repeating units.[7] The longer block length provided a high number of negative groups that can interact electrostatically with Dox. In comparison, our system was composed of four branches of 19 PAGE-COOH units each. To further improve the loading efficiency, the length of the PAGE blocks in CA-(PAGE-*b*-PEG)$_4$ can be increased. However, it should be noted that the longer chain length will result in larger micelles. Section 1.2.3 explained

that larger micelles are characterized with a lower extravasation into tumor tissues which limits their therapeutic potential.

Table 6.1 Comparison of drug loading efficiency of Dox using different polymer-drug interactions.

Polymer	Dox loading (wt%)	Interaction	Cytotoxicity (mg/mL)	LD_{50} (μM)	Reference
PEG-*b*-PBCL	3.1	π-π stacking	0.2	N/A	8
PEG-*b*-PCL	0.96	Hydrophobic	0.2	N/A	8
PEG-*b*-PHEA	3.3	Hydrophobic	1	2.7	7
PEG-*b*-PPBA	49	Donor-receptor coordination	1	1.3	7
PU-*alt*-PEG	14.1	Electrostatic	0.1	2.2	9
PEG-*b*-PBLAsp-*b*-hyPEI	5.5	Hydrophobic	0.06	14	10
PEG-*b*-PMA	50	Electrostatic	N/A	0.8	11
Literature Specifications	1 – 5.5	Hydrophobic	0.06 – 1	0.8 – 14	N/A
	14 – 50	Electrostatic			

PBCL: poly (γ-benzyl-ε-caprolactone)
PCL: poly ε-caprolactone
PHEA: poly-(N-2-hydroxyethyl)-aspartamide
PPBA: poly-(N-2-hydroxyethyl)-aspartamide functionalized with phenyl boronic acid
PU-*alt*-PEG: polyurethane-*alt*-poly(ethylene glycol)
PEG-*b*-PBLAsp-*b*-hyPEI: poly(ethylene glycol)-*b*-poly(β-benzyl L-aspartate)-*b*-poly(ethyleneimine)
PMA: poly(methacrylic acid)

To obtain quantitative specifications for each of the performance attributes of the CA-(PAGE-*b*-PEG)$_4$ and CA-(PAGE-COOH-*b*-PEG)$_4$, comparisons were made with promising polymer-based Dox delivery systems found in the literature. These literature specifications are used to assess if the objectives outlined in Section 1.3 of the introduction were met. These literature specifications are obtained by setting as an interval the lowest

and highest value obtained for the specific performance attribute found in examples in the literature. Unfortunately, no polymer-based system has reached the clinic for the formulation of Dox, therefore the most promising systems were identified. With regards to cytotoxicity, CA-(PAGE-*b*-PEG)$_4$ and CA-(PAGE-COOH-*b*-PEG)$_4$ have comparable values to the other systems described in Table 6.2 except for PEG-*b*-PHEA and PEG-*b*-PPBA which were well tolerated up to 1 mg/mL. Therefore, CA-(PAGE-*b*-PEG)$_4$ and CA-(PAGE-COOH-*b*-PEG)$_4$ are relatively non-toxic, however the use of CA-(PAGE-*b*-PEG)$_4$ does not provide a better toxicity profile than what has been described in the literature. Hence, the objective of obtaining biocompatible materials using bile acid-based block copolymers was met. The great advantage in the use of cholic acid as building block in the design of DDS was to obtain higher drug loading which was indeed achieved as discussed previously. The amount of Dox loaded when using hydrophobic interactions is much higher than the literature specifications, whereas the loading *via* electrostatic interaction was within the specifications. The objective of high Dox loading was achieved. When comparing the LD_{50} of the different Dox-loaded drug delivery systems presented in Table 6.2, the results show that CA-(PAGE-*b*-PEG)$_4$ is significantly less efficacious than the other systems. This lower efficacy was attributed to the lower cell uptake observed for CA-(PAGE-*b*-PEG)$_4$ and CA-(PAGE-COOH-*b*-PEG)$_4$. To improve the efficacy, the challenges in cell uptake for the cholic acid-based micelles need to be addressed. Therefore, the objective of higher cell uptake with bile acid-based block copolymers was not reached and more research is needed to address this issue.

In terms of siRNA loading, reports showed that branched polymers have higher loading than linear polymers.[12-13] Branched polymers allow more flexibility and folding options in a 3-dimensional space to complex with siRNA which is thought to be more rigid and less amenable to folding and rearrangement.[12-13] The branched structure of CA-(PAGE-*b*-PEG)$_4$ allows a higher siRNA loading and decreases the amount of polymers needed to elicit a therapeutically relevant transfection response. In Chapter 5, the allyl groups of CA-(PAGE-*b*-PEG)$_4$ were functionalized to bear pendant amine groups to promote complexation with siRNA. Two types of amines were studied, primary and tertiary amines. The primary amine-functionalized polymers had a higher siRNA loading than the tertiary amine-functionalized polymers; N/P ratios of 4 and 16, respectively. This

observation was correlated to the lower pK_a of tertiary amine and lower surface potential. The most successful polymers at complexing siRNA include poly(ethylene imine) (PEI), poly(2-(dimethylamino) ethyl methacrylate) (PDMAEMA), poly(L-lysine) (PLL) and chitosan.[14-15] To obtain quantifiable specifications for each of the performance attributes, the most promising polyplexes used as excipients have been identified and literature specifications are compiled in Table 6.2. A N/P ratio of 10 has been reported in the literature for branched PEI whereas a N/P ratio of 5 was reported for PDMAEMA.[16-18] Although these represent examples of high siRNA loading, these formulations showed high toxicity. Only formulations that presented suitable specifications for all performance attributes were chosen for comparison.

In this thesis, it was observed that the amine-functionalized CA-(PAGE-*b*-PEG)$_4$ system successfully complexed siRNA at levels comparable to the polyplexes with highest loading. Therefore, with respect to loading of therapeutic compounds, such as Dox and siRNA, the different CA-(PAGE-*b*-PEG)$_4$ formulations afforded high loading and confirmed our initial hypothesis that the branched architecture of the bile acid-based block copolymers and the hydrophobic reservoir is favorable to obtain high loading. In terms of cytotoxicity, CA-(PAGE-NH_2-*b*-PEG)$_4$ and CA-(PAGE-Et_2-*b*-PEG)$_4$ had comparable toxicities to the other polyplexes with a toxicity of 0.05 mg/mL which is well within the literature specifications. However, the lipid-polymer mixed micelles (LPM) of CA-(PAGE-Et_2-*b*-PEG)$_4$ with DSPE-PEG_{2k} and DSPE-PEG_{5k} were significantly less toxic with cells tolerating concentrations up to 1 mg/mL. This low toxicity was only matched by cyclodextrin-based formulations. Therefore, in terms of toxicity, the objective of designing an amine-functionalized CA-(PAGE-*b*-PEG)$_4$ formulation for siRNA delivery with low cytotoxicity was met. Finally, with regards to the transfection potential of the CA-based polyplexes, the objective of high efficacy was not met. Both CA-(PAGE-NH_2-*b*-PEG)$_4$ and CA-(PAGE-Et_2-*b*-PEG)$_4$ yielded transfections less than 5% and the LPM yielded transfections between 35-43%. Both were ascribed to low cell uptake of the polyplexes. Although, the LPM are close to the literature specifications, most polyplexes in the literature provide significantly higher transfection potential. Although the siRNA loading was high and the cytotoxicity of the polyplexes was low, the transfection potential remains lower than desired, hence, the objective of designing a bile acid-based polyplex

for achieving high transfection was not met. Further study into the challenges with cell uptake is needed to address the low transfection observed.

Table 6.2 Comparison of siRNA loading efficiency of different polyplexes found in the literature.

Polymer	**Cytotoxicity (mg/mL)**	**siRNA loading (N/P)**	**Transfection (%)**	**Reference**
Poly(cyclodextrin-*co*-dimethylsuberimidate)	3.0	50	60	19-20
Chitosan	0.2	6	78*	21
Chitosan-*g*-PEI	0.01	21	> 90	22
FC-PEI_{600}	0.01	30	80	23
Poly-L-Lysine dendrimer	0.004	8	90†	24
PEG-*b*-P(CBA-ABOL/EDA)	N/A	12	50	25
PDMAEMA-*b*-PCL-*b*-PDMAEMA	0.01	12	40	26
Literature Specifications	0.004 – 3.0	6 – 50	40 – 90	N/A

PEI: Polyethyleneimine
FC: Fluorocarbon
P(CBA-ABOL/EDA): Poly(cystaminebisacrylamide-*co*-4-amino-1-butanol-*co*-ethylene diamine)
PCL: Poly(ε-caprolactone)
PDMAEMA: Poly(dimethylaminoethyl methacrylate)
* Transfection obtained only with N/P ratio > 50.
† Transfection results with respect to PEI only.

6.1.2 Solution properties of star-shaped cholic acid-based block copolymers

Cholic acid star-shaped block copolymers formed aggregates in solution with the PEG chain length greatly influencing the stability of these aggregates. Throughout this thesis, aggregates of CA-(PAGE-*b*-$PEG)_4$ were prepared with varying PAGE and PEG

chain length, in the presence or absence of different co-surfactants and with the loading of different therapeutic compounds. These different formulations gave rise to interesting observations with a range of aggregate sizes. Table 6.2 compares the size of the aggregates as a function of chain length for the different CA-(PAGE-*b*-PEG)$_4$. In Chapter 3, the shorter PEG chains were not as efficient as the longer ones at preventing micellar clusters and led to larger aggregates with a higher polydispersity for the CA-(PAGE-*b*-PEG)$_4$ with 21 repeating units of PEG. This observation agrees with the literature which shows that increasing PEG chain length tends to favor an extended conformation for PEG and aides in preventing particle aggregation.[27-28] Low molecular weight PEG provides a lesser coverage of the hydrophobic core and increases its contact with the aqueous environment thereby favoring micellar aggregation.[27-28] In Chapter 4, the PEG chain length was increased to 30 repeating units and led to micelles with a lower diameter and dispersity, a further indication of the importance of tuning the PEG chain length to obtain a stable micellar aggregate. There is an advantage for the micelles with smaller diameters and smaller nanoparticles have a greater potential for extravasation and tumor tissue penetration than larger nanoparticles.[29]

Table 6.3 Comparison of micelle size for the different CA-(PAGE-*b*-PEG)$_4$ polymers synthesized in this thesis project.

Polymer	Aggregate diameter (nm)	Polydispersity
CA-(AGE$_7$-*b*-EG$_{21}$)$_4$	84	0.3
CA-(AGE$_{19}$-*b*-EG$_{30}$)$_4$	62	0.2
CA-(AGE$_9$-*b*-EG$_{41}$)$_4$	16	0.09
CA-((AGE-COOH)$_{19}$-*b*-EG$_{30}$)$_4$	27	0.2
CA-((AGE-NH$_2$)$_6$-*b*-EG$_{17}$)$_4$	N/A	N/A
CA-((AGE-HN$_2$)$_8$-*b*-EG$_{49}$)$_4$	209	0.2

6.1.2.1 Size and shape of the micellar aggregates

PAGE-*b*-PEG block copolymer aggregates have been studied before.[30-32] Linear block copolymers of PAGE-*b*-PEG typically formed emulsion-like aggregates when the

PAGE block was < 2,000 g/mol and micellar particles when the PAGE block was >2,000 g/mol.[30] Moreover, the size of the aggregates was typically small, where the emulsion-like aggregates had diameters of ca. 60 nm and the micellar aggregates had diameters ca. 10 nm. In comparison, the star-shaped CA-(PAGE-*b*-PEG)$_4$ system produced micellar aggregates with diameters ranging from 16 to 84 nm depending on the size of the PAGE and PEG blocks. TEM micrographs of CA-(PAGE-*b*-PEG)$_4$ show micellar aggregates with spherical morphology. Larger aggregate size was observed for star-shaped block copolymers than for linear block copolymers.[33] Further characterization of the CA-(PAGE-*b*-PEG)$_4$ aggregate morphology would be interesting to examine the impact of the block lengths and presence of co-surfactant on solution morphology. As discussed in Section 1.1, morphology has been identified as an important parameter governing cell uptake.

There are reports that describes the use of bile acids as building blocks for the preparation of drug delivery systems in manners that are different from the star-shaped CA-(PAGE-*b*-PEG)$_4$ system. In one example, hyaluronic acid was conjugated with deoxycholic acid (DCA) for the encapsulation of paclitaxel.[34] The hyaluronic acid-deoxycholic acid conjugate formed large micelles with diameters ranging from 140 to 292 nm depending on the number of DCA conjugated. Similarly, TEM showed that the conjugates formed spherical micellar aggregates.[34] In another report, hydrophilic carboxylic acid-functionalized curdlan was conjugated with DCA for the encapsulation of doxorubicin.[35] The size of the aggregates ranged from 214 to 380 nm with decreasing DCA content. The aggregate size decreased with increasing DCA content due to the formation of a more compact hydrophobic core with increasing hydrophobicity.[35] Comparing with CA-(PAGE-*b*-PEG)$_4$, the size of these constructs are substantially larger and indicate the potential of using a star shaped block copolymer architecture for the optimization of micelle size in the design of bile acid-based drug delivery systems. In accordance with this hypothesis, telodendrimers of PEG and cholic acid were prepared for the encapsulation of paclitaxel.[36] In this case, the ends of the PEG chains were conjugated with multiple cholic acid residues assembled as telodendrimers with varying amount of cholic acid groups. These micelles typically had low diameters between 10 and 20 nm depending on the number of cholic acid residues.

6.1.2.2 Effect of co-surfactants

The CA-(PAGE-*b*-PEG)$_4$ polymers were also incubated in the presence of a co-surfactant. In Chapter 4, the presence of oleic acid caused a significant decrease in micellar size. When the PAGE blocks of CA-(PAGE-*b*-PEG)$_4$ were functionalized to bear a carboxylic acid group, the micelles decreased in size. These block copolymers formed micelles that were significantly smaller than their non-functionalized counterparts. Here, the presence of carboxylic acid produced a negative charge on the surface of the micelles which decreased the association of micelles into clusters due to the electrostatic repulsion. TEM images of these micelles showed they formed spherical micelles. Adding oleic acid as a cosurfactant produced micelles with a denser core than the micelles without oleic acid and the size of the micelle was significantly smaller (27 vs 62 nm).

The addition of a co-surfactant to increase the cloud point and ultimately the colloidal stability is a strategy that has been previously described. The addition of a co-surfactant to bile acid micelles is currently being employed in the pharmaceutical industry to improve the solubilization capacity and lower the CMC.[37] Bile acids combines well with lipids and their synergistic interaction leads to improved physico-chemical properties.[37] For example, amphotericin B was commercialized as a micellar dispersion in the presence of sodium deoxycholate for parenteral administration.[37] This observation drove the idea towards addition of co-surfactants to stabilize the polyplexes in Chapter 5. The choice of co-surfactant was based on the fact that 1,2-dioleoyl-sn-glycero-3-phosphoethanolamine (DOPE) is known to promote endosomal escape, whereas PEGylated 1,2-distearoyl-sn-glycero-3-phosphorylethanolamine (DSPE-PEG) has good stabilization potential and is currently used in the Doxil formulation. In Chapter 5, it was discovered that the presence of the co-surfactant stabilized the polyplexes through the increase of the cloud points. Although the solution stability for CA-((PAGE-NEt$_2$)-*b*-PEG)$_4$ was greatly improved, further formulation testing with other co-surfactants that can improve the cell uptake and endosomal escape is warranted.

6.1.2.3 Thermoresponsive properties of CA-(PAGE-*b*-PEG)$_4$ block copolymers

In Chapters 3 and 5, the thermoresponsive properties of CA-(PAGE-*b*-PEG)$_4$ were observed. The block copolymers with shorter PEG chains were characterized with cloud points at varying concentrations from which a phase diagram was constructed. However, cloud points were not observed for the block copolymers with longer PEG chains. The presence of a cloud point for bile acid-based block copolymers is a phenomenon that has been observed previously. In one report, thermoresponsive PNIPAM-*b*-Poly(2-(acryloyloxy)ethyl cholate) (PNIPAM-*b*-PCAE) with pendant cholic acid groups were synthesized.[38] The authors observed a transition temperature between 30 and 35 °C similar to what was obtained for the CA-(PAGE-*b*-PEG)$_4$ with short PEG block. The PNIPAM-*b*-PCAE formed large aggregates above the LCST and precipitated out of solution. This precipitation results from the strong hydrophobicity of the PCAE block which enhances the dehydration of the PNIPAM block and causes an unwanted aggregation and precipitation of the DDS. To solve the colloidal instability problem, the authors added poly(acrylic acid) (PAAc) as a third block and they observed that 2% PAAc was sufficient to increase the LCST and prevent the aggregation process. They hypothesized that the presence of PAAc increased the hydrophilicity of the system. Other reports proposed the use of PEG blocks as a replacement to PNIPAM to enhance the stability of the copolymer system, but we saw that there is a minimal PEG length needed to provide higher stability above the LCST presumably due to the higher hydrophobicity of the cholic acid. The presence of thermoresponsive properties for bile acid-based block copolymers of the form CA-(PAGE-*b*-PEG)$_4$ were also studied previously and has been ascribed to the dehydration of the PEG block.[39] In this report, it was also identified that a minimal PEG block is necessary to achieve colloidal stability and an increase in the LCST. Therefore, our results indicate that there is a minimal PEG length needed to provide sufficient colloidal stability for the star-shaped architecture of CA-(PAGE-*b*-PEG)$_4$.

6.1.2.4 The presence of amine groups

In order to use CA-(PAGE-*b*-PEG)$_4$ as gene delivery vectors, it was necessary to functionalize the allyl groups to bear pendant amine groups. In the case of the amine-

functionalized block copolymers, the block copolymers displayed an increase in cloud point with respect to their non-functionalized counterpart. The increase in the cloud point results from an increase in the hydrophilicity of the block copolymer. This hypothesis is in tune with the observations for the PCAE-*b*-PNIPAM-*b*-PAAc system discussed above. However, in the presence of salt this trend was reversed, and the cloud point decreased drastically. Similarly, in Chapter 5, the cloud point of the amine functionalized block copolymers was only observed in the presence of salt. The lowering of the LCST of thermoresponsive block copolymers has been previously observed for bile acid-based block copolymers. Block copolymers of PNIPAM with methacrylate monomers derived with cholic acid were prepared and their LCST was measured in varying salt concentrations.[40] The LCST decreased with increasing salt concentration as a salting-out effect. The effect of salt on the stability of drug delivery systems can have a negative impact on their colloidal stability under physiological conditions as previously reported.[41] In a study of the effect of salt concentration on the transfection of PEI, PEI was complexed with pDNA and the polyplex was incubated with varying NaCl concentration.[41] The results showed that there is a large increase in particle size when incubated with salts. At a NaCl concentrations of 150 mM, which is the typical concentration observed in cell culture media, the nanoparticle size doubled after 10 min and quadrupled after 120 min. Moreover, the transfection efficiency decreased to 23% after 120 min incubation in salt-containing culture media. Similarly, in another report, the authors prepared PEGylated poly(amido amine) poly(N,N′-cystaminebisacrylamide-*co*-4-amino-1-butanol-*co*-ethylene diamine (P(CBA-ABOL/EDA)) and studied the effect of PEG on solution stability of the polyplexes in physiological salt concentrations.[25] They found that there was a threshold of 45 wt% PEG to prevent polyplex aggregation and that the aggregation was relatively fast with large increases in micelle size only 2 h after incubation. The PEG used in this study had 3,000 g/mol whereas the length of the PEG used in Chapter 5 had 2,100 g/mol. Therefore, it is reasonable to argue that the limited solution stability for the CA-((PAGE-NEt_2)-*b*-PEG)$_4$ polyplex resulted from insufficiently long PEG blocks which fail at preventing micellar aggregation. The decrease in cloud point observed for CA-((PAGE-NEt_2)-*b*-PEG)$_4$ in the presence of salt is an issue that is common in the literature for amine-functionalized polymers and strategies to improve their colloidal stability are

necessary. In this thesis, the addition of co-surfactants to aid in stabilizing the micelles in salt containing solutions was attempted.

These results demonstrate the importance in controlling the solution properties of drug delivery systems. These excipients are often modified to bear various functional groups to aide in the loading and release of their therapeutic cargos. For example, amine groups are frequently used to complex siRNA for gene therapy. However, these functional groups can significantly alter the solution properties of these drug delivery systems and limit their efficacy. The presence of a cloud point at physiological temperature can cause unwanted solution instability and precipitation, as observed in Chapters 3 and 5 and previous reports. This precipitation of the DDS can limit its therapeutic efficiency and solutions to this limitation needs further investigation. The results presented in this thesis indicates that either the addition of a co-surfactant, an increase in PEG block length, or the choice of another hydrophilic block may provide solutions to the colloidal instability of the DDS.

6.1.3 Bile acid-based drug delivery systems: Advantages and shortcomings

One of the hypotheses described in Section 1.3 is the use of biocompatible materials in the preparation of the DDS would provide better biocompatibility. A main driving force for the use of bile acids in the development of pharmaceutical formulations is their biocompatibility.[37, 42] In Chapters 4 and 5, the toxicity of blank formulations were tested in HeLa cells and the results demonstrated that the formulations were relatively non-toxic. In Chapter 4, the micelles were non-toxic up to concentrations of 0.17 mg/mL. In Chapter 5, the amine functionalized-blank micelles were more toxic with toxicities reported at concentrations higher than 0.05 mg/mL. The increased toxicity is a result of the presence of positive charges which favors the interaction of the micelles with the negatively charged surfaces of cells. However, this toxicity decreased substantially with the addition of the co-surfactants which were well tolerated up to 1 mg/mL. With respect to polymer systems described in the literature, our polymers present similar toxicities. For amine functionalized polymers, in one report PDMAEMA-based polymers was toxic at 0.04 mg/mL,[43] whereas poly(L-lysine) is toxic at 0.02 mg/mL[44] and PEI toxicity is reported to

0.01 mg/mL.[45] Therefore, CA-((PAGE-NEt_2)-*b*-PEG)$_4$ is slightly less toxic than other polyplexes presented in the literature and the mixed micelle system is substantially less toxic further showing the advantages of our proposed mixed micelle formulation. With regards to biocompatibility, the initial hypothesis holds true, and the use of biocompatible starting materials yields formulations with better tolerability. However, as mentioned in Section 1.1.2, the therapeutic response depends on the amount of the drug delivered to the site of action and systems with higher drug loading would decrease the number of polymers administered. In this thesis, it was demonstrated that CA-(PAGE-*b*-PEG)$_4$ gave rise to higher loading and combined with the low toxicities observed, there is a great potential of our system to be biocompatible and well tolerated.

The biggest shortcoming of CA-(PAGE-*b*-PEG)$_4$ formulations was apparent in Chapters 4 and 5 and is related to cell uptake. In the case of CA-((PAGE-COOH)-*b*-PEG)$_4$, the low cell uptake correlated with an increase in the IC_{50} as compared to free Dox and for CA-((PAGE-NEt_2)-*b*-PEG)$_4$ the low cell uptake correlated with lower transfection efficiency than lipofectamine. Conjugating the CA-((PAGE-NEt_2)-*b*-PEG)$_4$ with folic acids for receptor-mediated endocytosis improved cell uptake, however, even in this case, a moderate improvement was obtained where the cell uptake increased from 5 to 24%. This low cell uptake is what hinders the therapeutic potential of CA-(PAGE-*b*-PEG)$_4$ formulations and needs to be addressed. Unfortunately, cell uptake is a complicated phenomenon with multiple parameters affecting its efficiency. As mentioned in the previous section, the length of PEG influences the colloidal stability of polyplexes in physiological salt concentrations, but this comes at the expense of cell uptake. In the article mentioned above using PEGylated poly(amido amine) (P(CBA-ABOL/EDA)), increasing the PEG content increased colloidal stability but also decreased cell uptake to barely detectable levels.[25] This decrease in uptake was attributed to reduced interactions with cell membranes. Interestingly, certain reports describe the effect of PEG density on ligand-mediated cell uptake. In one report, nano-emulsions of soybean oil and DSPE-PEG were conjugated with $\alpha_v\beta_3$-integrin specific arginine-glycine-aspartic acid peptide (RGD) ligand at the end of the PEG chains and they discovered that higher PEG densities decreased the interaction between RGD peptide and ligand with a decrease in cell uptake.[46] Furthermore, another report studied the uptake of RGD-functionalized

PEGylated liposomes.[47] In this report, the RGD-functionalized liposomes had similar levels of cell uptake as the non-functionalized liposomes. Once again, the lower cell uptake was ascribed to diminished liposome-cell interaction due to the PEGylated surfaces. However, care must be exercised when drawing conclusions from these reports since there are numerous examples in the literature using PEG-based polymers and PEGylated liposomes with various ligands that successfully increased cell uptake. Moreover, there are other potential causes for the low cell uptake, most notably particle size and surface charge. In terms of size, the literature is unequivocal, the larger nanoparticles do not favor cell uptake.[48] In one report, a theoretical model was developed to predict the optimal size of spherical nanoparticles for ligand-mediated cell uptake.[48-50] It was discovered that for larger nanoparticles the wrapping process of the cell membrane around the nanoparticle depends on receptor diffusion over long distances and requires long wrapping time which is not optimal for cell uptake. These authors concluded that cell uptake was optimal for nanoparticles of 27-30 nm, a value that was validated empirically.[49-52] In the case of the CA-((PAGE-NEt_2)-*b*-PEG)$_4$ polyplexes, nanoparticles with large diameters of 188 to 221 nm were obtained and this may explain the low cell uptake achieved even with the presence of folic acid. Finally, the ligand density on the surface of nanoparticles has been reported to be an important factor affecting cell uptake.[53] In one report, polystyrene (PS) nanoparticles were prepared, and folic acid-functionalized albumin was adsorbed to the PS nanoparticles to varying degree.[54] The extent of cell uptake varied drastically from 10 to 60% cell uptake with increasing ligand density. A similar observation was also reported elsewhere further corroborating the importance of controlling ligand density.[55] In the case of CA-((PAGE-NEt_2)-*b*-PEG-FA)$_4$, the folic acid (FA) ligand density was not measured, and the low cell uptake may be a result of an insufficient ligand density. Further optimization of the ligand density on the surface of CA-((PAGE-NEt_2)-*b*-PEG-FA)$_4$ may result in improved cell uptake.

6.2 Perspective and outlook

An advantage demonstrated throughout this thesis for the proposed cholic acid-based star-shaped block copolymers is their versatility. Via a simple thiol-ene click reaction, the polymers can be functionalized and tailored for drug delivery of a range of

compounds. Indeed, functionalizing the PAGE blocks with pendant carboxylic acids provided electrostatic interactions which enabled high loading of Dox. Similarly, functionalizing the PAGE blocks with pendant amine groups enabled siRNA loading for gene delivery. With the same block copolymer, different therapeutic agents with varying physico-chemical properties were encapsulated with high efficiency and drug loading content. Moreover, it was observed in both Chapters 4 and 5, that the block copolymers have low toxicity and fulfill the criteria of biocompatibility.

There are advantages in using the star-shaped CA-(PEG-*b*-PEG)$_4$ as drug delivery systems in the treatment of breast cancer. CA-(PAGE-*b*-PEG)$_4$ possesses good biocompatibility, tunable drug release and high drug and gene loading. The high loading should be further explored through the combination of both drug and gene in the same drug delivery system to provide a synergistic response and increase the therapeutic efficiency of the formulation. However, as observed in this thesis, there are also disadvantages for the bile acid-based star-shaped block copolymers, i.e. low colloidal stability, large micellar diameters, and poor cell uptake, which can limit the therapeutic potential of the formulation. These limitations need to be addressed to access their clinical translatability, and in the following sections, solutions and alternatives are proposed for each of these identified challenges.

6.2.1 Protein adsorption

The topic of protein adsorption and its impact on the pharmacokinetics of drug delivery systems has been thoroughly reviewed in Chapter 1. In light of this discussion, a necessary step before the successful clinical translatability of cholic acid-based drug delivery systems is to examine the extent and the fingerprint of proteins adsorbed to its surface. The success of these drug delivery systems, especially pertaining to the delivery of chemotherapeutic agents, relies on the passive diffusion of the nanoparticles into tumor tissues via the EPR effect.[56] The extent of tumor accumulation depends on the amount of time the nanoparticles remain in circulation inside the blood stream. Numerous reports demonstrate that protein adsorption can severely limit the blood circulation of nanoparticles.[57-58] Therefore, a thorough understanding of the factors affecting protein

adsorption and methods to control it are necessary to secure a successful drug delivery system.

The group of Chan et al. have used a bioinformatics-inspired approach to quantitatively characterize the protein corona fingerprint of gold nanoparticles.[59] Using a similar approach, the protein adsorption on the surface of the cholic acid-based star-shaped block copolymers should be examined. In this case, the DDS loaded with either Dox or siRNA or both can be incubated with serum proteins and the DDS characterized for its physico-chemical properties using DLS, zeta potential and TEM measurements and for its protein fingerprint using polyacrylamide gel electrophoresis and LC/MS/MS. Depending on the type and extent of protein adsorption, different solutions can be developed. The length of the hydrophilic block, the length of PAGE block and number of amines can be varied to optimize the protein corona that favors colloidal stability and cell uptake. Moreover, the nanoparticles can be pre-incubated with certain proteins that favors higher cell uptake and stability to promote their presence on the surface of the nanoparticle.

The study of protein corona and optimization is highly important with regards to the translatability of *in vitro* to *in vivo* results. Unfortunately, one common trend in the experimental design of polymer-based DDS is the incubation of the DDS with cells in the absence of serum. This experimental setup is customary and does not represent the environment a NP will encounter following parenteral administration. Therefore, studying the cell interaction and uptake of NP in an environment closely mimicking that found *in vivo* will provide a better prediction of the success of the DDS in pre-clinical models.

6.2.2 Improved cell uptake

A common limitation of the cholic acid-based star-shaped block copolymers that was observed in both Chapters 4 and 5 is the poor cell uptake. In Chapter 5, the ends of the PEG chains of the block copolymers were conjugated with folic acid to promote targeting and cell uptake since folic acid receptors are overexpressed in numerous cancerous cell lines.[60] Folic acid is often used in nanoparticle design to promote cell targeting for tumor therapy.[61-64] Unfortunately, even when conjugated with folic acid, the block copolymers suffered from poor cell uptake. Therefore, an important aspect of the

proposed DDS that needs to be addressed is the factors limiting cell uptake. In light of recent reports into the EPR effect, one ligand that seems to promote high cell uptake while improving transcytosis significantly is the cyclic 9-amino acid RGD peptide (iRGD).[65] Therefore, rather than pursuing with FA, the iRGD ligand may present higher advantages for DDS to tumor tissues since it is involved in transcytosis and can increase extravasation from the blood circulation and uptake in tumor tissues.[65] Moreover, iRGD binds to $\alpha_v\beta_3$ and $\alpha_v\beta_5$ integrins which are overexpressed at the cancer site thereby favoring the accumulation of these nanoparticles in tumor tissues over healthy tissues conferring a targeting approach to the nanoparticles.[66] Similarly to FA ligands, RGD ligands possess tumor targeting potential for the treatment of cancer.[66] At the tumor site and through proteolytic cleavage, the iRGD releases its C-terminal motif which triggers NRP-1-mediated transcytosis.[66] As mentioned previously, the density of folic acid ligands on the surface of the nanoparticle plays an important role on the cell uptake. Therefore, the first step that should be taken would be to vary the density of ligand (whether iRGD or FA) on the surface of the CA-((PAGE-NEt_2)-*b*-PEG)$_4$ particles and quantify its impact on cell uptake. Addressing these limitations will ensure that a higher number of nanoparticles are internalized inside the cell and a greater therapeutic response is observed. It has been previously observed that positively-charged nanoparticles are characterized with high cell uptake.[67] Finding a balance between sufficient surface zeta potential to promote cell uptake without causing toxicity can be a potential strategy to increase cell uptake. Therefore, varying the length of the PAGE block and ultimately the number of amine groups should be also optimized to find the right balance between cell uptake and adequate biocompatibility. Furthermore, the presence of PEG as hydrophilic corona should also be challenged. In light of the previous discussion, PEG may decrease cell uptake and does not completely prevent micellar aggregation, therefore PEG may be replaced by other hydrophilic polymer blocks such as PVP which is biocompatible and, contrary to PEG, does not cause accelerated blood clearance.[68] In this case, the length of PVP should first be optimized to determine the optimal PVP length that enables colloidal stability while permitting cell interaction. To realize these experiments, a library of polymers with varying PAGE and PVP lengths should first be prepared and their cell

uptake evaluated. Once, the optimal polymer length is determined, the effect of ligand density on cell uptake should be evaluated.

Moreover, as mentioned in Section 1.2.5, the shape of the nanoparticle is an important factor controlling the extent of cell uptake. TEM may be used to study the shape of the nanoparticles while varying the length of both hydrophobic and hydrophilic blocks to further evaluate the impact of the nanoparticle shape on cell uptake.

6.2.3 Improved solution stability

In Chapter 3, the thermoresponsive properties of the cholic acid-based block copolymers have been examined. The results presented herein indicate that the presence of pendant amine on the PAGE block can significantly decrease the cloud point of the block copolymer in the presence of salt and lead to precipitation of the DDS. Unfortunately, these amine groups are necessary for the complexation of siRNA for gene therapy and the salt concentrations typically found in vivo are sufficient to cause colloidal instability of amine-functionalized polymers. The colloidal instability of CA-(PAGE-*b*-PEG)$_4$ and CA-(CPAGE-NEt$_2$)-*b*-PEG)$_4$ was demonstrated to result from insufficiently long PEG chains. However, per the discussion on cell uptake, increasing the PEG chain length may exacerbate the poor cell uptake. In addition, there is an increasing body of evidence that suggests PEGylated formulations stimulate an immune response which increases their uptake by macrophage cells thereby decreasing their overall efficiency and increasing their toxicity.[69-70] Taken together, these observations suggest that PEG may not be the optimal hydrophilic block for our application and should be replaced with other hydrophilic candidate polymers. As discussed in Section 1.1.1, other alternatives include PVP, dextran, PVA, poly(glutamic acid) and polyacrylamides, with PVP being a strong candidate due to its biocompatibility, high LCST, FDA-approval, and good colloidal stability of PVP-based micelles. Therefore, the use of PVP as a replacement of PEG is envisaged. Moreover, it is necessary to further investigate the influence of the block copolymer chain length and number of amines on the PAGE blocks to determine the optimal conditions to maintain colloidal stability. Shortening of the PAGE block may also provide further colloidal stability which unfortunately will come at the expense of siRNA loading. Therefore, the aforementioned library of polymers with of varying PAGE and

PVP length should be tested for their siRNA loading and solution stability in both low and high salt concentration.

6.2.4 Dual drug and gene loading

From Chapter 5 it is apparent that controlling the type of amine used for the complexation of siRNA is important for high transfection potential. To afford a successful release of the nanoparticle from within the endosome and ensure gene silencing, the polyplex requires protonable amine groups with buffering capacity.[71] PEI is successful at transfection and possesses strong siRNA condensing capacity due to the presence of both primary and secondary amines for linear PEI and primary, secondary and tertiary amines for branched PEI.[71-72] The secondary and tertiary amines have protonable amines and enable endosomal escape.[71] More importantly, recent reports identified a pK_a of 5.8 to 6.2 as the optimal pK_a for amines to ensure highest siRNA transfection.[73-74] Based on these observations, suitable amine substituents with pK_a's between 5.8 to 6.2 should be selected and investigated. Figure 6.1 lists amine candidates that can be attached to the block copolymer to favor high transfection.[73] A library of block copolymers with the different amine substituents presented in Figure 6.1 would first be synthesized. Of notable importance, pK_a values are affected by non-covalent interactions, such as π-π stacking and hydrophobic interactions, and by the length of hydrophobic blocks.[73, 75-76]

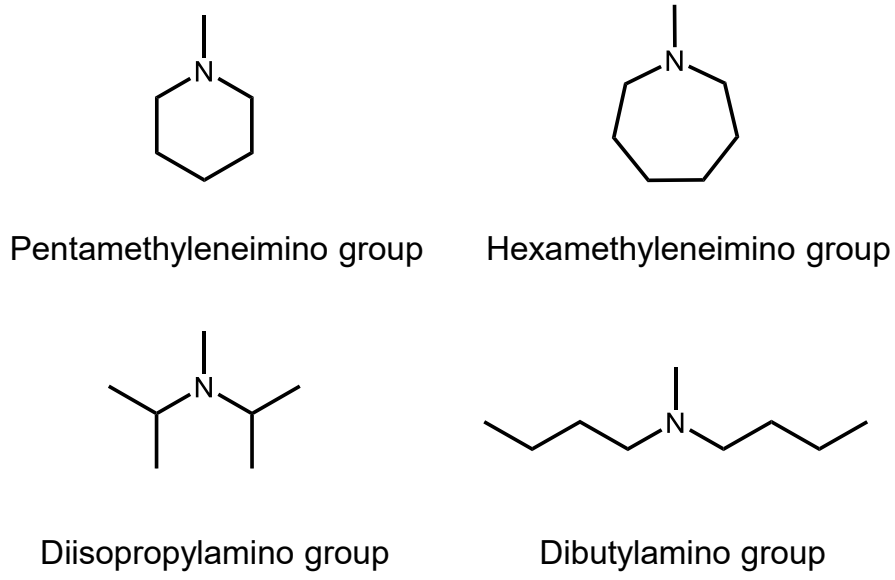

Figure 6.1. Potential amine substituents for functionalization of CA-(PAGE-*b*-PEG)$_4$.

The encapsulation of multiple therapeutic agents in combinatorial therapies either as dual drug or drug and gene product provides an opportunity to decrease the individual toxicities of each drug and ensures a strong therapeutic response.[77-78] This strategy has been recently outlined as a potential tool for overcoming multidrug resistance and achieve a synergistic response.[78-79] One major hurdle in the use of chemotherapeutic agent is the development of multi-drug resistance and combinatorial therapy was proven to be a successful solution to this issue.[79-80] In light of these observations, one potential optimization for the cholic acid-based block copolymers is the dual loading of drug and gene product to afford combinatorial therapy. Pursuing in the field of drug delivery system for the treatment of breast cancer, the ideal combination is doxorubicin and anti-estrogen receptor (ER) siRNA. Doxorubicin is the standard of care in terms of chemotherapeutic drug currently used in the clinic,[81] whereas the most common type of diagnosed breast cancers is ER-positive.[82] Therefore, combining Dox and anti-ER siRNA within the same drug delivery system is a promising strategy that is worth exploring.

6.3 References

1. Shen, S.; Wu, Y.; Liu, Y.; Wu, D., High drug-loading nanomedicines: progress, current status, and prospects. *Int. J. Nanomedicine* **2017,** *12*, 4085-4109.
2. Kolate, A.; Baradia, D.; Patil, S.; Vhora, I.; Kore, G.; Misra, A., PEG — A versatile conjugating ligand for drugs and drug delivery systems. *J. Control. Release* **2014,** *192*, 67-81.
3. Casalini, T.; Rossi, F.; Castrovinci, A.; Perale, G., A perspective on polylactic acid-based polymers use for nanoparticles synthesis and applications. *Front. Bioeng. Biotechnol.* **2019,** *7* (259), 1-16.
4. De Jong, W. H.; Borm, P. J. A., Drug delivery and nanoparticles: applications and hazards. *Int. J. Nanomedicine* **2008,** *3* (2), 133-149.
5. Patra, J. K.; Das, G.; Fraceto, L. F.; Campos, E. V. R.; Rodriguez-Torres, M. d. P.; Acosta-Torres, L. S.; Diaz-Torres, L. A.; Grillo, R.; Swamy, M. K.; Sharma, S.; Habtemariam, S.; Shin, H.-S., Nano based drug delivery systems: recent developments and future prospects. *J. Nanobiotechnol.* **2018,** *16* (1), 71-104.
6. Zhang, R.; Qin, X.; Kong, F.; Chen, P.; Pan, G., Improving cellular uptake of therapeutic entities through interaction with components of cell membrane. *Drug Deliv.* **2019,** *26* (1), 328-342.
7. Lv, S.; Wu, Y.; Cai, K.; He, H.; Li, Y.; Lan, M.; Chen, X.; Cheng, J.; Yin, L., High drug loading and sub-quantitative loading efficiency of polymeric micelles driven by donor–receptor coordination interactions. *J. Am. Chem. Soc.* **2018,** *140* (4), 1235-1238.

8. Washington, K. E.; Kularatne, R. N.; Biewer, M. C.; Stefan, M. C., Combination loading of doxorubicin and resveratrol in polymeric micelles for increased loading efficiency and efficacy. *ACS Biomater. Sci. Eng.* **2018,** *4* (3), 997-1004.
9. Huang, D.; Zhou, Y.; Xiang, Y.; Shu, M.; Chen, H.; Yang, B.; Liao, X., Polyurethane/doxorubicin nanoparticles based on electrostatic interactions as pH-sensitive drug delivery carriers. *Polym. Int.* **2018,** *67* (9), 1186-1193.
10. Feng, H.; Chu, D.; Li, Z.; Guo, Z.; Jin, L.; Fan, B.; Zhang, J.; Li, J., A Dox-loaded polymer micelle for effectively inhibiting cancer cells. *RSC Advances* **2018,** *8* (46), 25949.
11. Kim, J. O.; Kabanov, A. V.; Bronich, T. K., Polymer micelles with cross-linked polyanion core for delivery of a cationic drug doxorubicin. *J. Control. Release* **2009,** *138* (3), 197-204.
12. Boeckle, S.; von Gersdorff, K.; van der Piepen, S.; Culmsee, C.; Wagner, E.; Ogris, M., Purification of polyethylenimine polyplexes highlights the role of free polycations in gene transfer. *J. Gene Med.* **2004,** *6* (10), 1102-1111.
13. Scholz, C.; Wagner, E., Therapeutic plasmid DNA versus siRNA delivery: common and different tasks for synthetic carriers. *J. Control. Release* **2012,** *161* (2), 554-565.
14. Agarwal, S.; Zhang, Y.; Maji, S.; Greiner, A., PDMAEMA based gene delivery materials. *Mater. Today* **2012,** *15* (9), 388-393.
15. Lächelt, U.; Wagner, E., Nucleic acid therapeutics using polyplexes: A journey of 50 years (and beyond). *Chem. Rev.* **2015,** *115* (19), 11043-11078.
16. Cheng, Q.; Du, L.; Meng, L.; Han, S.; Wei, T.; Wang, X.; Wu, Y.; Song, X.; Zhou, J.; Zheng, S.; Huang, Y.; Liang, X.-j.; Cao, H.; Dong, A.; Liang, Z., The promising nanocarrier for doxorubicin and siRNA co-delivery by PDMAEMA-based amphiphilic nanomicelles. *ACS Appl. Mater. Interfaces* **2016,** *8* (7), 4347-4356.
17. Kim, J.; Kim, S. W.; Kim, W. J., PEI-g-PEG-RGD/small interference RNA polyplex-mediated silencing of vascular endothelial growth factor receptor and its potential as an anti-angiogenic tumor therapeutic strategy. *Oligonucleotides* **2011,** *21* (2), 101-107.
18. Nicolì, E.; Syga, M. I.; Bosetti, M.; Shastri, V. P., Enhanced gene silencing through human serum albumin-mediated delivery of polyethylenimine-siRNA polyplexes. *PLOS ONE* **2015,** *10* (4), e0122581.
19. Hu-Lieskovan, S.; Heidel, J. D.; Bartlett, D. W.; Davis, M. E.; Triche, T. J., Sequence-specific knockdown of EWS-FLI1 by targeted, nonviral delivery of small interfering RNA inhibits tumor growth in a murine model of metastatic Ewing's sarcoma. *Cancer Res.* **2005,** *65* (19), 8984-8992.
20. Hwang, S. J.; Bellocq, N. C.; Davis, M. E., Effects of structure of beta-cyclodextrin-containing polymers on gene delivery. *Bioconjug. Chem.* **2001,** *12* (2), 280-290.
21. Howard, K. A.; Rahbek, U. L.; Liu, X.; Damgaard, C. K.; Glud, S. Z.; Andersen, M. Ø.; Hovgaard, M. B.; Schmitz, A.; Nyengaard, J. R.; Besenbacher, F.; Kjems, J., RNA interference in vitro and in vivo using a novel chitosan/siRNA nanoparticle system. *Mol. Ther.* **2006,** *14* (4), 476-484.

22. Jiang, H.-L.; Kim, Y.-K.; Arote, R.; Nah, J.-W.; Cho, M.-H.; Choi, Y.-J.; Akaike, T.; Cho, C.-S., Chitosan-graft-polyethylenimine as a gene carrier. *J. Control. Release* **2007,** *117* (2), 273-280.
23. Johnson, M. E.; Shon, J.; Guan, B. M.; Patterson, J. P.; Oldenhuis, N. J.; Eldredge, A. C.; Gianneschi, N. C.; Guan, Z., Fluorocarbon modified low-molecular-weight polyethylenimine for siRNA delivery. *Bioconjug. Chem.* **2016,** *27* (8), 1784-1788.
24. Inoue, Y.; Kurihara, R.; Tsuchida, A.; Hasegawa, M.; Nagashima, T.; Mori, T.; Niidome, T.; Katayama, Y.; Okitsu, O., Efficient delivery of siRNA using dendritic poly(L-lysine) for loss-of-function analysis. *J. Control. Release* **2008,** *126* (1), 59-66.
25. Vader, P.; van der Aa, L. J.; Engbersen, J. F. J.; Storm, G.; Schiffelers, R. M., Physicochemical and biological evaluation of siRNA polyplexes based on PEGylated poly(amido amine)s. *Pharm. Res.* **2012,** *29* (2), 352-361.
26. Zhu, C.; Jung, S.; Luo, S.; Meng, F.; Zhu, X.; Park, T. G.; Zhong, Z., Co-delivery of siRNA and paclitaxel into cancer cells by biodegradable cationic micelles based on PDMAEMA–PCL–PDMAEMA triblock copolymers. *Biomaterials* **2010,** *31* (8), 2408-2416.
27. Owen, S. C.; Chan, D. P. Y.; Shoichet, M. S., Polymeric micelle stability. *Nano Today* **2012,** *7* (1), 53-65.
28. Owens, D. E.; Peppas, N. A., Opsonization, biodistribution, and pharmacokinetics of polymeric nanoparticles. *Int. J. Pharm.* **2006,** *307* (1), 93-102.
29. Vu, M. N.; Rajasekhar, P.; Poole, D. P.; Khor, S. Y.; Truong, N. P.; Nowell, C. J.; Quinn, J. F.; Whittaker, M.; Veldhuis, N. A.; Davis, T. P., Rapid assessment of nanoparticle extravasation in a microfluidic tumor model. *ACS Appl. Nano Mater.* **2019,** *2* (4), 1844-1856.
30. Hrubý, M.; Koňák, Č.; Ulbrich, K., Poly(allyl glycidyl ether)-block-poly(ethylene oxide): A novel promising polymeric intermediate for the preparation of micellar drug delivery systems. *J. Appl. Polym. Sci.* **2005,** *95* (2), 201-211.
31. Wagner, M.; Barthel, M. J.; Freund, R. R. A.; Hoeppener, S.; Traeger, A.; Schacher, F. H.; Schubert, U. S., Solution self-assembly of poly(ethylene oxide)-block-poly(furfuryl glycidyl ether)-block-poly(allyl glycidyl ether) based triblock terpolymers: a field-flow fractionation study. *Polym. Chem.* **2014,** *5* (24), 6943-6956.
32. Wang, R.; Hu, X.; Yue, J.; Zhang, W.; Cai, L.; Xie, Z.; Huang, Y.; Jing, X., Luteinizing-hormone-releasing-hormone-containing biodegradable polymer micelles for enhanced intracellular drug delivery. *J. Mater. Chem. B* **2013,** *1* (3), 293-301.
33. Yun, J.; Faust, R.; Szilágyi, L. S.; Kéki, S.; Zsuga, M., Effect of architecture on the micellar properties of amphiphilic block copolymers: Comparison of AB linear diblock, AAB, and A2B heteroarm star block copolymers. *Macromolecules* **2003,** *36* (5), 1717-1723.
34. Li, J.; Huo, M.; Wang, J.; Zhou, J.; Mohammad, J. M.; Zhang, Y.; Zhu, Q.; Waddad, A. Y.; Zhang, Q., Redox-sensitive micelles self-assembled from amphiphilic hyaluronic acid-deoxycholic acid conjugates for targeted intracellular delivery of paclitaxel. *Biomaterials* **2012,** *33* (7), 2310-2320.

35. Yan, J.-K.; Ma, H.-L.; Chen, X.; Pei, J.-J.; Wang, Z.-B.; Wu, J.-Y., Self-aggregated nanoparticles of carboxylic curdlan-deoxycholic acid conjugates as a carrier of doxorubicin. *International J. Bio. Macromol.* **2015,** *72*, 333-340.
36. Luo, J.; Xiao, K.; Li, Y.; Lee, J. S.; Shi, L.; Tan, Y.-H.; Xing, L.; Holland Cheng, R.; Liu, G.-Y.; Lam, K. S., Well-defined, size-tunable, multifunctional micelles for efficient paclitaxel delivery for cancer treatment. *Bioconjug. Chem.* **2010,** *21* (7), 1216-1224.
37. Faustino, C.; Serafim, C.; Rijo, P.; Reis, C. P., Bile acids and bile acid derivatives: use in drug delivery systems and as therapeutic agents. *Exp. Opin. Drug Deliv.* **2016,** *13* (8), 1133-1148.
38. Castro-Hernández, A.; Cortez-Lemus, N. A., Thermo/pH responsive star and linear copolymers containing a cholic acid-derived monomer, N-isopropylacrylamide and acrylic acid: synthesis and solution properties. *Polymers* **2019,** *11* (11), 1859-1892.
39. Li, C.; Lavigueur, C.; Zhu, X. X., Aggregation and thermoresponsive properties of new star block copolymers with a cholic acid core. *Langmuir* **2011,** *27* (17), 11174-11179.
40. Benrebouh, A.; Avoce, D.; Zhu, X. X., Thermo- and pH-sensitive polymers containing cholic acid derivatives. *Polymer* **2001,** *42* (9), 4031-4038.
41. Sang, Y.; Xie, K.; Mu, Y.; Lei, Y.; Zhang, B.; Xiong, S.; Chen, Y.; Qi, N., Salt ions and related parameters affect PEI-DNA particle size and transfection efficiency in Chinese hamster ovary cells. *Cytotechnology* **2015,** *67* (1), 67-74.
42. Pavlović, N.; Goločorbin-Kon, S.; Đanić, M.; Stanimirov, B.; Al-Salami, H.; Stankov, K.; Mikov, M., Bile acids and their derivatives as potential modifiers of drug release and pharmacokinetic profiles. *Front. Pharmacol.* **2018,** *9* (1283), 1-23.
43. Teo, J.; McCarroll, J. A.; Boyer, C.; Youkhana, J.; Sagnella, S. M.; Duong, H. T. T.; Liu, J.; Sharbeen, G.; Goldstein, D.; Davis, T. P.; Kavallaris, M.; Phillips, P. A., A rationally optimized nanoparticle system for the delivery of RNA interference therapeutics into pancreatic tumors in vivo. *Biomacromolecules* **2016,** *17* (7), 2337-2351.
44. Zheng, C.; Zheng, M.; Gong, P.; Deng, J.; Yi, H.; Zhang, P.; Zhang, Y.; Liu, P.; Ma, Y.; Cai, L., Polypeptide cationic micelles mediated co-delivery of docetaxel and siRNA for synergistic tumor therapy. *Biomaterials* **2013,** *34* (13), 3431-3438.
45. Zakeri, A.; Kouhbanani, M. A. J.; Beheshtkhoo, N.; Beigi, V.; Mousavi, S. M.; Hashemi, S. A. R.; Karimi Zade, A.; Amani, A. M.; Savardashtaki, A.; Mirzaei, E.; Jahandideh, S.; Movahedpour, A., Polyethylenimine-based nanocarriers in co-delivery of drug and gene: a developing horizon. *Nano Rev. Exp.* **2018,** *9* (1), 1-14.
46. Hak, S.; Helgesen, E.; Hektoen, H. H.; Huuse, E. M.; Jarzyna, P. A.; Mulder, W. J. M.; Haraldseth, O.; Davies, C. d. L., The effect of nanoparticle polyethylene glycol surface density on ligand-directed tumor targeting studied in vivo by dual modality imaging. *ACS nano* **2012,** *6* (6), 5648-5658.
47. Estelrich, J.; Busquets, M. A.; Del Carmen Morán, M., Effect of PEGylation on ligand-targeted magnetoliposomes: A missed goal. *ACS Omega* **2017,** *2* (10), 6544-6555.

48. Gao, H.; Shi, W.; Freund, L. B., Mechanics of receptor-mediated endocytosis. *Proc. Natl. Acad. Sci.* **2005,** *102* (27), 9469-9474.
49. Nakai, T.; Kanamori, T.; Sando, S.; Aoyama, Y., Remarkably size-regulated cell invasion by artificial viruses. saccharide-dependent self-aggregation of glycoviruses and its consequences in glycoviral gene delivery. *J. Am. Chem. Soc.* **2003,** *125* (28), 8465-8475.
50. Li, Y.; Kröger, M.; Liu, W. K., Endocytosis of PEGylated nanoparticles accompanied by structural and free energy changes of the grafted polyethylene glycol. *Biomaterials* **2014,** *35* (30), 8467-8478.
51. Aoyama, Y.; Kanamori, T.; Nakai, T.; Sasaki, T.; Horiuchi, S.; Sando, S.; Niidome, T., Artificial viruses and their application to gene delivery. Size-controlled gene coating with glycocluster nanoparticles. *J. Am. Chem. Soc.* **2003,** *125* (12), 3455-3457.
52. Osaki, F.; Kanamori, T.; Sando, S.; Sera, T.; Aoyama, Y., A quantum dot conjugated sugar ball and its cellular uptake. On the size effects of endocytosis in the subviral region. *J. Am. Chem. Soc.* **2004,** *126* (21), 6520-6521.
53. Alkilany, A. M.; Zhu, L.; Weller, H.; Mews, A.; Parak, W. J.; Barz, M.; Feliu, N., Ligand density on nanoparticles: A parameter with critical impact on nanomedicine. *Adv. Drug Deliv. Rev.* **2019,** *143* (15), 22-36.
54. Moradi, E.; Vllasaliu, D.; Garnett, M.; Falcone, F.; Stolnik, S., Ligand density and clustering effects on endocytosis of folate modified nanoparticles. *RSC Advances* **2012,** *2* (7), 3025-3033.
55. Li, L.; Zhang, Y.; Wang, J., Effects of ligand distribution on receptor-diffusion-mediated cellular uptake of nanoparticles. *R. Soc. Open Sci.* **2017,** *4* (5), 170063-170063.
56. Fang, J.; Nakamura, H.; Maeda, H., The EPR effect: Unique features of tumor blood vessels for drug delivery, factors involved, and limitations and augmentation of the effect. *Adv. Drug Deliv. Rev.* **2011,** *63* (3), 136-151.
57. Gunawan, C.; Lim, M.; Marquis, C. P.; Amal, R., Nanoparticle–protein corona complexes govern the biological fates and functions of nanoparticles. *J. Mater. Chem. B* **2014,** *2* (15), 2060-2083.
58. Nguyen, V. H.; Lee, B. J., Protein corona: a new approach for nanomedicine design. *Int. J. Nanomedicine* **2017,** *12* (18), 3137-3151.
59. Walkey, C. D.; Olsen, J. B.; Song, F.; Liu, R.; Guo, H.; Olsen, D. W. H.; Cohen, Y.; Emili, A.; Chan, W. C. W., Protein corona fingerprinting predicts the cellular interaction of gold and silver nanoparticles. *ACS Nano* **2014,** *8* (3), 2439-2455.
60. Cheung, A.; Bax, H. J.; Josephs, D. H.; Ilieva, K. M.; Pellizzari, G.; Opzoomer, J.; Bloomfield, J.; Fittall, M.; Grigoriadis, A.; Figini, M.; Canevari, S.; Spicer, J. F.; Tutt, A. N.; Karagiannis, S. N., Targeting folate receptor alpha for cancer treatment. *Oncotarget* **2016,** *7* (32), 52553-52574.
61. Khan, M. M.; Madni, A.; Filipczak, N.; Pan, J.; Rehman, M.; Rai, N.; Attia, S. A.; Torchilin, V. P., Folate targeted lipid chitosan hybrid nanoparticles for enhanced anti-tumor efficacy. *Nanomedicine* **2020,** *28*, 102228.
62. Angelopoulou, A.; Kolokithas-Ntoukas, A.; Fytas, C.; Avgoustakis, K., Folic acid-functionalized, condensed magnetic nanoparticles for targeted delivery of

doxorubicin to tumor cancer cells overexpressing the folate receptor. *ACS Omega* **2019,** *4* (26), 22214-22227.
63. Kularatne, S. A.; Low, P. S., Targeting of nanoparticles: folate receptor. *Methods Mol. Biol.* **2010,** *624*, 249-265.
64. Stella, B.; Arpicco, S.; Peracchia, M. T.; Desmaële, D.; Hoebeke, J.; Renoir, M.; D'Angelo, J.; Cattel, L.; Couvreur, P., Design of folic acid-conjugated nanoparticles for drug targeting. *J. Pharm. Sci.* **2000,** *89* (11), 1452-1464.
65. Liu, X.; Lin, P.; Perrett, I.; Lin, J.; Liao, Y. P.; Chang, C. H.; Jiang, J.; Wu, N.; Donahue, T.; Wainberg, Z.; Nel, A. E.; Meng, H., Tumor-penetrating peptide enhances transcytosis of silicasome-based chemotherapy for pancreatic cancer. *J. Clin. Invest.* **2017,** *127* (5), 2007-2018.
66. Nel, A.; Ruoslahti, E.; Meng, H. New insights into "permeability" as in the enhanced permeability and retention effect of cancer nanotherapeutics. *ACS Nano* **2017,** *11* (10), 9567-9569.
67. Behzadi, S.; Serpooshan, V.; Tao, W.; Hamaly, M. A.; Alkawareek, M. Y.; Dreaden, E. C.; Brown, D.; Alkilany, A. M.; Farokhzad, O. C.; Mahmoudi, M., Cellular uptake of nanoparticles: journey inside the cell. *Chem. Soc. Rev.* **2017,** *46* (14), 4218-4244.
68. Kierstead, P. H.; Okochi, H.; Venditto, V. J.; Chuong, T. C.; Kivimae, S.; Fréchet, J. M. J.; Szoka, F. C., The effect of polymer backbone chemistry on the induction of the accelerated blood clearance in polymer modified liposomes. *J. Control. Release* **2015,** *213*, 1-9.
69. Shiraishi, K.; Yokoyama, M., Toxicity and immunogenicity concerns related to PEGylated-micelle carrier systems: a review. *Sci. Tech. Adv. Mater.* **2019,** *20* (1), 324-336.
70. Mohamed, M.; Abu Lila, A. S.; Shimizu, T.; Alaaeldin, E.; Hussein, A.; Sarhan, H. A.; Szebeni, J.; Ishida, T., PEGylated liposomes: immunological responses. *Sci. Technol. Adv. Mater.* **2019,** *20* (1), 710-724.
71. Hall, A.; Lächelt, U.; Bartek, J.; Wagner, E.; Moghimi, S. M., Polyplex evolution: understanding biology, optimizing performance. *Mol. Ther.* **2017,** *25* (7), 1476-1490.
72. Boussif, O.; Lezoualc'h, F.; Zanta, M. A.; Mergny, M. D.; Scherman, D.; Demeneix, B.; Behr, J. P., A versatile vector for gene and oligonucleotide transfer into cells in culture and in vivo: polyethylenimine. *Proc. Natl. Acad. Sci.* **1995,** *92* (16), 7297-7301.
73. Du, L.; Wang, C.; Meng, L.; Cheng, Q.; Zhou, J.; Wang, X.; Zhao, D.; Zhang, J.; Deng, L.; Liang, Z.; Dong, A.; Cao, H., The study of relationships between pKa value and siRNA delivery efficiency based on tri-block copolymers. *Biomaterials* **2018,** *176*, 84-93.
74. Whitehead, K. A.; Dorkin, J. R.; Vegas, A. J.; Chang, P. H.; Veiseh, O.; Matthews, J.; Fenton, O. S.; Zhang, Y.; Olejnik, K. T.; Yesilyurt, V.; Chen, D.; Barros, S.; Klebanov, B.; Novobrantseva, T.; Langer, R.; Anderson, D. G., Degradable lipid nanoparticles with predictable in vivo siRNA delivery activity. *Nat. Comm.* **2014,** *5* (1), 4277-4287.

75. Li, Y.; Wang, Z.; Wei, Q.; Luo, M.; Huang, G.; Sumer, B. D.; Gao, J., Non-covalent interactions in controlling pH-responsive behaviors of self-assembled nanosystems. *Polymer Chemistry* **2016,** *7* (38), 5949-5956.
76. Huang, X.; Huang, G.; Zhang, S.; Sagiyama, K.; Togao, O.; Ma, X.; Wang, Y.; Li, Y.; Soesbe, T. C.; Sumer, B. D.; Takahashi, M.; Sherry, A. D.; Gao, J., Multi-chromatic pH-activatable 19F-MRI nanoprobes with binary ON/OFF pH transitions and chemical-shift barcodes. *Angew. Chem. Int. Ed.* **2013,** *52* (31), 8074-8078.
77. Jadia, R.; Scandore, C.; Rai, P., Nanoparticles for effective combination therapy of cancer. *Int. J. Nanotechnol. Nanomed.* **2016,** *1* (1), 1-27.
78. Li, Y.; Thambi, T.; Lee, D. S., Co-delivery of drugs and genes using polymeric nanoparticles for synergistic cancer therapeutic effects. *Adv. Healthc. Mater.* **2018,** *7* (1), 1700886.
79. Zhang, M.; Liu, E.; Cui, Y.; Huang, Y., Nanotechnology-based combination therapy for overcoming multidrug-resistant cancer. *Cancer Biol. Med.* **2017,** *14* (3), 212-227.
80. Scarano, W.; de Souza, P.; Stenzel, M. H., Dual-drug delivery of curcumin and platinum drugs in polymeric micelles enhances the synergistic effects: a double act for the treatment of multidrug-resistant cancer. *Biomater. Sci.* **2015,** *3* (1), 163-174.
81. Frezza, A. M.; Stacchiotti, S.; Gronchi, A., Systemic treatment in advanced soft tissue sarcoma: what is standard, what is new. *BMC Med.* **2017,** *15* (1), 109-121.
82. DeSantis, C.; Ma, J.; Bryan, L.; Jemal, A., Breast cancer statistics, 2013. *CA Cancer J. Clin.* **2014,** *64* (1), 52-62.